UNIVERSITÀ VITA-SALUTE SAN RAFFAELE

CORSO DI DOTTORATO DI RICERCA
IN NEUROSCIENZE COGNITIVE

Multimodal in vivo assessment of Lewy-body pathology: toward a new definition of LBD-spectrum subtypes

DoS: Prof. Daniela Perani

Tesi di DOTTORATO di RICERCA di Cecilia Boccalini

matr. 017371

Ciclo di dottorato XXXVI

M-PSI/02

Anno Accademico 2022/2023

UNIVERSITÀ VITA-SALUTE SAN RAFFAELE

CORSO DI DOTTORATO DI RICERCA
IN NEUROSCIENZE COGNITIVE

Multimodal in vivo assessment of Lewy-body pathology: toward a new definition of LBD-spectrum subtypes

DoS: Prof. Daniela Perani

Tesi di DOTTORATO di RICERCA di Cecilia Boccalini

matr. 017371

Ciclo di dottorato XXXVI

M-PSI/02

Anno Accademico 2022/2023



CONSULTAZIONE TESI DI DOTTORATO DI RICERCA

Il/la sottoscritto/I CECILIA BOCCALINI

Matricola / *registration number* 017371

nata a/ *born at* PIACENZA

il/*on* 18/08/1995

autore della tesi di Dottorato di ricerca dal titolo / *author of the PhD Thesis titled*

Multimodal in vivo assessment of Lewy-body pathology: toward a new definition of LBD-spectrum subtypes

□ AUTORIZZA la Consultazione della tesi / AUTHORIZES *the public release of the thesis*

X NON AUTORIZZA la Consultazione della tesi per 12 mesi /DOES NOT AUTHORIZE *the public release of the thesis for 12 months*

a partire dalla data di conseguimento del titolo e precisamente */ from the PhD thesis date, specifically*

Dal / *from* 15/10/2023 Al / *to 15*/10/2024

Poiché /*because*:

□ l'intera ricerca o parti di essa sono potenzialmente soggette a brevettabilità/ *The whole project or part of it might be subject to patentability;*

X ci sono parti di tesi che sono già state sottoposte a un editore o sono in attesa di pubblicazione/ *Parts of the thesis have been or are being submitted to a publisher or are in press;*

□ la tesi è finanziata da enti esterni che vantano dei diritti su di esse e sulla loro pubblicazione/ *the thesis project is financed by external bodies that have rights over it and on its publication.*

E' fatto divieto di riprodurre, in tutto o in parte, quanto in essa contenuto / *Copyright the contents of the thesis in whole or in part is forbidden*

Data /Date 15/10/2023 Firma /Signature 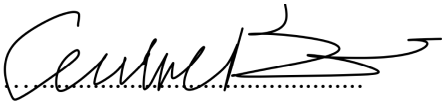

DECLARATION

This thesis has been:

- composed by myself and has not been used in any previous application for a degree. Throughout the text I use both 'I' and 'We' interchangeably.
- has been written according to the editing guidelines approved by the University.

Almost all images come from open-access sources. Permission to use images and other material covered by copyright has been sought and obtained. For the following image/s (Figures 19, 20, 21), it was not possible to obtain permission and is/are therefore included in the thesis under the "fair use" exception (Italian legislative Decree no. 68/2003).

The results of Studies II, IV, V, VI, VII, VIII, IX have been already published in scientific journals and acknowledged by means of reference.

All the results presented here were obtained by myself, except for:

1) ***[^{123}I]FP-CIT-SPECT SUVr and molecular connectivity analyses (Study VII)***
   were performed in collaboration with Dr Giulia Carli, In Vivo Human Molecular and Structural Neuroimaging Unit, Division of Neuroscience, IRCCS San Raffaele Scientific Institute, Milan, Italy.

2) ***Analyses of [^{123}I]MIBG planar images (Study II)***
   were performed in collaboration with Dr Giulia Carli, In Vivo Human Molecular and Structural Neuroimaging Unit, Division of Neuroscience, IRCCS San Raffaele Scientific Institute, Milan, Italy.

3) ***[^{18}F]FDG-PET and metabolic connectivity analyses (Study III and Study IX)***
   were performed in collaboration with Dr Silvia Paola Caminiti, In Vivo Human Molecular and Structural Neuroimaging Unit, Division of Neuroscience, IRCCS San Raffaele Scientific Institute, Milan, Italy.

All sources of information are acknowledged by means of reference.

Acknowledgments

This doctoral dissertation would not have been possible without the support and patience of its first supervisor and mentor, Prof. Perani, whom I sincerely and warmly thank, also for the great opportunities she offered me. Among all of them, the possibility of doing my visiting period abroad, without which I could not have completed my PhD with the same passion and dedication. Sincere and heartfelt thanks go to Prof. Garibotto who supervised and accompanied all my work in Geneva, becoming a point of reference in my professional and personal growth. I would like to thank Giulia and Federica, who represent for me the healthy and supportive part of the two environments in which I worked, which are sometimes enough to counteract the dark side of academia.

Finally, I will not contradict myself and mix my private life with my work life, adding only that this doctoral dissertation also goes to my family and all the people who have filled my life with love these past three years.

Abstract

The clinical syndromes known as Lewy body disorders (LBDs)—Parkinson's disease (PD), PD with dementia, and dementia with Lewy bodies (DLB)—are characterized by the neuropathological aggregation of α-synuclein in the central nervous system. Clinical and preclinical LBDs exhibit highly distinct disease progression and remarkable heterogeneity of motor and nonmotor symptoms. The mechanisms underpinning this clinical heterogeneity are still unclear. Cognitive impairment is a particularly strong predictor of faster progression to dementia in PD, which is likely inevitable but happens at widely variable times after the onset of motor symptoms. Early attempts to establish clinical subgroups were based on the finding that disease progression was more benign in some patients with a specific set of motor symptoms than in others, as observed in large cohort studies and therapeutic trials. New genetic markers, imaging features, and cerebrospinal fluid compounds have been included in both hypothesis- and data-driven investigations. Strong, repeatable clinical subgroups, however, have proved challenging to find.

This thesis aims to investigate the neurobiological mechanisms underlying different phenotypes and clinical trajectories in LBDs since the preclinical stages. The studies address this topic through molecular imaging biomarkers by applying different methodological approaches and different study designs. Multimodal brain molecular techniques are combined with connectivity and graph-theory measures, as well as, with clinical information, to assess *in vivo* pathology spreading and variability of network dysfunction in the whole LBD spectrum. Specifically, the exploration of molecular connectivity allows a detailed *in vivo* evaluation of the dynamic neurobiological changes underlying neurodegeneration. Moreover, the studies relied on these methods to disentangle the sources of clinical variability, focusing mainly on sex/gender contribution to α-synuclein-related neurodegeneration process and phenotypes.

Overall, the final goal is to clarify the heterogeneity of LBD neurodegenerative mechanisms using different molecular neuroimaging approaches within and between different disorders, which also is essential for prognostic considerations and the future development of personalized preventive and treatment strategies.

TABLE OF CONTENTS

LIST OF STUDIES 6

ACRONYMS AND ABBREVIATION 9

LIST OF FIGURES AND TABLES 11

1. Introduction 14

1.1 α-synuclein and neurodegeneration 14

1.2 Lewy body disorders (LBD) clinical spectrum 18

1.2.1 REM sleep behaviour disorder 19

1.2.2 Parkinson's disease 21

1.2.3 Dementia with Lewy bodies 25

1.3 *In vivo* molecular imaging for the underlying pathology 27

1.3.1 Biomarkers for diagnosis and prognosis 27

[^{123}I]FP-CIT-SPECT 28

[^{123}I]MIBG myocardial scintigraphy 31

[^{18}F]FDG-PET 33

1.3.2 Brain molecular connectivity 35

1.4 Fix and flexible factors — key to understand LBD heterogeneity 37

1.4.1 Clinical variability in phenotypes and progression trajectories 37

1.4.2 Sources of phenotypic variability 40

Variable spread of synucleinopathy 41

Genetic factors 44

Sex and gender differences in LBDs 46

2. Aim of the work 50

3. Results 52

3.1 Imaging biomarkers for diagnosis and progression 52

3.1.1 Study 1: Distinctive clinical and imaging trajectories in SWEDD and Parkinson's disease patients (Boccalini, et al.) – submitted article 52

3.1.2 Study 2: Manual and semi-automated approaches to MIBG myocardial scintigraphy in patients with Parkinson's disease (Boccalini, Carli*, et al., 2022) – Published article* 64

3.1.3 Study 3: Mapping brain metabolism, connectivity and neurotransmitters topography in early and late onset dementia with Lewy bodies (Caminiti, Galli, et al.,2023) – submitted article 68

3.2 Brain molecular connectivity to achieve novel insights into the pathophysiology of neurodegenerative diseases 75

3.2.1 Study 4: Review - Brain Molecular Connectivity in Neurodegenerative Conditions (Carli, Tondo*, Boccalini*, et al., 2021) – Published article* 75

3.2.2 Study 5: Metabolic connectivity of resting-state networks in α synucleinopathies, from prodromal to dementia phase (Boccalini, et al., 2022) – Published article 81

3.3 Sex and gender as crucial sources of variability in LBD 90

3.3.1 Study 6: Gender-Related Vulnerability of Dopaminergic Neural Networks in Parkinson's Disease (Boccalini, et al., 2021) – Published article 90

3.3.2 Study 7: Gender differences in dopaminergic system dysfunction in de novo Parkinson's disease clinical subtypes (Boccalini, Carli*, et al., 2022) – Published article* 94

3.3.3 Study 8: Sex differences in dementia with Lewy bodies: an imaging study of neurotransmission pathways (Boccalini, et al., 2023) – Published article 108

3.3.4 Study 9: Sex differences in brain metabolic connectivity architecture in probable dementia with Lewy bodies (Caminiti, Boccalini, et al., 2023) –Published article 115

4. Discussion 123

4.1 Imaging biomarkers for diagnosis and progression 123

4.1.1 Study 1: Distinctive clinical and imaging trajectories between SWEDD and Parkinson's disease patients (Boccalini, et al.) – submitted article 123

4.1.2 Study 2: Manual and semi-automated approaches to MIBG myocardial scintigraphy in patients with Parkinson's disease (Boccalini, Carli*, et al., 2022) – Published article* 127

4.1.3 Study 3: Mapping brain metabolism, connectivity and neurotransmitters topography in early and late onset dementia with Lewy bodies – submitted article 128

4.2 Brain molecular imaging to achieve novel insights into the pathophysiology of neurodegenerative diseases 132

4.2.1 Study 5: Metabolic connectivity of resting-state networks in α synucleinopathies, from prodromal to dementia phase (Boccalini, et al., 2022) – Published article.....132

4.3 Sex and gender as crucial sources of variability in LBD 137

4.3.1 Study 6: Gender-Related Vulnerability of Dopaminergic Neural Networks in Parkinson's Disease (Boccalini, et al., 2021) – Published article 137

4.3.2 Study 7: Gender differences in dopaminergic system dysfunction in de novo Parkinson's disease clinical subtypes (Boccalini*, Carli*, et al., 2022) – Published article 141

4.3.3 Study 8: Sex differences in dementia with Lewy bodies: an imaging study of neurotransmission pathways (Boccalini, et al., 2023) – Published article 146

4.3.4 Study 9: Sex differences in brain metabolic connectivity architecture in probable dementia with Lewy bodies (Caminiti, Boccalini, et al., 2023) – Published article.....150

4.4 Conclusion..... 155

5. Materials and Methods..... 157

5.1 Clinical and cognitive assessment..... 157

5.2 [^{18}F]FDG-PET 157

5.2.1 Imaging acquisition.....157

5.2.2 Pre-processing and single-subject analyses 158

5.3 [^{123}I]FP-CIT-SPECT..... 159

5.3.1 Imaging acquisition.....159

5.3.2 Pre-processing and imaging analyses 159

5.4 [^{123}I]MIBG myocardial scintigraphy..... 162

5.4.1 Imaging acquisition.....162

5.4.2 Pre-processing and imaging analyses 162

5.5 Metabolic and molecular connectivity analyses 163

5.5.1 Inter-regional correlation analysis (IRCA) for large-scale networks 163

5.5.2 Whole-brain and neurotransmitter networks analysis.....164

5.6 Sample, methods and statistical analyses applied in different studies 166

5.6.1 Study 1: Distinctive clinical and imaging trajectories between SWEDD and Parkinson's disease patients (Boccalini, et al.) – submitted article 166

Sample..... 166

Statistical analyses and voxel-wise analyses..... 166

Connectivity analysis 167

Spatial correlation analysis 167

5.6.2 Study 2: Manual and semi-automated approaches to MIBG myocardial scintigraphy in patients with Parkinson's disease (Boccalini*, Carli*, et al., 2022) – Published article.....168

Sample..... 168

The inter-rater agreements 168

The intra-rater agreements 169

5.6.3 Study 3: Mapping brain metabolism, connectivity, and neurotransmitters topography in early and late onset dementia with Lewy bodies (Caminiti et al., 2023) – submitted article 169

Sample..... 169

Brain hypometabolism maps..... 169

Connectivity analysis 170

Metabolic Spatial Distribution of Neurotransmitter Systems 170

5.6.4 Study 5: Metabolic connectivity of resting-state networks in α-synucleinopathies, from prodromal to dementia phase (Boccalini, et al., 2022) – Published article.....171

Sample..... 171

Metabolic connectivity comparison and metrics..... 172

5.6.5 Study 6: Gender-Related Vulnerability of Dopaminergic Neural Networks in Parkinson's Disease (Boccalini, et al., 2021) – Published article 174

Sample..... 174

Metabolic connectivity measures and statistical analyses..... 175

5.6.6 Study 7: Gender differences in dopaminergic system dysfunction in de novo Parkinson's disease clinical subtypes (Boccalini, Carli*, et al., 2022) – Published article* 175

Sample 175

Statistical analyses 176

Connectivity analysis 177

5.6.7 Study 8: Sex differences in dementia with Lewy bodies: an imaging study of neurotransmission pathways (Boccalini, et al., 2023) – Published article 177

Sample 177

Statistical analyses 178

[^{123}I]FP-CIT-SPECT voxel-wise analyses 178

Connectivity 179

5.6.8 Study 9: Sex differences in brain metabolic connectivity architecture in probable dementia with Lewy bodies (Caminiti, Boccalini, et al., 2023) – Published article 179

Sample 179

[^{18}F]FDG-PET voxel-wise analyses 180

Metabolic connectivity measures and statistical analyses 180

6. Bibliography 182

LIST OF STUDIES

Papers included in this dissertation:

Review:

1. Carli, G., Tondo, G., **Boccalini, C.**, & Perani, D. (2021). Brain molecular connectivity in neurodegenerative conditions. Brain Sciences, 11(4), 433. https://doi.org/10.3390/brainsci11040433

Research studies:

2. **Boccalini, C.**, Bortolin, E., Carli, G., Pilotto, A., Galbiati, A., Padovani, A., ... & Perani, D. (2022). Metabolic connectivity of resting-state networks in alpha synucleinopathies, from prodromal to dementia phase. Frontiers in Neuroscience. 16, 930735. 10.3389/fnins.2022.930735
3. **Boccalini, C.**, Carli, G., Pilotto, A., Padovani, A., & Perani, D. (2021). Gender-Related Vulnerability of Dopaminergic Neural Networks in Parkinson's Disease. Brain Connectivity, 11(1), 3-11. https://doi.org/10.1089/brain.2020.0781
4. **Boccalini, C.**, Carli, G., Pilotto, A., Padovani, A., & Perani, D. (2022). Gender differences in dopaminergic system dysfunction in de novo Parkinson's disease clinical subtypes. Neurobiology of Disease, 167, 105668. https://doi.org/10.1016/j.nbd.2022.105668
5. **Boccalini C.**, Nicastro N., Perani D., & Garibotto, V. (2023). Distinctive clinical and imaging trajectories between SWEDD and Parkinson's disease patients. Submitted paper
6. **Boccalini, C.**, Carli, G., Vanoli, E. G., Cocco, A., Albanese, A., Garibotto, V., & Perani, D. (2022). Manual and semi-automated approaches to MIBG myocardial scintigraphy in patients with Parkinson's disease. Frontiers in Medicine, 9, 1073720. 10.3389/fmed.2022.1073720
7. Caminiti, S. P., **Boccalini, C.**, Nicastro, N., Garibotto, V., Perani, D., & Alzheimer's Disease Neuroimaging Initiative. (2023). Sex differences in brain metabolic connectivity architecture in probable dementia with Lewy bodies. Neurobiology of Aging. https://doi.org/10.1016/j.neurobiolaging.2023.02.004

8. **Boccalini, C.**, Nicastro, N., Peretti, D. E., Caminiti, S. P., Perani, D., & Garibotto, V. (2023). Sex differences in dementia with Lewy bodies: an imaging study of neurotransmission pathways. European Journal of Nuclear Medicine and Molecular Imaging, 1-11. https://doi.org/10.1007/s00259-023-06132-4
9. Caminiti, S.P., Galli A., Jonghi-Lavarini L., **Boccalini C.**, Nicastro N., Garibotto V. & Perani D. (2023). Mapping brain metabolism, connectivity and neurotransmitters topography in early and late onset dementia with Lewy bodies. Submitted paper

Studies published/submitted but not included in this dissertation:

1. **Boccalini, C.**, Ribaldi, F., Hristovska I., Arnone A., Peretti, D. E., Mu L., Scheffler M., Perani D., Frisoni G.B. & Garibotto, V. (2023). The impact of tau deposition and hypometabolism on cognitive impairment and longitudinal cognitive decline. Alzheimer's & Dementia. https://doi.org/10.1002/alz.13355
2. **Boccalini, C.**, Peretti, D. E., Ribaldi, F., Scheffler, M., Stampacchia, S., Tomczyk, S., ... & Garibotto, V. (2023). Early-phase 18F-Florbetapir and 18F-Flutemetamol images as proxies of brain metabolism in a memory clinic setting. Journal of Nuclear Medicine, 64(2), 266-273. https://doi.org/10.2967/jnumed.122.264256
3. Tondo, G., **Boccalini, C.**, Vanoli, E. G., Presotto, L., Muscio, C., Ciullo, V., ... & Perani, D. (2022). Brain Metabolism and Amyloid Load in Individuals With Subjective Cognitive Decline or Pre–Mild Cognitive Impairment. Neurology, 99(3), e258-e269. https://doi.org/10.1212/WNL.0000000000200351
4. **Boccalini, C.**, Carli, G., Tondo, G., Polito, C., Catricalà, E., Berti, V., ... & Perani, D. (2022). Brain metabolic connectivity reconfiguration in the semantic variant of primary progressive aphasia. Cortex, 154, 1-14. https://doi.org/10.1016/j.cortex.2022.05.010
5. Catricalà, E., Santi, G. C., Polito, C., Conca, F., Esposito, V., Caminiti, S. P., **Boccalini, C.**, … & Cappa, S. F. (2022). Comprehensive qualitative characterization of linguistic performance profiles in primary progressive aphasia: a multivariate study with FDG-PET. Neurobiology of Aging, 120, 137-148. https://doi.org/10.1016/j.neurobiolaging.2022.09.001

6. Polito, C., Conca, F., Santi, G. C., Esposito, V., Caminiti, S. P., **Boccalini, C.**, ... & Catricalà, E. (2023). Comparing two picture naming tasks in Primary Progressive Aphasia: insights from behavioural and neural results. Cortex. https://doi.org/10.1016/j.cortex.2023.04.014

ACRONYMS AND ABBREVIATION

Abbreviation	Full-lenght Word
AAL	Automated Anatomical Labeling
ACC	Anterior Cingulate Cortex
AChE	Acetylcholinesterase
AD	Alzheimer's Disease
ADL	Activities of Daily Living
ADMN	Anterior Default Mode Network
AI	Asymmetry index
ATN	Attentional Network
CBS	Corticobasal Syndrome
CNS	Central Nervous System
CR	Cognitive Reserve
CSF	Cerebrospinal Fluid
DA	Dopamine
DAT	DA Transporter
DC	Dice coefficient
DLB	Dementia with Lewy Bodies
DLPFC	Dorsolateral Prefrontal Cortex
ECN	Executive Control Network
EEG	Elettroencelography
EMG	Electromyography
ET	Essential Tremor
FWE	Family Wise Error
GBA	Glucosylceramidase Beta
GDS	Geriatric Depression Scale
GWAS	Genome-wide association studies
H/M	Heart-to-mediastinum
HC	Healty Controls
HLVT-R	Hopkins Verbal Learning Test-Revised
HVN	High Visual Network
i	Idiopathic
ICSD-3	3rd edition of the international classification of sleep disorders
ImCalc	Image Calculator
iRBD	Isolated RBD
IRCA	Interregional Correlation Analysis
JOLO	Benton Judgment of Line Orientation
JSC	Jaccard similarity coefficient
LB	Lewy Bodies
LBD	Lewy Bodies disorders
LC	Locus Coeruleus
LEDD	Levodopa Equivalent Daily Dose
LN	Lewy neurites
LNS	Letter-Number Sequencing
LRRK2	The leucine-rich repeat kinase 2
MCC	Middle Cingulate Cortex
MCI	Mild Cognitive Impairment

MDS	Movement Disorder Society
MMSE	Mini-Mental State Examination
MoCA	Montreal Cognitive Assessment
MSA	Multiple System Atrophy
NBM	Nucleus Basalis of Meynert
NE	Norepinephrine
NMSs	Non-motor symptoms
PD	Parkinson's Disease
PDD	Parkinson disease with dementia
PDMN	Posterior Default Mode Network
PET	Positron Emission Tomography
PIGD	Postural Instability Gait Difficulty
PNS	Periphery Nervous System
PPMI	Parkinson's Progression Markers Initiative
PSG	Polysomnography
PSP	Progressive Supranuclear Palsy
PVN	Primary Visual Network
QSPT	Qualitative Scoring of Pentagon Test
QUIP	Questionnaire for Impulsive-Compulsive Disorders
RAVLT	Rey Auditory Verbal Learning Test
RBD	REM Sleep Behavuoir Disorder
RBDQ	RBD Questionnaire
RBE	REM-sleep-related behavioural events
REM	Rapid Eye Movement
ROCF	Rey–Osterrieth Complex Figure
ROIs	Regions Of Interest
SBR	Specific binding ratio
SCOPA-AUT	Scale for Outcomes for Parkinson’s Disease—autonomic function
SD	Standard Deviation
SDMT	Symbol-Digit Modalities Test
SERT	Serotonin transporter
SMA	Supplementary Motor Area
SN	Substantia Nigra
SPECT	Single Photon Emission Computed Tomography
SPM	Statistical Parametric Mapping
SSM/PCA	Scaled Subprofile Model/Principal Component Analysis
STAI	State-Trait Anxiety Inventory
SUVr	Specific Uptake Value ratio
SWEDD	Scan without evidence of dopaminergic deficit
TFCE	Threshold-free Cluster Enhancement
UPDRS	Unified Parkinson’s Disease Rating Scale
UPSIT	40- item University of Pennsylvania Smell Identification Test
VTA	Ventral Tegmental Area
wDC	Weighted Dice Coefficient
[^{123}I]MIBG	^{123}I-metaiodobenzylguanidine
[^{18}F]FDG	^{18}fluorodeoxyglucose
[^{123}I]FP-CIT	Iodine[^{123}I]N-ω-fluoropropyl-2β-carbomethoxy-3β-(4-iodophenyl)nortropane

LIST OF FIGURES AND TABLES

Figure 1. α-synuclein pathology in Parkinson's disease (Open Access Source).
Figure 2. Staging of Lewy pathology in Parkinson's disease (Open Access Source).
Figure 3. Characteristics of proposed body-first and brain-first subtypes of Parkinson's disease (Open Access Source).
Figure 4. Conversion of RBD to α-synucleinopathy (Open Access Source).
Figure 5. Clinical symptoms associated with Parkinson disease progression (Open Access Source).
Figure 6. Motor and cognitive baseline differences and clinical trajectories over time.
Figure 7. Voxel-wise differences in [^{123}I]FP-CIT binding.
Figure 8. Results of spatial correlation analysis with neurotransmitter maps for PD and SWEDD.
Figure 9. Dopaminergic connectivity results in SWEDD and iPD groups.
Figure 10. Manual and fixed-size regions of interest (ROIs) on planar ^{123}I-metaiodobenzylguanidine (MIBG) images (Open access source).
Figure 11. Group analysis in EO- and LO- DLB.
Figure 12. Whole-brain metabolic connectivity architecture in EO- and LO- DLB.
Figure 13. Resting State Networks in EO- and LO- DLB.
Figure 14. Neurotransmitter topography analysis.
Figure 15. Metabolic connectivity alterations in Lewy bodies disease spectrum (Open access source).
Figure 16. RSNs analysis (Open access source).
Figure 17. Brain networks spatial overlap and extension (Open access source).
Figure 18. wDC Similarity coefficient between clinical groups (Open access source).
Figure 19. Nigro-striato-cortical dopaminergic network analyses (Open access source).
Figure 20. Mesolimbic dopaminergic network analyses (Open access source).
Figure 21. Percentage of altered connections (Opens access source).

Figure 22. Dopaminergic connectivity analyses in the whole group with idiopathic Parkinson's disease (Open access source).
Figure 23. Dopaminergic connectivity analyses in the clinical subtypes of idiopathic Parkinson's disease (Open access source).
Figure 24. Voxel-wise sex differences in [^{123}I]FP-CIT binding (Open access source).
Figure 25. Results of spatial correlation analysis with neurotransmitter maps for DLB females and males (Open access source).
Figure 26. Dopaminergic connectivity results in the whole group, and separately in females and males (Open access source).
Figure 27. Topographical distribution of brain hypometabolism (Open access source).
Figure 28. Whole-brain network analysis (Open access source).
Figure 29. Neurotransmitter networks analysis (Open access source).
Figure 30. Resting state network analysis (Open access source).
Figure 31. Subject-specific Regions of Interest (ROIs) (Open access source).

Table 1. Demographic and clinical features of the sample of Study 1 at baseline.
Table 2. Clinical features of the sample of Study 1 at 2 years follow-up.
Table 3. Regional analysis of [^{123}I]FP-CIT-SPECT imaging bindings in SWEDD and iPD patients at baseline and 2 years follow-up.
Table 4. Inter and intra-rater indices on MIBG parameters in Study 2.
Table 5. Clinical, CSF and demographic features of the EO and LO DLB groups in Study 3.
Table 6. Comparisons of brain hypometabolism (Z scores) between EO-DLB and LO-DLB groups of Study 3.
Table 7: Selected seeds for resting-state networks (RSNs) analyses.
Table 8: Demographic and clinical features of the samples.
Table 9: wDC coefficient for comparison in clinical groups.
Table 10: Demographic and clinical features of the PD sample included in Study 6.
Table 11. Demographic and clinical features of the whole iPD sample of Study 7.
Table 12. Demographic and clinical features of iPD subtypes.
Table 13. [^{123}I]FP-CIT SPECT imaging gender differences in the whole group.

Table 14. [^{123}I]FP-CIT SPECT imaging gender differences in the subtypes.

Table 15. Demographic and clinical features of Study 8 sample.

Table 16. Regional analysis of [^{123}I]FP-CIT-SPECT imaging bindings in the male and female DLB patients.

Table 17. Demographic and clinical features of Study 9 sample.

1. Introduction

1.1 α-synuclein and neurodegeneration

α-synuclein is a 140 amino acid tiny intracellular neuronal protein, encoded by the SNCA gene, and it is predominantly localized in the presynaptic terminals. Together with ß- and γ-synuclein, it belongs to the synuclein family and is physiologically prevalent in the brain (Goedert, Jakes and Spillantini, 2017). The physiological function of α-synuclein is incompletely understood, it has been suggested to fulfil roles in synaptic function and plasticity, such as maintaining neurotransmitter homeostasis by regulating synaptic vesicle fusion, clustering, and trafficking between the reserve and ready-releasable pools, as well as interacting with neurotransmitter membrane transporters (Calo *et al.*, 2016). Under pathological conditions, α-synuclein misfolds and aggregates into multiple soluble oligomeric species and insoluble amorphous or fibrillar assembles, which spread from one cell to another in a prion-like manner via synapsis and linked neural pathways (Goedert, Clavaguera and Tolnay, 2010) (**Figure 1**). A-synucleinopathies are neurodegenerative conditions characterized by the formation of intracellular inclusions of filamentous aggregated protein in neuronal cell bodies and processes (Lewy bodies [LBs], Lewy neurites [LNs]) and glial cells (glial cytoplasmic inclusion). LBs are a prerequisite for Parkinson's disease (PD) and dementia with Lewy body (DLB), also known as Lewy body diseases (LBD); instead, multiple system atrophy (MSA) is characterized by glial cytoplasmic inclusion. Patients with idiopathic REM sleep behavior disorder (iRBD) also showed LB pathology in the brains (Boeve *et al.*, 2013; Iranzo *et al.*, 2013; Iranzo, Gelpi, *et al.*, 2014), sustaining RBD as prodromal of α-synucleinopathies (Schenck, 2019).

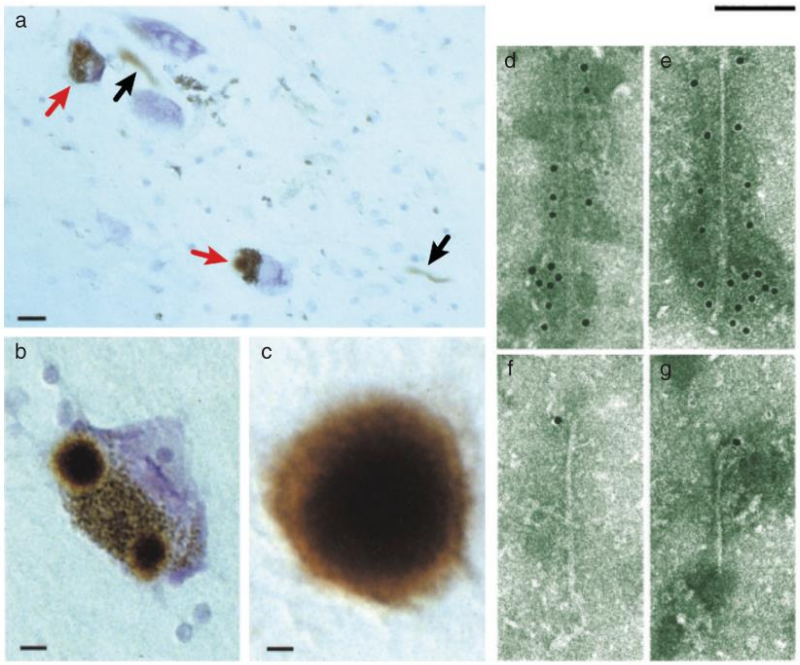

Figure 1. α-synuclein pathology in Parkinson's disease (Open Access Source). *They are shown here at light (a-c) and electron microscopic (d-g) levels, labelled by α-synuclein antibodies. (a), Two pigmented nerve cells, each containing an α-synuclein -positive Lewy body (red arrows). Lewy neurites (black arrows) are also immunopositive. Scale bar, 20 µm. (b), Pigmented nerve cell with two α-synuclein-positive Lewy bodies. Scale bar, 8µm. (c) α-synuclein-positive extracellular Lewy body. Scale bar, 4µm. (d-g), Isolated filaments from the substantia nigra of patients with Parkinson's disease are decorated with an antibody directed against the carboxy-terminal (d and e) or the amino-terminal (f,g) region of α-synuclein. The gold particles conjugated to the second antibody appear as black dots. Note the uniform decoration (d,e), and the labelling of only one filament end (f,g). Scale bar, 100 nm. Figure from (Goedert, Jakes and Spillantini, 2017)*

Since the synapse is the site of primary α-synuclein pathology in the cell, synaptic dysfunction is essential in the pathogenesis of α-synucleinopathies and occurs prior to cell death in the course of the disease (Calo *et al.*, 2016). The aggregation of α-synuclein in presynaptic terminals is likely to be the initial event in cellular α-synuclein pathology preceding α-synuclein in cell bodies, according with the dopaminergic neurotransmission dysfunction occurring before the loss of dopaminergic neurons in PD (Milber *et al.*, 2012). Thus, the aggregated α-synuclein in the synaptic apparatus affects first synaptic function and neurotransmitter release. Moreover, synaptic α-synuclein pathology seems to be directly involved in the spreading of α-synucleinopathy to other cells and tissues

and in retro-grade transfer of pathology leading to the death of the neurons. The pathology appears to spread across cells and tissues via prion-like self-propagation of pathogenic α-synuclein aggregates (Henderson, Trojanowski and Lee, 2019). Pathological spreading occurs via aggregate release from the original cell and uptake by another cell, where they induce misfolding of endogenous α-synuclein and the generation of new aggregates. Notably, according to the Braak hypothesis of staged progression of Lewy pathology in PD (Braak, Del Tredici, *et al.*, 2003), α-synuclein spreads through neural connections rather than anatomical proximity, indicating transsynaptic transfer of α-synuclein. The staging scheme by Braak and colleagues (Braak, Del Tredici, *et al.*, 2003; Braak *et al.*, 2006) states that α-synuclein pathology in PD rostrocaudally progresses: it begins in the brainstem and then spreads progressively to the limbic lobe and the cerebral neocortex in 6 stages (**Figure 2**). The first pathological changes (Stage 1) appear in the dorsal motor nucleus of the vagus nerve, the intermediate reticular zone (medulla oblongata and pontine tegmentum), the anterior olfactory nucleus and olfactory bulb. Then the second stage (Stage 2) involves brainstem nuclei, such as caudal raphe nuclei, magnocellular reticular nucleus, and noradrenergic coeruleus–subcoeruleus complex. In stage three (Stage 3) basal portions of the midbrain and forebrain, substantia nigra, amygdala, tegmental pedunculopontine nucleus and cholinergic magnocellular nuclei of the basal forebrain are involved. Prosencephalic lesions characterize stage four (Stage 4), however cortical involvement is confined to the temporal mesocortex (transentorhinal region) and allocortex (CA2-plexus). During stage 3/4 the pathology becomes clinically manifest. Sensory association areas of the neocortex and prefrontal neocortex are involved during stage five (Stage 5). In the last stage (Stage 6) neuropathology affects the neocortex, specifically neocortical association areas (motor and sensory areas). According to this staging scheme, the disease progress worsens stage by stage and the areas involved in the previous stage show more severe α-synuclein pathology in the next stage. According to Braak, the cognitive status has a significant positive association with the proposed six neuropathological stages (Braak *et al.*, 2006). Pathology of α-synuclein can be identified in the cortical regions in later disease stages when patients' cognitive ability declines. Motor dysfunction is an early symptom in the disease's progression, and α-synuclein pathology is most prevalent in these areas at this time. Despite the paucity of studies concerning the applicability of Braak staging to DLB, α-synuclein pathology seems to

display a similar predictable topographic distribution in DLB patients (Marui *et al.*, 2002; Saito *et al.*, 2003; Deramecourt *et al.*, 2006; Parkkinen, Pirttilä and Alafuzoff, 2008).

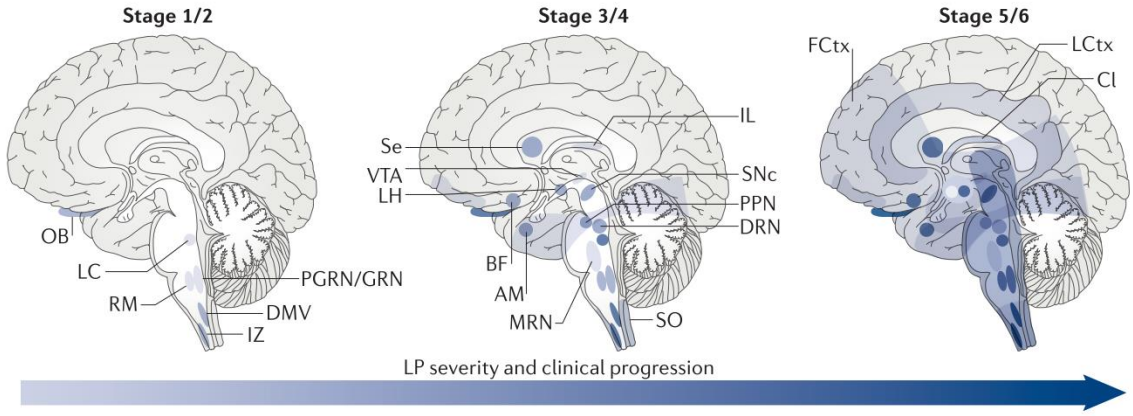

Figure 2. Staging of Lewy pathology in Parkinson's disease (Open Access Source). *The spread Lewy pathology (LP) within different brain structures is based on the study of Braak et al. (Braak, Del Tredici, et al., 2003). The anatomical progression of disease through the brain increases over time (from left to right), and the darker the colour the more LP is present in each region at a given stage. Figure from (Surmeier, Obeso and Halliday, 2017).*

In summary, the Braak staging scheme supports the hypothesis that α-synuclein aggregates originate in the peripherical nervous system (PNS) and then spread into the central nervous system (CNS) via retrograde vagal transport. However, PD is a highly heterogeneous condition and not all cases follow this scheme. An alternative route has been advanced by supporting the existence of two main subtypes of PD according to the pathology spreading: PNS-first (or body-first) and CNS-first (or brain-first) subtypes (Borghammer and Van Den Berge, 2019). A brain-first (top-down) subtype differs from a body-first (bottom-up) subtype because the pathology associated with α-synuclein arises in the brain itself, most frequently in the limbic system or occasionally secondary to entry via the olfactory bulb and descends through the brainstem and into the periphery (**Figure 3**). The evidence gathered from post-mortem studies and the clinical variation in the symptom occurrence order are well represented by these subtypes (Borghammer *et al.*, 2022). According to this theory, premotor RBD is associated with the body-first type because ascending α-synuclein pathology impacts pontine structures before nigral dopamine neurons. While top-down RBD can occur once the pons has been damaged,

patients with the brain-first subtype typically do not have RBD when motor symptoms first appear (Berg *et al.*, 2021).

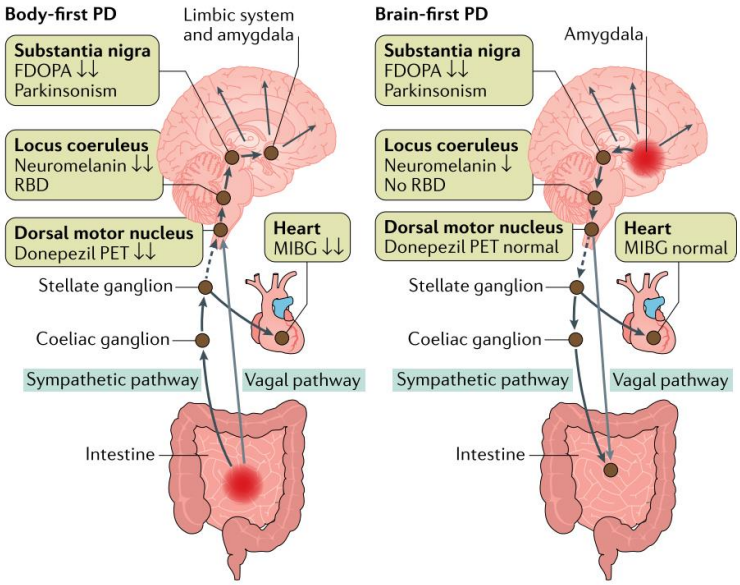

Figure 3. Characteristics of proposed body-first and brain-first subtypes of Parkinson's disease (Open Access Source). *The orange boxes represent the predicted imaging findings and symptoms at the time when motor symptoms first appear, and the arrows indicate the direction of spread of α-synuclein pathology. In body-first Parkinson disease (PD; left), the first α-synuclein aggregation occurs in the gut and propagates through the autonomic nervous system to the spinal cord and brainstem. In brain-first PD (right), the initial α-synuclein pathology arises in vulnerable structures of the brain, such as the limbic system, or enters via an olfactory route, and then descends through the brainstem. During the later disease stages, nearly all patients have widespread pathology in these systems and their symptomatology therefore converges. FDOPA, fluorodopa; MIBG, meta-iodobenzylguanidine. Figure from (Berg et al., 2021).*

1.2 Lewy body disorders (LBD) clinical spectrum

LBDs, which include PD, PD with dementia (PDD), and DLB, are clinically and pathologically heterogeneous groups of neurodegenerative diseases characterized by intracellular α-synuclein Lewy pathology at autopsy. PDD and DLB share multiple clinical characteristics, and it is still debatable how to differentiate the two (Jellinger and Korczyn, 2018). The "one-year rule" is the only criteria now in use to distinguish between PDD and DLB, although there is no evidence supporting a precise time gap between the beginning of motor symptoms and dementia (McKeith *et al.*, 2017). The one-year rule states that although dementia in DLB develops before to the beginning of motor

symptoms, dementia in PDD develops at least a year after the onset of motor symptoms. IRBD is considered in the LBD clinical spectrum since it represents a prodromal phase of α-synucleinopathies (Schenck, 2019).

1.2.1 REM sleep behaviour disorder

IRBD is a REM sleep parasomnia caused by early α-synuclein accumulation in the locus coeruleus in Braak Stage 2 (Knudsen *et al.*, 2018a). IRBD is defined by recurrent dream enactment behavior, including vocalizations, jerks, and movements mimicking dream content during REM sleep, associated with the absence of chin and limb electromyographic (EMG) atonia (Dauvilliers *et al.*, 2018; Ferini-Strambi *et al.*, 2019). The combination of clinical history and video-polysomnography (PSG) were used to diagnose iRBD. The following are the current diagnostic criteria, according to ICSD-3: (I) PSG or reports of dream enactment must show recurrent episodes of behavior or vocalization occurring during the REM phase, and (II) evidence of REM sleep without atonia (RSWA) on PSG (as determined by manual scoring). If the other clinical requirements are satisfied and RSWA fails to appear during the video-PSG recording, the diagnosis may be made provisionally (Sateia, 2014). The correct diagnosis of iRBD requires video-PSG, thus data on the prevalence are limited. According to those, up to 1.06% of the general population is affected (Haba-Rubio *et al.*, 2018), with age of onset ranging from 40 to 70 years, and more frequently men with a male-to-female ratio ranging from 5:1 to 8:1 (Boeve, 2010). RBD clinical implications range from unnoticed sleep disruption to injuries on themselves or their bed partners if dreams have lively or aggressive features (Högl, Stefani and Videnovic, 2018; Ferini-Strambi *et al.*, 2019). Patients with RBD may also exhibit cognitive impairments, such as deficits in attentional, executive, verbal, and visuospatial short-term memory abilities resembling DLB (Massicotte-Marquez *et al.*, 2008; Leitner *et al.*, 2023). Mild cognitive impairment (MCI) is a common condition in iRBD, affecting up to 50% of patients (Gagnon *et al.*, 2009), and it has been suggested as a predictor of conversion into dementia phenotypes (Terzaghi *et al.*, 2013).

RBD can be classified as *primary* or *idiopathic* when it occurs without other conditions or trigger factors, or as *secondary* when it is caused by medications or other neurodegenerative or neurological conditions, autoimmune diseases, or brainstem lesions (Högl, Stefani and Videnovic, 2018). The iRBD is a prodromal phase for

neurodegeneration, especially α-synucleinopathies (Högl, Stefani and Videnovic, 2018; Lin and Chen, 2018): >97% of iRBD patients have been demonstrated to convert into PD, PDD, DLB, or, more rarely, MSA after 14 years follow-up (Galbiati *et al.*, 2019). Consequently, the term idiopathic seems not to be appropriate anymore: many patients with iRBD may exhibit an early clinical manifestation of an evolving neurodegenerative disorder. The term "isolated" has been proposed as more suitable for indicating a prodromal manifestation of neurodegeneration (Ferini-Strambi *et al.*, 2019).

There is an increasing agreement in considering iRBD as a red flag for a malignant α-synucleinopathy (i.e., PDD, DLB) (Högl, Stefani and Videnovic, 2018; Lin and Chen, 2018), supported by α-synuclein accumulation in most brain regions (Boeve *et al.*, 2013; Iranzo *et al.*, 2013; Iranzo, Gelpi, *et al.*, 2014), fast worsening in motor and non-motor symptoms and molecular alterations resembling those of an overt clinical phenotype (Meles *et al.*, 2018; Boeve, 2019; G. Carli, Caminiti, Galbiati, *et al.*, 2020). According to longitudinal data, the estimated risk of a neurodegenerative disease was 33.1% five years after the diagnosis, 75.7% after 10 years and 90.9% after 14 years (Iranzo, Fernández-Arcos, *et al.*, 2014) (**Figure 4**). Specifically, 90% of patients with iRBD develop PD (43%), DLB (25%), or, rarely, MSA (5%) after 15 years of disease duration (Galbiati *et al.*, 2019). Several studies investigating the patterns of hypometabolism in patients with iRBD discovered early neurodegeneration signs supporting iRBD as a prodromal phase (Wu *et al.*, 2014; Ge *et al.*, 2015; Meles *et al.*, 2018; G. Carli, Caminiti, Galbiati, *et al.*, 2020). The majority of iRBD individuals reported a significant occipital hypometabolism that will then spread to other posterior regions (G. Carli, Caminiti, Galbiati, *et al.*, 2020). This hypometabolism pattern is considered a key feature of DLB that helps to discriminate DLB from other conditions (Teune *et al.*, 2010; S.P. Caminiti *et al.*, 2019). Moreover, PD patients with these specific hypometabolic pattern have shown an increased risk of developing dementia (Andrea Pilotto *et al.*, 2018). The existence of similar neural vulnerabilities between iRBD and overt neurodegeneration is also supported by metabolic connectivity studies investigating the neurotransmission vulnerabilities in the whole LBD clinical spectrum (Giulia Carli, Caminiti, *et al.*, 2020). By targeting the dopaminergic, noradrenergic, and cholinergic systems, that are affected by α-synuclein pathology (Uchihara and Giasson, 2016), many pathological similarities emerged between iRBD and DLB (Giulia Carli, Caminiti, *et al.*, 2020). Precisely, iRBD

and DLB were defined by similar cholinergic alterations, whereas PD revealed limited cholinergic impairment, suggesting less vulnerability to dementia. Shared underlying pathological mechanisms between iRBD and a severe phenotype have been identified also in similar genetic mutations in iRBD and PD with cognitive impairment (Lin and Chen, 2018). GBA mutations in PD patients are associated with lower memory, executive, and visuospatial abilities together with a greater risk of developing dementia (Alcalay *et al.*, 2012; Szwedo *et al.*, 2022). Such mutations occur in iRBD where patients with severe GBA variants may have an earlier age at onset and may convert faster to overt neurodegenerative disease (Lin and Chen, 2018; Krohn *et al.*, 2020).

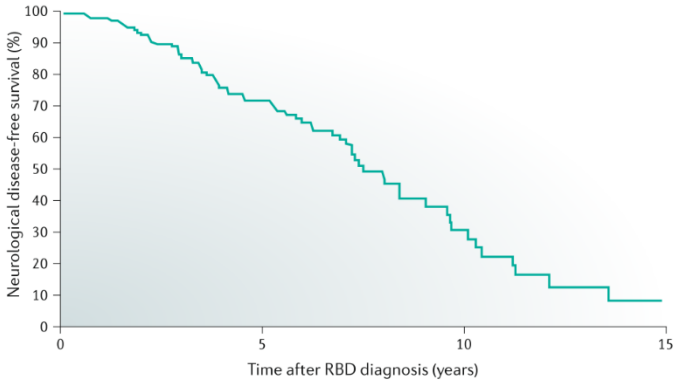

Figure 4. Conversion of RBD to α-synucleinopathy (Open Access Source). *In 174 patients diagnosed with video polysomnography-confirmed rapid eye movement (REM) sleep behaviour disorders (RBD), the estimated risk of a neurodegenerative syndrome was 33.1% 5 years after the diagnosis of idiopathic RBD, 75.7% after 10 years and 90.9% after 14 years. Figure from (Dauvilliers et al., 2018).*

Following all this evidence, iRBD is now considered not merely parasomnia but rather a clinical entity with meaningful pathophysiological and prognostic relevance, and it represents the manifestation of early-stage α-synucleinopathies. In particular, the reported existence of shared neural vulnerabilities between iRBD and DLB/PD with cognitive impairment supports iRBD as a prodromal phase of overt neurodegenerative diseases.

1.2.2 Parkinson's disease

PD is an age-related neurodegenerative disorder affecting 2-3% of the population ≥ 65 years of age (Poewe *et al.*, 2017). It is twice as common in men than in women in most populations and seems to vary by race, ethnicity, genotype and/or environment factors

(Van Den Eeden *et al.*, 2003). The clinical diagnosis of PD relied on specific motor symptoms including bilateral or unilateral/asymmetrical motor deficits (Ronald B Postuma *et al.*, 2015) caused by the loss of dopaminergic neurons in the substantia nigra and widespread intracellular α-synuclein accumulation. After the establishment of patient's parkinsonism, which is defined as bradykinesia, in combination with at least 1 of rest tremor or rigidity, the presence of supportive and absence of exclusionary features and red flags are considered to make a clinical diagnosis according to the International Parkinson and Movement Disorder Society (MDS) criteria (Ronald B Postuma *et al.*, 2015; Postuma *et al.*, 2018). Despite motor symptoms remain central to the diagnosis of PD, neuropsychiatric symptoms as well as posture instability and increasing gait difficulties are gaining recognition as being of similar relevance (Tolosa *et al.*, 2021; Weintraub *et al.*, 2022). In fact, PD is associated with several non-motor symptoms, including hyposmia, constipation, urinary dysfunction, orthostatic hypotension, memory loss, depression, pain, and sleep disturbances. Whereas the classic motor signs of PD are linked to nigral degeneration and striatal dopamine depletion, non-motor symptoms are associated with neurodegeneration of other structures and peripheral autonomic nervous system (Tolosa *et al.*, 2021). Non-motor symptoms can manifest before movement dysfunctions, including sleep dysfunction (i.e., RBD), anosmia, and constipation, together with cognitive and behavioral deficits, such as depression, anxiety, and apathy (Schrag *et al.*, 2015; Zis *et al.*, 2015). Together with a wide range of clinical features, PD patients show also variable disease progressions (**Figure 5**): some have a more benign disease course with a high incidence of motor symptoms (PD stable), while others show a more malignant progression defined by initial severe motor and non-motor symptoms (Obeso *et al.*, 2017). Only in the worst scenario, PD patients progress to dementia during the disease course (PDD). Specifically, about 30% of patients develop dementia (prevalence increases with disease duration), affecting visual spatial recognition and construction, and semantic and episodic memory, frequently associated with hallucinations and psychosis (Tolosa *et al.*, 2021).

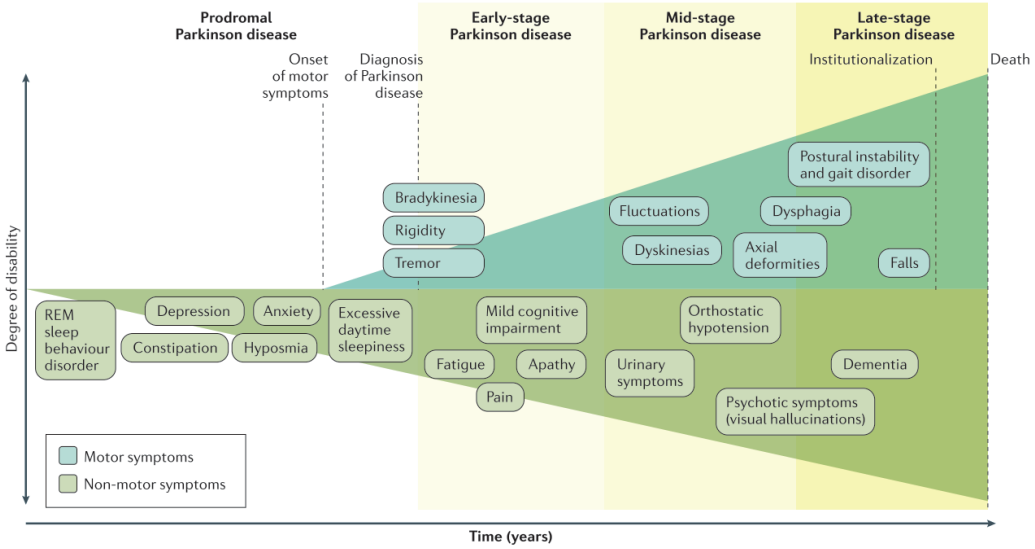

Figure 5. Clinical symptoms associated with Parkinson disease progression (Open Access Source). *The graph depicts the progression of disability in Parkinson's disease (PD) from the prodromal stage to the end stage of the disease. Even if non-motor symptoms become more prevalent and visible throughout the diseases, they can be present to varying degrees at all stages. The PD progression is highly variable. Patients can experience cognitive decline ranging from minor cognitive deficits to severe dementia, or they can remain cognitively stable over time. Figure from (Poewe et al., 2017).*

Given the heterogeneity of clinical manifestations and prognosis, previous literature focused on identifying different subcategories of PD to shed light on underlying pathological mechanisms and predict individual prognosis (Berg *et al.*, 2021). The National Institutes of Health has suggested to prioritize the identification of PD subtypes with the goal of providing sufficient rationale to initiate proof-of-concept prevention trials that initially target high-risk populations (Sieber *et al.*, 2014). Empirical and data-driven classifications approaches have been used to subtype PD. These approaches can vary in how they take into account clinical features, biomarkers, genetic information, disease progression, and/or the presence of different clinical manifestations (Obeso *et al.*, 2017). The most popular method of PD subtyping based on cardinal motor traits is a good representation of an empirical technique. According to the prevalence of some cardinal motor traits on the others, clinical types of PD have been identified. These include tremor-dominant, akinetic-rigid dominant, and postural instability gait difficulty (PIGD) (Eisinger *et al.*, 2017). A data-driven analytical strategy without any a priori

preconceptions can likewise be used for PD subtyping. For instance, with this method, three distinct PD subtypes have been recently defined based on the presence of motor symptoms and three non-motor features (cognitive impairment, RBD, and dysautonomia): the mild motor-predominant, the intermediate and the diffuse malignant (Fereshtehnejad *et al.*, 2017). Patients with the diffuse malignant subtype showed the most severe motor and non-motor symptoms, with both the dopaminergic and non-dopaminergic pathways involved at baseline. These subjects also had a poorer response to levodopa and a faster progression of their condition in outcome and motor/non-motor features, such as somnolence, depression, anxiety, and cognition (Fereshtehnejad *et al.*, 2017; De Pablo-Fernández *et al.*, 2019). On the contrary, the mild motor predominant subtype had minor motor and non-motor impairments at baseline, a younger age of onset, a better response to levodopa, and a slower progression (Fereshtehnejad *et al.*, 2017; De Pablo-Fernández *et al.*, 2019). A later longitudinal study corroborated this PD subtype categorization in an independent cohort, confirming its usefulness in clinical practice and in predicting long-term disease progression (De Pablo-Fernández *et al.*, 2019). Furthermore, the diffuse malignant subtype is the categorization that most closely resembles PDD and DLB phenotypes. The major challenge remains to identify reliable prognostic markers for high-risk progression since the prodromal PD phases (Berg *et al.*, 2021).

Advanced age, advanced disease stage, akinetic-rigid PD motor subtype, cognitive impairment, RBD, and dysautonomia are considered the main risk factors for dementia development. However, the pathophysiology of dementia in PD is still unclear. These clinical phenotypic variations represent the consequence of the involvement of the central, peripheral, and autonomic nervous system associated with a widespread occurrence of LB, resulting from the deposition of abnormal α-synuclein in the brain (Jellinger, 2012). PD's phenotype is not just a dopaminergic motor syndrome, but a dysfunctional multisystem or multiorgan disorder, with the variable involvement of the cholinergic, serotoninergic and noradrenergic systems too (Titova *et al.*, 2017). In PD, the dual syndrome hypothesis (Kehagia, Barker and Robbins, 2013) states that while the tremor-dominant phenotype and dysexecutive syndrome are linked to failure of the frontostriatal dopaminergic system, the onset of dementia seems to be connected to a posterior cholinergic deficiency generating visuospatial and semantic fluency difficulties.

1.2.3 Dementia with Lewy bodies

DLB is the second most common cause of neurodegenerative dementia after Alzheimer's disease (AD) in people older than 65 years (Geser *et al.*, 2005). The clinical onset age of the DLB ranges from 50 at 85 years, with an average of 68 years (Heidebrink, 2002). It accounts for 10–20% of dementia cases, contributing substantially to the overall burden of dementia (Zaccai, McCracken and Brayne, 2005). Although the differential diagnosis could be challenging and mixed pathology is frequent, DLB patients show different cognitive symptoms than AD patients in the early stages (Tiraboschi *et al.*, 2006) and a less favourable prognosis, with accelerated cognitive decline, shorter lifespan, and increased admission to residential care than AD patients, probably because of the increased prevalence and early emergence of neuropsychiatric symptoms in DLB (Mueller *et al.*, 2017). Early-onset dementia (EO) is used when the disorder begins before the age of 65 and is frequently characterized by more severe behavioral and psychiatric symptoms as well as a greater mortality rate than late-onset dementia (LO) (Koedam *et al.*, 2008). Visual hallucinations, parkinsonism, fluctuating cognition, and RBD are among the core clinical symptoms shared by EO and LO DLB (McKeith *et al.*, 2017, 2020); however, LO-DLB exhibits more severe memory impairment than EO-DLB, while EO-DLB has more rapid deterioration and neuropsychiatric symptoms at the beginning (Sim *et al.*, 2022).

According to the most recent criteria (McKeith *et al.*, 2017), DLB diagnosis can be distinguished into *probable* or *possible* DLB depending on clinical features (core and supportive) and diagnostic biomarkers (indicative and supportive). The diagnosis of probable DLB relied on the presence of two or more core clinical features even in the absence of indicative biomarkers, or the presence of only one core clinical feature together with at least one indicative biomarker (McKeith *et al.*, 2017). Possible DLB is diagnosed in the presence of only one clinical feature and no indicative biomarkers, or only indicative biomarkers but no core clinical features (McKeith *et al.*, 2017). Core clinical features include fluctuations, visual hallucinations, parkinsonism, and RBD, occurring in the context of dementia interfering with usual daily functioning. Fluctuations refer to spontaneous alterations in cognition, attention, and arousal and include inconsistent behaviour, incoherent speech, variable attention, and altered consciousness involving staring or zoning out. Visual hallucinations are well-formed, mostly

representing people, animals, and body parts, and may be accompanied by passage hallucinations, a sense of presence, and visual illusions. Complex visual hallucinations have been identified as the most powerful predictor of DLB (Tiraboschi *et al.*, 2006) and are present in 80% of patients (McKeith *et al.*, 2017). They occur before the clinical diagnosis in 77% of patients (Auning *et al.*, 2011) and are associated with negative prognostic outcomes in DLB (Mueller *et al.*, 2017). Parkinsonism is quite common in DLB, affecting 85% of patients. It includes symptoms typically present in PD, namely bradykinesia, together with rest tremors and rigidity (McKeith *et al.*, 2017). Lastly, RBD is present in the majority (75% - 100%) of autopsy-confirmed DLB cases (Ferman *et al.*, 2011) and appears many years or decades before the onset of dementia and other extrapyramidal symptoms (McKeith *et al.*, 2017). DLB patients show a specific neuropsychological profile characterized by impairments of attentional, executive, and visual-spatial abilities, whereas memory is relatively preserved during the early stages. Agnosia, prosopagnosia, and ideomotor apraxia are present. Speech disorders include confabulation, perseveration, and the reduction of verbal fluency. With the disease progression, the memory and the global impairment worsen, and this makes differential diagnosis difficult, specifically with AD. Psychiatric symptoms such as delusions, apathy, and anxious state are frequent in DLB patients and they occur from the early stages of the disease, persisting over time. Thus, these psychiatric symptoms are considered among the supporting clinical features (McKeith *et al.*, 2017). Another supportive feature for DLB diagnosis is the autonomic dysfunction with several different signs and symptoms that are associated with more rapid disease progression and shorter survival (Stubendorff *et al.*, 2012). The important role of prodromal DLB is supported by the fact that the first clinical signs indicative of DLB may present 15 years or more prior to the development of dementia. Cognitive deficits, motor problems, autonomic dysfunction, sleep disorders, and neuropsychiatric disorders are all signs of prodromal DLB. The proposed research criteria distinguish three different subtypes: DLB-MCI onset, DLB-delirium onset, and DLB-psychiatric onset (McKeith *et al.*, 2020). RBD is frequently the first clinical hallmark of the transitional state dominated by cognitive alterations (DLB-MCI onset), followed by cognitive decline, the diagnosis of MCI, and further clinical development of DLB leading to the definition of RBD-MCI-DLB continuum (Boeve, 2019).

Regarding biomarkers, the presence of an indicative biomarker in combination with a single core clinical feature is sufficient for a diagnosis of probable DLB, while supportive biomarkers are consistent with DLB but lack the specificity of the indicative biomarkers (McKeith *et al.*, 2017). Indicative biomarkers include reduced DAT uptake in basal ganglia, abnormal (low uptake) MIBG myocardial scintigraphy, and polysomnographic confirmation of REM sleep without atonia. Other imaging investigations have been proven as helpful for DLB diagnosis, indeed relative conservation of temporal lobe structures assessed by magnetic resonance (MRI), occipital hypoperfusion (SPECT) and hypometabolism (FDG-PET), and prominent slow wave activity on EEG were added as supportive biomarkers for diagnosis (McKeith *et al.*, 2017). The development of other biomarkers for the diagnosis of LBD, and thus DLB, is an active area of research. Much of this effort is focused on the development of an α-synuclein biomarker to complement the β-amyloid and tau biomarkers that have been developed for AD. α-synuclein imaging ligands are currently under study (Korat *et al.*, 2021). α-synuclein biomarkers in other tissues such as skin (Donadio *et al.*, 2017), and gut (Stokholm *et al.*, 2016) are currently being investigated.

1.3 *In vivo* molecular imaging for the underlying pathology

1.3.1 Biomarkers for diagnosis and prognosis

Given the frequent overlap in clinical pictures of different neurodegenerative diseases, the clinical research paradigm has increasingly transitioned from solely clinical diagnosis to biomarker-supported diagnosis during the last few decades (Perani *et al.*, 2020). Neuroimaging tools have given essential contributions to research and diagnosis/prognosis of neurodegenerative conditions. Single-photon emission computed tomography (SPECT), positron emission tomography (PET), and ^{123}I-metaiodobenzylguanidine ([^{123}I]MIBG) scintigraphy are powerful tools for investigating underlying molecular alterations in LBDs. In nuclear medicine clinical practice, the most widely used tools for detecting PD and DLB are the DaTSCAN and [^{123}I]MIBG scintigraphy, which assess the integrity of neurotransmitter systems, specifically the nigrostriatal dopaminergic and the noradrenergic systems, respectively. The usefulness of both DaTSCAN and [^{123}I]MIBG scintigraphy for the diagnosis of PD and DLB has been widely confirmed by meta-analysis studies (Orimo *et al.*, 2012; Papathanasiou *et al.*, 2012; Treglia, Cason and Giordano, 2012; Bega *et al.*, 2021), especially in making the

differential diagnosis. Furthermore, [^{18}F]FDG-PET has demonstrated high accuracy in distinguishing PD from different atypical Parkinsonism disorders (Tang, Poston, Eckert, *et al.*, 2010; S.P. Caminiti *et al.*, 2019), as well as DLB from AD (McKeith *et al.*, 2017), giving a helpful contribution in the diagnosis.

[^{123}I]FP-CIT-SPECT

The nigrostriatal dopaminergic system can be evaluated with molecular imaging techniques used to assist with diagnosis (Politis, 2014). Among them, dopamine transporters (DAT) imaging has largely been employed with SPECT using the [^{123}I]FP-CIT ligand (also known as ^{123}I-ioflupane or DaTSCAN). *In vivo* DAT imaging is currently considered one of the most useful diagnostic tools for degenerative parkinsonism and related movement disorders since the loss of striatal dopamine nerve terminal function led to neurodegenerative parkinsonism. Thus, DaTSCAN selectively and reliably measures the presynaptic dopaminergic deficit, providing the possibility of an objective and quantitative biomarker of degeneration in PD (Saeed *et al.*, 2017) and DLB (McKeith *et al.*, 2017). In PD, DAT imaging displays a striatal binging reduction, predominantly in the striatum contralateral to the clinically most affected side, and has high diagnostic accuracy for distinguishing degenerative parkinsonisms from essential tremor (Marshall *et al.*, 2009) and in helping the early diagnosis of PD. Particularly, dopaminergic denervation progresses from putamen to caudate contralateral to the clinically affected side, which is strongly related to disease severity and duration, as well as rigidity and bradykinesia, but not with tremor severity (Palermo *et al.*, 2021). However, a proportion of patients clinically diagnosed with PD have normal scans (Scans Without Evidence of Dopaminergic Deficit (SWEDD)), generating debates on the underlying biological mechanisms characterizing these subjects. Large imaging studies for PD found SWEDDs to be up to 20% (Erro *et al.*, 2016). These patients usually report different clinical features in posture, gait, and tremor, with great presence of non-motor symptoms, such as orthostatic hypotension, cardiovascular and thermoregulatory dysfunction, daytime sleepiness, cognitive impairment, sleep disturbances, and almost in all, no hyposmia (Balestrino *et al.*, 2021). Previous studies on SWEDD populations found minimal evidence of disease progression, suggesting that SWEDD subjects are unlikely to have idiopathic PD (Marshall *et al.*, 2009; Marek *et al.*, 2014; Erro *et al.*, 2016; Nicastro, Burkhard and Garibotto, 2018; Balestrino *et al.*, 2021). Follow-up studies of SWEDD

cases showed that in a significant proportion of these patients the diagnosis was revised in favor of non-degenerative conditions, including psychogenic parkinsonism, musculoskeletal co-morbidity, dystonia, or essential tremor (Schneider *et al.*, 2007; Sixel-Döring *et al.*, 2011; Marek *et al.*, 2014). It should also be considered that a small proportion of SWEDD subjects, however, may have false-negative imaging in a degenerative condition, arguably PD, because of a misleading SPECT assessment (Nicastro, Garibotto, Badoud, *et al.*, 2016). Until recently and in many studies, the interpretation of [^{123}I]FP-CIT SPECT images has been based mostly on visual assessment (Catafau *et al.*, 2004). Despite its reliability (Davidsson *et al.*, 2014), the visual interpretation leads to difficult-to-classify scans and inter-observer variability that represent a serious problem, particularly in the early-phase cases. Adding semi-quantitative evaluation to the standard visual assessment improved the detection of hitherto undetected changes (Söderlund *et al.*, 2013; Nicastro, Burkhard and Garibotto, 2018).

Also in DLB, low DAT reuptake in the basal ganglia as revealed by SPECT or PET imaging is now considered an indicative biomarker (McKeith *et al.*, 2017). The diagnostic accuracy of DaTSCAN has been demonstrated to be sufficiently high to distinguish DLB from AD, with sensitivity (78%) and specificity (90%) (McKeith, 2007), since severe nigrostriatal dopaminergic degeneration occurs in DLB but not in AD. Some attempts have been made to use DaTSCAN for a differential diagnosis between PD and atypical parkinsonian disorders. DLB patients showed an extended involvement of basal ganglia, with a significantly lower binding in the caudate nucleus than the PD patients, whereas PD patients had a more asymmetric loss of binding sites in the posterior putamen than DLB patients and controls (Walker *et al.*, 2004). However, DaTSCAN still lacks sufficient specificity to distinguish PD from other atypical parkinsonism disorders (Ferrando and Damian, 2021). Therefore, other exams might be useful to discriminate against these patients, such as [^{123}I]MIBG scintigraphy and [^{18}F]FDG-PET.

The presynaptic dopaminergic integrity has been also assessed in iRBD, with a percentage of dopaminergic impairment in the striatum varying among studies (Baucknehtet *et al.*, 2018). Moreover, the presence of nigrostriatal dopaminergic dysfunction, as investigated by DaTSCAN, was able to identify iRBD patients at high risk of short-time phenoconversion to overt α-synucleinopathy (Iranzo *et al.*, 2017; Li *et al.*, 2017; Arnaldi

et al., 2021). Specifically, Li et al. (2017) found that patients with decreased binding of the DAT ligand in the left striatum and putamen were at higher risk of developing an α-synucleinopathy after five years (Li *et al.*, 2017). Iranzo et al. (2017) demonstrated that a decrease of putaminal binding higher than 25% predicts a phenoconversion in three years (Iranzo *et al.*, 2017). A recent multicenter study found that iRBD patients older than 70, with constipation and reduced putaminal dopaminergic function, are at high risk of phenoconversion within 3 years (Arnaldi *et al.*, 2021). The severity of striatal dopaminergic depletion is correlated with iRBD clinical impairment, with the deficiency being worse as the disease progresses. According to this evidence, presynaptic striatal impairment in iRBD patients may serve as a biomarker of neurodegeneration (Bauckneht *et al.*, 2018). Presynaptic dopaminergic impairment, however, cannot distinguish between patients progressing to primary dementia (PDD/DLB) or to PD (Postuma *et al.*, 2019). Therefore, it appears that the striatal dopaminergic deficiency is a biomarker that indicates the early development of unspecific α-synucleinopathy.

Despite the clinical focus on striatal DAT binding in LBD patients, in the last years, the research addressed also extrastriatal [^{123}I]FP-CIT bindings, given the affinity of [^{123}I]FP-CIT for transporters involved in distinct neurotransmission systems (i.e., high-to-low affinity for DAT, serotonin (SERT), and norepinephrine (NET) transporters, respectively) (Scheffel *et al.*, 1997; Booij *et al.*, 2007; Booij and Kemp, 2008). Thus, the study of [^{123}I]FP-CIT binding in the extrastriatal regions offers the chance to study other neurotransmission pathways, particularly the serotoninergic one since extrastriatal binding mainly (70%) derives from SERT density. Serotonin regulates many higher brain functions including cognition, mood, and motor behaviour – all being impaired in LBDs. In PD, decreased [^{123}I]FP-CIT uptake was found in frontal regions (Premi *et al.*, 2017), amygdala (Nicastro, Garibotto and Burkhard, 2020), insula, thalamus, and cingulate (Pilotto, Schiano di Cola, *et al.*, 2019). The few studies in DLB patients reported lower [^{123}I]FP-CIT bindings in the midbrain (Roselli *et al.*, 2010), hypothalamus (Joling *et al.*, 2019), insula (Nicastro *et al.*, 2020), cingulate, and thalamus (Pilotto, Schiano di Cola, *et al.*, 2019), as compared to controls. These alterations may explain the wide range of non-motor symptoms expressed in LBDs, which should not be considered merely dopaminergic diseases.

[^{123}I]MIBG myocardial scintigraphy

[^{123}I]MIBG scintigraphy is used to assess the denervation of the autonomic nervous system (Knudsen and Borghammer, 2018), representing a supportive diagnostic technique in LBDs (McKeith *et al.*, 2017; Postuma *et al.*, 2018). The quantity of [^{123}I]MIBG retention over several hours following injection reflects neuronal integrity since MIBG is an analog of noradrenaline that is actively taken up into the presynaptic cardiac sympathetic neurons by the norepinephrine uptake-1 transporter (Sisson and Wieland, 1986). Therefore, [^{123}I]MIBG cardiac scintigraphy assesses the postganglionic presynaptic cardiac sympathetic nerve endings of the noradrenergic nervous system. It started out as a tool for the evaluation of heart conditions (Carrió, 2001). After then, cardiac [^{123}I]MIBG scintigraphy was clinically used in PD and most patients had lower cardiac uptake (Orimo *et al.*, 2012) supporting its sensitivity for this clinical condition.

The image acquisition usually consists of an early 10-minute anterior planar view 15 minutes after injection, and a late 10-minute planar view 4 hours after injection (Van Vickle and Thompson, 2015). The heart-to-mediastinum (H/M) ratio is calculated to obtain the cardiac uptake by setting regions of interest (ROIs) over the heart and the upper mediastinum on the anterior planar view of the chest (Orimo *et al.*, 2016). Thus, cardiac [^{123}I]MIBG uptake is quantified by comparing the [^{123}I]MIBG radiation emitted from ROIs selected over the heart and the mediastinum (H/M ratio) on planar images of the thoracic anterior view for the early and late acquired images. The method used to obtain these parameters is generally based on manually drawing cardiac ROIs and a low H/M ratio indicates a reduced [^{123}I]MIBG cardiac uptake (van der Veen, Scholte and Stokkel, 2010). Since the loss of postganglionic myocardial sympathetic nerve fibers is a significant characteristic of autonomic dysfunction in LBDs, cardiac [^{123}I]MIBG scintigraphy is currently considered a supportive criterion of PD (Postuma *et al.*, 2018) and an indicative biomarker of DLB together with DaTSCAN (McKeith *et al.*, 2017). In general, 90% of PD patients show pathological [^{123}I]MIBG scintigraphy during the disease course, while around 40%-50% of PD patients may show normal scans in the early disease stage (Chung and Kim, 2015). This evidence fit well with the presence of gut-first and brain-first subtypes characterizing by two different starting points of LBD (Borghammer and Van Den Berge, 2019). Interestingly, [^{123}I]MIBG alteration in PD has also been associated with great cognitive deterioration and the risk of dementia

(PDD/DLB) (Kim *et al.*, 2009; Anang *et al.*, 2014). The majority of DLB patients show abnormal [^{123}I]MIBG scintigraphy (Chung and Kim, 2015), which has been included now as an indicative biomarker in the fourth DLB consensus criteria (McKeith *et al.*, 2017). Patients with DLB and PDD have a lower cardiac uptake than those with PD (Oka *et al.*, 2007), and the [^{123}I]MIBG scintigraphy was highly accurate at predicting likely DLB in patients with suspected DLB after one year of follow-up (Ishii *et al.*, 2013).

Thus, alterations at [^{123}I]MIBG scintigraphy are considered a supportive biomarker for PD and DLB but also helpful for making differential diagnosis (King, Mintz and Royall, 2011). [^{123}I]MIBG scintigraphy can accurately distinguish LBDs (i.e., PD, DLB) and non-LBDs (e.g., AD, MSA, and progressive supranuclear palsy (PSP)) (King, Mintz and Royall, 2011). A meta-analysis demonstrated 94% of sensitivity and 91% of specificity for [^{123}I]MIBG scintigraphy in distinguishing LBDs from non-LBDs (King, Mintz and Royall, 2011). Differently from PD, patients with PSP, MSA, and CBS show normal or marginally reduced [^{123}I]MIBG uptakes (Saeed *et al.*, 2017; Giannoccaro *et al.*, 2020). The evidence of normal values of [^{123}I]MIBG uptake showed by MSA patients is consistent with the fact that autonomic dysfunction defining MSA is caused by preganglionic rather than postganglionic denervation, as opposed to PD and DLB (Rascol and Schelosky, 2009). [^{123}I]MIBG scintigraphy can discriminate DLB from AD since the early stage of the disease (Komatsu *et al.*, 2018), with sensitivity (69%) and specificity (87%) (McKeith *et al.*, 2017). AD patients showed a normal mean H/M ratio and a lower proportion of orthostatic hypotension than DLB (Kim *et al.*, 2015), in line with the absence of non-motor dysfunction, such as constipation, iRBD, or cardiovascular autonomic dysfunction in AD.

Alterations in [^{123}I]MIBG uptake are already present in the iRBD phase with iRBD subjects presenting abnormal H/M ratios compared to controls, with the percentage ranging from 82% to 100% (Miyamoto *et al.*, 2008; Knudsen *et al.*, 2018b). By comparing cardiac [^{123}I]MIBG scintigraphy in iRBD, PD, and DLB patients, the impairment in iRBD was as severe as in PD and DLB and was already evident at an early stage after onset (Miyamoto *et al.*, 2008). Moreover, cardiac peripheral nerve degeneration occurs more frequently in the early stages of DLB and iRBD than in PD (Miyamoto *et al.*, 2008).

[^{18}F]FDG-PET

The glucose analog FDG is the radiotracer used to measure cellular glucose metabolism. [^{18}F]FDG-PET emerged in the 1980s and is an established relevant clinical tool in the diagnostic work-up of neurodegenerative diseases and movement disorders (Iaccarino *et al.*, 2017; Perani *et al.*, 2020). The [^{18}F]FDG-PET signal, which reflects both oxidative metabolism in neurons and aerobic glycolysis in astrocytes, is highly coupled to synaptic function and dysfunction (Stoessl, 2017). Many different neuropathological events contribute to synaptic dysfunction and altered glucose metabolism and can be detected by [^{18}F]FDG–PET from the early clinical disease stages (Cerami *et al.*, 2015; G. Carli, Caminiti, Galbiati, *et al.*, 2020; Perani *et al.*, 2020; Tondo *et al.*, 2022).

The abnormal aggregations of α-synuclein lead to neural and synaptic dysfunction, thus, disease-specific altered metabolic patterns have been systematically detected in LBDs (Poston and Eidelberg, 2010; Tang, Poston, Eckert, *et al.*, 2010; Teune *et al.*, 2010; Garcia-Garcia *et al.*, 2012; Hellwig *et al.*, 2012; Wu *et al.*, 2014; Ge *et al.*, 2015; S. P. Caminiti *et al.*, 2017; A. Pilotto *et al.*, 2018; Meles *et al.*, 2018; G. Carli, Caminiti, Galbiati, *et al.*, 2020) allowing also differential diagnoses with high accuracy (Tang, Poston, Eckert, *et al.*, 2010; Teune *et al.*, 2013; Silvia Paola Caminiti *et al.*, 2019). PD patients typically exhibit a normal brain metabolism or heterogeneous but limited cortical hypometabolism, involving bilateral parietal, premotor, and supplementary motor regions compared to controls (Poston and Eidelberg, 2010; Tang, Poston, Dhawan, *et al.*, 2010; Zhao, Zhang and Gao, 2012; A. Pilotto *et al.*, 2018). A disease-specific pattern for PD, namely PDRP, was first identified by Eidelberg and colleagues and validated in multiple independent populations (Niethammer and Eidelberg, 2012; Teune *et al.*, 2013; Meles *et al.*, 2020) using the scaled sub-profile model and principal component analysis (SSM/PCA) approach (Eidelberg *et al.*, 1994). The hypermetabolism involves the globus pallidus and putamen, thalamus, cerebellum, pons, and sensorimotor cortex, whereas hypometabolism characterizes the lateral frontal and parieto-occipital areas. It has been shown that pattern expression increases with disease progression and decreases with effective therapy. Interestingly, when PD patients were stratified by their clinical symptoms (Albrecht *et al.*, 2019), patients with cognitive impairment showed prevalent parietal involvement. Consistently, PD patients who progress to dementia showed a prevailing occipital and posterior parietal-temporal hypometabolism, variably associated

with frontal hypometabolism (Pappatá *et al.*, 2011; Gasca-Salas *et al.*, 2016; Baba *et al.*, 2017; A. Pilotto *et al.*, 2018).

A significative hypometabolism in occipital brain regions, including the calcarine cortex, middle and inferior occipital gyrus bilaterally, and parietal regions is considered a key feature of DLB, helping to discriminate DLB from other diseases (Teune *et al.*, 2010; Garcia-Garcia *et al.*, 2012; S. P. Caminiti *et al.*, 2017; Silvia Paola Caminiti *et al.*, 2019). It is recognized as a supportive biomarker (McKeith *et al.*, 2017) able to distinguish DLB from AD with high accuracy (Minoshima *et al.*, 2001). The temporo-parietal hypometabolism has also been reported in AD (Teune *et al.*, 2010; Kantarci *et al.*, 2012), but the occipital hypometabolism is the hallmark of DLB (McKeith *et al.*, 2017). Moreover, the typical DLB metabolic pattern can be influenced by disease severity and different core features that were associated with more severe hypometabolism in specific regions, thus, suggesting a close clinical–imaging correlation (Morbelli *et al.*, 2019). Parkinsonism has been negatively covaried with bilateral parietal, precuneus, and anterior cingulate metabolism; visual hallucinations with bilateral dorsolateral–frontal cortex, posterior cingulate, and parietal metabolism; RBD with bilateral parieto-occipital cortex, precuneus, and ventrolateral–frontal metabolism; and cognitive fluctuations with occipital metabolism.

The occipito-parietal hypometabolic pattern observed in DLB patients has been also reported, even if less extended, in iRBD patients (up to 84%) (Wu *et al.*, 2014; Ge *et al.*, 2015; Meles *et al.*, 2018; G. Carli, Caminiti, Galbiati, *et al.*, 2020), supporting the existence of strong similarities of the underlying pathological processes. Applying SSM/PCA approach, a RBD-related pattern was characterized by hypermetabolism in the cerebellum, brain stem, thalamus, sensorimotor cortex, hippocampus, and hypometabolism in the middle cingulate, temporal, occipital, and parietal cortices (Meles *et al.*, 2018). More recently, a similar brain metabolic pattern has been demonstrated to reflect changes associated with phenoconversion from iRBD to PD or DLB (Mattioli *et al.*, 2023). Specifically, metabolic changes in occipital and parietal areas have been related to MCI in iRBD and the phenoconversion to PD or DLB (Yoon *et al.*, 2022). Indeed, the occipital metabolic alterations observed in iRBD may represent an early signature of neurodegeneration that may spread to other posterior regions as in DLB. Since occipital hypometabolism has been associated with an increased risk of dementia

conversion, it might represent a risk of iRBD progression toward a malignant α-synucleinopathy, such as PDD/DLB. However, further longitudinal studies are warranted to differentiate patterns predicting conversion to different α-synucleinopathies (Miglis *et al.*, 2021).

1.3.2 Brain molecular connectivity

Nowadays, the research focus has shifted from studying the effect of pathology on local neuron functions to investigating the long-distance effects on the interconnected nervous systems. This change is grounded on the evidence that pathology does involve a set of vulnerable interconnected regions, namely brain networks (Seeley *et al.*, 2009; Rubinov and Sporns, 2010; Pievani *et al.*, 2014; Fornito, Zalesky and Breakspear, 2015; Yakushev, Drzezga and Habeck, 2017; Sala and Perani, 2019; Carli *et al.*, 2021; Sala *et al.*, 2022). The pathophysiological models of neurodegenerations see the brain as composed of inter-regional anatomical and functional networks, considered on both sides as passive targets of the pathology and active participants in its spread (Carli *et al.*, 2021). For these reasons, in the last decade, there has been increasing interest in the study of brain connectivity in neurodegenerative diseases, mainly using resting state (RS) functional MRI. Connectome approach is integral to understanding neuropathology, since brain-network topology shapes neural responses to damage through maladaptive and adaptive processes (Palop, Chin and Mucke, 2006; Fornito, Zalesky and Breakspear, 2015). Previous neuroimaging studies supported that pathology starts in disease-specific region of the brain, and then progresses to the most connected regions following healthy functional connectivity networks (estimated using functional MRI) in neurodegenerative diseases, perhaps due to trans-synaptic spread of abnormally folded proteins through connected neuronal pathways (Zhou *et al.*, 2012; Mandelli *et al.*, 2016). Within this framework, pathological changes occur in a specific region of the brain that is especially vulnerable to each disorder. Thus, connectivity approach has major implications for understanding diseases pathogenesis and progression within the same clinical spectrum. Despite the majority of available studies are based on functional MRI, PET studies on brain connectivity are increasing since they can provide unique information inaccessible to MRI-based and electrophysiological techniques (Sala *et al.*, 2022). The combination between molecular neuroimaging techniques and multivariate brain connectivity methods represents an innovative and powerful approach to obtain a unique insight into the pathophysiology of

neurodegenerative diseases. However, literature on molecular connectivity is still limited (Sala *et al.*, 2022), with most studies mainly focusing on [^{18}F]FDG-PET metabolic connectivity, as the most popular and established radiotracer. Studying neurodegenerative diseases with metabolic connectivity identifies disease-specific patterns of alterations consistent with the underlying pathology and it might provide important insights into the link between local vulnerabilities, long-range disconnection, and the effects of neuropathology (Sala and Perani, 2019). In addition, metabolic connectivity may add important complementary information to RS functional connectivity obtained with fMRI (Ripp *et al.*, 2020; Jamadar *et al.*, 2021).

To detect and evaluate the connectivity of complex brain networks using PET data, multivariate methods have been implemented allowing the assessment of changes in the relationship between regions that go beyond local regional variations. Given that brain regions with significantly correlated PET uptake are functionally interconnected, molecular connectivity approaches are based on the assessment of regional covariation in PET tracer uptake across subjects. The strengths of the connections are proportional to the magnitude of their correlation coefficients, and the pattern is representative of the entire population of subjects used for the analysis. Based on this assumption, there are three main approaches to assess such relationships: (i) seed correlation or interregional correlation analysis (IRCA) (Lee *et al.*, 2008), (ii) independent component analysis (ICA) (Di and Biswal, 2012), and (iii) regions of interest (ROI)-based approaches (Huang *et al.*, 2010; Veronese *et al.*, 2019) (for more comprehensive methodological reviews, also see (Yakushev, Drzezga and Habeck, 2017; Sala and Perani, 2019; Sala *et al.*, 2022)). Moreover, graph theory indexes (such as the brain hubs and modules, changes in node and global network characteristics) can be computed to study the brain connectome and network's organization in health and disease (Rubinov and Sporns, 2010).

The study of molecular and metabolic connectivity has been very relevant also in investigating α-synucleinopathies showing them as multi-network neurodegenerative disorders in which both local and global networks are affected. The α-synuclein accumulations lead to dysfunctions in synaptic transmission and widespread impacts on functional and molecular connectivity, which result in neural network alterations. In LBDs, most molecular connectivity studies are based on [^{18}F]FDG-PET data, and studies that have used different radiotracers for neurotransmission systems represent a small

proportion of the literature (Carli *et al.*, 2021). Reviewing the available evidence of molecular and metabolic connectivity studies in LBDs has resulted in one recent publication by my group and I (Carli *et al.*, 2021), which is fully described below (**Paragraph 3.2.1**). Briefly, PD was characterized by a metabolic connectivity derangement in the large-scale frontal networks (Sala, S.P. Caminiti, *et al.*, 2017), which are strictly related to dopaminergic depletion and the consequent clinical manifestations. On the other hand, DLB patients showed a metabolic connectivity pattern characterized by a severe involvement of the posterior cortical, limbic, and attention networks, that are related to diverse clinical symptoms (Sala *et al.*, 2019). The multisystem derangement of large-scale networks in PD and DLB has also been demonstrated by molecular connectivity studies on neurotransmission systems, targeting the dopaminergic, noradrenergic, and cholinergic ones (S.P. Caminiti *et al.*, 2017; Silvia Paola Caminiti *et al.*, 2017; Giulia Carli, Caminiti, *et al.*, 2020; Caminiti, Pilotto, *et al.*, 2023).

1.4 Fix and flexible factors — key to understand LBD heterogeneity

1.4.1 Clinical variability in phenotypes and progression trajectories

Although all LBDs share the neuropathological accumulation of α-synuclein in the central nervous system, these clinical entities have marked heterogeneity of motor and nonmotor symptoms with highly variable disease progression. The heterogeneity starts in the prodromal phase (Berg *et al.*, 2021) and its biological basis remains poorly understood (Coughlin, Hurtig and Irwin, 2020). Whereas α-synuclein is the hallmark pathology of LBDs, tau and beta-amyloid (Aβ) copathology is common and overall ~50% of all LBD have a secondary neuropathological diagnosis of medium- or high-level AD in most large autopsy series (Irwin, Lee and Trojanowski, 2013; Irwin and Hurtig, 2018; Jellinger and Korczyn, 2018). AD copathology not only contributes to decreased survival and a shortened motor-dementia interval but also influences specific motor and cognitive features (Coughlin, Hurtig and Irwin, 2020). Postmortem works suggest those patients with moderate- to high-level AD neuropathological change at death have a worse prognosis and altered clinical phenotypes, with, especially, tau appearing to have a strong influence on dementia and survival (Coughlin *et al.*, 2019; Coughlin, Hurtig and Irwin, 2020).

PD itself is heterogeneous and could be considered a syndrome, or as an umbrella term under which different and overlapping clinical and pathological subtypes fit (Menšíková *et al.*, 2022). Cognitive impairment is present in up to 25% of PD patients in the early stages of the disease and predicts faster progression to dementia (Yarnall *et al.*, 2014), which is likely inevitable but occurs at widely variable times after the onset of motor parkinsonism (Hely *et al.*, 2008). Early efforts to create clinical subgroups were based on the observation in large cohort studies and clinical trials that disease progression was more benign in some patients with a particular set of motor symptoms than in others. Subsequent work has integrated new genetic markers, imaging characteristics, and cerebrospinal fluid (CSF) data in both hypothesis-driven studies and data-driven analyses. However, despite the priority of the identification of PD subtypes (Sieber *et al.*, 2014), robust and reproducible subgroups have been difficult to identify (Coughlin, Hurtig and Irwin, 2020). According to the empirical clinical approach, PD patients have been clustered based on clinical features, namely age-at-onset, major motor phenotypes, cognitive impairment, and nonmotor symptoms. The most used clinical classification is based on the dominance of some cardinal motor features. According to that, the tremor-dominant, the akinetic-rigid dominant, and the PIGD subtypes have been described (Stebbins *et al.*, 2013) as different forms of PD with an indeterminate group of patients who do not fall into these categories. The tremor-dominant patients were characterized by a slow and benign motor progression, whereas PIGD phenotypes are linked to faster cognitive decline and a higher prevalence of nonmotor symptoms than other forms. Despite their wide acceptance, the solidity of these motor subtypes is still on debate, since different subtypes may represent different phases of the disease (Nutt, 2016).

Another approach to identifying subtypes is data-driven methods using various forms of cluster analyses without any a priori hypothesis. However, these methods are influenced by the variables that are included in the analysis, the number of subtypes that the investigators allow in the final model, and the population that is studied. Cluster analyses of large groups of PD patients generally group populations into 3 to 5 clusters, but the groups differ in each report (Nutt, 2016). These studies usually include several clinical motor and nonmotor features, as well as different kinds of biomarkers (Obeso *et al.*, 2017). In a recent study (Fereshtehnejad *et al.*, 2017), criteria for categorizing newly diagnosed patients into various subtypes were developed using the extensive phenotypic

and biomarker data (i.e., neuroimaging, genetic, blood, and CSF biomarkers) available from the Parkinson's Progression Markers Initiative (PPMI) (Marek *et al.*, 2011). Three distinct subtypes, including the diffuse malignant, the intermediate, and the mild motor predominate, have been identified (Fereshtehnejad *et al.*, 2017). Diffuse malignant PD patients exhibit earlier onset, more severe motor and nonmotor symptoms, inadequate drug response, and rapid disease progression. Patients with mild motor predominate subtype had milder motor and nonmotor symptoms, slower development, younger onset age, and better treatment response. The intermediate subtype falls between the mild and malignant phenotypes in terms of its onset, clinical severity, and rate of progression. In contrast to patients with other subtypes, patients with the diffuse malignant subtype stand out for having a more pronounced striatal dopaminergic deficiency and the highest degree of caudate dopaminergic denervation. Further evidence for the prognostic significance of this subtype classification came from longitudinal clinical data and postmortem results in a separate PD cohort (De Pablo-Fernández *et al.*, 2019). When individuals are categorized this way, the mild motor-predominant form is the most common (49%-53%), followed by the intermediate form (35%-39%). The diffuse malignant form is the least common (9%-16%) (Fereshtehnejad *et al.*, 2017; De Pablo-Fernández *et al.*, 2019; Armstrong and Okun, 2020). Whether this subtyping is the best approach remains unclear, and individuals with PD are not routinely categorized in clinical practice. However, clinicians should recognize that there are diverse presentations of PD with implications for diagnosis, prognosis, and expected treatment response (Armstrong and Okun, 2020).

Despite controversies and differences in labels, the diffuse-malignant subtype, where "diffuse" denotes a broad pattern of nonmotor and motor traits and "malignant" denotes a bad prognosis overall, has been regularly reported as a subtype with a poor prognosis. This subtype is generally characterized by an older age at onset, dominant nonmotor manifestations, particularly in the cognitive domain, and a more rapid progression to dementia, the need for gait assistance, institutionalization, and death (de Lau *et al.*, 2014; Fereshtehnejad *et al.*, 2015, 2017; De Pablo-Fernández *et al.*, 2019). RBD, dysautonomia, and cognitive impairment are highly prevalent nonmotor symptoms in patients with the diffuse-malignant subtype from the disease's earliest stages. The AD-like CSF profile has also been linked to the diffuse-malignant subtype of PD (Fereshtehnejad *et al.*, 2017). Many patients diagnosed with DLB likely fall into this subtype, which shares similarities

with DLB. Patients with DLB usually had low CSF levels of amyloid, which reinforces the similarity with diffuse-malignant PD subtypes. According to the evidence of iRBD as a warning sign for severe clinical presentation in PD, many patients with idiopathic RBD develop this diffuse-malignant subtype of PD when they phenoconvert (Lin and Chen, 2018). As result, iRBD represents the strongest clinical hallmark of prodromal α-synucleinopathy and is linked to cognitive decline, severe autonomic dysfunction, rapid motor progression (especially in gait) and loss of independence, and mortality.

Although individuals can enormously differ in the onset and progression of motor and non-motor symptoms even during the prodromal phase (Berg *et al.*, 2021), subtyping in this phase has not been conducted systematically yet. Some features, such as RBD, early cognitive deficits, autonomic dysfunction, and genetic risk factors, are well-known and recognized as associated with faster progression (Fereshtehnejad *et al.*, 2015; Szwedo *et al.*, 2022) and a shorter life expectancy (De Pablo-Fernández *et al.*, 2019). However, identifying reliable prognostic markers since the prodromal phases for differentiating between different clinical evolutions over time represents still a challenge (Berg *et al.*, 2021).

1.4.2 Sources of phenotypic variability

Heterogeneity in the clinical expression of LBDs reflects differences in pathological spread as well as the dysfunction and possible failure of both neurochemical and structural neural networks within a complex interaction with fixed (e.g., genotype and sex) and modifiable (e.g., gender, education, occupation, and leisure activity) factors. Many of these factors are typically regarded as risk factors. Clinical phenotypes can be influenced by genetics; genetic variants for PD account for around 22% of the heritable risk of the disease, and a high polygenic risk score is linked to more severe motor and cognitive deterioration in PD patients (Paul *et al.*, 2018). Genetics can also moderate the impact of environmental factors including pesticide exposure, smoking, and head trauma, in addition to the direct effects of gene variants on disease. Prodromal and clinical subtypes could also be influenced by environmental factors. For instance, disparities in motor and cognitive reserve are related to education levels, with highly educated patients having greater baseline motor and cognitive performance than those with less education (Lee *et al.*, 2019). In this context, the concept of reserve wants to explain differences between individuals in susceptibility to age-related brain changes and pathology, such as that seen

in neurodegenerative diseases (Stern, 2013; Stern and Barulli, 2019; Stern *et al.*, 2020). The reserve has been suggested as a protective factor against both age-related and pathological cognitive decline (Drag and Bieliauskas, 2010). Individuals with a high reserve start with more resources and therefore require more time to reach the critical threshold to which the deficits linked to physiological aging or neurological diseases are clinically manifested (delay in the onset of clinical symptoms). Once the threshold has been reached, the decline is accelerated, since the patients have already reached a high level of pathology (Hall *et al.*, 2007; Van Loenhoud *et al.*, 2019). This reserve capacity is designed to reflect the resilience and plasticity of brain networks that shield people from the harmful impacts of aging and pathology or ultimately make up for them.

In addition, gender represents a crucial epidemiological variable influencing the clinical expression of neurodegenerative diseases. A mounting body of evidence supports the notion that sex and gender differences exist, from clinical symptoms to the risk of onset and conversion and response to pharmacological treatment (Picillo *et al.*, 2017; Cerri, Mus and Blandini, 2019; Ullah *et al.*, 2019; Ferretti *et al.*, 2020; Meoni, Macerollo and Moro, 2020). Studies on how sex/gender influences neurodegenerative processes related to α-synuclein pathology are now growing. The expression of neurodegenerative diseases differs depending on many genetic and hormonal factors as well as a range of broader social factors (e.g., role expectations and social attitudes). For instance, due to gender roles, inequalities can be seen in the types of education and occupation, behaviors, and activities. Thus, sex has a biological connotation that refers to the classification of human beings according to their sex chromosomal compliment, while gender finds its origin in social and cultural perspectives and refers to a person's psychosocial and cultural self-identification as being male or female (Ullah *et al.*, 2019).

In the next section, some relevant factors (pathological spread, genetics, and sex) that influence clinical phenotypes in LDBs will be described with a particular focus given to sex and gender differences as one of the main research goals of my thesis.

Variable spread of synucleinopathy

The study of phenotypes to identify subtypes is only a starting point for detection of biological differences underlying different subtypes. The heterogeneity of LBDs indicates that the underlying mechanisms must differ.

As anticipated above (**Paragraph 1.1**), the prodromal and clinical variability of PD may not be fully reflected by the Braak staging system. According to several research, the gut-brain hypothesis may need to be revised in order to explain exceptions to the Braak spreading pattern and why some patients develop dementia first (Kosaka, 2014). The Braak model has been supplemented by other alternatives (Borghammer, 2023). The inclusion of PD with and without dementia and DLB as three subgroups of LBD with varying pathological spread has been proposed (Kosaka, 2014). Another hypothesis proposes that stage 1 of all LBDs involves disease in the olfactory bulb, with stage 2 being either brainstem dominating spread or limbic-predominant spread (Adler *et al.*, 2019). The synuclein, origin, and connectome (SOC) model was recently proposed as a theoretical disease model to understand the pathogenesis of LBDs and may have greater explanatory power than previous models as it is well-matched with the two main profiles of α-synuclein pathology proven by postmortem studies (Borghammer, 2023). The SOC model predicts the brain-first and body-first clinical subtypes (**Figure 3**), integrating two aspects of α-synuclein pathology that influence the disease course for each patient: the anatomical location of the initial α-synuclein inclusion, and α-synuclein spread dependent on the ipsilateral connections that govern connectivity of the human brain (Borghammer, 2021). Brain-first subtype includes patients where pathology arises uni-focally in the olfactory bulb, and then spread to the anterior olfactory nucleus, and medial temporal structures and patients where the first pathology may appear in the amygdala itself, and then spread to the olfactory bulb. In these cases, the pathology reaches the substantia nigra quite rapidly due to mono-synaptic connections from the amygdala (Poulin *et al.*, 2018) and possibly also via direct connections from the olfactory bulb (Höglinger *et al.*, 2015). The prodromal phase is, therefore, relatively short, and the patients have few or no non-motor symptoms during the prodromal phase. From the amygdala and substantia nigra, the pathology then spreads caudally to the mid and lower brainstem structures, and eventually the enteric nervous system, parasympathetic, and sympathetic structures. Characteristic non-motor symptoms including constipation and RBD, therefore, most often appears after parkinsonism. On the other hand, in the body-first subtype, representing most patients, the first pathology appears in the enteric nervous system and then propagates via the vagus to the dorsal motor nucleus of the vagus, and via sympathetic connections to the coeliac or mesenteric ganglia, and then to the sympathetic

trunk and heart. Most patients develop autonomic symptoms including constipation and orthostatic hypotension, and RBD before parkinsonism appears. They almost universally develop severe sympathetic, cardiac denervation many years before diagnosis evidenced by [^{123}I]MIBG scintigraphies and the majority develop enlarged colon and delayed colonic transit time during the prodromal phase (Fedorova *et al.*, 2022). These non-motor manifestations are probably mainly caused by damaged neurons and neural circuitry located in the pons, medulla, and peripheral autonomic nervous system, i.e., caudal to the substantia nigra. The prodromal phase is probably longer in body-first patients.

It might seem rational that brain-first PD would predispose to rapid cognitive decline since the initial α-synuclein pathology appears inside the CNS. However, in contrast, the increased risk of cognitive decline and dementia groups with RBD, constipation, and orthostatic hypotension—all hallmarks of the body-first subtype. Moreover, the majority of DLB patients, perhaps around 70%, are considered to be body-first, since approximately 70% develop RBD years before diagnosis (van de Beek *et al.*, 2020). In contrast, only one-third of PD develops RBD before diagnosis pointing to body-first etiology (Högl, Stefani and Videnovic, 2018). The temporal profile of (pre-motor) RBD is a key clinical indicator of the body-first subtype. It is consistent with post-mortem data showing that the presence of RBD can not only reliably identify an a-synucleinopathy (Boeve *et al.*, 2013), but within PD can also identify those with higher synuclein burden on autopsy (Postuma *et al.*, 2015).

Yet unidentified variables may contribute to the variety in pathological spreading and require additional research since the variability in pathological spreading may reflect the heterogeneity in LBDs. Particularly, other pathologies that interact with the Lewy pathology, such amyloid- and tau-pathologies, may affect the clinical subtypes and progression patterns. The coexisting extracellular amyloid-β and intracellular tau deposition in PD represent risk factors for early progression to dementia and have been reported to increase the amount of limbic and neocortical α-synuclein pathology, such that the severity of α-synuclein and Alzheimer-pathologies are correlated (Toledo *et al.*, 2016; Smith *et al.*, 2019). The synergistic contribution influences progression routes and clinical phenotypes in LBDs (Raunio *et al.*, 2019). Although the frequent coexistence, α-synuclein and Alzheimer-pathologies also contribute independently to the clinical phenotype in DLB (Ferreira *et al.*, 2020). Amyloid-β pathology was the main predictor

of lower cognitive performance, whereas tau pathology was associated with a lower frequency of clinical features, such as parkinsonism and probable RBD (Ferreira *et al.*, 2020). Consistently, DLB clinical features have been associated with more widespread α-synuclein relative to tau at postmortem, whereas patients with both α-synuclein and tau extending to the neocortex exhibited a combination of DLB and Alzheimer's clinical features and a more rapid dementia trajectory (Ferman *et al.*, 2020). All in all, evidence highlights the clinical relevance of co-pathology since it is associated with faster time to dementia, decreased overall survival (Irwin and Hurtig, 2018), and contributes to specific cognitive and motor features in LBDs (Peavy *et al.*, 2016; Coughlin *et al.*, 2019, 2020; Ferman *et al.*, 2020; Ferreira *et al.*, 2020).

Genetic factors

According to genome-wide association studies (GWAS) and candidate gene association studies, intricate gene-environment interactions help to increase (or decrease) the risk for LBDs (Nussbaum, 2018). Although rare, mutations in SNCA, the gene encoding α-synuclein, have been unequivocally implicated in hereditary, autosomal dominant forms of PD, DLB, or neurodegenerative disease with parkinsonism (Nussbaum, 2018). A severe early-onset form of PD caused by specific mutations in the SNCA gene (deleterious point mutations and multiplications) is characterized by akinetic-rigid predominance, pyramidal indications, psychiatric symptoms, cognitive impairment, and a moderate response to levodopa. Leucine-rich repeat kinase 2 (LRRK2) gene missense mutations cause the most prevalent autosomal dominant form of parkinsonism. Carriers of the LRRK2 mutation are at an increased risk of developing PD from 28% at age 59 to 51% at age 69 and up to 74% at age 79 (Healy *et al.*, 2008). Although there is a reduced risk of cognitive dysfunction, the clinical symptoms associated with LRRK2 mutation are quite comparable to those of idiopathic PD (Thenganatt and Jankovic, 2014). In addition to PD caused by the SNCA and LRRK2 genes, there are the autosomal recessive forms of parkinsonism that include mutations in the parkin gene (PARK2), the phosphatase and tensin homologue–induced putative kinase 1 gene (PINK1), and the DJ1 gene. PARK2 and PINK1 cooperate to remove damaged mitochondria, whereas DJ1 preserves mitochondria from oxidative stress. These mutations are generally associated with early onset, a good response to levodopa and early development of dyskinesias, but not with early cognitive impairment. Mutations in PINK1 and DJ1 are not frequent (1% to 8% in

early-onset sporadic PD), whereas 50% of familial cases and about 15% of sporadic cases with early-onset PD have shown parkin mutations (Lücking *et al.*, 2000; Periquet *et al.*, 2003).

Numerically, the main genetic risk factor for developing PD is heterozygous mutations in the GBA gene, which codes for the enzyme glucocerebrosidase (Sidransky *et al.*, 2009). Due to the low frequency of GBA mutations, this gene was originally left out of GWAS analysis. The α-synuclein accumulation may be triggered by glycosylceramide5, and it may also result in glucocerebrosidase activity decline, in a vicious circle (Mazzulli *et al.*, 2011). Clinically, GBA-PD show an earlier onset and increased risk for cognitive deterioration than idiopathic PD. They are distinguished by an early cognitive decline that affects executive functions, abstraction and orientation domains, working and visual-short memories, memory, and visuospatial abilities (Balestrino and Schapira, 2018). Patients with GBA-PD appear to be especially susceptible to psychiatric symptoms, despite the conflicting results regarding depression, anxiety, and apathy (Balestrino and Schapira, 2018).

GBA mutations was found to be also associated with iRBD in both preclinical and PD populations (Gan-Or *et al.*, 2015). Specifically, carriers of GBA mutations showed a high risk of developing iRBD. Over the course of two years of follow-up, a longitudinal study showed that GBA mutation carriers develop RBD, depression, autonomic dysfunction, cognitive performance, and parkinsonian movement symptoms (Beavan *et al.*, 2015). In terms of subtypes, GBA mutations may be associated more with RBD-associated PD. Indeed, patients with PD who have GBA mutation (GBA-PD) and those with RBD-associated PD share several clinical symptoms, including faster motor worsening (Fereshtehnejad *et al.*, 2015), the PIGD phenotype (Postuma, Gagnon, Vendette and Montplaisir, 2009), cognitive decline and progression to dementia (Brockmann *et al.*, 2011). Consistent with the notion that GBA mutations are linked to a malignant phenotype, GBA is considered a strong genetic risk factor also for DLB. Patients with DLB have an eight-fold higher likelihood of carrying the GBA mutation than the general population (Nalls *et al.*, 2013). Additionally, DLB patients have a considerably higher risk of GBA mutation than PD patients (Sidransky *et al.*, 2009). GBA mutations in DLB has been linked to a clinical manifestation characterized by an earlier age of onset and a more severe disease progression (Outeiro *et al.*, 2019).

Sex and gender differences in LBDs

In LBDs, sex/gender differences are described not only in brain anatomy and function but also in pathogenesis, clinical features, and response to treatment. Many studies have been conducted in LBDs, especially in PD, providing evidence of links between sex/gender and risk for diagnosis, clinical manifestation, or mortality (Cerri, Mus and Blandini, 2019; Ullah *et al.*, 2019; Meoni, Macerollo and Moro, 2020; Chiu *et al.*, 2023).

The role of sex as a relevant factor in PD has been widely discussed in the past decade, demonstrating clear sex-related differences in epidemiological and clinical features of PD (Cerri, Mus and Blandini, 2019). PD has been found predominantly in men than in women by an approximate ratio of 2:1; therefore, male sex is considered a risk factor (Baldereschi *et al.*, 2000). Many observational studies have investigated the relationship between estrogen exposure and PD risk (Cerri, Mus and Blandini, 2019). Males and post-menopausal females seem to have a similar risk of developing PD because their levels of estrogen are lower than those of premenopausal females (Currie *et al.*, 2004). On the contrary, women with higher cumulative estrogen exposure over their lifetime have a significantly reduced PD risk (Gatto *et al.*, 2014). There is also evidence that parity (number of children), age at menopause, and duration of the fertile life span were all associated with a later age at onset of PD (Haaxma *et al.*, 2007). Moreover, some studies show how medical conditions leading to estrogen depletion (i.e. hysterectomy, oophorectomy), or short fertile life span, increase the risk of PD (Benedetti *et al.*, 2001), while later menopause and a longer fertile life span, increasing cumulative estrogen levels (Currie *et al.*, 2004), delay the age at onset. Several studies point toward a neuroprotective effect of estrogens on dopamine system and consequent reduction of risk for PD (Cereda *et al.*, 2013; Jurado-Coronel *et al.*, 2018). Women tend to be older than men at symptom onset, and this slightly delayed development of symptomatic PD can be explained by higher initial physiological striatal dopamine levels in women compared with men, possibly due to the action of estrogens (Haaxma *et al.*, 2007). This could explain the epidemiological observations of older age at onset and a lower prevalence of PD in women. Clinical phenotypes of PD have shown sex/gender differences, particularly in terms of the onset of symptoms, the nature of motor and non-motor symptoms, medication use, levodopa bioavailability, and quality of life (Cerri, Mus and Blandini, 2019). In comparison to males, PD women had a later onset of the disease and a more

benign motor phenotype, which may be because estrogens have a protective impact by increasing the availability of dopamine in synapses by lowering DAT activity (Haaxma *et al.*, 2007). Molecular neuroimaging studies have demonstrated higher striatal dopamine levels in women than males during the entire disease history (Haaxma *et al.*, 2007; Kaasinen *et al.*, 2015), despite the fact that few research have studied variations in imaging biomarkers. Regardless of body weight, women have a higher risk than males of getting levodopa-related motor problems (such as dyskinesia) when the condition worsens. This is possibly explained by the fact that women have lower levodopa clearance levels and higher levodopa bioavailability than men (Bjornestad *et al.*, 2016). Instead, females tend to experience more frequent and severe psychiatric symptoms, namely fatigue, feeling of nervousness, pain, anxiety, and depression (Martinez-Martin *et al.*, 2012). Conversely, the males are more likely to experience impulse control disorders in people with PD than the females (Cerri, Mus and Blandini, 2019). Regarding cognitive domains, males exhibit more severe executive and processing speed deficiencies than females, suggesting a major susceptibility to cognitive deterioration (Reekes *et al.*, 2020). Despite the increasing interest in different clinical PD subtypes, the impact of sex/gender is unknown leaving open a possible gender and subtype interaction leading to distinct vulnerabilities.

Sex/gender differences in LBDs are present since the early preclinical stage, namely iRBD. This preclinical condition is characterized by a high prevalence of males, up to 90% (Iranzo *et al.*, 2005; Postuma, Gagnon, Vendette and Montplaisir, 2009). However, increasing evidence has suggested that women with iRBD could be underdiagnosed because of less aggressive and violent REM sleep behaviors (Zhou *et al.*, 2015) and decreased polysomnography sensitivity in detecting iRBD women (Bodkin, 2019). Estrogens may have a role in these phenotypical differences modulating neurotransmission systems, with higher estrogen levels correlated with low noradrenergic activity, leading to reduced phasic REM activity (Schwartz and Roth, 2008). The proportion of women enrolled in the studies is recently growing, suggesting more understanding of women with RBD (Bodkin, 2019) and no gender differences in the likelihood of neurodegenerative disorder. Indeed, in one study of 93 patients with iRBD, the 12-year risk of progressing to a neurodegenerative disease was 52.4%, from the time of iRBD diagnosis, and it was similar in men and women (Postuma, Gagnon, Vendette,

Fantini, *et al.*, 2009). A more recent study demonstrated that symptoms were first recognized later in female iRBD patients than in males, but females showed elevated electromyogram activity during REM sleep and a similar deteriorated olfactory and cognitive function to male patients at the first medical consultation (Takeuchi, Sasai-Sakuma and Inoue, 2020). Moreover, the disease progression in female RBD patients was confirmed to be equivalent to that in male patients (Takeuchi, Sasai-Sakuma and Inoue, 2020).

Despite the relevance of sex/gender differences in LBDs, these have been long undervalued and understudied in DLB. The historical preclusion of the examination of sex/gender differences in DLB may be because the disease is more commonly diagnosed in men (Chiu *et al.*, 2023). However, recent multicenter collaborations now have large cohorts available for addressing potential sex/gender differences. These recent studies have shown higher proportions of men with RBD (Utsumi *et al.*, 2020) and parkinsonism (Utsumi *et al.*, 2020; Bayram *et al.*, 2021), but not in all cohorts (Bayram *et al.*, 2021), and higher (Van De Beek *et al.*, 2020; Chiu *et al.*, 2023) or similar (Bayram *et al.*, 2021) proportions of women with visual hallucinations. Moreover, the temporal sequence of the core features changes between men and women: men were more likely to have RBD and were diagnosed with probable DLB earlier than women, whereas visual hallucinations appeared late in men, differently than in women where they happened earlier and concurrently with fluctuations and parkinsonism (Choudhury *et al.*, 2022). In accordance with a more aggressive disease course and a more frequent AD co-pathology than men, women have shorter symptom duration before diagnosis, are older, and score lower on cognitive tests (Van De Beek *et al.*, 2020). According to a new postmortem investigation, sex influences the relationships between AD co-pathology and clinical phenotype in DLB patients. Both men and women demonstrated a decreased likelihood of the LB clinical phenotype in the context of severe AD co-pathology or high tau staging; however, women experienced greater dementia and cognitive decline (Bayram, Coughlin and Litvan, 2022). Notably, there is no study on sex/gender differences addressing changes in molecular neurotransmission that are strongly related to motor, cognitive, and psychiatric symptoms variably characterizing patients.

Clinical awareness of possible sex/gender differences in clinical presentation and biomarker status of LBDs will support more accurate and timely diagnoses, including at

prodromal stages. Additional research is needed to address the presented gaps in the current understanding of potential sex and gender differences in biomarkers and treatment responses in LBDs.

2. Aim of the work

This thesis aims to investigate the neurobiological mechanisms underlying different phenotypes and clinical trajectories in LBDs since the preclinical stages. The studies address this topic through molecular imaging biomarkers by applying different methodological approaches and different study designs. Multimodal brain molecular techniques are combined with connectivity and graph-theory measures, as well as, with clinical information, to assess *in vivo* pathology spreading and variability of network dysfunction in the whole LBDs spectrum. Specifically, the exploration of molecular connectivity allows a detailed *in vivo* evaluation of the dynamic neurobiological changes underlying neurodegeneration.

Moreover, a deep focus is given to sex/gender contribution to α-synuclein-related neurodegeneration process and phenotypes. The multi-factorial protocol integrates epidemiological (e.g., sex) and clinical data, with neuroimaging measures to better understand the main sources of variability in LBD.

The work is organized into three main lines of research: i) Imaging biomarkers for diagnosis and progression; ii) Brain metabolic connectivity to achieve novel insights into the pathophysiology of neurodegenerative diseases; iii) Sex and gender as crucial sources of phenotypic variability in LBD.

Section 1 includes three studies focusing on three main molecular biomarkers, widely implemented in LBDs clinical practice, namely [^{18}F]FDG-PET for the brain metabolism, [^{123}I]FP-CIT-SPECT for the presynaptic dopaminergic activity and [^{123}I]MIBG myocardial scintigraphy for the noradrenergic system. Both studies 1 and 2 investigated neurobiological changes in PD at an early stage. *Study 1* specifically addresses different clinical and dopaminergic longitudinal trajectories in PD patients with and without positive [^{123}I]FP-CIT SPECT, drawing conclusions concerning the SWEDD cases. *Study 2* represents a methodological study addressing the lack of standardized semi-automated methods to interpret [^{123}I]MIBG scintigraphy in clinical practice, despite its importance as a supportive biomarker for PD detection and differential diagnosis. *Study 3* used [^{18}F]FDG-PET imaging to assess the differences between EO DLB and LO DLB regarding brain hypometabolism, related neurotransmitter functional topography and brain metabolic connectivity.

Section 2 focuses on brain molecular connectivity as an emerging approach to deeply study the pathophysiology of neurodegenerative diseases, complementing the LBD knowledge acquired with univariate analyses on established biomarkers. *Study 4* is a review overviewing concepts and methods for molecular and metabolic connectivity encompassing evidence in neurodegenerative conditions, including the LBD spectrum. *Study 5* investigates shared and disease-specific changes in the large-scale networks across the LBDs, including iRBD, PD, and DLB groups, using a brain metabolic connectivity approach.

Section 3 assesses sex/gender differences in clinical phenotypes and endophenotypes (as measured by [^{18}F]FDG-PET and [^{123}I]FP-CIT SPECT) in PD and DLB patients, given sex/gender as a main source of variability. *Studies 6* and *7* focused on gender differences in dopaminergic activity and metabolic and molecular connectivity as well as clinical symptoms in PD patients with stable disease progression (*Study 6*) and patients with distinct clinical subtypes (*Study 7*). *Studies 8* and *9* address gender differences in the dementia stage (DLB), investigating the neurotransmission systems with [^{123}I]FP-CIT-SPECT (*Study 8*) or metabolic connectivity with [^{18}F]FDG-PET (*Study 9*).

Overall, the final goal is to clarify the heterogeneity of LBD neurodegenerative mechanisms using different molecular neuroimaging approaches within and between different disorders, which also is essential for prognostic considerations and the future development of personalized preventive and treatment strategies.

3. Results

Most of following data are published (Boccalini *et al.*, 2020, 2023; Carli *et al.*, 2021; Boccalini, Bortolin, *et al.*, 2022; Boccalini, Carli, Pilotto, *et al.*, 2022; Boccalini, Carli, Vanoli, *et al.*, 2022; Caminiti, Boccalini, *et al.*, 2023).

3.1 Imaging biomarkers for diagnosis and progression

3.1.1 Study 1: Distinctive clinical and imaging trajectories in SWEDD and Parkinson's disease patients (Boccalini, et al.) – submitted article

The aggregation of misfolded α-synuclein in PD causes synaptic dysfunction and neurodegeneration in the substantia nigra. [^{123}I]FP-CIT SPECT is commonly used in clinical settings to evaluate the integrity of presynaptic dopaminergic nerve terminals. However, a proportion of patients clinically diagnosed with PD can have normal scans (SWEDD), generating a controversial debate on the underlying biological mechanisms characterizing these subjects. *Study 1* investigated differences in clinical features, [^{123}I]FP-CIT binding, molecular connectivity, and clinical and imaging progression between SWEDD cases and patients with idiopathic PD, as compared to healthy controls (HC).

Data used in this study were obtained in September 2021 from the PPMI database (www.ppmi-info.org/data), an international, multiple-site, prospective, longitudinal cohort study. The aims and methodology of PPMI are published elsewhere (Marek *et al.*, 2011, 2018). Study protocols and manuals are available online at www.ppmi-info.org/study-design. The institutional review board approved the study at each site, and the participants provided written informed consent. We included 49 SWEDD patients from the PPMI who underwent baseline [^{123}I]FP-CIT SPECT imaging and T1-weighted MRI within one year. SWEDD subjects have no evidence of dopaminergic deficit in presynaptic dopaminergic scans and no expectation of PD medication within six months from baseline. The visual interpretation for normality was determined by the imaging core of PPMI and was informed to the referring physician. We randomly selected 49 de novo idiopathic PD (iPD) and 49 HC with baseline [^{123}I]FP-CIT SPECT imaging and T1-weighted MRI within one year, for comparison. PD patients were drug naïve and subjects with verified genetic mutations known to cause PD (GBA, LRRK2) have been excluded. For all SWEDD and iPD subjects, we collected baseline clinical data from the PPMI database

(Marek *et al.*, 2011, 2018). 38 SWEDD and 40 iPD patients underwent clinical assessment at 2 years follow-up and for 36 SWEDD and 39 iPD of them [^{123}I]FP-CIT SPECT scans at 2 years follow-up were also available.

After semiquantitative single-subject analysis, 13 SWEDD showed significant striatal dopaminergic depletion and were excluded for further analyses. Thus, the final SWEDD group includes 36 cases. Of these 27 subjects had a clinical follow-up and 26 an imaging follow-up.

Clinical and demographic features in SWEDD and PD groups at baseline and follow-up are reported in **Tables 1** and **2**, respectively, and **Figure 6**. [^{123}I]FP-CIT imaging results are reported in **Figures 7** and **Table 3**. Our sample included a limited proportion of subjects on antidepressant medication (SSRI/SNRI) (12.2%), equally distributed among PD, SWEDD, and HC (p = 0.807).

Table 1. Demographic and clinical features of the sample of Study 1 at baseline

	iPD	Swedd	p-values
Demographics features			
Age	65 (7.3)	61.8 (9.28)	0.11
Education	16 (2.6)	14.4 (3.87)	0.09
Sex (Female, %)	19 (38.8%)	13 (36.1%)	0.98
Clinical non-motor assessment			
MoCA	26.6 (2.11)	26.6 (2.60)	0.96
REM Sleep Disorder Questionnaire	4.78 (3.15)	4.91 (3.13)	0.84
Epworth Sleepiness Scale	5.65 (3.08)	8.57 (4.27)	**0.001**
Scopa-AUT	13.4 (9.33)	16.7 (12.1)	0.18
MDS-UPDRS I	5.12 (4.13)	8.22 (6.30)	**0.013**
UPSIT	22.7 (8.00)	29.2 (8.05)	**<0.001**
Motor assessment			
Hoehn and Yahr Staging	1.51 (0.51)	1.42 (0.50)	0.4
MDS-UPDRS II	4.78 (2.73)	6.83 (6.33)	0.07
MDS-UPDRS III	18.5 (6.87)	15.1 (9.11)	0.06
MDS-UPDRS total score	28.4 (9.91)	30.2 (17.3)	0.59
Motor Subtype:			0.84
Postural and Instability Gait Disorder Dominant, PIGD	5 (10.2%)	4 (11.1%)	
Tremor Dominant, TD	38 (77.6%)	29 (80.6%)	
Intermediate type, IT	6 (12.2%)	3 (8.3%)	
Neurobehavioral assessment			
GDS	5.20 (1.32)	5.60 (1.79)	0.27
QUIP	0.27 (0.57)	1.64 (1.13)	**<0.001**
STAI-total score	94.3 (7.71)	92.3 (6.67)	0.19
STAI-state score	47.8 (4.67)	46.5 (4.50)	0.24
STAI-trait score	46.6 (4.07)	45.7 (4.31)	0.35
Cognitive assessment			
Benton Judgment of Line Orientation	11.6 (3.37)	12.5 (3.00)	0.22
Letter number sequencing	11.1 (2.40)	9.89 (2.72)	0.034
HVLT total immediate recall t- score	45.4 (12.3)	44.4 (10.4)	0.67
HVLT delayed recall t-score	42.0 (13.3)	41.8 (12.4)	0.95
HVLT recognition t-score	42.4 (14.1)	36.9 (13.8)	0.08
Semantic Fluency t-score	50.4 (9.32)	47.9 (10.4)	0.26

Results are reported as mean values and standard deviations (SD, in parentheses).
Abbreviations: Swedd, scans without evidence for dopaminergic deficit; iPD, idiopathic Parkinson's disease; SD, standard deviation; y, years; MoCA, Montreal Cognitive Assessment; UPSIT, Smell identification test; MDS-UPDRS, Movement Disorders Society-Unified Parkinson's Disease Rating Scale; GDS, Geriatric Depression Scale; QUIP, Questionnaire for Impulsive-Compulsive Disorders in Parkinson's Disease–Rating Scale; STAI, State-Trait Anxiety Inventory; HVLT, Hopkins Verbal Learning Test.
Significant p-values are reported in bold.

Baseline clinical differences – PD and SWEDD patients did not significantly differ in motor impairments or subtypes (**Table 1** and **Figure 6**). PD patients presented significantly worse smell impairment as measured by UPSIT than SWEDD ($p<0.001$). SWEDD patients presented higher MDS-UPDRS part I scores, indicating more, even if mild, nonmotor deficits of daily living compared to PD. PD and SWEDD significantly differed in the Epworth Sleepiness Scale and in QUIP (measuring impulsive-compulsive behaviors), but both groups presented average scores within normal values.

Table 2. Clinical features of the sample of Study 1 at 2 years follow-up

	iPD at BL	**iPD at FU**	**p-value *paired t-test in iPD***	**Swedd at BL**	**Swedd at FU**	**p-value *paired t-test in Swedd***	**p-value *t-test between Swedd vs iPD at FU***
Clinical non-motor assessment							
MoCA	26.6 (2.11)	25.6 (3.54)	0.059	26.6 (2.60)	26.0 (2.48)	0.164	0.566
REM Sleep Disorder Questionnaire	4.78 (3.15)	5.47 (3.86)	0.343	4.91 (3.13)	4.59 (3.00)	0.242	0.298
Epworth Sleepiness Scale	5.65 (3.08)	6.15 (3.06)	0.415	8.57 (4.27)	7.74 (4.52)	0.532	0.118
Scopa-AUT	13.4 (9.33)	16.2 (8.39)	0.063	16.7 (12.1)	17.3 (10.9)	0.988	0.678
MDS-UPDRS I	5.12 (4.13)	6.97 (4.94)	**0.001**	8.22 (6.30)	9.11 (5.82)	0.264	0.124
Motor assessment							
Hoehn and Yahr Staging	1.51 (0.51)	1.77 (0.42)	**0.023**	1.42 (0.50)	1.00 (1.00)	**0.030**	**<0.001**
MDS-UPDRS II	4.78 (2.73)	7.10 (4.28)	**<0.001**	6.83 (6.33)	8.59 (7.29)	0.064	0.344
MDS-UPDRS III	18.5 (6.87)	24.3 (10.7)	**<0.001**	15.1 (9.11)	14.4 (11.1)	0.771	**<0.001**
MDS-UPDRS total score	28.4 (9.91)	38.4 (14.9)	**<0.001**	30.2 (17.3)	45.6 (31.8)	**0.001**	0.279
Neurobehavioral assessment							
GDS	5.20 (1.32)	5.70 (1.77)	0.158	5.60 (1.79)	5.59 (1.76)	0.826	0.808
QUIP	0.27 (0.57)	1.52 (1.01)	**<0.001**	1.64 (1.13)	2.00 (2.30)	0.386	0.321
STAI-total score	94.3 (7.71)	93.0 (5.33)	0.345	92.3 (6.67)	91.2 (8.97)	0.865	0.360
STAI-state score	47.8 (4.67)	47.0 (3.94)	0.612	46.5 (4.50)	45.9 (6.92)	0.807	0.449
STAI-trait score	46.6 (4.07)	46.0 (3.18)	0.291	45.7 (4.31)	45.4 (3.79)	0.987	0.464
Cognitive assessment							
Benton Judgment of Line Orientation	11.6 (3.37)	11.6 (2.99)	0.851	12.5 (3.00)	11.6 (3.03)	**0.036**	0.979
Letter number sequencing	11.1 (2.40)	11.3 (3.28)	0.607	9.89 (2.72)	10.7 (3.20)	0.705	0.443

HVLT total immediate recall t-score	45.4 (12.3)	41.7 (10.2)	0.084	44.4 (10.4)	43.2 (12.4)	0.106	0.615
HVLT delayed recall t-score	42.0 (13.3)	41.2 (13.2)	0.881	41.8 (12.4)	39.4 (13.8)	**0.043**	0.605
HVLT recognition t-score	42.4 (14.1)	45.0 (12.5)	0.881	36.9 (13.8)	45.2 (9.88)	**0.003**	0.950
Semantic Fluency t-score	50.4 (9.32)	49.6 (11.0)	0.347	47.9 (10.4)	50.2 (9.10)	0.415	0.810

Results are reported as mean values and standard deviations (SD, in parentheses).

Abbreviations: Swedd, scans without evidence for dopaminergic deficit; iPD, idiopathic Parkinson's disease; BL, baseline; FU, follow-up; y, years; MoCA, Montreal Cognitive Assessment; UPSIT, Smell identification test; MDS-UPDRS, Movement Disorders Society-Unified Parkinson's Disease Rating Scale; GDS, Geriatric Depression Scale; QUIP, Questionnaire for Impulsive-Compulsive Disorders in Parkinson's Disease–Rating Scale; STAI, State-Trait Anxiety Inventory; HVLT, Hopkins Verbal Learning Test.

Significant p-values are reported in bold.

Follow-up clinical differences – PD and SWEDD patients significantly differed in the motor assessment, with PD showing higher Hoehn and Yahr stages and MDS-UPDRS part III scores compared to SWEDD (**Table 2**). Paired t-test results showed a worsening from baseline to follow-up in all motor scales and QUIP (**Table 2**). SWEDD patients presented a worsening in memory (HVLT), and visuospatial skills (JOLO) at 2 year-follow-up. Moreover, MDS-UPDRS total score increased for SWEDD and PD. Linear mixed effect models indicated that PD group showed a significantly faster decline over time on MDS-UPDRS part III ($p<0.001$) and MDS-UPDRS total score ($p=0.04$) compared to SWEDDs (**Figure 6**).

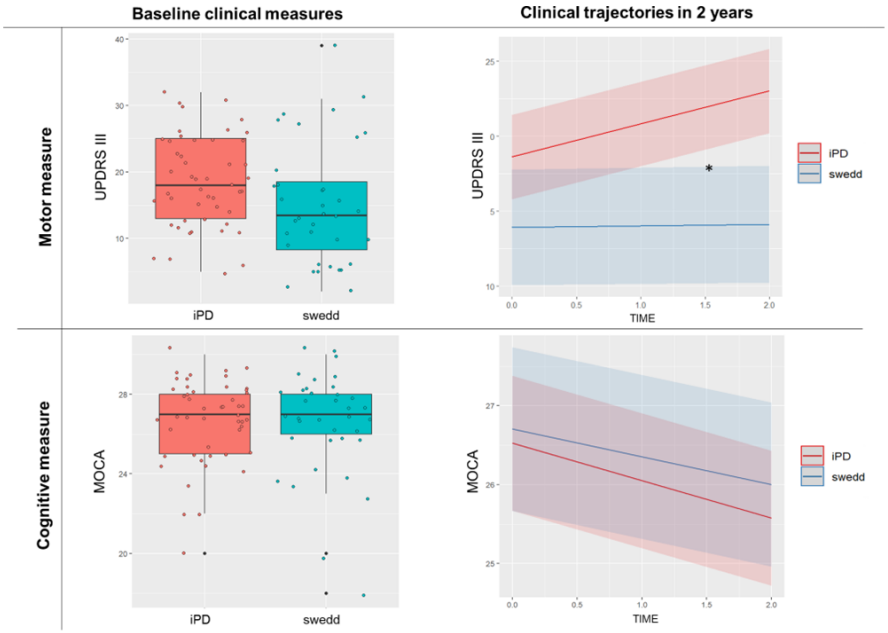

Figure 6. Motor and cognitive baseline differences and clinical trajectories over time. *Boxplots in the left column show the motor (UPDRS III) and cognitive (MOCA) scores' distribution in HC, iPD, and SWEDD groups at baseline. Both SWEDD and iPD significantly differ in motor and cognitive performance from HC, but they do not differ from each other at baseline. The right column shows the longitudinal linear mixed models results for UPDRIII and MOCA scores. iPD declines faster than SWEDD, instead remains stable, in the motor symptoms. No differences are found in the cognitive trajectories.*

Baseline [^{123}I]FP-CIT SPECT imaging differences – ROI-based results showed more significant SBR decreases for PD patients than SWEDD in several striatal (ventral striatum, dorsal caudate, and dorsal putamen) and extrastriatal (amygdala, hippocampus, parahippocampus, insula) ROIs within the nigrostriatal and mesocorticolimbic dopaminergic systems (**Table 3**). SWEDD showed lower binding than PD only in the ACC as shown by ROI-based results (**Table 3**). Voxel-wise analysis did not find any difference between SWEDD and HC, whereas PD exhibited lower binding in the striatal and limbic extrastriatal regions in comparison with HC (**Figure 7A**) and SWEDD (**Figure 7B**). Notably, at variance with voxel-wise analyses, ROI-based results showed lower SBR in SWEDD patients compared to HC in striatal regions, insula, hippocampus, and olfactory cortex, without reaching the same severity of PD.

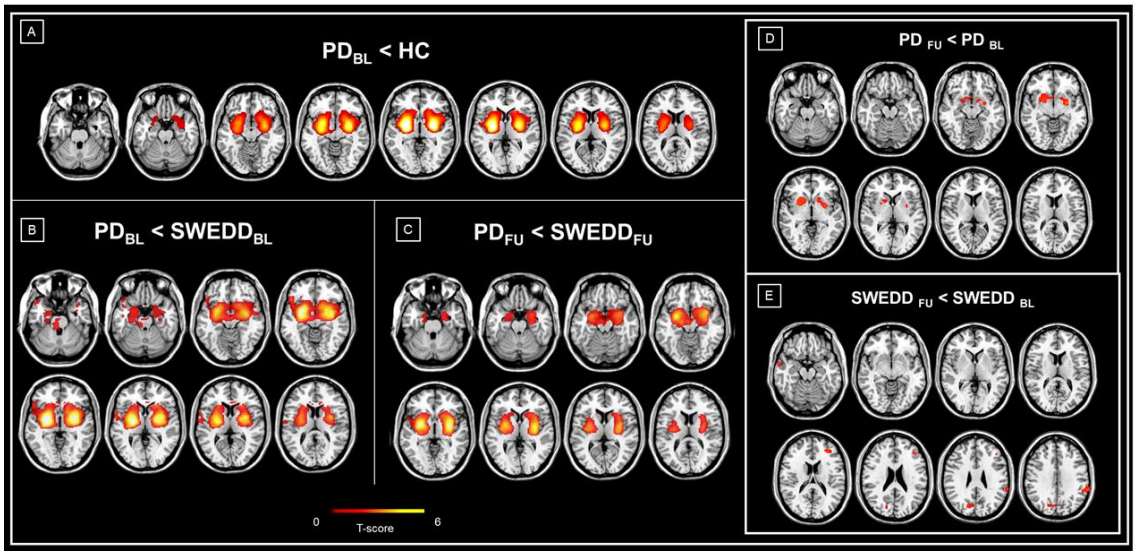

Figure 7. Voxel-wise differences in [^{123}I]FP-CIT binding. *Panels A shows the distribution of voxel-wise differences in [^{123}I]FP-CIT SBR for PD resulting from statistical comparison with HC. Of note, no voxel survived in comparison between SWEDD vs. HC. Panel B shows the results from the direct voxel-wise comparison between SWEDD and PD patients at baseline. Panel C shows the distribution of voxel-wise differences in [^{123}I]FP-CIT SBR between PD and SWEDD groups at follow-up. Panels D and E show the results from the direct voxel-wise paired t-test between scans at follow-up and baseline in PD (D) and SWEDD (E) groups. The magnitude of the difference is reported by means of t-score. Abbreviations: PD, Parkinson's disease; SWEDD, scans without evidence of dopaminergic deficit; HC, healthy controls.*

Table 3. Regional analysis of [^{123}I]FP-CIT-SPECT imaging bindings in SWEDD and iPD patients at baseline and 2 years follow-up

	iPD at BL	**iPD at FU**	**p-value *paired t-test in iPD***	**Swedd at BL**	**Swedd at FU**	**p-value *paired t-test in Swedd***	**p-value *t-test Swedd vs iPD at BL***	**p-value *t-test Swedd vs iPD at FU***
Left dorsal caudate	1.34 (0.43)	1.01 (0.44)	**<0.001**	1.59 (0.55)	1.69 (0.58)	0.416	0.065	**<0.001**
Right dorsal caudate	1.44 (0.45)	1.15 (0.47)	**<0.001**	1.77 (0.70)	1.72 (0.61)	0.509	0.022	**<0.001**
Left dorsal putamen	1.34 (0.48)	0.98 (0.37)	**<0.001**	2.33 (0.73)	2.29 (0.55)	0.874	<0.001	**<0.001**
Right dorsal putamen	1.33 (0.49)	1.03 (0.44)	**<0.001**	2.25 (0.74)	2.34 (0.50)	0.771	<0.001	**<0.001**
Left ventral striatum	1.16 (0.44)	0.85 (0.36)	**<0.001**	1.52 (0.54)	1.60 (0.59)	0.382	<0.001	**<0.001**
Right ventral striatum	1.22 (0.47)	0.87 (0.37)	**<0.001**	1.50 (0.59)	1.63 (0.60)	0.118	0.017	**<0.001**
Left amygdala	0.31 (0.16)	0.33 (0.17)	0.308	0.56 (0.48)	0.48 (0.19)	0.383	<0.001	**0.003**
Right amygdala	0.36 (0.20)	0.29 (0.16)	0.173	0.53 (0.50)	0.49 (0.19)	0.680	0.041	**<0.001**
Left hippocampus	0.29 (0.11)	0.29 (0.10)	0.900	0.47 (0.35)	0.41 (0.12)	0.441	0.003	**<0.001**
Right hippocampus	0.30 (0.12)	0.29 (0.12)	0.854	0.46 (0.33)	0.41 (0.14)	0.550	0.010	**<0.001**
Left parahippocampus	0.16 (0.10)	0.17 (0.11)	0.324	0.34 (0.45)	0.25 (0.10)	0.312	0.026	**0.013**
Right parahippocampus	0.17 (0.12)	0.15 (0.12)	0.195	0.31 (0.50)	0.24 (0.11)	0.375	0.126	**0.003**
Left insula	0.36 (0.14)	0.29 (0.13)	**<0.001**	0.47 (0.21)	0.50 (0.21)	0.098	0.057	**<0.001**
Right insula	0.34 (0.11)	0.29 (0.10)	**0.013**	0.45 (0.16)	0.48 (0.19)	0.542	0.010	**<0.001**
Left olfactory cortex	0.38 (0.22)	0.31 (0.24)	0.084	0.48 (0.24)	0.47 (0.30)	0.749	0.106	**0.022**

Right olfactory cortex	0.39 (0.24)	0.30 (0.23)	**0.007**	0.48 (0.28)	0.44 (0.27)	0.924	0.165	**0.027**
Left anterior cingulate	0.21 (0.10)	0.17 (0.11)	**0.035**	0.18 (0.15)	0.18 (0.12)	0.613	0.316	0.657
Right anterior cingulate	0.22 (0.10)	0.18 (0.11)	**0.007**	0.17 (0.14)	0.20 (0.13)	0.112	0.034	0.492
Left middle cingulate	0.25 (0.12)	0.21 (0.12)	0.054	0.28 (0.11)	0.29 (0.13)	0.235	0.436	**0.012**
Right middle cingulate	0.25 (0.12)	0.23 (0.12)	0.293	0.29 (0.12)	0.30 (0.15)	0.666	0.224	**0.014**
Left postcentral gyrus	0.07 (0.07)	0.04 (0.06)	0.098	0.05 (0.06)	0.05 (0.06)	0.396	0.568	0.505
Right postcentral gyrus	0.06 (0.05)	0.05 (0.07)	0.438	0.06 (0.07)	0.06 (0.07)	0.432	0.982	0.927
Right precentral gyrus	0.16 (0.12)	0.15 (0.12)	0.561	0.17 (0.12)	0.16 (0.11)	0.941	0.623	0.767
Left precentral gyrus	0.15 (0.11)	0.14 (0.11)	0.733	0.16 (0.10)	0.16 (0.11)	0.487	0.743	0.588

Results are reported as mean values and standard deviations (SD, in parentheses).

Abbreviations: Swedd, scans without evidence for dopaminergic deficit; iPD, idiopathic Parkinson's disease; BL, baseline; FU, follow-up.

Significant p-values are reported in bold.

Follow-up [^{123}I]FP-CIT SPECT imaging differences – PD patients showed lower SBR than SWEDD in all striatal and many extrastriatal ROIs, namely the amygdala, insula, hippocampus, parahippocampus, olfactory cortex, and middle cingulate (**Table 3**). These differences were confirmed in voxel-wise analysis (**Figure 7C**). No SBR decreases were observed over time in any ROIs for SWEDD patients, whereas SBR significantly decreased for PD at follow-up in the striatum, insula, and right olfactory cortex (**Table 3**, **Figure 7D** and **7E**). Linear mixed effect models indicated that the PD group showed a faster decline over time in striatal dopaminergic denervation in all ROIs ($p<0.05$) compared to SWEDDs.

Neurotransmitter mapping - Extrastriatal mapping of [^{123}I]FP-CIT binding alterations in other monoaminergic systems was assessed. We observed a significant spatial correlation between DAT and SERT alterations ($p < 0.001$) for PD compared to HC (z-scores). However, we found only a trend for significance in the correlation between ^{123}I-FP- CIT alterations and serotonergic map in SWEDD ($p = 0.059$). **Figure 8** shows Fisher's z-transformed correlation coefficients with respective neurotransmitter maps for each subject (individual points) and contrast.

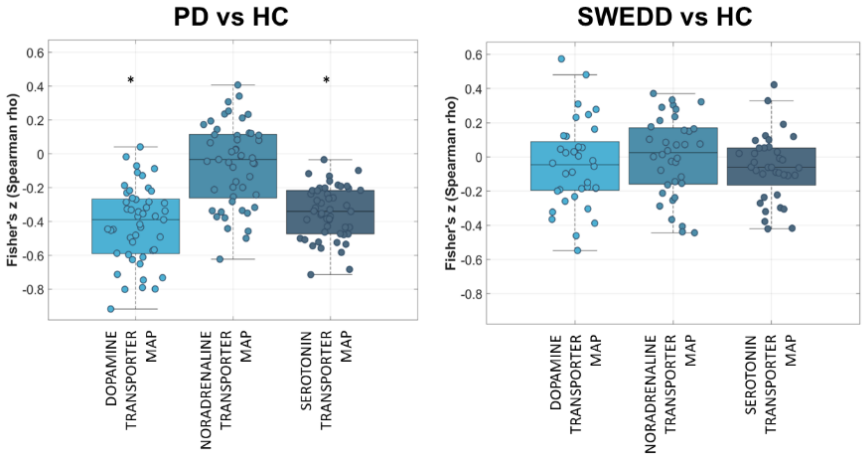

Figure 8. Results of spatial correlation analysis with neurotransmitter maps for PD and SWEDD. *Fisher's z-transformed correlation coefficients with respective neurotransmitter maps are displayed for each subject and contrast. [^{123}I]FP-CIT binding alterations in PD but not in SWEDD as compared to controls are significantly associated with the topographies of DAT and SERT. Error bars represent the parametric 95% confidence interval of the mean. Exact permutation-based p values (1000 permutations) were computed for all analyses: * indicates p values < 0.001. See text for details. Abbreviations: PD, Parkinson's disease; SWEDD, scans without evidence of dopaminergic deficits; HC, healthy controls.*

Nigrostriatal dopaminergic connectivity – Several connectivity alterations affected both SWEDD and PD nigrostriatal system, with 12.5% of altered connections for both groups compared to HC. However, these were characterized by different connectivity patterns (**Figure 9**). PD connectivity pattern showed only short-distance local subcortical alterations within the striatum. SWEDD patients also showed short-distance cortical

alterations between the precentral and postcentral gyri, specifically connectivity increases characterizing ipsilateral regions and connectivity decreases contralateral ones.

Mesolimbic dopaminergic connectivity – SWEDD and PD patients showed 15.2% and 6.2% altered connections, respectively, compared to HC (**Figure 9**). 64.7% of the altered connections in SWEDD were represented by increases compared to HC, whereas in PD most of the alterations (71.5%) were represented by decreased in connectivity. For SWEDD, the alterations involved many extrastriatal regions, mostly insula, hippocampus, and amygdala as well as the right olfactory cortex. For PD, we observed altered connectivity between ventral striatum and insula, between insula and hippocampus, in addition to ACC and MCC. Interestingly, SWEDD showed more connectivity alterations compared to PD ($\chi 2 = 4.30$, $p = 0.03$).

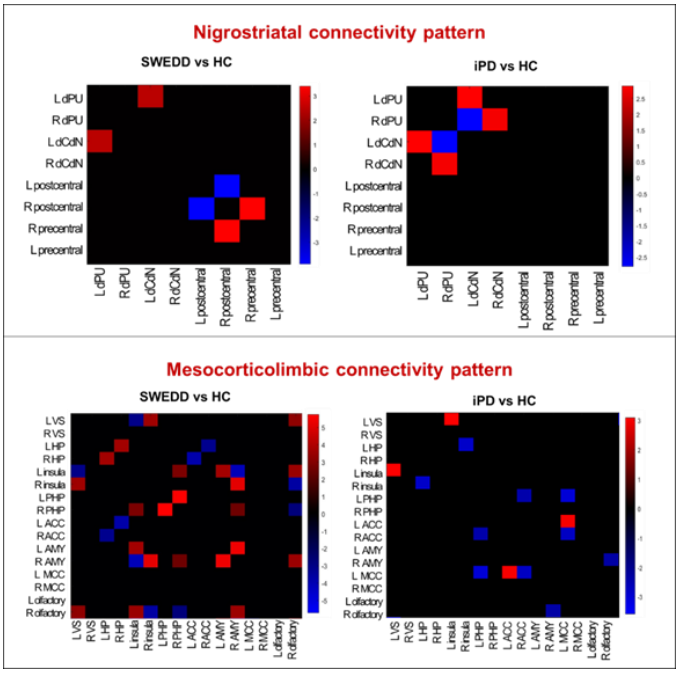

Figure 9. Dopaminergic connectivity results in SWEDD and iPD groups. *The matrices represent the significant differences obtained when comparing partial correlation coefficients between SWEDD vs HC, and iPD vs HC in the dopaminergic networks. The color bar displays the Z scores' values to compare partial correlation coefficients' strengths. Altered connections are presented: in red, the increased and in blue, the decreased connections compared with HC. Abbreviations: iPD, idiopathic Parkinson's disease; SWEDD, scans without evidence of dopaminergic deficits; HC, healthy controls; L, left; R, right; dCdN, dorsal caudate nucleus;*

dPU, dorsal putamen, VS, ventral striatum, HIP, hippocampus; PHP, parahippocampus; AMY, amygdala; ACC, anterior cingulate cortex, MCC, middle cingulate cortex.

To sum up, *Study 1* confirmed that SWEDD cases showed significantly less amount of striatal and extrastriatal presynaptic dopaminergic depletion than PD at the same symptoms' severity. Longitudinal imaging results further supported that the majority of SWEDDs were unlikely to have PD since they did not worsen in motor symptoms and neither in striatal nor extrastriatal dopaminergic depletion in 2 years. On the other hand, for the first time, we found extensive altered connectivity in dopaminergic systems, however with different patterns in PD and SWEDD. The latter group was characterized by more severe extrastriatal cortical connectivity derangement. When we map the [^{123}I]FP-CIT binding alterations with monoaminergic neurotransmitter topography in the two groups, we found significant spatial associations with dopaminergic and serotonergic systems only in PD, and a trend with the serotonergic one in SWEDD. In conclusion, [^{123}I]FP-CIT SPECT imaging reliably revealed iPD deficits and progression. The limited dopaminergic impairment observed in SWEDD, stable at follow-up, confirms that SWEDD subjects suffer from different conditions other than iPD. The presence of cortical and extrastriatal alterations in [^{123}I]FP-CIT binding might suggest other possible neurotransmission abnormalities contributing to SWEDD symptomatology.

3.1.2 Study 2: Manual and semi-automated approaches to MIBG myocardial scintigraphy in patients with Parkinson's disease (Boccalini, Carli*, et al., 2022) – Published article*

The denervation of the autonomic nervous system can be assessed by [^{123}I]MIBG cardiac scintigraphy, which measures the postganglionic presynaptic cardiac sympathetic nerve endings of the noradrenergic nervous system. In PD, cardiac [^{123}I]MIBG scintigraphy showed reduced cardiac uptake in most patients, representing a sensitive tool for clinical and differential diagnosis. The most used quantitative measurements of [^{123}I]MIBG uptake are the heart-to-mediastinum (H/M) ratios calculated from early (15 min) and late (3–4 h) [^{123}I]MIBG static planar images. The method used to obtain these parameters is mainly based on manually drawing cardiac regions of interest (ROIs). However, the position and size of the cardiac ROI, as well as the level of experience in drawing the

ROIs on the planar [^{123}I]MIBG images, might affect the final H/M ratio measures. *Study 2* aimed to compare two different methods of assessing the H/M ratios in a series of PD patients, (i) the typical manual-drawing method and (ii) the fixed-size ROIs approach following Veltman's guidelines for the standardisation of [^{123}I]MIBG parameters. Veltman et al. (Veltman *et al.*, 2012) demonstrated good reproducibility of fixed-size mediastinal and cardiac ROIs in assessing H/M ratios in patients with heart failure; in this study, we wanted to extend these findings to PD. The guidelines for the semi-automated method applied (Veltman *et al.*, 2012) are shown in **Figure 10**. [^{123}I]MIBG images of 35 PD patients were analysed by highly expert, moderate-expert, and inexpert raters. We evaluated the influences of cardiac ROI size and position and the impact of raters' experience on assessing the H/M ratios.

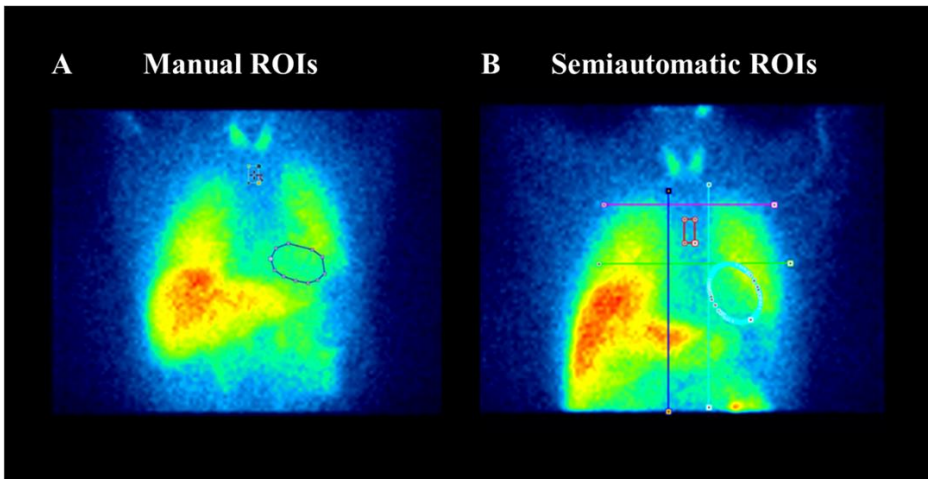

Figure 10. Manual and fixed-size regions of interest (ROIs) on planar 123I-metaiodobenzylguanidine (MIBG) images (Open Access Source). *Panel (A) depicts the manual ROIs method. A rectangular mediastinal ROI is used with unspecified size and located on planar MIBG images below the thyroid. The manual-drawn cardiac ROI is polygonal and includes the myocardium and the left ventricular cavity. Panel (B) represents the semi-automatic ROIs method. An "anatomical landmark square" is formed by the lung apexes (upper square border), the upper cardiac border (lower square border), and the medial contours of the lungs (medial square borders) to place fixed-size mediastinum and oval cardiac ROIs. Precisely, a fixed-size rectangular mediastinal ROI (13 × 20 pixel) and an oval cardiac ROI are placed on MIBG planar images. The mediastinal ROI is placed in the half of the "anatomical landmark square" formed by lungs apexes, the upper cardiac border, and the medial contours of the lung. The cardiac oval ROI (60 × 70 pixel) is placed in the lower-right quadrant, over the myocardium, including the*

left ventricular cavity. The figure is from (Boccalini, Carli, Vanoli, *et al.*, 2022) *in accordance to the fair use principle.*

A total of 35 PD patients [63.66 ± 9.74 years of age, 27 (77%) men] were included in the study. **Table 4** reported the number of PD patients that fell into the category of "pathological sympathetic innervation," according to the cut-off value of early and late H/M ratios, obtained with manual approach and semi-automatic approach for the three raters.

Table 4. Inter and intra-rater indices on MIBG parameters in Study 2

	Early H/M ratio		**Delayed H/M ratio**	
	manual method	semiautomatic method	manual method	semiautomatic method
Inter-raters analysis				
Continue values				
Expert (1)	1.49±0.27	1.59±0.27	1.41±0.37	1.51±0.35
Moderate-expert (2)	1.54±0.28	1.53±0.26	1.46±0.35	1.44±0.33
Inexpert (3)	1.65±0.32	1.62±0.28	1.56±0.40	1.51±0.36
ICC (95% CI)	0.94 (0.80-0.97)	0.95 (0.90-0.97)	0.95 (0.89-0.97)	0.97 (0.95-0.98)
Categorical values (n pathological /35)				
Expert (1)	32	28	24	20
Moderate-expert (2)	31	31	24	26
Inexpert (3)	26	28	20	23
Fleiss Kappa (95% CI)	0.45 (0.44-0.46)	0.78 (0.78-0.79)	0.69 (0.69-0.71)	0.78 (0.78-0.79)
Cohen Kappa 1-2	0.63	0.76	0.66	0.68
Cohen Kappa 1-3	0.29	0.90	0.69	0.87
Cohen Kappa 2-3	0.54	0.68	0.75	0.79
Intra-rater analysis				
Spearman Coefficient 1	p= 0.92, *p*=0.000		p= 0.92, *p*=0.000	
Spearman Coefficient 2	p= 0.86, *p*=0.000		p= 0.93, *p*=0.000	
Spearman Coefficient 3	p= 0.91, *p*=0.000		p= 0.91, *p*=0.000	

The inter-rater agreement results - The raters showed excellent reliability measured by intraclass correlation coefficient (ICC) in both methods (i.e., manual and semi-automatic) (**Table 4**). Of note, the agreement among raters tends to be higher in the semi-automatic procedure (ICC = 0.95 and ICC = 0.97, early and delayed H/M ratio, respectively) compared to the manual one (ICC = 0.94 and ICC = 0.95, early and delayed H/M ratio, respectively) (**Table 4**). Fleiss' kappa showed moderate agreement in the raters' classification of normal and pathological scores regarding early H/M ratio values (κ = 0.45, $p < 0.0005$) by using the manual method. Instead, the agreement was good when the early H/M ratio was obtained with the semi-automatic method ($\kappa = 0.78$). Similarly, the late H/M ratios showed increased raters' compliance moving from manual ($\kappa = 0.69$) to semi-automatic approaches ($\kappa = 0.78$). Of note, with the semi-automatic method, fewer PD patients fell under the category "non-pathological" for the inexpert and the moderate-expert raters (**Table 4**), with a more significant agreement among raters (**Table 4**). Specifically, the chi-square test found significant differences between the proportion of subjects classified as pathological or not by expert versus inexpert raters and moderate expert versus inexpert raters ($p < 0.05$) only with the manual method. The differences were not significant between raters when they applied the semi-automatic method ($p > 0.05$). Cohen Kappa values revealed that applying a semi-automatic method instead of the manual one leads to an improvement in agreement, especially between expert and inexpert raters; the agreement moved from 0.29 (fair, in early H/M ratios) and 0.69 (substantial, in late H/M ratios) to 0.90 (perfect, in early H/M ratios) and 0.87 (perfect, late H/M ratios).

The intra-rater agreement results - The Spearman correlation analysis showed a robust intra-rater agreement in the assessment of early and delayed H/M values (Spearman Coefficient > 0.80, $p < 0.001$).

In conclusion, the use of the semi-automatic method improves the agreement among raters in classifying' H/M ratios as pathological or non-pathological, namely for inexpert readers. These results may have important implications for semi-quantitative assessment of [^{123}I]MIBG images in clinical routine.

3.1.3 <u>Study 3</u>: Mapping brain metabolism, connectivity and neurotransmitters topography in early and late onset dementia with Lewy bodies (Caminiti, Galli, et al.,2023) – submitted article

EO-DLB and LO-DLB are similar in terms of core symptoms. However, LO-DLB presents with more amnestic deficits, while EO-DLB shows rapid cognitive decline and more severe neuropsychiatric symptoms at onset. A contribution of neurotransmitter dysfunction was suggested, but never explored, as a possible factor contributing to the reported clinical differences. By using [^{18}F]FDG-PET brain metabolism imaging, *Study 3* aimed to assess the differences between EO-DLB and LO-DLB regarding brain hypometabolism, related neurotransmitter functional topography and metabolic connectivity. The EO and LO DLB groups were similar regarding clinical and demographical features, except age at onset ($p<0.001$), by definition (**Table 5**). DLB groups were comparable for frequency of neuropsychiatric symptoms, namely depression ($p=0.25$), apathy ($p=0.29$), irritability ($p=0.99$), and anxiety ($p=0.92$). CSF p-tau load resulted higher in the LO-DLB than EO-DLB group ($p=0.03$). REM sleep behaviour disorder was more frequent in the LO-DLB group (49% vs 21%, $p=0.07$).

Table 5. Clinical, CSF and demographic features of the EO and LO DLB groups in Study 3.

	EO-DLB	**LO-DLB**	**p value**
N	21	41	
Age (years)	59.1 ± 3.8	74.8 ± 5.9	<0.001
Sex (female/male)	8/13	13/28	0.62
Disease Duration (years)	2.7± 1.7	2.3 ± 1.4	0.45
Education (years)	10.6 ± 3.3	10.7 ± 4.8	0.95
MMSE, total	19.8 ± 4.9	19.1 ± 4.8	0.65
CSF Aβ 1-42 (z-score) †	-0.8±1.3	0.04±0.8	0.36
CSF total-Tau (z-score) †	-0.2±0.8	0.08±1.1	0.63
CSF total-Tau/Aβ 1-42 (z-score) †	0.42±1.4	-0.08±0.9	0.44
CSF phosphorylated-Tau (z-score) †	-0.5±0.7	0.2±1.1	0.03
CSF phosphorylated-Tau/Aβ 1-42 (z-score) †	-0.03±0.5	0.01±1.09	0.95
Neuropsychiatric Features, Number and (%) °			
Depression	7 (54%)	12 (35%)	0.25
Apathy	8 (62%)	15 (44%)	0.29

Irritability	5 (39%)	13 (38%)	0.99
Anxiety	4 (31%)	12 (32%)	0.92
Core DLB criteria, Number (%)			
Parkinsonism	13 (87%)	36 (88%)	0.91
Fluctuating Cognition	7 (50%)	20 (49%)	0.94
Visual Hallucinations	7 (50%)	26 (63%)	0.38
REM sleep behavior disorder	3 (21%)	20 (49%)	0.07
† CSF z-scores are calculated based on the distribution of the Milan and Geneva DLB groups. ° Data available for 47 out of 62 DLB participants. MMSE= Mini-Mental State Examination; CSF= cerebrospinal fluid; DLB = dementia with Lewy Bodies. Numbers in bold indicate significant results.			

[^{18}F]FDG-PET univariate results - SPM voxel-wise analysis showed a significant hypometabolism in middle and superior occipital lobe, angular gyrus, supramarginal gyrus, precuneus, inferior frontal gyrus and middle frontal gyrus, bilaterally (**Figure 11**). Regarding direct comparison of DLB groups, we found no differences in terms of brain hypometabolism in the DLB core regions (**Table 6**). However, differences emerged in extra-DLB typical regions. Namely, the EO-DLB group showed a more severe hypometabolism in the superior parietal cortex and PCC. Instead, the LO-DLB group presented a significant hypometabolism in the insula, supplementary motor area, and parahippocampal gyrus when compared to the EO-DLB group (**Figure 11** and **Table 6**).

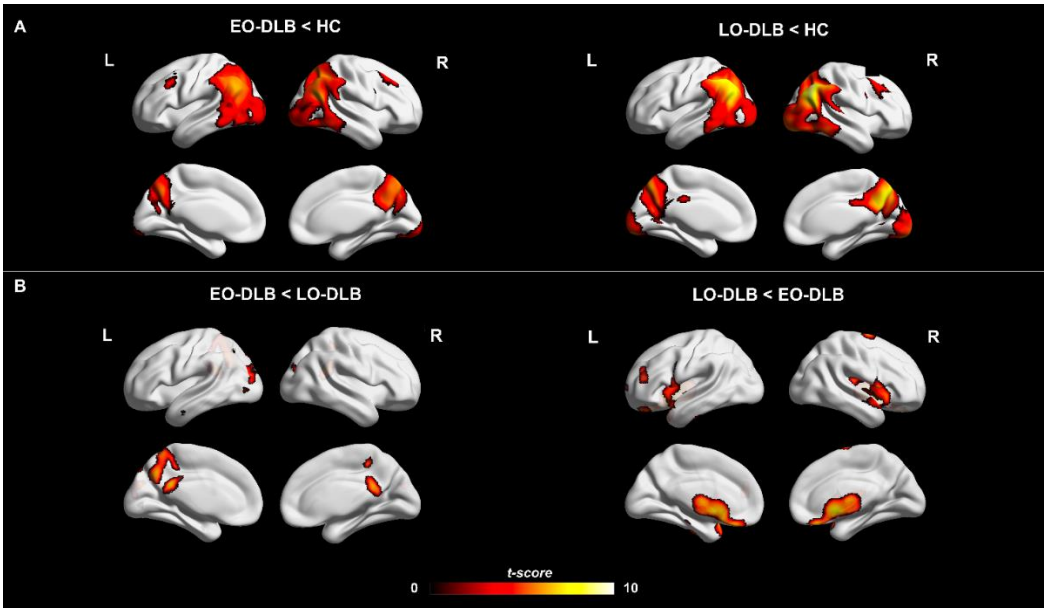

Figure 11. Group analysis in EO- and LO- DLB. *(A) Voxel-wise SPM comparison between each DLB group and a validated FDG-PET database of HC (N = 112). (B) Voxel-wise SPM direct comparison between EO-DLB (N=21) and LO-DLB (N=41). Hypometabolism is represented in a lateral and medial view. Each comparison was FWE-corrected, with a significance level at p<0.05. SPM, Statistical Parametric Mapping; EO-DLB, early-onset dementia with Lewy bodies; LO-DLB, late-onset dementia with Lewy bodies; HC, healthy controls; FWE, Family-wise Error; FDG-PET, Fluorodeoxyglucose-positron emission tomography.*

Table 6. Comparisons of brain hypometabolism (Z scores) between EO-DLB and LO-DLB groups of Study 3

	EO-DLB	**LO-DLB**	**p value**
ROIs			
Angular Gyrus	2.25±1.36	2.02±0.9	0.49
Calcarine Cortex	0.82±0.77	0.94±0.58	0.48
Middle Frontal Gyrus	0.51±0.91	0.53±0.81	0.95
Fusiform Gyrus	-0.37±0.59	-0.16±0.65	0.23
Superior Temporal Gyrus	0.006±0.96	0.37±82	0.12
Inferior Temporal Gyrus	0.28±0.82	0.32±0.71	0.84
Lingual Gyrus	0.49±0.75	0.57±0.60	0.66
Inferior Occipital Lobe	1.44±0.68	1.29±0.89	0.52
Middle Occipital Lobe	1.66±0.88	1.45±0.82	0.35
Superior Occipital lobe	1.16±0.71	0.91±0.78	0.12
Superior Parietal Cortex	1.22±0.91	0.84±0.86	**0.04**
Posterior Cingulate Cortex	0.81±0.98	0.76±0.72	**0.03**
Insula	-1.14±0.87	-0.63±0.64	**0.01**
Supplementary Motor Area	-0.23±0.73	-0.12±0.72	**0.03**
Parahippocampal Gyrus	-1.47±0.83	-0.97±0.78	**0.01**
CIS	0.43±0.03	0.42±0.03	0.30

CIS = cingulate island sign; EO-DLB= early-onset dementia with Lewy bodies; LO-DLB= late-onset dementia with Lewy bodies. Significant p-values are reported in bold.

Metabolic connectivity results - Overall, comparable whole-brain connectivity alterations were found in the two clinical groups as compared to HC (**Figure 12**). We showed decreases and increase in connectivity, the latter more evident in the posterior regions of the EO-DLB group. Some discrepancies were also evident in the pathological nodes. Namely, the EO-DLB showed pathological nodes in precuneus, inferior and

superior parietal cortex, angular gyrus, inferior temporal cortex and middle occipital cortex, the LO-DLB, in the lingual gyrus, inferior occipital cortex, fusiform, middle temporal cortex, and cerebellar vermis. The RSN metabolic connectivity in EO-DLB, LO-DLB and HC as reference, revealed: i) for the EO-DLB, a reduced connectivity in the frontal components of the EXN, aDMN and pDMN and in the LIN, a loss of connectivity in thalamus and pons and an increased connectivity between ventral putamen and amygdala; ii) for the LO-DLB, a loss of connectivity in the ATN, involving the dorsolateral prefrontal cortex (**Figure 13**).

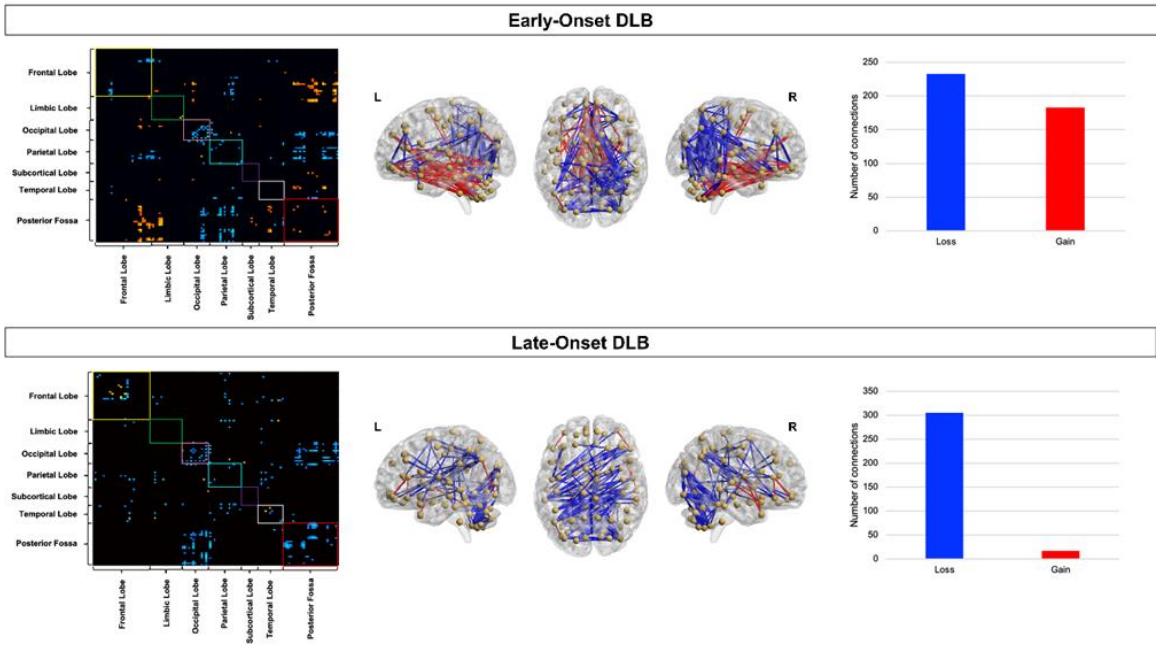

Figure 12. Whole-brain metabolic connectivity architecture in EO- and LO- DLB. *The matrices represent the significant differences obtained comparing adjacency matrices of each clinical cohort (EO-DLB and LO-DLB) with the HC group in the whole-brain network ($p<0.001$). The connectivity loss is shown in cyan-blue, the gained connectivity in yellow-red, and the unchanged connectivity in black. 3D brain showing altered connections (blue edges for losses and red for gains) for EO-DLB and LO-DLB. Box-plot representing number of loss (blue) and gained (red) connections. AAL labels[20] were grouped into 7 macro-ROIs:* ***Frontal Lobe*** *(precentral gyrus, superior frontal gyrus, middle frontal gyrus, inferior frontal gyrus, Rolandic operculum, supplementary motor area, olfactory lobe, rectus gyrus),* ***Limbic Lobe*** *(insula, anterior cingulate cortex, middle cingulate cortex, posterior cingulate cortex, hippocampus, parahippocampal gyrus, amygdala),* ***Occipital Lobe*** *(calcarine cortex, cuneus, lingual gyrus, superior occipital gyrus, middle occipital gyrus, inferior occipital gyrus),* ***Parietal Lobe***

(precentral gyrus, superior parietal lobule, inferior parietal lobule, supramarginal gyrus, angular gyrus, precuneus, paracentral lobule), ***Subcortical Lobe*** *(caudate, putamen, thalamus, pallidum), Temporal Lobe (fusiform gyrus, Heschl gyrus, superior temporal gyrus, superior temporal pole, middle temporal gyrus, middle temporal pole, inferior temporal gyrus), and* ***Posterior Fossa*** *(cerebellum crus 1, crus 2, cerebellum 3-10, vermis). EO-DLB, early-onset dementia with Lewy bodies; LO-DLB, late-onset dementia with Lewy bodies; HC, healthy controls; AAL, Automated anatomical labelling atlas.*

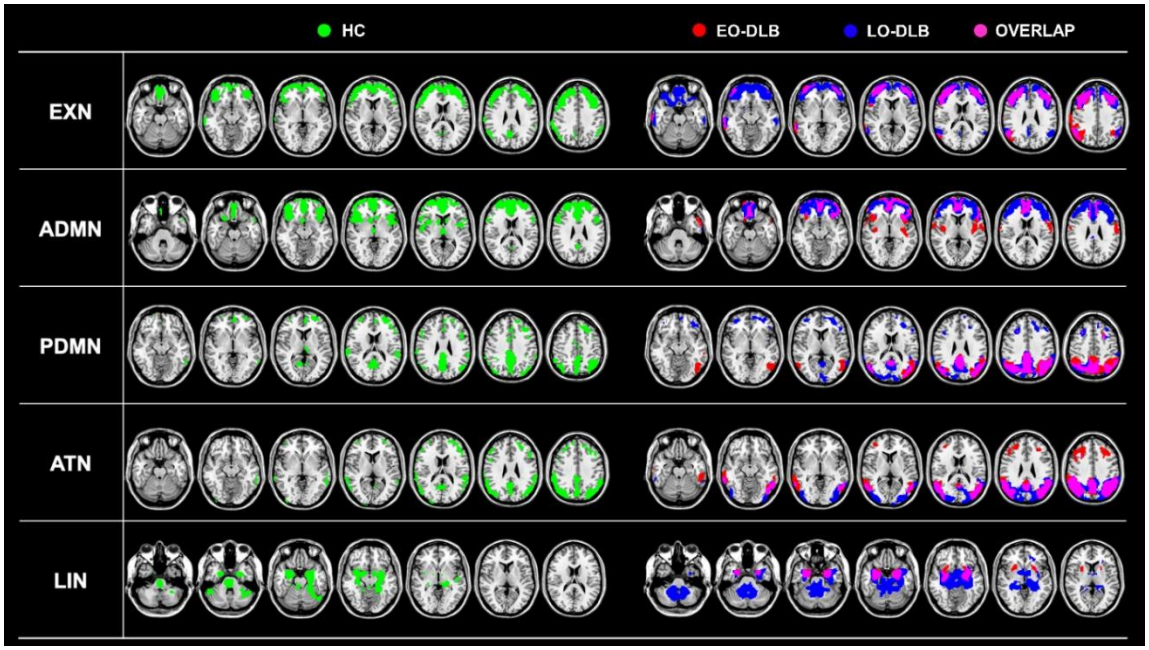

Figure 13. Resting State Networks in EO- and LO- DLB. *Figure illustrates resting-state networks topography in (left) HC (green overlaid to the anatomical template), (right) EO-DLB (red overlaid to the anatomical template) and LO-DLB (blue overlaid to the anatomical template) for anterior and posterior default mode network; attentive, executive networks, limbic network. Overlap in the RSNs between EO-DLB and LO-DLB is represented by pink color. A connectivity derangement is more prominent for EO-DLB than LO-DLB, showing reduced connectivity in the frontal components of the EXN, aDMN and pDMN, and increased connectivity in the LIN. The LO-DLB showed reduced connectivity in ATN. Resting-state networks were obtained using seed-based intercorrelation analysis. Clusters with a minimum spatial extent of 100 voxels are shown, with a voxel-wise significant threshold of $p<0.001$. EO-DLB, early-onset dementia with Lewy bodies; LO-DLB, late-onset dementia with Lewy bodies; HC, healthy controls; aDMN, anterior default mode network; pDMN, posterior default mode network; ATN, attentive network; EXN, executive network, LIN, limbic network.*

Spatial Distribution of Neurotransmitter Systems - The hypometabolism z-score maps were spatially correlated with AChT (r=-0.368, p <0.001), GABAa (r=0.331, p=0.004), SERT (r=-0.256, p<0.001), and DAT (r=-0.220, p<0.001) neurotransmitter maps in the whole DLB group. As for the EO-DLB group, we found a significant association between hypometabolism z-score maps and the distribution of AChT (r=-0.414, p <0.001), GABAa (r=0.348, p=0.005), SERT (r=-0.326, p<0.001), DAT (r=-0.292, p<0.001) and 5HT4 (r=-0.133, p=0.04) maps. As for the LO-DLB group, hypometabolism z-score maps were significantly associated with the distribution of AChT (r=-0.345, p<0.001), GABAa (r=0.333, p=0.004), SERT (r=-0.22, p<0.001), and DAT (r=-184, p=0.002) maps (**Figure 14**). The resulting negative correlation coefficients indicate that the hypometabolism characterizing each group was present in structures specific for each neurotransmitter. The post-hoc direct comparison between EO and LO-DLB Fisher's z scores showed differences only in the SERT map (p=0.029), and the largest hypometabolism cluster driving the relationship between hypometabolism and SERT neurotransmitter maps was localized in the in PCC [MNI XYZ coordinates= 8 -66 42, T=7.45, FWE-corrected p<0.001] (**Figure 14**).

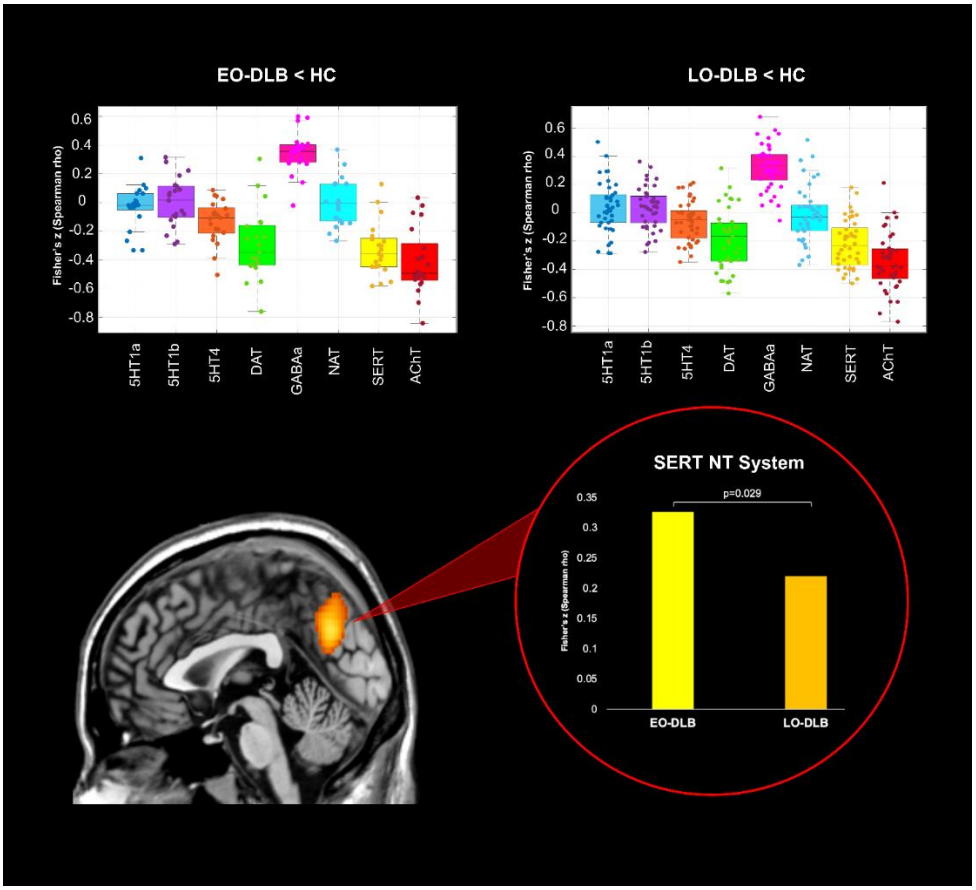

Figure 14. Neurotransmitter topography analysis. *(top) Bar plots representing Fisher's z-scores resulting from the Spearman correlation analysis between hypometabolism z-scores and neurotransmitter systems in EO-DLB (left) and LO-DLB (right); (bottom) Bar plot representing the significant difference between the two DLB groups within the serotonin transporter (SERT) circuit resulting from the post-hoc direct comparison. FDG-PET hypometabolism in posterior cingulate cortex overlaid on a T1-template image, which is associated to alterations within the serotonergic network. Significance level was set at FWE-p<0.05. EO-DLB, early-onset dementia with Lewy bodies; LO-DLB, late-onset dementia with Lewy bodies; HC, healthy controls; FDG-PET, Fluorodeoxyglucose-positron emission tomography.*

3.2 Brain molecular connectivity to achieve novel insights into the pathophysiology of neurodegenerative diseases

3.2.1 <u>Study 4:</u> Review - Brain Molecular Connectivity in Neurodegenerative Conditions (Carli, Tondo*, Boccalini*, et al., 2021) – Published article*

Study 4 is a review of concepts and methods for PET molecular and metabolic connectivity assessment. Moreover, we reported on available metabolic and molecular PET connectivity studies in LBDs with most of the evidence in PD and DLB.

In PD and DLB, connectivity alterations of resting-state large-scale networks revealed a widespread derangement of the brain connectome, suggesting them as multi-network neurodegenerative disorders (**Figure 15.B**) (S.P. Caminiti *et al.*, 2017; Sala, Silvia Paola Caminiti, *et al.*, 2017; Sala *et al.*, 2019; G. Carli, Caminiti, Sala, *et al.*, 2020). PD patients are characterized by a connectivity derangement in several resting-state networks, specifically in the frontal components (Sala, Silvia Paola Caminiti, *et al.*, 2017). These networks involve the attentional network, the anterior DMN, and the executive and motor networks. These networks are strictly related to the critical pathological events leading to neurodegeneration (e.g., dopaminergic depletion) and the consequent clinical manifestations during the disease course. For example, the metabolic connectivity in the DMN is preserved in early-stage PD patients, showing, however, a progressive disruption with the emergence of mild cognitive impairment occurring in PD later stages (Spetsieris *et al.*, 2015). DMN alteration seems to be closely associated with PD dopaminergic depletion and partial restoration of DMN connectivity after dopaminergic therapy (Spetsieris *et al.*, 2015). Moreover, for the executive network, prefrontal and orbitofrontal networking impairment might follow the frontal–striatal dopaminergic imbalance (Pagonabarraga and Kulisevsky, 2012). Although the role of frontal lobe dysfunction in executive deficits is recognized in PD, it is not clear whether it contributes to cognitive decline and dementia development (Gratwicke, Jahanshahi and Foltynie, 2015). The early predictor of PD dementia, instead, is posterior cortical damage [107]. The dual syndrome hypothesis suggests that prefrontal and striatal dysfunctions are features of stable non-dementia PD patients and that the posterior cortex and temporal lobe derangements are signs of rapid cognitive decline (Kehagia, Barker and Robbins, 2013). The pathological involvement of the frontal networks in PD seems to be associated with the

neuropsychiatric manifestation, typically characterizing this condition (Schwartz *et al.*, 2019). A recent study tried to map common PD non-motor symptoms—i.e., impulsivity and hypomania—using seed-based metabolic connectivity analyses (Premi *et al.*, 2016). Impulsivity and metabolism showed an association in the medial part of the right superior frontal gyrus, brain structure functionally connected with brain regions belonging to the anterior DMN. The impulse control disorder in PD patients was associated with severe impairment of the mesocorticolimbic metabolic connectivity (Verger *et al.*, 2018) and a functional loss of covariance, as measured with DaTSCAN SPECT imaging, between basal ganglia and frontal associative cortex (Premi *et al.*, 2016). This evidence further highlights the link between dopaminergic deficits and network integrity in PD.

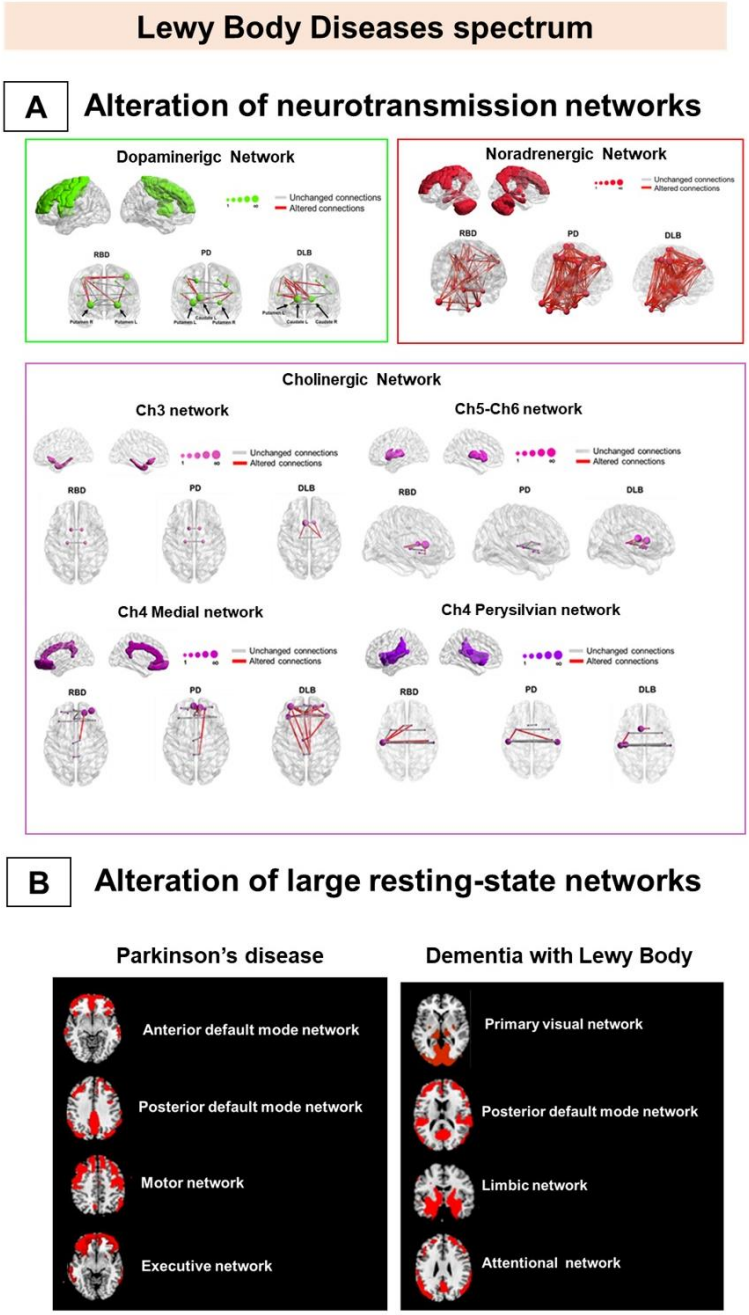

Figure 15. Metabolic connectivity alterations in Lewy bodies disease spectrum (Open access source). *The figure represents the main metabolic connectivity findings in Parkinson's disease (PD), dementia with Lewy bodies (DLB), and isolated rapid eye movement (REM) sleep behavior disorders (iRBD). The figure depicts the neurotransmission networks (A) and the large-scale resting-state network alterations (B). (A) DLB and PD share connectivity changes, mainly in noradrenergic and cholinergic (Ch)4 perisylvian (P) cholinergic networks. The iRBD and DLB groups show high similarity in noradrenergic and Ch5-Ch6 cholinergic networks. IRBD and PD show a high degree of similarity in the noradrenergic network. Finally, the dopaminergic network*

impairment is limited and localized in iRBD and moderate-to-severe in DLB and PD. (B) PD is characterized by alteration of the frontal component of anterior default mode network DMN, posterior DMN, and motor and executive networks (right), and DLB by alteration of the posterior component of PVN, pDMN, and limbic and attentional networks (left). All the evidence supports that α-synucleinopathies should be considered multisystem disorders since the prodromal stage. Panel A modified by Carli et al. (2020) [95] with the permission of Elsevier 2021. Abbreviations: RBD = REM sleep behavior disorder, PD = Parkinson's disease; DLB = dementia with Lewy bodies; DMN: default mode network; Ch5-Ch6 = cholinergic Ch5-Ch6 divisions networks; Ch4 medial = cholinergic medial Ch4 division network; Ch4 perisylvian = cholinergic lateral perisylvian Ch4 division networks; Ch3 = cholinergic Ch3 division network; Ch1-Ch2 = cholinergic Ch1-Ch2 division network. The figure is from (Carli *et al.*, 2021) *in accordance to the fair use principle.*

In DLB, metabolic connectivity evidence showed a severe involvement of the posterior cortical, the limbic, and the attention networks, consistently with the pathological and clinical heterogeneity intrinsic to this condition (Sala *et al.*, 2019). DLB connectivity alterations in large-scale resting-state networks are strongly related to clinical symptoms (Sala *et al.*, 2019). Visual hallucinations (VH) are associated with impaired connectivity in posterior DMN, the attention network, and visual networks (Iaccarino *et al.*, 2018; Sala *et al.*, 2019). The biological explanation for these findings points to cholinergic damage, leading to the breakdown of the functional relationship among the calcarine cortex, lateral occipital cortex, and parietal cortex (Klein *et al.*, 2010). These studies demonstrated that the neural correlates of complex neurological symptoms, such as VH, encompass multiple large-scale brain networks. Visual attention and executive, visuoperceptive, and visuospatial deficits in DLB patients are associated with specific large-scale network connectivity changes (Sala *et al.*, 2019). Visual attention and visuospatial neuropsychological deficits are related to impaired metabolic connectivity in the primary and associative visual networks, whereas executive dysfunction is related to a frontal metabolic connectivity impairment (Sala *et al.*, 2019). Of note, the association between visual selective attention and integrity of metabolic connectivity in the primary visual network crucially supports the hypothesis that visual cortex desynchronization is a key factor in DLB visual attention deficits. The multisystem derangement of large-scale networks in PD and DLB is also confirmed by metabolic connectivity studies targeting neurotransmission systems (S.P. Caminiti *et al.*, 2017; G. Carli, Caminiti, Sala, *et al.*,

2020). A-synuclein aggregations play a crucial role in the neurotransmitter impairment observed in these syndromes, affecting different systems—the dopaminergic, noradrenergic, and cholinergic sytems (Uchihara and Giasson, 2016). Degeneration of dopaminergic nigro-striatal neurons is the pathological hallmark of PD and DLB associated with typical motor impairment (Goedert, Jakes and Spillantini, 2017). According to neuropathological findings, several pieces of metabolic and molecular connectivity data have consistently reported relevant connectivity reconfigurations within the nigro-striato-cortical dopaminergic network in PD and DLB (S.P. Caminiti *et al.*, 2017; Sala, Silvia Paola Caminiti, *et al.*, 2017; G. Carli, Caminiti, Sala, *et al.*, 2020). Moreover, metabolic connectivity alterations are present in the noradrenergic network in PD and DLB, in agreement with post-mortem observations (Nahimi *et al.*, 2018). Of note, limited metabolic cholinergic network alterations characterize PD, while a widespread and severe metabolic connectivity impairment features DLB (G. Carli, Caminiti, Sala, *et al.*, 2020).

These data led to a comparative picture of the metabolic connectome in the LBDs (**Figure 15**). PD and DLB conditions both revealed consistencies and substantial differences. PD patients show an extensive decrease in connectivity in frontal regions and a compensatory connectivity increase in occipital and posterior cortical regions (Sala, Silvia Paola Caminiti, *et al.*, 2017). In contrast, an occipital connectivity impairment is the hallmark of DLB, together with a more preserved frontal connectivity (Sala, Silvia Paola Caminiti, *et al.*, 2017). The different patterns of metabolic connectivity alterations might reflect vulnerabilities of the cholinergic system in PD and DLB (Pagonabarraga and Kulisevsky, 2012), leading to disease-specific patterns of dysfunction (Bohnen and Albin, 2011; Garcia-Garcia *et al.*, 2012), as confirmed by recent metabolic connectivity evidence (G. Carli, Caminiti, Sala, *et al.*, 2020). In this regard, PD and DLB patients present common and disease-specific neurotransmission network reconfigurations. Both clinical syndromes show moderate-to-severe alterations in the nigrostriatal dopaminergic and noradrenergic networks, whereas the DLB condition presented more severely affected cholinergic networks (**Figure 15.A**). PET molecular connectivity in DLB was also investigated at different stages, as measured by [^{123}I]FP-CIT SPECT (Huber *et al.*, 2020). The connectivity analysis showed alterations in the limbic circuits and basal ganglia with differences in DLB with mild or intermediate/severe dopamine deficiency. Connectivity

alterations increased slightly in DLB with mild dopamine deficiency but degenerated strongly when dopamine deficiency became intermediate or severe (Huber *et al.*, 2020). All the above findings indicate that PD and DLB conditions must be considered complex and multisystem disorders. Metabolic connectivity findings indicate that the whole α-synuclein spectrum is a multisystem neurotransmission disease since the early stages (**Figure 15.A**). Notably, in iRBD, today considered the early stage of DLB, patients showed severe impairment of noradrenergic network connectivity, as well as an initial derangement of the cholinergic networks (G. Carli, Caminiti, Sala, *et al.*, 2020). IRBD shared some cholinergic alterations with DLB, indicating an early occurrence and a role in this system's phenotypic expressions. Conversely, the nigro-striato-cortical dopaminergic network featured limited connectivity changes in iRBD. This metabolic signature is consistent with molecular neuroimaging findings, demonstrating a nigrostriatal dopamine innervation within normal limits in iRBD cases (Knudsen *et al.*, 2018b). These connectivity data also represent an in vivo confirmation of Braak staging of α-synuclein propagation (Braak *et al.*, 2018). Two other in vivo studies support the Braak staging hypothesis in PD and DLB conditions only, reporting the brain regions' metabolic disconnection affected by α-synuclein spreading (S.P. Caminiti *et al.*, 2017; Sala, Silvia Paola Caminiti, *et al.*, 2017). Despite a common molecular pathological substrate and a backbone of shared neuronal vulnerabilities, α-synucleinopathies show significant clinical differences, particularly regarding the timing and severity of symptoms. Since connectivity is a marker of the clinical phenotype, distinct network dysfunction patterns—related to the severity and extent of neurodegenerative processes—might help explain these differences.

Other factors may influence metabolic connectivity changes and help to explain the heterogeneous clinical manifestation of neurodegenerative disorders. Recent evidence suggests that education and occupation can modulate resting-state network metabolic connectivity in DLB (Giulia Carli, Boccalini, *et al.*, 2020). Education seems to act through compensatory mechanisms since it showed a specific influence on the executive, attentive, and posterior DMN in which a highly educated DLB sub-group engaged the anterior brain regions to cope with more severe brain posterior pathology. On the other hand, occupation acts through neural reserve mechanisms, with a specific effect on anterior DMN and associative visual network, in subjects with high occupational

attainment. Thus, CR induces brain plasticity, resulting in neural reserve, making the brain more resistant to pathological changes and preserving cognitive functions. Moreover, the same article investigated the occupation considering specific occupational profiles—different metabolic connectivity patterns emerged in association with occupational proxies and types (Giulia Carli, Boccalini, *et al.*, 2020).

3.2.2 Study 5: Metabolic connectivity of resting-state networks in α synucleinopathies, from prodromal to dementia phase (Boccalini, et al., 2022) – Published article

Previous evidence suggests that the derangement of large-scale brain networks reflects structural, molecular, and functional mechanisms underlying neurodegenerative diseases. Despite the above-described large-scale brain network alterations in PD and DLB separately, a comprehensive study on connectivity reconfiguration starting from the preclinical phase is still lacking. *Study 5* investigates shared and disease-specific changes in the large-scale networks (resting-state networks, RSNs), in three clinical groups (iRBD, PD without cognitive deterioration over time, and DLB) throughout the brain metabolic connectivity approach. We included 30 patients with iRBD, 28 with stable PD, 30 with DLB, and 30 HC for comparison. We evaluated metabolic connectivity changes by applying a seed-based interregional correlation analysis (IRCA) on [^{18}F]FDG-PET data. We considered the seeds of RSNs previously validated. Specifically, we considered the RSNs affected in PD and DLB, following the previous literature (discussed above), namely, the anterior and posterior default mode networks (ADMN and PDMN), the attentive network (ATTN), the frontal executive network (EXN), the limbic network (LIN), the motor network (MN), the somatosensory network (SN), the primary, and high visual networks (PVN and HVN; details on the selected ROIs are provided in **Table 7**). We assessed the topographical similarities and differences between diagnostic groups vs. HC and between each other through specific connectivity metrics, such as the weighted and unweighted Dice similarity coefficients (DC).

Table 7: Selected seeds for resting-state networks (RSNs) analyses

	SEEDS	**DERIVATION ATLASES**
ADMN	Ventromedial frontal cortex	Shirer 2012 Functional RSNs atlas
ATTN	Angular gyrus, supramarginal gyrus	Shirer 2012 Functional RSNs atlas
EXN	Dorsolateral Prefrontal Cortex	Sallet's Dorsal Frontal Parcellation atlas
HVN	Inferior occipital cortex, middle occipital cortex	Shirer 2012 Functional RSNs atlas
LIN	Amygdala	Anatomical Automatic Labeling (AAL) atlas
MN	Precentral gyrus	Anatomical Automatic Labeling (AAL) atlas
PDMN	Posterior cingulum, precuneus	Shirer 2012 Functional RSNs atlas
PVN	Calcarine cortex	Shirer 2012 Functional RSNs atlas
SN	Postcentral gyrus	Anatomical Automatic Labeling (AAL) atlas
Abbreviations: ADMN= anterior default mode network; ATTN= attentive network; EXN= executive network; HVN=high visual network; LIN=limbic network; MN=motor network; PDMN=posterior default mode network; PVN=primary visual network; SN= somatosensory network.		

The demographic and clinical features of the study groups are reported in **Table 8**. PD patients were significantly younger than iRBD and DLB ($p<0.05$), whereas MMSE excluded significant cognitive changes in iRBD and PD compared to DLB ($p<0.05$). Thus, the iRBD cohort was characterized by the absence of relevant cognitive impairments ($MMSE_{mean} \pm SD = 27.46 \pm 2.65$) and motor signs ($UPDRS\ III_{mean} \pm SD = 0.54 \pm 1.2$). At the same time, 97% of the DLB group featured parkinsonism.

Table 8: Demographic and clinical features of the samples

	iRBD	PD	DLB	HC	Statistic
N	30	28	30	30	
Gender (F/M)	2/28	12/16	13/17	13/17	p = 0,002[1 a, b, e]
Age, y (Mean ± SD)	70,0± 6,82	62,6± 10,82	70,8± 8,45	63,0± 2,8	p = 0,000[2 a, c, d, e]
Education, y (Mean ± SD)	11,1± 4,79	8,25± 4,26	9,3± 4,14	-	p = 0,053[2]
Disease duration, y (Mean ± SD)	5,33± 3,12	4,25± 2,59	2,3± 2,12	-	p = 0,000[2 b, c]
MMSE, score (Mean ± SD)	27,46± 2,65	28,7 ± 1,49	17,3± 4,59	-	p = 0,000[2 b, c]

[1]Chi-squared test

[2]One-way ANOVA

Significant differences at post-hoc comparisons, significant at p < 0.05, using Bonferroni-correction for multiple comparisons.

a= iRBD ≠ PD, b= iRBD ≠ DLB, c= PD ≠ DLB, d= DLB ≠ HC, e= iRBD ≠ HC

Abbreviations: iRBD = isolated REM sleep behaviour disorder; PD = Parkinson's disease; DLB = dementia with Lewy Bodies, N= number, y= year, F = female, M = Male, MMSE = Mini Mental State Examination, SD = standard deviation

Isolated REM sleep behavior disorder subjects vs. healthy controls: The MN (DC = 0.19; Δvoxel = -7543), PDMN (DC = 0.29; Δvoxel = 8717), and ATTN (DC = 0.39; Δvoxel = 7463) were the most altered networks in iRBD. Specifically, MN seed (i.e., precentral gyrus) lost metabolic connectivity mainly with the bilateral supplementary motor area and superior frontal gyrus. PDMN and ATTN showed instead increased connectivity compared to HC. In PDMN, the seeds (i.e., posterior cingulum and precuneus) showed increased metabolic connectivity with the angular gyrus, cuneus, precuneus, and superior frontal gyrus, bilaterally. In ATTN, the seed showed increased connectivity with the angular gyrus, posterior cingulum, and middle temporal gyrus, bilaterally. The other RSNs showed moderate differences compared to HC in terms of topography extension and overlap. The ADMN (DC = 0.44; Δvoxel = 3449), EXN (DC = 0.43; Δvoxel = 799), HVN (DC = 0.53; Δvoxel = 2244), and PVN (DC = 0.47; Δvoxel = 3775) showed an

increase of metabolic connectivity compared to HC. On the other hand, SN (DC = 0.41; Δvoxel = - 7151) and LIN (DC = 0.29; Δvoxel = -1005) showed a decrease in metabolic connectivity in comparison to HC. See **Figures 16** and **17** for the graphical representation.

Parkinson's disease patients vs. healthy controls: The MN (DC = 0.18; Δvoxel = -5846) and SN (DC = 0.23; Δvoxel = -9561) were the most altered networks in PD patients, both characterized by a decrease of connections compared to HC. Specifically, MN seed extensively lost metabolic connections mainly with the bilateral supplementary motor area and middle and superior frontal gyrus. In SN, the seed (i.e., bilateral postcentral gyrus) showed a widespread connectivity decrease with inferior and superior parietal gyrus, precuneus, and paracentral lobule. The other RSNs showed moderate differences compared to HC in terms of topography extension and overlap. The ADMN (DC = 0.50; Δvoxel = 1552), EXN (DC = 0.45; Δvoxel = -3061), HVN (DC= 0.41; Δvoxel = -4,675), PVN (DC= 0.48; Δvoxel = - 2259), PDMN (DC = 0.41; Δvoxel = -3035), ATTN (DC = 0.42; Δvoxel = -1068), and LIN (DC = 0.36; Δvoxel = -1632). See **Figures 16** and **17** for the graphical representation.

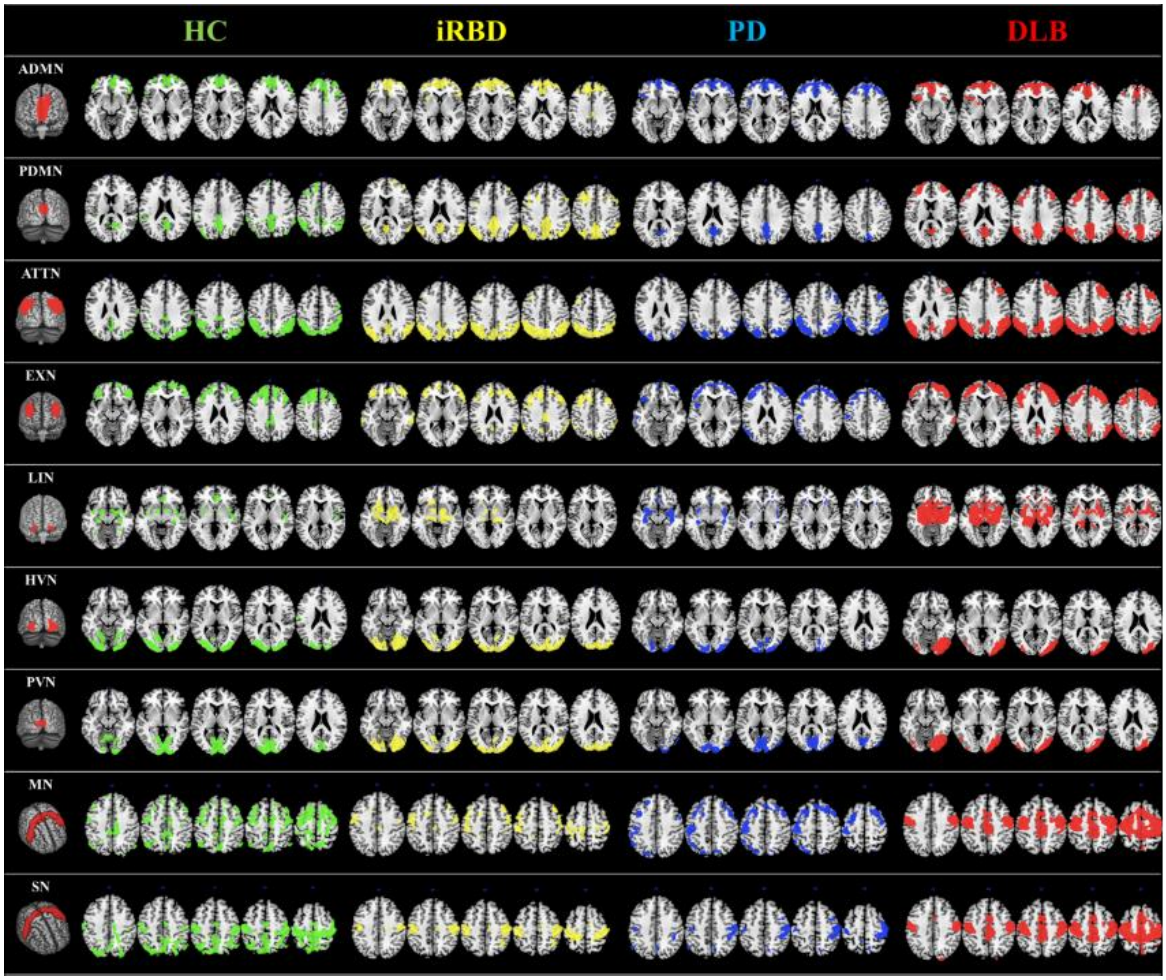

Figure 16. RSNs analysis (Open access source). *RSNs topography in HC (green overlaid to the anatomical template), iRBD (yellow overlaid to the anatomical template), PD (blue overlaid to the anatomical template), and DLB (red overlaid to the anatomical template) for the ADMN, PDMN, ATTN, EXN, LIN, HVN, PVN, MN, and SN. The selected seed for each network is shown in the first column. A connectivity derangement is present in all the RSNs. RSNs were obtained using seed-based intercorrelation analysis. Clusters with a minimum spatial extent of 100 voxels are shown, with a voxel-wise significant threshold of p = 0.001. iRBD, isolated REM sleep behavior disorder; PD, Parkinson's disease; DLB, dementia with Lewy Bodies; HC, healthy controls; ADMN, anterior default mode network; ATTN, attentive network; EXN, executive network; HVN, high visual network; LIN, limbic network; MN, motor network; PDMN, posterior default mode network; PVN, primary visual network; SN, somatosensory network. The figure is from* (Boccalini, Bortolin, *et al.*, 2022) *in accordance to the fair use principle.*

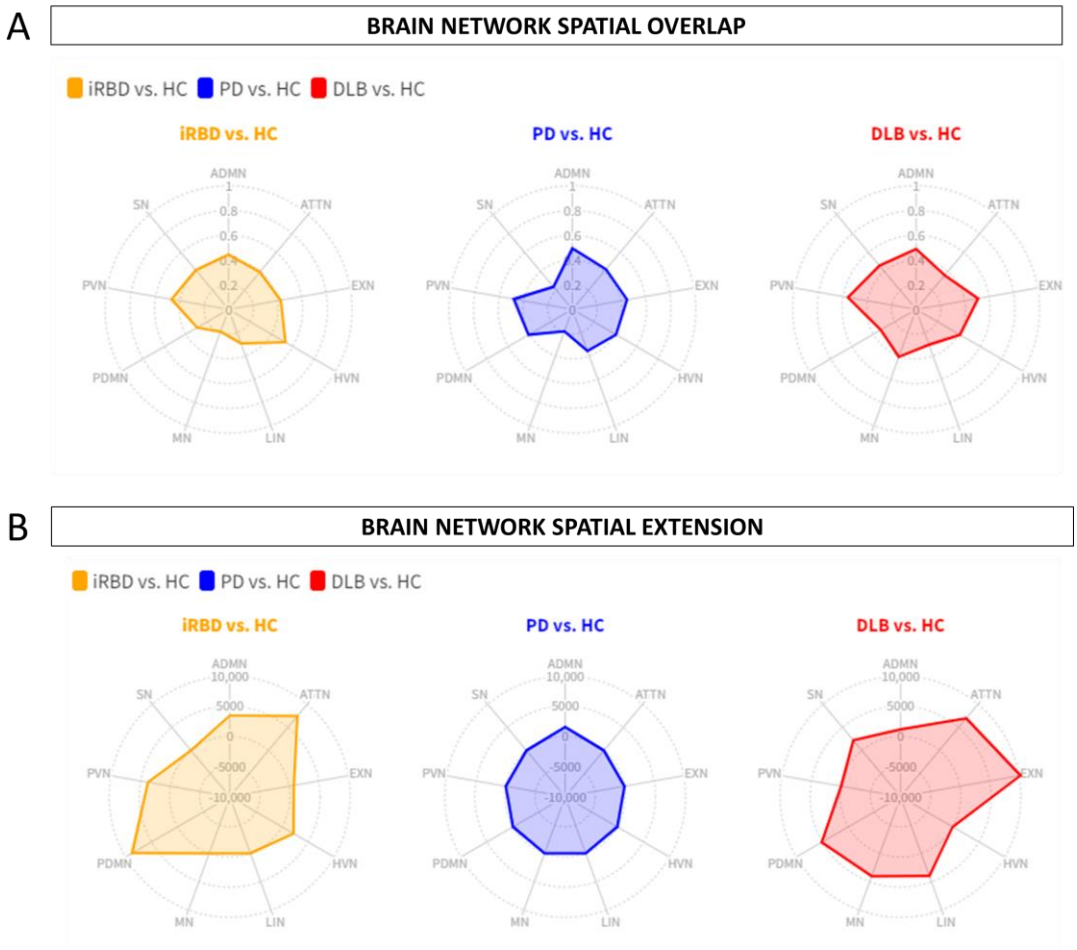

Figure 17. Brain networks spatial overlap and extension (Open access source). *A) Figure shows the spatial overlap between HC and iRBD (orange), PD (blue) and DLB (red) in the ADMN, PDMN, ATTN, EXN, LIN, HVN, PVN, MN, SN, expressed by DC. B) The spatial extension of all networks in RBD (orange), PD (blue) and DLB (red) compared to HC, expressed as the difference between HC and each clinical group (Δ). Abbreviations: iRBD = isolated REM sleep behaviour disorder; PD = Parkinson's disease; DLB = dementia with Lewy Bodies; HC= healthy controls; ADMN= anterior default mode network; ATTN= attentive network; EXN= executive network; HVN=high visual network; LIN=limbic network; MN=motor network; PDMN=posterior default mode network; PVN=primary visual network; SN= somatosensory network. The figure is from* (Boccalini, Bortolin, *et al.*, 2022) *in accordance to the fair use principle.*

Dementia with Lewy bodies patients vs. healthy controls: The LIN (DC = 0.30; Δvoxel = 3988), PDMN (DC = 0.33; Δvoxel = 5136), and ATTN (DC = 0.36; Δvoxel = 6963) were the most altered networks in DLB patients, all characterized by an increase of metabolic connectivity compared to HC. Specifically, LIN seed (i.e., amygdala) showed increased metabolic connectivity mainly with the bilateral hippocampus, parahippocampus, and

middle temporal pole. In PDMN, we found increased metabolic connectivity between the posterior seed and frontal brain regions (i.e., bilateral middle frontal gyrus and superior frontal gyrus). Similarly, in ATTN, IRCA revealed increased connectivity between posterior and anterior regions. The ATTN seed (i.e., angular gyrus and supramarginal gyrus) showed increased metabolic connectivity, mainly with the right middle frontal gyrus and middle orbital frontal cortex. The seed showed higher connectivity with the posterior portion of the middle temporal gyrus bilaterally. The other RSNs showed moderate differences compared to HC in terms of spatial extension and overlap. The ADMN (DC= 0.48; Δvoxel = 1138), EXN (DC= 0.51; Δvoxel = 10233), MN (DC = 0.41; Δvoxel = 4027), and SN (DC = 0.46; Δvoxel = 2225). Only the visual networks, namely PVN (DC = 0.56; Δvoxel = -2876) and HVN (DC = 0.41; Δvoxel = -1424), showed a reduction of metabolic connectivity compared with controls. See **Figures 16** and **17** for the graphical representation.

The direct comparisons between clinical groups are summarized in **Table 9** and **Figures 16** and **18** for the weighted DC (wDC) and DC values and their graphical representation and are explained below.

Isolated REM sleep behavior disorder subjects vs. Parkinson's disease patients: iRBD and PD patients showed an overall low degree of overlap in RSNs metabolic reconfiguration, with most values close to 0 (wDC ranging from -0.60 to 0.81). According to the ranking strategy, PD and iRBD showed five similar RSNs (i.e., ADMN, LIN, MN, PVN, SN) and four dissimilar RSNs (i.e., ATTN, EXN, HVN, and PDMN). Similar and dissimilar RSNs showed a significant difference in wDC mean values (similar mean ± SD: 0.51 ± 0.18; not similar mean ± SD: 0.01 ± 0.41; p = 0.016). The PDMN was the network where the two groups showed the lowest similarity value (wDC = -0.60). The highest level of similarity was found in SN (wDC = 0.81), where both groups showed a decrease in network extension compared to HC.

Isolated REM sleep behavior disorder subjects vs. dementia with Lewy bodies patients: iRBD patients showed an overall high degree of overlap with DLB patients in RSNs metabolic reconfigurations (wDC ranging from 0.06 to 1.81). According to the rank strategy, in DLB and iRBD, most RSNs were similar (i.e., ADMN, ATTN, EXN, HVN, PDMN PVN, and SN), and only two were not similar RSNs (i.e., LIN and MN). Similar

(mean ± SD: 0.75 ± 0.58) RSNs showed slightly higher wDC compared to dissimilar (mean ± SD: 0.17 ± 0.16) RSNs without reaching the statistical significance in wDC (p = 0.111), further demonstrating a high degree of similarity between iRBD and DLB. The highest similarities were found in PDMN (wDC = 1.81) and ATTN (wDC = 1.30), where both DLB and iRBD networks showed increased connectivity between frontal and posterior regions. Accordingly, both groups showed an increased extension of these two networks compared to HC, with increased anterior–posterior connectivity.

Parkinson's disease patients vs. dementia with Lewy bodies patients: DLB and PD patients showed an overall low degree of overlap in RSNs metabolic reconfigurations, with all the values close to 0 (wDC ranging from -0.18 to 0.61). PD and DLB showed four similar RSNs (i.e., ADMN, HVN, LIN, and PVN) and five dissimilar RSNs (i.e., ATTN, EXN, MN, PDMN, and SN) with significant differences in wDC mean values (similar mean ± SD: 0.46 ± 0.13; not similar mean ± SD: 0.05 ± 0.16; p = 0.016). The PDMN was the network where they showed the lowest overlap value (wDC = -0.18). The PD group showed a decreased extension in this network compared to HC; an increased network extension characterized the DLB cohort.

From a topographical point of view, PD patients showed functional isolation of the seed that lost its metabolic connection with the brain, and the DLB cohort showed recruitment of frontal cortical regions, especially on the right side.

Table 9: wDC coefficient for comparison in clinical groups

	wDC PD vs. iRBD	**wDC DLB vs. PD**	**wDC iRBD vs. DLB**
ADMN	0.52	0.54	0.52
ATTN	0.18	0.18	1.30
EXN	0.30	0.21	0.46
HVN	0.16	0.37	0.48
LIN	0.37	0.33	0.29
MN	0.47	-0.04	0.06
PDMN	-0.60	-0.18	1.81
PVN	0.37	0.61	0.27
SN	0.81	0.10	0.35

Abbreviations: iRBD = isolated Rem sleep behaviour disorder; PD = Parkinson's disease; DLB = dementia with Lewy bodies; WDC= weighted Dice coefficient; ADMN= anterior default mode network; ATTN= attentive network; EXN= executive network; HVN=high visual network; LIN=limbic network; MN=motor network; PDMN=posterior default mode network; PVN=primary visual network; SN= somatosensory network.

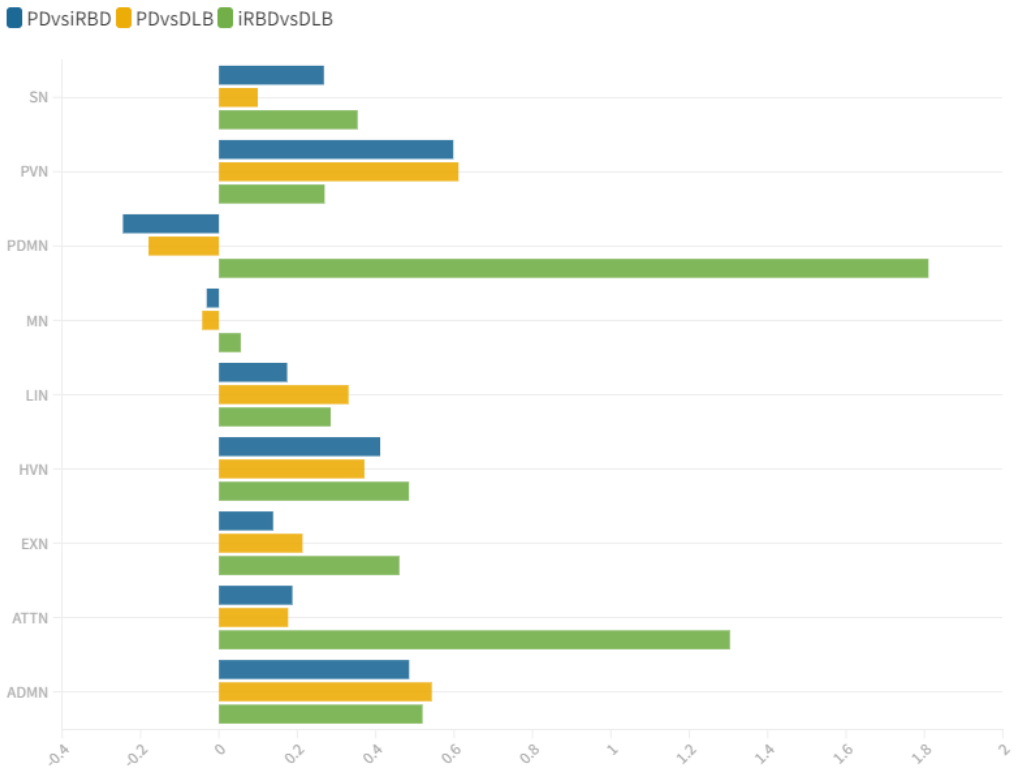

Figure 18. wDC Similarity coefficient between clinical groups (Open access source). *wDC for every RSN are shown. The length of the bars represents the degree of similarity between clinical groups, i.e., PD vs iRBD (blue), PD vs DLB (orange) and iRBD vs DLB (green), in the ADMN, PDMN, ATTN, EXN, LIN, HVN, PVN, MN, SN. iRBD and DLB (green) showed the highest wDC values, especially in PDMN and ATTN. The figure is from* (Boccalini, Bortolin, *et al.*, 2022) *in accordance to the fair use principle.*

3.3 Sex and gender as crucial sources of variability in LBD

3.3.1 <u>Study 6:</u> Gender-Related Vulnerability of Dopaminergic Neural Networks in Parkinson's Disease (Boccalini, et al., 2021) – Published article

Multivariate methods to [^{18}F]FDG-PET brain data enable to reconstruct brain connectivity patterns within and between neurotransmitter systems, thus providing an *in vivo* window to the functional architecture of these systems. Previous evidence revealed a significant coupling between neurotransmission impairment and the integrity of metabolic networks (Niethammer *et al.*, 2013; Holtbernd *et al.*, 2015; Ko, Lee and Eidelberg, 2017; Massa *et al.*, 2019; Huber *et al.*, 2020). Specifically, in PD and DLB, [^{18}F]FDG-PET-based metabolic network expression and dopamine availability were found to provide consistent information underlying the disease process (Niethammer *et al.*, 2013; Ko, Lee and Eidelberg, 2017; Massa *et al.*, 2019; Huber *et al.*, 2020). *Study 6* focused on the dopaminergic nigro-striato-cortical and mesolimbic networks to investigate gender differences in idiopathic PD. 34 PD patients (mean age in years – standard deviation [SD]: 62.97 – 10.48; gender [F/M]: 16/18) without cognitive impairment at baseline were retrospectively collected from the clinical and imaging database of the Neurology Unit, Department of Clinical and Experimental Sciences, at the University of Brescia, Brescia, Italy. The clinical diagnosis of PD was made according to the Movement Disorder Society Clinical Diagnostic Criteria (Ronald B Postuma *et al.*, 2015). All patients underwent MRI or computed tomography (CT) to exclude cerebrovascular diseases or brain/iron accumulation. Patients with deep brain stimulation, verified genetic mutation known to cause PD, concomitant psychiatric or other neurological disorders, hallucination, psychosis or antipsychotic drug use, a background of drug or alcohol addiction, and mild cognitive impairment were excluded. Gender groups in the PD cohorts were compared through a one-way analysis of variance (**Table 10**), running in SPSS 21.0 software for Windows (SPSS, Chicago, IL). A group of 34 healthy age-matched volunteers (mean age in years – SD: 62.52 – 4.52; gender [F/M]: 16/18) were retrospectively collected from the internal database of the in vivo Human Molecular and Structural Neuroimaging Unit, San Raffaele Scientific Institute for Research and Healthcare (IRCCS), Milan, Italy. The subjects presented a negative

medical history for neurological or other chronic diseases, and they were not taking psychoactive medication.

Table 10: Demographic and clinical features of the PD sample included in Study 6

Demographic and clinical features	**PD whole Group**	**PD Female**	**PD Males**	***Statistic***
Number of patients	34	16	18	
Gender (F/M)	16/18	-	-	-
Age in year, y (means ± SD)	62.97±10.48	63.35±11.36	63.31±10.54	p=0.935
Disease durations, y (means ± SD)	4.16±2.52	4.00±2.41	4.31±2.67	p=0.741
MMSE, corrected scores (means ± SD)	28.56±1.54	28.50±1.60	28.62±1.54	p=0.830
Years of education, y (means ± SD)	8.03±4.19	6.92±4.00	9.00±4.22	p=0.181
UPDRS III, corrected scores (means ± SD)	14.63±6.94	15.14±7.79	14.18±6.33	p=0.714
Daily LED, mg (means ± SD)	125.08±128.35	126.45±156.81	124.06±107.79	p=0.962

M: male, F: female; Y: years; S.D: standard deviation; MMSE: Mini-Mental State Examination; UPDRS: Unified Parkinson's Disease Rating Scale; LED: levodopa equivalent dose; p: p-value.
The differences were tested using a one-way analysis of variance (ANOVA)

Males and females with PD did not show significant differences in demographical and clinical data, including both cognitive and motor assessment and medication state (**Table 10**). However, we found gender differences in the brain metabolic connectivity of the two dopaminergic networks, namely the nigro-striato-cortical and the mesolimbic networks.

Nigro-striato-cortical network: A widespread alteration of metabolic connectivity characterized PD males within the nigro-striato-cortical dopaminergic network, with 34.69% of altered connections in comparison with HC (p-value <0.01, corrected for Bonferroni multiple comparisons) (**Figure 19**). On the contrary, the connectivity reconfiguration of the same network was relatively spared in PD females (only 17.35% changes in comparison with HC) (p-value <0.01, corrected for Bonferroni multiple

comparisons) (**Figure 19**). The direct comparison between PD males and females showed that the metabolic connectivity alteration of nigro-striato-cortical network was significantly more severe in PD males compared with PD females (χ^2 = 7.65, p-value <0.005) (**Figure 19**). Since the p-value is significant, the observed difference is not due to chance (assumption H0), but due to the gender factor.

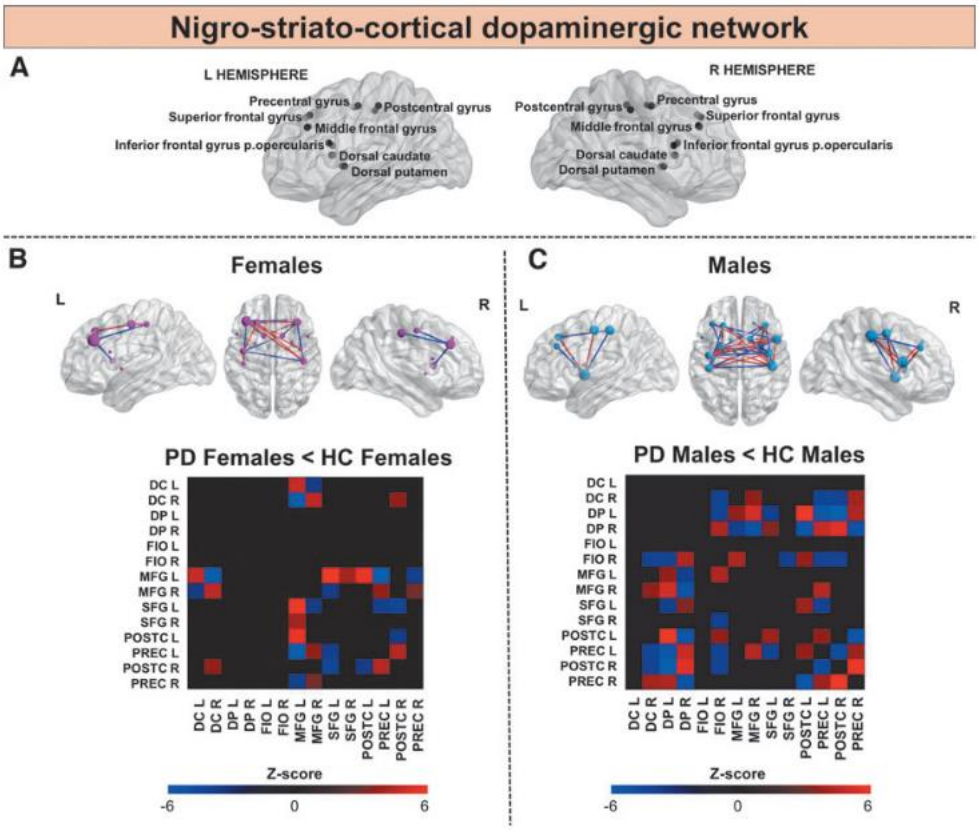

Figure 19. Nigro-striato-cortical dopaminergic network analyses (Open access source). *3D brain templates display (A) the nodes of the network in the left and right hemispheres; (B) the PD network connectivity graphs for females; and (C) the PD network connectivity graphs for males. In (B, C), only the altered connections are presented: the increased and the decreased connections compared with HC. The dimension of each node depends on the total node number of connections and is represented by the size of each dot. A nigro-striato-cortical connectivity derangement and reconfiguration are evident in males versus females. Below, dopaminergic nigro-striato-cortical network's connectivity matrices of PD females (B) and males (C) are displayed. The matrices represent the significant differences obtained when comparing partial correlation coefficients between PD females < HC (B) and PD males < HC (C) in the dopaminergic nigro-striato-cortical network. The color bar displays values of the Z scores, for the comparison of partial correlation*

coefficients' strengths. The figure is from (Boccalini et al., 2021) in accordance to the fair use principle.

Mesolimbic network: Significant widespread alterations of connections within the mesolimbic dopaminergic network characterized PD females, reporting 55.10% of altered connections in comparison with HC (p-value <0.01, corrected for Bonferroni multiple comparisons). On the contrary, the connectivity reconfiguration of the same network was limited in PD males compared with HC (1.02%) (p-value <0.01, corrected for Bonferroni multiple comparisons) (**Figures 20** and **21**). The direct comparison between PD males and females showed that the metabolic connectivity alteration of the mesolimbic network was significantly more severe in PD females compared with PD males (χ^2= 70.99, p-value <0.00001) (**Figures 20** and **21**). Since the p-value is significant, the observed difference is not due to chance (assumption H0), but due to the gender factor.

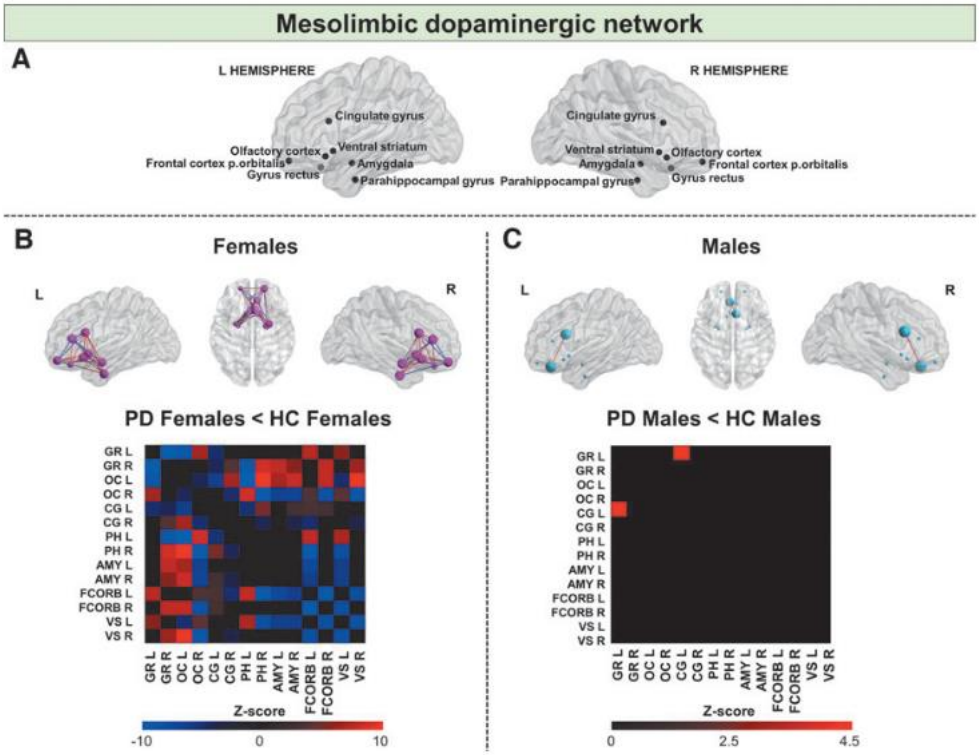

Figure 20. Mesolimbic dopaminergic network analyses (Open access source). *3D brain templates display (A) the nodes of the network in the left and right hemispheres; (B) the PD network connectivity graphs for females; and (C) the PD network connectivity graphs for males. In (B, C), only the altered connections are presented: the increased and the decreased connections compared with HC. The dimension of each node depends on the total node number of connections*

and is represented by the size of each dot. A severe mesolimbic connectivity derangement and reconfiguration are evident in females versus males. Below, dopaminergic mesolimbic network's connectivity matrices in PD females (B) and males (C). The matrices represent the significant differences obtained when comparing partial correlation coefficients between PD females < HC (B) and PD males < HC (C) in the dopaminergic mesolimbic network. The color bar displays values of the Z scores, for the comparison of partial correlation coefficients' strengths. The figure is from (Boccalini et al., 2021) in accordance to the fair use principle.

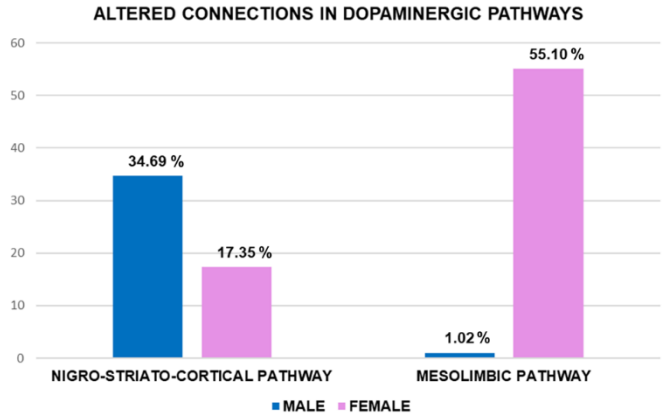

Figure 21. Percentage of altered connections (Opens access source). *The histograms show the percentage of altered connections in the dopaminergic pathways compared with the control group: nigro-striato-cortical and mesolimbic networks in PD females (pink) and males (blue). The figure is from (Boccalini et al., 2021) in accordance to the fair use principle.*

3.3.2 <u>Study 7</u>: Gender differences in dopaminergic system dysfunction in de novo Parkinson's disease clinical subtypes (Boccalini, Carli*, et al., 2022) – Published article*

Gender differences in neural anatomy and function, as well as the existence of different subtypes, are fundamental determinants of phenotypic variability in PD. Clinical criteria for subtypes, defined as mild motor predominant, intermediate, and diffuse-malignant, have been recently proposed in PD (Fereshtehnejad *et al.*, 2017). Despite the increasing interest in gender-related vulnerabilities, the impact of gender on different clinical subtypes is unknown. Gender and phenotype could interact, leading to distinct vulnerabilities. *Study 7* investigates gender differences in clinical subtypes, because of

their relevance in the clinical trajectories and underlying neurodegeneration (Fereshtehnejad *et al.*, 2017; De Pablo-Fernández *et al.*, 2019). In a large PPMI cohort of 286 newly diagnosed and drug-naïve idiopathic PD (iPD) patients (Males/Females: 189/97, age [mean ± SD]: 61.99 ± 9.67; disease duration: 2.08 ± 2.21), we studied whether gender modulates the clinical phenotypes and molecular endophenotype of patients stratified according to clinical criteria provided by Fereshtehnejad et al. (2017) (Fereshtehnejad *et al.*, 2017). We investigated gender differences in i) the presenting symptoms, ii) the amount of dopaminergic presynaptic dysfunction in nigrostriatal and mesolimbic systems, also considering extra-striatal targets, as assessed by [^{123}I]FP-CIT bindings, and iii) the molecular connectivity of the dopaminergic systems.

Clinical and demographic features in the whole iPD group (M/F:189/97) and the subtypes are reported in **Tables 11** and **12**, respectively. DAT imaging features are reported in **Tables 11** and **12**. According to clinical criteria (Fereshtehnejad *et al.*, 2017), 155 out of 286 patients with iPD presented the mild motor subtype (M/F: 116/39), 119 the intermediate (M/F, 68/51), and 12 the diffuse malignant subtype (M/F, 5/7).

Clinical gender differences:

Whole iPD group: Male patients presented a significantly higher education level and visuospatial performance, assessed by the JOLO test, compared to females. Females showed significantly higher STAI, SCOPA-AUT, HVLT, Semantic fluency, and SDMT scores than males (**Table 11**). The thermos- regulatory component produced the significant gender difference in SCOPA-AUT, where females showed higher scores than males (mean and SD females = 1.54 ± 1.51; mean and SD males = 0.91 ± 1.21; p = 0.000). Female patients showed higher motor symptoms asymmetry than males (mean and SD females = 8.15 ± 4.65; mean and SD males = 7.02 ± 4.06; p = 0.066).

Table 11. Demographic and clinical features of the whole iPD sample of Study 7

	iPD Males	**iPD Females**	**t-statistic**
Demographic Features			
N	189	97	
Age (mean±sd)	62.32±9.69	61.35±9.65	p=0.24
Education (mean±sd)	15.71±2.80	15.02±3.06	**p=0.03**
Disease Duration, y (mean±sd)	2.05±2.15	2.14±2.34	p=0.561

Clinical non-motor assessment (mean±sd)			
MoCA	27.02±2.30	27.41±2.24	p=0.233
REM Sleep Disorder Questionnaire	4.40±2.90	4.26±2.61	p=0.748
Epworth Sleepiness Scale	5.94±3.33	5.51±3.42	p=0.33
Scopa-AUT	10.99±8.68	15.89±9.65	**p=0.000**
UPSIT	22.08±8.18	24.05±8.63	p=0.096
Motor assessment (mean±sd)			
Schwab and England ADL scale	93.54±5.77	93.65±6.09	p=0.775
Hoehn and Yahr Staging	0.45±0.85	0.42±0.66	p=0.472
UPDRS total score	31.67±13.69	31.21±13.51	p=0.893
UPDRS I	5.48±3.96	6.27±4.68	p=0.129
UPDRS II	5.7±4.04	5.59±4.53	p=0.921
UPDRS III	20.5±9.17	19.34±8.02	p=0.369
Neurobehavioral assessment (mean±sd)			
GDS	5.3±1.46	5.27±1.23	p=0.792
QUIP	0.31±0.781	0.42±1.11	p=0.368
STAI- state score	46.81±5.40	48.48±5.29	**p=0.012**
STAI- trait score	45.66±4.57	47.01±3.60	**p=0.01**
STAI- total score	92.47±8.44	95.49±7.03	**p=0.002**
Cognitive assessment (mean±sd)			
Benton Judgment of Line Orientation	12.53±2.75	11.19±3.05	**p=0.000**
Letter Number Sequencing	11.33±2.63	11.42±2.78	p=0.862
HVLT total immediate recall t-score	43.81±10.98	48.91±9.93	**p=0.000**
HVLT delayed recall t-score	43.38±10.83	47.27±11.10	**p=0.005**
HVLT recognition t-score	43.84±10.862	46.55±11.83	p=0.064
Semantic Fluency t-score	46.05±10.62	52.65±11.05	**p=0.000**
Symbol Digit t-score	44.68±8.85	47.89±8.50	**p=0.004**

Abbreviations: iPD, idiopathic Parkinson's disease; N, Number; sd, standard deviation; y, years; MoCA, Montreal Cognitive Assessment; UPSIT, Smell identification test; UPDRS, Unified Parkinson's Disease Rating Scale; GDS, Geriatric Depression Scale; QUIP, Questionnaire for Impulsive-Compulsive Disorders in Parkinson's Disease–Rating Scale; STAI, State-Trait Anxiety Inventory; HVLT, Hopkins Verbal Learning Test

Mild motor subtype: Females showed significantly higher/better performances in memory (HVLT), executive functions (Semantic fluency), and processing speed (SDMT) than males (**Table 10**). Female and male patients did not differ in motor symptoms asymmetry (p = 0.183).

Intermediate subtype: Males presented significantly higher visuospatial performance (JOLO) than females, and more severe sleep disorders, as measured by Epworth Sleepiness Scale and RBD Questionnaire, compared to females. Females showed significantly higher anxiety (STAI) and autonomic deficits (SCOPA-AUT) and better cognitive performances – memory (HVLT), executive function (semantic fluency), and processing speed (SDMT) – than males (**Table 10**). Female and male patients did not differ in motor symptoms asymmetry (p = 0.225).

Diffuse malignant subtype: Males presented significantly higher MDS-UPDRS total and MDS-UPDRS III scores than females (**Table 10**). Female and male patients did not differ in motor symptoms asymmetry (p = 0.126).

Table 12. Demographic and clinical features of iPD subtypes

	MILD MOTOR-PREDOMINANT iPD				**INTERMEDIATE iPD**				**DIFFUSE MALIGNANT iPD**			
	whole group	**M**	**F**	***t-statistic***	**whole group**	**M**	**F**	***t-statistic***	**whole group**	**M**	**F**	***t-statistic***
Demographic Features												
N	155	116	39		119	68	51		12	5	7	
Age	60.27 ±9.46	60.58 ±9.60	59.36 ±9.09	*p=0.24*	64.11 ±9.31	64.53 ±9.12	63.55 ±9.62	*p=0.505*	63.17 ±12.24	72.6 ±8.50	56.43 ±9.98	***p=0.018***
Education	15.76 ±2.98	15.89 ±2.90	15.38 ±3.21	*p=0.322*	15 ±2.70	15.26 ±2.612	14.65 ±2.81	*p=0.157*	16.58 ±3.28	17.8 ±1.30	15.71 ±4.07	*p=0.343*
Disease Duration, y	1.81 ±1.48	1.78 ±1.46	1.91 ±1.54	*p=0.389*	2.40 ±2.93	2.47 ±2.98	2.30 ±2.89	*p=0.859*	2.37 ±1.50	2.67 ±1.36	2.16 ±1.66	*p=0.432*
Clinical non-motor Assessment (mean±sd)												
MoCA	27.55 ±2.03	27.48 ±2.08	27.74 ±1.89	*p=0.572*	26.58 ±2.51	26.31 ±2.50	26.96 ±2.50	*p=0.177*	27.58 ±1.88	26.00 ±1.58	28.71 ±1.11	*p=0.073*
REM Sleep Disorder Questionnaire	3.57 ±2.23	3.54 ±2.31	3.67 ±2.02	*p=0.733*	5.11 ±2.99	5.66 ±3.14	4.36 ±2.61	***p=0.019***	7.00 ±3.91	7.20 ±4.21	6.86 ±4.02	*p=0.805*
Epworth Sleepiness Scale	5.66 ±3.33	5.59 ±3.24	5.90 ±3.63	*p=0.599*	5.93 ±3.39	6.56 ±3.45	5.08 ±3.14	***p=0.019***	6.08 ±3.70	5.60 ±3.36	6.43 ±4.16	*p=0.485*

Scopa-AUT	6.87 ±3.47	6.84 ±3.57	6.95 ±3.19	*p=0.768*	19.34 ±9.67	17.56 ±10.59	21.76 ±7.71	***p=0.008***	21.33 ±5.91	18.00 ±2.0	23.71 ±6.75	***p=0.046***
UPSIT	23.73 ±7.87	23.21 ±7.89	25.28 ±7.71	*p=0.207*	21.63 ±8.83	20.56 ±8.46	23.08 ±9.20	*p=0.169*	21.00 ±8.94	16.60 ±6.35	24.14 ±9.60	*p=0.362*
Motor Assessment (mean±sd)												
Schwab and England ADL scale	94.16 ±5.18	93.97 ±5.08	94.74 ±5.49	*p=0.292*	93.52 ±6.24	93.31 ±6.55	93.8 ±5.85	*p=0.65*	86.67 ±6.51	87 ±6.70	86.43 ±6.90	*p=0.66*
Hoehn and Yahr Staging	0.26 ±0.54	0.26 ±0.53	0.28 ±0.56	*p=0.133*	0.64 ±1.00	0.78 ±1.17	0.46 ±0.68	*p=0.962*	0.67 ±0.78	0.40 ±0.55	0.86 ±0.90	*p=0.36*
UPDRS total score	27.61 ±11.39	28.3 ±11.89	25.56 ±9.59	*p=0.241*	33.84 ±12.26	35.06 ±12.43	32.18 ±11.94	*p=0.223*	59.08 ±16.37	63.8 ±18.56	55.71 ±15.16	***p=0.008***
UPDRS I	4.32 ±3.11	4.31 ±3.19	4.33 ±2.91	*p=0.926*	6.84 ±4.2	6.94 ±4.13	6.7 ±4.32	*p=0.652*	13.42 ±5.69	12.6 ±4.393	14 ±6.758	*p=0.691*
UPDRS II	4.68 ±3.44	4.97 ±3.73	3.79 ±2.20	*p=0.072*	6.03 ±3.78	6.43 ±3.97	5.48 ±3.48	*p=0.224*	14.83 ±5.68	12.6 ±4.61	16.43 ±6.16	*p=0.749*
UPDRS III	18.62 ±8.08	19.02 ±8.28	17.44 ±7.43	*p=0.36*	20.97 ±8.34	21.69 ±8.48	20 ±8.13	*p=0.306*	30.83 ±13.46	38.6 ±16.72	25.29 ±7.74	***p=0.000***
Neurobehavioral assessment (mean±sd)												
GDS	5.23 ±1.26	5.25 ±1.33	5.15 ±1.04	*p=0.613*	5.41 ±1.54	5.44 ±1.67	5.36 ±1.36	*p=0.7*	4.92 ±1.31	4.4 ±1.14	5.29 ±1.38	*p=0.31*
QUIP	0.24 ±0.81	0.22 ±0.57	0.31 ±1.30	*p=0.549*	0.47 ±1.01	0.49 ±1.04	0.46 ±0.99	*p=0.842*	0.5 ±0.67	0.2 ±0.44	0.71 ±0.75	*p=0.089*
STAI- state score	47.1 ±5.36	46.86 ±5.53	47.82 ±4.82	*p=0.326*	47.86 ±5.33	46.97 ±5.18	49.06 ±5.34	***p=0.034***	46.08 ±6.88	43.4 ±5.32	48 ±7.59	*p=0.099*
STAI- trait score	45.94 ±4.42	45.63 ±4.63	46.85 ±3.65	*p=0.124*	46.64 ±4.04	45.96 ±4.5	47.58 ±3.13	***p=0.03***	43.25 ±4.39	42.4 ±3.36	43.86 ±5.17	*p=0.346*
STAI- total score	93.04 ±8.13	92.49 ±8.48	94.67 ±6.81	*p=0.137*	94.5 ±7.83	92.93 ±8.38	96.64 ±6.48	***p=0.01***	89.33 ±9.42	85.8 ±6.79	91.86 ±10.68	*p=0.094*
Cognitive Assessment (mean ±sd)												
Benton Judgment of Line Orientation	12.97 ±2.42	13.15 ±2.27	12.44 ±2.81	*p=0.081*	10.97 ±3.19	11.49 ±3.24	10.27 ±3.00	***p=0.038***	11.38 ±2.02	12.19 ±0.99	10.81 ±2.43	*p=0.089*
Letter Number Sequencing	11.57 ±2.49	11.66 ±2.49	11.31 ±2.49	*p=0.382*	11.03 ±2.94	10.84 ±2.86	11.30 ±3.05	*p=0.381*	11.83 ±1.99	10.40 ±0.55	12.86 ±2.04	*p=0.12*
HVLT total immediate recall t-score	45.99 ±10.23	44.89 ±10.52	49.28 ±8.63	***p=0.021***	44.92 ±12.04	42.1 ±11.93	48.76 ±11.21	***p=0.002***	45.5 ±6.86	42.2 ±3.70	47.86 ±7.86	*p=0.218*

HVLT delayed recall t-score	45.68 ±10.52	44.85 ±10.67	48.15 ±97.73	*p=0.095*	43.42 ±11.58	40.94 ±11.02	46.8 ±11.56	***p=0.005***	44.25 ±12.32	42.2 ±6.09	45.71 ±15.73	*p=0.41*
HVLT recognition t-score	45.53 ±11.12	44.84 ±11.00	47.56 ±11.38	*p=0.214*	44.26 ±11.17	42.84 ±10.15	46.2 ±12.27	*p=0.103*	39.5 ±12.859	34 ±12.981	43.43 ±12.15	*p=0.53*
Semantic Fluency t-score	49.63 ±11.51	47.45 ±10.10	56.10 ±13.06	***p=0.000***	46.65 ±10.49	43.99 ±11.09	50.28 ±8.44	***p=0.002***	46.67 ±12.31	41.60 ±12.3	50.29 ±11.81	*p=0.727*
Symbol Digit t-score	47.17 ±7.90	46.25 ±7.44	49.89 ±8.66	***p=0.012***	44.52 ±9.78	42.68 ±10.36	47.02 ±8.40	***p=0.014***	39.88 ±6.99	35.50 ±6.66	43.00 ±5.73	*p=0.079*

Abbreviations: iPD, idiopathic Parkinson's disease; N, Number; sd, standard deviation; y, years; MoCA, Montreal Cognitive Assessment; UPSIT, Smell identification test; UPDRS, Unified Parkinson's Disease Rating Scale; GDS, Geriatric Depression Scale; QUIP, Questionnaire for Impulsive-Compulsive Disorders in Parkinson's Disease–Rating Scale; STAI, State-Trait Anxiety Inventory; HVLT, Hopkins Verbal Learning Test

[^{123}I]FP-CIT SPECT imaging differences:

Whole iPD group: Female patients presented more significant SUVr decreases than males in several ROIs innervated by the mesolimbic dopaminergic system, namely the amygdala, the parahippocampus and hippocampus, the insula, the anterior and middle cingulate cortex, the thalamus, bilaterally. The pallidum and the precentral cortex of females were also more depleted than males (**Table 13**). Female patients showed more significant DAT asymmetry in the putamen than males (mean and SD females = 0.36 ± 0.23; mean and SD males = 0.32 ± 0.27; p = 0.043). We observed a significant negative correlation between MDS-UPDRS III and SUVr in the putamen and globus pallidus in males (p = 0.001, r = − 0.233; p = 0.037, r = − 0.139, respectively) and in the precentral gyrus and the opIFG in females (p = 0.048, r = − 0.190; p = 0.029, r = − 0.216, respectively).

Table 13. [^{123}I]FP-CIT SPECT imaging gender differences in the whole group

	iPD Males N=189	**HC Males N=39**	**statistic HC vs iPD**	**iPD Females N=97**	**HC Females N=34**	**statistic HC vs iPD**	**statistic M iPD vs F iPD**
Ipsilateral Caudate	1.26±0.42	1.55±0.30	***p=0.000***	1.25±0.45	1.55±0.25	***p=0.000***	*p=0.649*
Contralateral Caudate	1.37±0.43	1.53±0.30	***p=0.021***	1.44±0.49	1.54±0.24	*p=0.140*	*p=0.394*
Ipsilateral Putamen	1.09±0.37	2.29±0.29	***p=0.000***	1.06±0.45	2.23±0.24	***p=0.000***	*p=0.286*
Contralateral Putamen	1.40±0.46	2.14±0.26	***p=0.000***	1.43±0.55	2.06±0.24	***p=0.000***	*p=0.911*

Ipsilateral Dorsal Caudate	1.32±0.54	1.61±0.34	***p=0.002***	1.26±0.61	1.63±0.27	***p=0.001***	*p=0.183*
Contralateral Dorsal Caudate	1.45±0.58	1.55±0.32	*p=0.198*	1.53±0.63	1.60±0.26	*p=0.465*	*p=0.594*
Ipsilateral Dorsal Putamen	1.19±0.44	2.56±0.32	***p=0.000***	1.07±0.48	2.50±0.24	***p=0.000***	***p=0.018***
Contralateral Dorsal Putamen	1.56±0.53	2.56±0.30	***p=0.000***	1.52±0.60	2.47±0.26	***p=0.000***	*p=0.302*
Ipsilateral Ventral Striatum	2.11±0.45	2.87±0.40	***p=0.000***	2.09±0.47	2.80±0.30	***p=0.000***	*p=0.783*
Contralateral Ventral Striatum	2.27±0.51	3.27±0.44	***p=0.000***	2.32±0.54	3.27±0.37	***p=0.000***	*p=0.484*
Ipsilateral Thalamus	0.57±0.22	1.12±0.16	***p=0.000***	0.38±0.16	1.05±0.16	***p=0.000***	***p=0.000***
Contralateral Thalamus	0.57±0.21	1.18±0.16	***p=0.000***	0.40±0.16	1.11±0.18	***p=0.000***	***p=0.000***
Ipsilateral Globus Pallidus	1.42±0.51	0.20±0.10	***p=0.000***	1.15±0.46	0.11±0.06	***p=0.000***	***p=0.000***
Contralateral Globus Pallidus	1.66±0.58	0.18±0.08	***p=0.000***	1.43±0.56	0.12±0.07	***p=0.000***	***p=0.001***
Ipsilateral Amygdala	0.42±0.25	0.71±0.22	***p=0.000***	0.31±0.24	0.64±0.17	***p=0.000***	***p=0.000***
Contralateral Amygdala	0.46±0.30	0.73±0.18	***p=0.000***	0.32±0.25	0.57±0.18	***p=0.000***	***p=0.000***
Ipsilateral Hippocampus	0.37±0.19	0.57±0.17	***p=0.000***	0.24±0.14	0.48±0.14	***p=0.000***	***p=0.000***
Contralateral Hippocampus	0.40±0.20	0.59±0.16	***p=0.000***	0.25±0.15	0.49±0.15	***p=0.000***	***p=0.000***
Ipsilateral Parahippocampus	0.26±0.18	0.30±0.14	*p=0.163*	0.14±0.15	0.21±0.13	***p=0.024***	***p=0.000***
Contralateral Parahippocampus	0.27±0.18	0.29±0.16	*p=0.624*	0.14±0.13	0.22±0.12	***p=0.006***	***p=0.000***
Ipsilateral Insula	0.38±0.15	0.67±0.13	***p=0.000***	0.29±0.12	0.63±0.15	***p=0.000***	***p=0.000***
Contralateral Insula	0.40±0.16	0.61±0.13	***p=0.000***	0.36±0.16	0.59±0.13	***p=0.000***	***p=0.033***
Ipsilateral Olfactory	0.57±0.37	1.03±0.25	***p=0.000***	0.54±0.37	0.96±0.25	***p=0.000***	*p=0.531*
Contralateral Olfactory	0.59±0.37	1.05±0.26	***p=0.000***	0.59±0.39	1.03±0.23	***p=0.000***	*p=0.959*
Ipsilateral Anterior Cingulate	0.25±0.14	0.42±0.11	***p=0.000***	0.14±0.09	0.34±0.12	***p=0.000***	***p=0.000***
Contralateral Anterior Cingulate	0.26±0.14	0.41±0.13	***p=0.000***	0.15±0.09	0.35±0.12	***p=0.000***	***p=0.000***
Ipsilateral Middle Cingulate	0.27±0.14	0.47±0.13	***p=0.000***	0.15±0.09	0.37±0.12	***p=0.000***	***p=0.000***
Contralateral Middle Cingulate	0.28±0.14	0.46±0.13	***p=0.000***	0.15±0.09	0.38±0.12	***p=0.000***	***p=0.000***
Ipsilateral opIFG	0.16±0.15	0.18±0.09	*p=0.890*	0.11±0.10	0.19±0.12	***p=0.003***	***p=0.016***
Contralateral opIFG	0.13±0.13	0.15±0.09	*p=0.534*	0.10±0.11	0.14±0.08	*p=0.060*	*p=0.075*
Ipsilateral precentral	0.13±0.13	0.28±0.10	***p=0.000***	0.06±0.06	0.22±0.12	***p=0.000***	***p=0.000***
Contralateral precentral	0.09±0.09	0.30±0.11	***p=0.000***	0.05±0.06	0.23±0.10	***p=0.000***	***p=0.007***

Abbreviations: iPD, idiopathic Parkinson's disease; HC, healthy controls; N, number; opIFG, inferior frontal gyrus pars opercularis

Mild motor subtype: As in the whole group, females showed lower SUVr than males in several dopaminergic mesolimbic targets, namely the amygdala, the parahippocampus and hippocampus, the insula, the anterior and middle cingulate cortex, thalamus, bilaterally (**Table 14**). Female and male patients did not differ in DAT asymmetry in the putamen (p = 0.574). A significant correlation between MDS-UPDRS III and SUVr in the puta- men and globus pallidus was found only in males (p = 0.007, r = − 0.247; p = 0.020, r = − 0.209, respectively). In females, lower SUVr in the amygdala was associated with higher STAI (trait scores) (p = 0.035, r = − 0.393).

Intermediate subtype: Female patients presented significantly decreased SUVr than males in several ROIs, namely the amygdala, the hippocampus and parahippocampus, the anterior and middle cingulate cortex, bilaterally, and the ipsilateral insula (**Table 14**). Female patients showed significantly higher DAT asymmetry in the putamen than males (mean and SD females = 0.34 ± 0.21; mean and SD males = 0.28 ± 0.27; p = 0.024. We observed a significant correlation between SUVr in the opIFG and STAI (trait scores) in females (p = 0.029, r = − 0.329).

Diffuse malignant subtype: Females showed significantly higher SUVR in the ipsilateral putamen compared to males. Female patients presented less significantly decreased SUVr than males in some dopaminergic mesolimbic targets, namely in the ipsilateral ventral striatum, ipsilateral anterior cingulate, contralateral insula, and ipsilateral opIFG (**Table 14**). Female and male patients did not differ in DAT asymmetry in the putamen (p = 0.082).

Table 14. [^{123}I]FP-CIT SPECT imaging gender differences in the subtypes

	MILD MOTOR-PREDOMINANT iPD				**INTERMEDIATE iPD**				**DIFFUSE MALIGNANT iPD**			
	whole group	**M**	**F**	**P value**	**whole group**	**M**	**F**	**P value**	**whole group**	**M**	**F**	**P value**
N	155	116	39		119	68	51		12	5	7	
Ipsilateral Caudate	1.28 ±0.43	1.27 ±0.42	1.29 ±0.45	*0.915*	1.23 ±0.44	1.24 ±0.43	1.21 ±0.45	*0.879*	1.27 ±0.50	1.31 ±0.49	1.24 ±0.54	*0.326*

Contralateral Caudate	1.39 ±0.42	1.37 ±0.41	1.43 ±0.45	*0.689*	1.40 ±0.48	1.37 ±0.45	1.44 ±0.52	*0.464*	1.42 ±0.45	1.35 ±0.40	1.47 ±0.51	*0.142*
Ipsilateral Putamen	1.07 ±0.36	1.08 ±0.36	1.03 ±0.35	*0.249*	1.09 ±0.44	1.12 ±0.39	1.07 ±0.49	*0.531*	1.14 ±0.45	1.09 ±0.25	1.18 ±0.57	***0.045***
Contralateral Putamen	1.41 ±0.48	1.42 ±0.45	1.40 ±0.54	*0.634*	1.40 ±0.51	1.39 ±0.49	1.41 ±0.55	*0.887*	1.52 ±0.59	1.32 ±0.34	1.66 ±0.71	*0.079*
Ipsilateral Dorsal Caudate	1.36 ±0.56	1.34 ±0.52	1.42 ±0.66	*0.673*	1.25 ±0.57	1.29 ±0.57	1.19 ±0.56	*0.324*	1.12 ±0.47	1.44 ±0.51	0.90 ±0.29	*0.756*
Contralateral Dorsal Caudate	1.51 ±0.59	1.47 ±0.59	1.63 ±0.60	*0.505*	1.44 ±0.61	1.41 ±0.56	1.48 ±0.68	*0.602*	1.37 ±0.45	1.39 ±0.59	1.36 ±0.38	*0.704*
Ipsilateral Dorsal Putamen	1.15 ±0.44	1.18 ±0.44	1.07 ±0.43	*0.127*	1.16 ±0.48	1.22 ±0.45	1.09 ±0.52	*0.141*	1.06 ±0.43	1.16 ±0.38	0.99 ±0.48	*0.150*
Contralateral Dorsal Putamen	1.56 ±0.53	1.57 ±0.51	1.51 ±0.60	*0.218*	1.54 ±0.58	1.55 ±0.56	1.53 ±0.60	*0.736*	1.44 ±0.63	1.39 ±0.57	1.48 ±0.71	*0.375*
Ipsilateral ventral Striatum	2.08 ±0.44	2.08 ±0.45	2.08 ±0.41	*0.963*	2.11 ±0.45	2.14 ±0.46	2.08 ±0.45	*0.478*	2.24 ±0.68	2.24 ±0.26	2.23 ±0.90	***0.042***
Contralateral ventral Striatum	2.27 ±0.49	2.27 ±0.49	2.29 ±0.50	*0.854*	2.30 ±0.53	2.28 ±0.55	2.32 ±0.50	*0.597*	2.46 ±0.77	2.34 ±0.37	2.54 ±0.99	*0.096*
Ipsilateral Thalamus	0.53 ±0.22	0.58 ±0.22	0.38 ±0.16	***0.000***	0.48 ±0.22	0.55 ±0.22	0.38 ±0.16	***0.000***	0.40 ±0.14	0.48 ±0.17	0.35 ±0.09	*0.301*
Contralateral Thalamus	0.54 ±0.22	0.58 ±0.22	0.41 ±0.17	***0.000***	0.49 ±0.20	0.56 ±0.20	0.40 ±0.16	***0.000***	0.41 ±0.12	0.47 ±0.12	0.37 ±0.11	*0.734*
Ipsilateral Globus Pallidus	1.36 ±0.50	1.45 ±0.49	1.11 ±0.42	***0.000***	1.30 ±0.53	1.38 ±0.54	1.18 ±0.50	*0.067*	1.28 ±0.38	1.43 ±0.36	1.16 ±0.38	*0.284*
Contralateral Globus Pallidus	1.62 ±0.61	1.69 ±0.61	1.42 ±0.57	***0.012***	1.53 ±0.54	1.62 ±0.52	1.42 ±0.55	*0.076*	1.62 ±0.53	1.61 ±0.52	1.63 ±0.58	*0.478*
Ipsilateral Amygdala	0.38 ±0.25	0.42 ±0.26	0.27 ±0.17	***0.001***	0.38 ±0.27	0.42 ±0.25	0.31 ±0.28	***0.028***	0.47 ±0.19	0.49 ±0.16	0.47 ±0.23	*0.262*

Contralateral Amygdala	0.42 ±0.29	0.45 ±0.30	0.33 ±0.22	***0.014***	0.39 ±0.29	0.48 ±0.29	0.28 ±0.27	***0.000***	0.48 ±0.25	0.48 ±0.27	0.48 ±0.25	*0.171*
Ipsilateral Hippocampus	0.33 ±0.18	0.37 ±0.18	0.22 ±0.11	***0.000***	0.32 ±0.19	0.37 ±0.20	0.24 ±0.15	***0.000***	0.33 ±0.20	0.31 ±0.19	0.35 ±0.21	*0.148*
Contralateral Hippocampus	0.36 ±0.20	0.39 ±0.20	0.25 ±0.14	***0.000***	0.33 ±0.19	0.40 ±0.20	0.24 ±0.15	***0.000***	0.37 ±0.18	0.42 ±0.13	0.33 ±0.20	*0.269*
Ipsilateral Parahippocampus	0.23 ±0.17	0.27 ±0.17	0.14 ±0.12	***0.000***	0.20 ±0.19	0.25 ±0.19	0.14 ±0.17	***0.003***	0.22 ±0.20	0.27 ±0.19	0.19 ±0.21	*0.416*
Contralateral Parahippocampus	0.24 ±0.19	0.28 ±0.19	0.15 ±0.14	***0.000***	0.22 ±0.18	0.28 ±0.19	0.13 ±0.13	***0.000***	0.24 ±0.16	0.27 ±0.16	0.22 ±0.17	*0.625*
Ipsilateral Insula	0.35 ±0.16	0.37 ±0.16	0.28 ±0.13	***0.000***	0.35 ±0.15	0.40 ±0.16	0.29 ±0.11	***0.000***	0.38 ±0.14	0.38 ±0.07	0.37 ±0.18	*0.110*
Contralateral Insula	0.40 ±0.16	0.41 ±0.17	0.35 ±0.15	***0.030***	0.39 ±0.16	0.40 ±0.17	0.38 ±0.15	*0.488*	0.38 ±0.22	0.41 ±0.07	0.35 ±0.29	***0.018***
Ipsilateral Olfactory	0.55 ±0.37	0.56 ±0.38	0.49 ±0.33	*0.227*	0.57 ±0.35	0.60 ±0.38	0.53 ±0.31	*0.378*	0.81 ±0.61	0.64 ±0.25	0.94 ±0.78	*0.148*
Contralateral Olfactory	0.57 ±0.36	0.58 ±0.36	0.53 ±0.35	*0.485*	0.60 ±0.37	0.60 ±0.39	0.58 ±0.35	*0.796*	0.89 ±0.56	0.76 ±0.32	0.98 ±0.69	*0.065*
Ipsilateral Anterior Cingulate	0.22 ±0.14	0.25 ±0.14	0.14 ±0.11	***0.000***	0.22 ±0.14	0.27 ±0.15	0.14 ±0.08	***0.000***	0.22 ±0.16	0.34 ±0.12	0.13 ±0.11	***0.034***
Contralateral Anterior Cingulate	0.23 ±0.14	0.26 ±0.14	0.15 ±0.10	***0.000***	0.22 ±0.15	0.28 ±0.16	0.15 ±0.09	***0.000***	0.22 ±0.14	0.30 ±0.06	0.16 ±0.16	*0.213*
Ipsilateral Middle Cingulate	0.24 ±0.14	0.27 ±0.14	0.15 ±0.10	***0.000***	0.23 ±0.14	0.29 ±0.15	0.16 ±0.09	***0.000***	0.19 ±0.11	0.27 ±0.08	0.13 ±0.09	*0.930*
Contralateral Middle Cingulate	0.25 ±0.15	0.28 ±0.15	0.15 ±0.10	***0.000***	0.23 ±0.14	0.29 ±0.14	0.16 ±0.09	***0.000***	0.19 ±0.12	0.28 ±0.10	0.13 ±0.10	*0.494*
Ipsilateral opIFG	0.14 ±0.15	0.15 ±0.16	0.11 ±0.09	*0.151*	0.16 ±0.14	0.18 ±0.16	0.13 ±0.11	*0.072*	0.13 ±0.17	0.22 ±0.08	0.07 ±0.19	***0.031***

Contralateral opIFG	0.12 ±0.13	0.13 ±0.13	0.11 ±0.12	*0.294*	0.12 ±0.12	0.14 ±0.14	0.10 ±0.09	*0.063*	0.18 ±0.17	0.20 ±0.13	0.17 ±0.20	*0.531*
Ipsilateral precentral	0.10 ±0.10	0.12 ±0.11	0.07 ±0.07	***0.009***	0.10 ±0.09	0.13 ±0.11	0.07 ±0.06	***0.002***	0.06 ±0.09	0.13 ±0.10	0.01 ±0.04	*0.188*
Contralateral precentral	0.09 ±0.09	0.09 ±0.09	0.07 ±0.08	*0.284*	0.07 ±0.08	0.09 ±0.10	0.05 ±0.06	***0.047***	0.08 ±0.09	0.13 ±0.11	0.04 ±0.05	*0.514*
Abbreviations: iPD, idiopathic Parkinson's disease; N, number; opIFG, inferior frontal gyrus pars opercularis												

Gender differences in molecular connectivity of nigrostriatal dopaminergic system

Whole iPD group: Male patients were characterized by a widespread alteration of molecular connectivity within the nigrostriatal dopaminergic system, with 15% of altered connections compared to HC. The connectivity alterations involved the dorsal caudate and dorsal putamen bilaterally (**Figure 18A**). On the contrary, the metabolic connectivity architecture of this network was relatively spared in females (only 6% changes in comparison with HC). The few molecular alterations affected the connections between the contralateral precentral gyrus and bilateral opIFG (**Figure 18B**). The direct comparison between males and females showed that the molecular connectivity alterations were significantly more severe in male patients than in females ($\chi^2 = 4.30$, $p = 0.037$).

Mild motor subtype: Male patients were characterized by 18% of altered connections within the nigrostriatal dopaminergic system compared to HC. Males displayed altered connections between the dorsal putamen and dorsal caudate and between the precentral gyri and ipsilateral opIFG (**Figure 19A**). The connectivity reconfiguration of the nigrostriatal network was spared in female patients (only 3% changes than HC), showing altered connections between the contralateral precentral gyrus and contralateral opIFG (**Figure 19B**). The direct comparison between male and female patients showed that the molecular connectivity alterations were significantly more severe in males than females ($\chi^2 = 11.97$, $p = 0.000$).

Intermediate subtype: Male patients were characterized by a 15% of altered connections within the nigrostriatal network compared to HC. The connectivity alterations involved

the dorsal caudate and dorsal putamen bilaterally (**Figure 19C**). The same network displayed 12% of connectivity changes in female patients in comparison with HC. Females' reconfiguration was characterized by altered connections between the dorsal caudate, the contralateral precentral gyrus, and the ipsilateral opIFG. Specifically, the ipsilateral opIFG lost connections with the contralateral precentral gyrus, which showed altered connectivity with the contralateral dorsal caudate (**Figure 19D**). Male patients showed a more severe connectivity alteration than females without reaching the threshold of significance ($\chi^2 = 0.385$; $p = 0.534$).

Gender differences in molecular connectivity of mesolimbic dopaminergic system

Whole iPD group: Mesolimbic system was relatively spared in male patients showing 7% of altered connections compared to HC. The connectivity alterations mainly affected the bilateral ventral striatum, the contralateral hippocampus, and the contralateral amygdala (**Figure 22C**). In the same network, female patients showed 11% of altered connections in comparison with HC. The molecular connectivity alterations characterized several structures: the contralateral ventral striatum, hippocampus, parahippocampus, insula, and anterior cingulate bilaterally (**Figure 22D**). Female patients showed higher connectivity alterations than males without reaching the threshold of significance ($\chi^2 = 0.976$; $p = 0.322$).

Mild motor subtype: Male patients were characterized by 15% of altered connections within the mesolimbic system compared to HC. The connectivity alterations mainly involved the bilateral hippocampus, parahippocampus, and amygdala, where the contralateral hippocampus featured the highest number of altered connections (**Figure 23E**). On the other hand, the mesolimbic network in female patients showed a 17% of altered connection. The contralateral insula showed the highest number of altered connections, followed by the bilateral middle cingulate, olfactory cortex, and the contralateral ventral striatum (**Figure 23F**). Female patients showed higher connectivity alterations than males, however, without reaching the threshold of significance ($\chi 2 = 0.148$; $p = 0.699$).

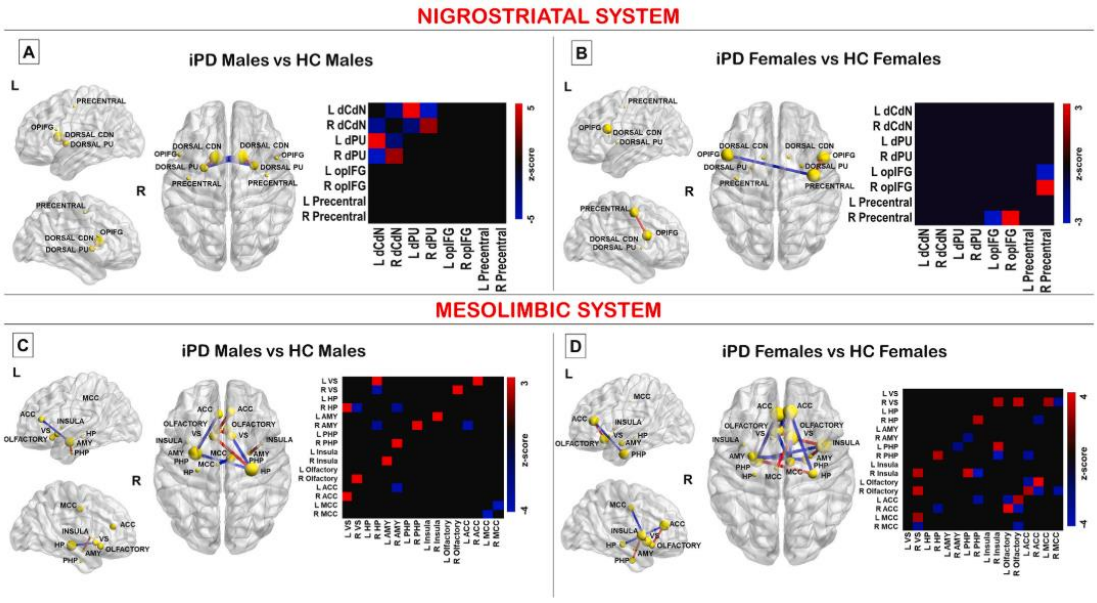

Figure 22. Dopaminergic connectivity analyses in the whole group with idiopathic Parkinson's disease (Open access source). *3D brain templates display the nodes and the edges of (A) the nigrostriatal system connectivity for male patients with idiopathic Parkinson's disease (iPD), and (B) the nigrostriatal system connectivity for iPD females; (C) the mesolimbic system connectivity for iPD males; and (D) the mesolimbic system connectivity for iPD females. Altered connections are presented: in red, the increased and in blue the decreased connections compared with healthy controls (HC). The dimension of each node depends on the total node number of connections represented by the size of each yellow dot. Next to each brain templates, the matrices represent the significant differences obtained when comparing partial correlation coefficients between iPD males < HC (A, C) and iPD females < HC (B, D) in the dopaminergic networks. The colour bar displays the Z scores' values to compare partial correlation coefficients' strengths. A nigrostriatal connectivity derangement and reconfiguration is evident in males versus females. A mesolimbic connectivity derangement and reconfiguration is evident in females versus males. Abbreviations: 3D, three-dimensional; iPD, idiopathic Parkinson's disease; HC, healthy controls, L, left; R, right; dCdN, dorsal caudate nucleus; dPU, dorsal putamen, opIFG, inferior frontal gyrus (pars opercularis); VS, ventral striatum, HP, hippocampus; AMY, amygdala; PHP, parahippocampus; ACC, anterior cingulate cortex, MCC, middle cingulate cortex. The figure is from* (Boccalini, Carli, Pilotto, *et al.*, 2022) *in accordance to the fair use principle.*

Intermediate subtype: Mesolimbic system was relatively spared in male patients showing 7% of altered connections. The alterations mainly involved the contralateral amygdala and the ipsilateral olfactory cortex, showing the highest number of altered connections (**Figure 23G**). The same network displayed 17% metabolic connectivity changes in

female patients. The contralateral ventral striatum showed the highest number of altered connections, followed by the contralateral middle cingulate, the ipsilateral parahippocampus, and the ipsilateral olfactory cortex (**Figure 23H**). The direct comparison between male and female patients showed that the molecular connectivity alterations were significantly more severe in females than males ($\chi^2 = 4.73$, $p = 0.029$).

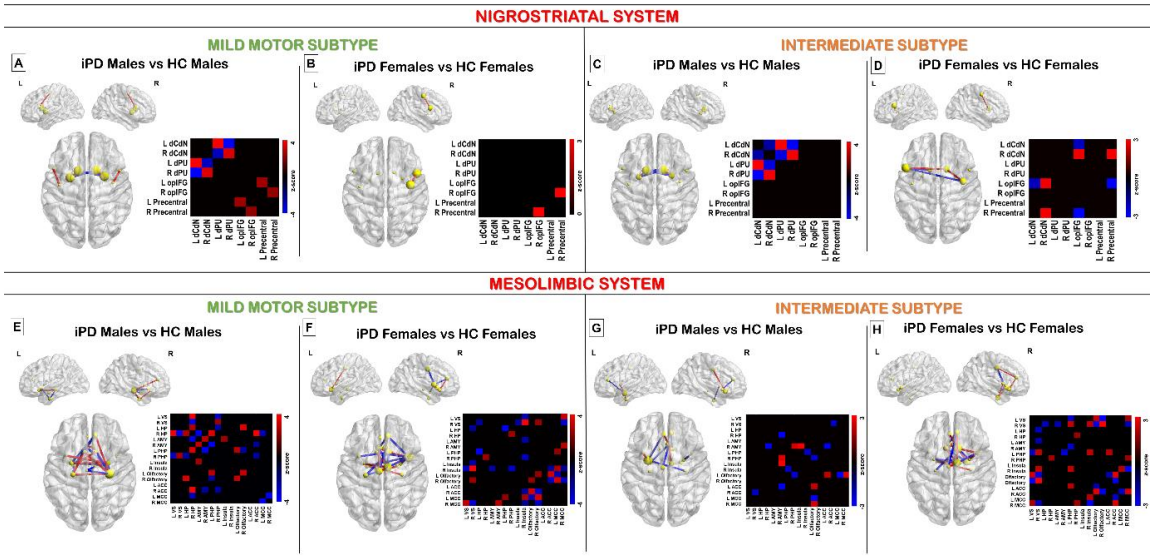

Figure 23. Dopaminergic connectivity analyses in the clinical subtypes of idiopathic Parkinson's disease (Open access source). *3D brain templates display the nodes and the edges of (A) the nigrostriatal system connectivity for male patients with idiopathic Parkinson's disease (iPD), and (B) the nigrostriatal system connectivity for iPD females; (C) the mesolimbic system connectivity for iPD males; and (D) the mesolimbic system connectivity for iPD females. Altered connections are presented: in red, the increased and in blue the decreased connections compared with healthy controls (HC). The dimension of each node depends on the total node number of connections rep- resented by the size of each yellow dot. Next to each brain templates, the matrices represent the significant differences obtained when comparing partial correlation coefficients between iPD males < HC (A, C) and iPD females < HC (B, D) in the dopaminergic networks. The colour bar displays the Z scores' values to compare partial correlation coefficients' strengths. A nigrostriatal connectivity derangement and reconfiguration is evident in males versus females. A mesolimbic connectivity derangement and reconfiguration is evident in females versus males. Abbreviations: 3D, three-dimensional; iPD, idiopathic Parkinson's disease; HC, healthy controls, L, left; R, right; dCdN, dorsal caudate nucleus; dPU, dorsal putamen, opIFG, inferior frontal gyrus (pars opercularis); VS, ventral striatum, HP, hippocampus; AMY, amygdala; PHP,*

parahippocampus; ACC, anterior cingulate cortex, MCC, middle cingulate cortex. The figure is from (Boccalini, Carli, Pilotto, *et al.*, 2022) *in accordance to the fair use principle.*

3.3.3 Study 8: Sex differences in dementia with Lewy bodies: an imaging study of neurotransmission pathways (Boccalini, et al., 2023) – Published article

Considering the recent reported clinical and pathological differences in DLB, *Study 8* aims to explore sex differences by using ^{123}I-FP- CIT binding in striatal and extrastriatal regions in female and male patients. We included 123 probable DLB (pDLB) patients (male/female: 77/46) and 78 control subjects (male/female: 34/44) for comparison. We assessed sex differences in the dopaminergic activity of the nigrostriatal and mesolimbic systems using regional-based and voxel-wise analyses of [^{123}I]FP-CIT binding. Considering the affinity of [^{123}I]FP-CIT for transporters involved in different neurotransmission systems (i.e., high-to-low affinity for dopaminergic (DAT), serotonin (SERT), and norepinephrine (NET) transporters, respectively) (Scheffel *et al.*, 1997; Booij *et al.*, 2007; Booij and Kemp, 2008), we tested whether sex-specific binding alterations would also pertain to these systems by applying spatial correlation analyses. Moreover, we investigated the molecular connectivity alterations in nigrostriatal and mesolimbic dopaminergic pathways focusing on sex differences.

Clinical and demographic features of the whole pDLB group (M/F = 77/46) are reported in **Table 15**. Female and male patients did not differ regarding clinical and demographic features, except for age with women being older than men at the time of diagnosis.

Table 15. Demographic and clinical features of Study 8 sample

	Whole DLB sample	**DLB males**	**DLB females**	**Statistic p-value**
Number	123	77	46	
Age, year	77.15±6.50	76.14±6.46	78.84±6.27	**0.025**[a]
Disease duration, year	1.81±1.72	1.92±1.68	1.62±1.80	0.397[a]
DatSCAN, N positive cases	112 (91%)	70 (91%)	42 (91%)	0.940[b]
Putamen asymmetry index (%)	22.02±14.76	20.87±13.55	23.94±16.57	0.265[a]
Clinical symptoms				

Parkinsonism, frequency	90.2%	88.6%	93.1%	0.519[b]
Visual hallucinations, frequency	73.2%	71.6%	75.8%	0.684[b]
Cognitive fluctuations, frequency	56.1%	62.2%	44.8%	0.128[b]
REM-sleep behaviour disorder, frequency	17.2%	21.3%	9.4%	0.147[b]
Abbreviations: DLB= Dementia with Lewy bodies; N= number [a] two-sample t-test [b] Chi-square test				

Sex differences in ^{123}I-FP-CIT SPECT imaging

The pDLB male and female cohorts showed significant reductions of [^{123}I]FP-CIT-SPECT bindings in comparison with CTL (**Figure 24** and **Table 16**). Voxel-wise analysis assessing differences between each sex group vs sex-matched CTL showed severe alterations of DAT binding density in the basal ganglia for both pDLB females and males (**Figure 24**). The binding reductions (t-scores) were higher for pDLB males than females as visible in **Figure 24B**. When we directly compared voxel-wise [^{123}I]FP-CIT binding of pDLB females vs pDLB males, we found reduced bindings in the thalamus, amygdala, insula, hippocampus, parahippocampus, ACC, MCC, orbitofrontal cortex, middle frontal gyrus, precentral and postcentral gyri, as well as the inferior parietal lobule in pDLB females (**Figure 24C**). No differences were found with the opposite contrast. The ROI-based analysis revealed more significant SBR decreases for pDLB females than males in several ROIs depending on the nigrostriatal (left opIFG, bilateral precentral and postcentral gyri ($p < 0.05$)), mesolimbic dopaminergic, and serotonergic systems, namely, the bilateral amygdala, insula, hippocampus, parahippocampus, OFC, ACC, and MCC ($p < 0.05$). Females showed more significant SBR decreases also in the bilateral thalamus as compared to males. In most of the aforementioned regions showing significantly lower SBR in females pDLB, we also found a trend toward a lower SBR in females CTL (**Table 16**). In CTL, significant sex differences were found only in the left opIFG, left precentral gyrus, left postcentral gyrus, ACC, and MCC. Results are fully reported in **Table 16**. Although both sex and group (pDLB vs CTL) have main effects on SBR, no significant

interaction effect between group and sex was found, indicating that sex effect on regional SBR does not differ between pDLB and CTL, after controlling for age. This confirms that sex and group are both significant and independent predictors of SBR decreases in the investigated ROIs.

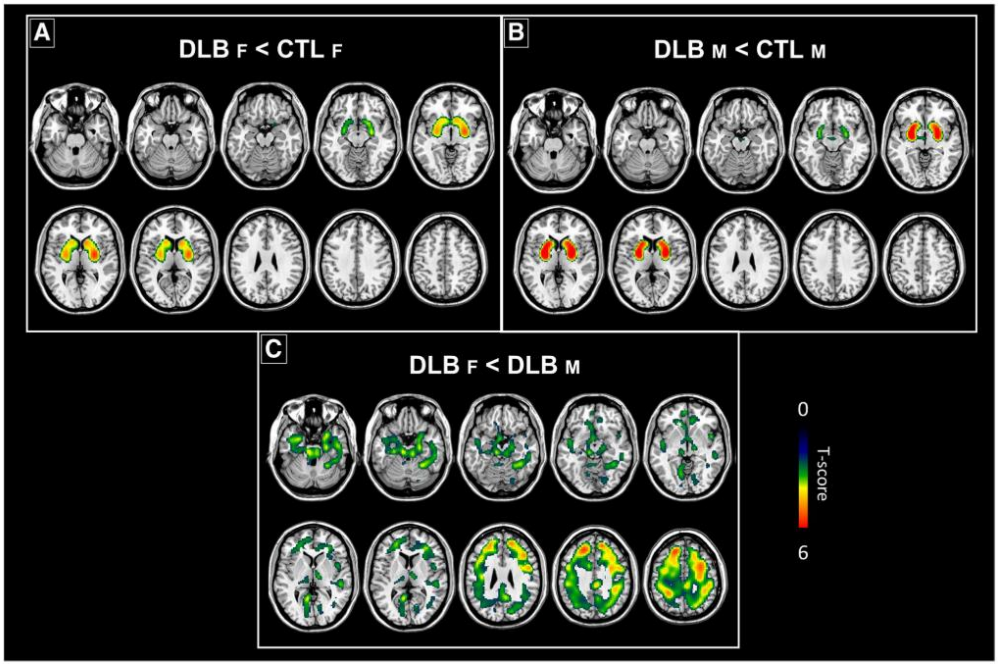

Figure 24. Voxel-wise sex differences in [^{123}I]FP-CIT binding (Open access source). *Panels A and B show the distribution of voxel-wise differences in [^{123}I]FP-CIT SBR for each sex group, resulting from statistical comparison with sex-matched CTL. Panel C shows the results from the direct voxel-wise comparison between females and males with DLB, after adjusting for age. The magnitude of the difference is reported by means of t-score. Abbreviations: DLB, dementia with Lewy bodies; CTL, controls; F, females; M, males. The figure is from* (Boccalini *et al.*, 2023) *in accordance to the fair use principle.*

Table 16. Regional analysis of [^{123}I]FP-CIT-SPECT imaging bindings in the male and female DLB patients.

	DLB males N=77	**CTL males N=34**	**statistic DLB_M vs CTL_M**	**DLB females N=46**	**CTL females N=44**	**statistic DLB_F vs CTL_F**	**statistic CTL_M vs CTL_F**	**statistic DLB_M vs DLB_F**
Nigrostriatal system ROIs								
Left Dorsal Caudate	3.68± 1.97	6.11± 2.38	**p<0.001**	3.46± 1.79	6.05± 2.38	**p<0.001**	0.826	0.597

Right Dorsal Caudate	3.39± 1.80	5.63± 2.29	**p<0.001**	3.00± 1.59	5.65± 2.28	**p<0.001**	0.864	0.275
Left Dorsal Putamen	4.93± 2.15	8.05± 2.09	**p<0.001**	4.72± 2.30	7.28± 2.07	**p<0.001**	0.063	0.499
Right Dorsal Putamen	5.00± 2.29	8.07± 2.11	**p<0.001**	4.61± 2.22	7.32± 2.20	**p<0.001**	0.079	0.241
Left opIFG	0.85± 0.59	0.93± 0.56	0.785	0.62± 0.36	0.71± 0.38	0.814	**0.016**	**0.028**
Right opIFG	0.69± 0.52	0.67± 0.47	0.817	0.54± 0.36	0.63± 0.54	0.546	0.482	0.088
Left precentral gyrus	1.01± 0.60	0.96± 0.48	0.808	0.67± 0.40	0.83± 0.39	0.156	**0.001**	**p<0.001**
Right precentral gyrus	0.89± 0.56	0.86± 0.49	0.678	0.64± 0.42	0.76± 0.40	0.253	0.060	**0.006**
Left postcentral gyrus	0.94± 0.54	0.88± 0.46	0.613	0.69± 0.37	0.79± 0.37	0.296	**0.018**	**0.004**
Right postcentral gyrus	0.85± 0.54	0.77± 0.47	0.416	0.63± 0.37	0.79± 0.41	0.093	0.907	**0.008**
Mesolimbic system ROIs								
Left Ventral Striatum	4.14± 2.01	6.14± 2.18	**0.001**	3.57± 1.61	5.69± 2.12	**p<0.001**	0.241	0.132
Right Ventral Striatum	3.93± 1.93	5.90± 2.15	**p<0.001**	3.37± 1.51	5.51± 2.03	**p<0.001**	0.360	0.109
Left Amygdala	1.48± 0.79	1.57± 0.58	0.533	1.13± 0.51	1.43± 0.64	0.101	0.256	**0.010**
Right Amygdala	1.67± 0.84	2.01± 0.80	0.117	1.34± 0.56	1.68± 0.66	**0.046**	0.055	**0.018**
Left Hippocampus	1.02± 0.59	0.98± 0.51	0.412	0.78± 0.37	0.88± 0.78	0.904	0.256	**0.025**
Right Hippocampus	1.18± 0.68	1.20± 0.56	0.558	0.93± 0.43	1.09± 0.50	0.467	0.266	0.057
Left parahippocampus	0.56± 0.51	0.50± 0.41	0.506	0.31± 0.30	0.39± 0.38	0.957	0.088	**0.006**
Right parahippocampus	0.83± 0.56	0.76± 0.49	0.276	0.51± 0.33	0.60± 0.39	0.881	**0.024**	**0.001**
Left Insula	1.22± 0.67	1.36± 0.61	0.454	0.99± 0.38	1.24± 0.56	0.225	0.346	**0.043**

Right Insula	1.01± 0.58	1.05± 0.55	0.872	0.74± 0.34	0.95± 0.52	0.376	0.273	**0.007**
Left Olfactory cortex	1.29± 0.76	1.41± 0.76	0.946	0.91 ±0.50	1.34± 0.75	0.095	0.491	**0.006**
Right Olfactory cortex	1.41± 0.85	1.72± 0.88	0.413	1.07± 0.50	1.60± 0.76	**0.020**	0.402	**0.028**
Left Anterior Cingulate	0.90± 0.62	0.90± 0.55	0.707	0.65± 0.37	0.68± 0.43	0.497	**0.018**	**0.021**
Right Anterior Cingulate	1.10± 0.68	1.10± 0.64	0.946	0.81± 0.42	0.79± 0.43	0.405	**0.007**	**0.009**
Left Middle Cingulate	1.16± 0.73	1.23± 0.66	0.865	0.82± 0.43	1.00± 0.61	0.435	**0.019**	**0.006**
Right Middle Cingulate	1.18± 0.71	1.28± 0.67	0.783	0.84± 0.43	1.09± 0.66	0.219	0.053	**0.005**
Other ROIs								
Left Thalamus	1.03± 0.64	1.10± 0.63	0.975	0.72± 0.36	1.04± 0.59	0.107	0.453	**0.011**
Right Thalamus	1.20± 0.67	1.26± 0.63	0.898	0.92± 0.37	1.22± 0.61	0.113	0.700	**0.020**
Left Globus Pallidus	4.64± 1.95	7.01± 2.11	**p<0.001**	4.29± 1.84	6.42± 2.06	**p<0.001**	0.142	0.287
Right Globus Pallidus	5.15± 2.31	8.38± 2.41	**p<0.001**	4.79± 2.22	7.65± 2.36	**p<0.001**	0.121	0.311

Abbreviations: DLB, Dementia with Lewy bodies; CTL, controls; N, number; opIFG, inferior frontal gyrus pars opercularis; ROIs, regions of interest

Since [^{123}I]FP-CIT can be used for the evaluation of other monoaminergic systems beyond DAT, especially in extrastriatal regions, we assessed the mapping of [^{123}I]FP-CIT binding alterations with different neurotransmission templates, using JuSpace toolbox (Dukart *et al.*, 2021). We showed a significant spatial correlation with the DAT alterations ($p < 0.005$) for both pDLB groups compared to CTL (z-scores). In addition, neurotransmitter alterations significantly correlated with SERT receptor map in both pDLB females and males ($p < 0.001$) and with NET receptor map only in pDLB females ($p < 0.001$). **Figure 25** shows Fisher's z-transformed correlation coefficients with respective neurotransmitter maps for each subject (individual points) and contrast.

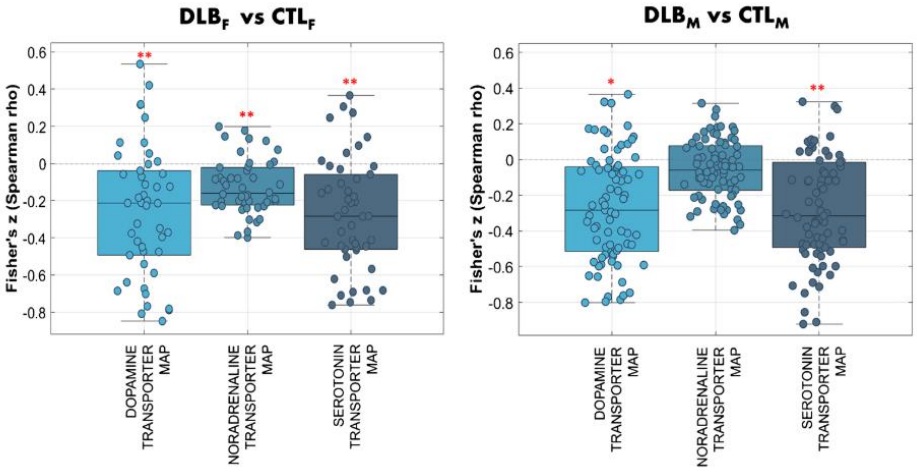

Figure 25. Results of spatial correlation analysis with neurotransmitter maps for DLB females and males (Open access source). *Fisher's z-transformed correlation coefficients with respective neurotransmitter maps are displayed for each subject and contrast. [^{123}I]FP-CIT binding alterations in DLB females and males as compared to controls are significantly associated with the topographies of DAT and SERT. [^{123}I]FP-CIT binding alterations in DLB females are associated with NET. Error bars represent the parametric 95% confidence interval of the mean. Exact permutation-based p values (10,000 permutations) were computed for all analyses: ** indicates p values < 0.001; whereas * indicates p values < 0.005. See text for details. Abbreviations: DLB, dementia with Lewy bodies; F, females; M, males; CTL, controls. . The figure is from* (Boccalini *et al.*, 2023) *in accordance to the fair use principle.*

Sex differences in molecular connectivity

Nigrostriatal dopaminergic system: Considering the whole pDLB group, several connectivity alterations (22.5%) affected the nigrostriatal system as compared to CTL. These alterations involved subcortical connections connections between the putamen and caudate nucleus, with a loss of connectivity with the contralateral striatum and increased pathological connections with the ipsilateral structures as compared to CTL. Moreover, pDLB lost subcortical-cortical connections between the striatum and the postcentral and precentral gyri as compared to CTL. pDLB males' connectivity pattern showed only short-distance local subcortical alterations within the striatum. The pDLB females showed long-distance alterations between the caudate nucleus and precentral and postcentral gyri, and between opIFG and precentral gyrus. However, a direct comparison

between males' and females' altered connections did not show any significant difference, i.e., females (20%) and males (10%) ($\chi^2 = 1.56$, $p = 0.21$).

Mesolimbic dopaminergic system: pDLB patients showed 6% of altered connections as compared to CTL. Specifically, there was altered connectivity between the amygdala and the ipsilateral ventral striatum, the MCC, and ACC. In turn, ACC showed altered connectivity with the hippocampus. pDLB females and males did not differ in the number of connectivity alterations ($\chi^2 = 0.14$, $p = 0.69$). However, we found sex differences in the connectivity patterns: altered connectivity patterns of pDLB females involved limbic structures, i.e., the amygdala, insula, OFC, MCC, and ACC, whereas connectivity alterations in pDLB males were more extensive, also affecting the hippocampus.

See **Figure 26** for the matrices resulting from the connectivity analyses.

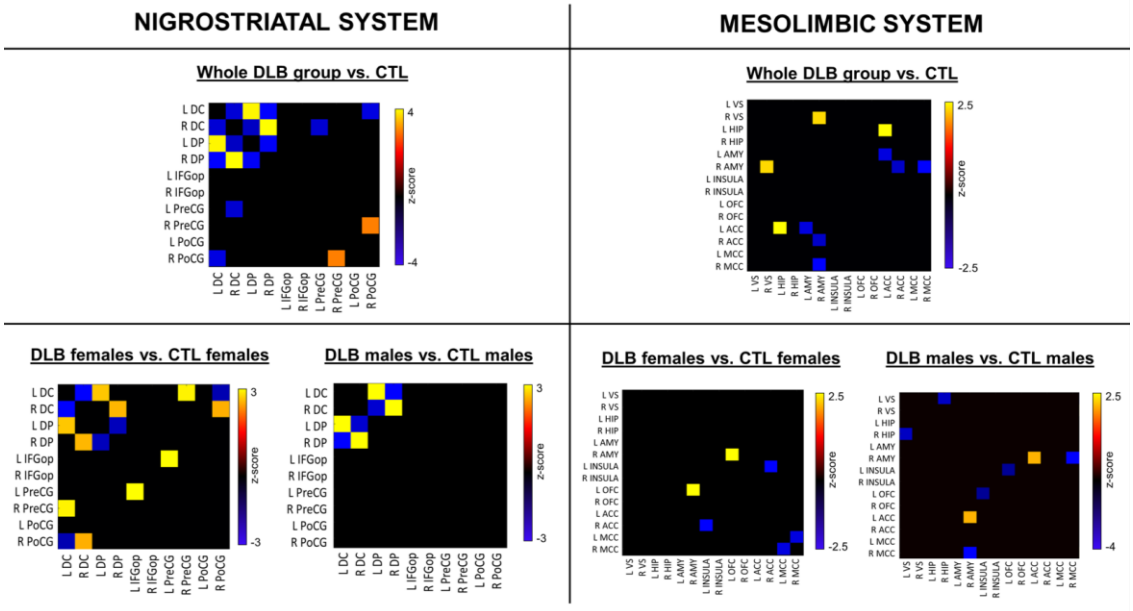

Figure 26. Dopaminergic connectivity results in the whole group, and separately in females and males (Open access source). *The matrices represent the significant differences obtained when comparing partial correlation coefficients between pDLB < HC, pDLB males < HC males and pDLB females < HC females, in the dopaminergic networks. The color bar displays the Z scores' values to compare partial correlation coefficients' strengths. Altered connections are presented: in red, the increased and in blue, the decreased connections compared with HC. The figure is from* (Boccalini *et al.*, 2023) *in accordance to the fair use principle.*

.

3.3.4 Study 9: Sex differences in brain metabolic connectivity architecture in probable dementia with Lewy bodies (Caminiti, Boccalini, et al., 2023) –Published article

Study 9 investigated how sex can modulate brain metabolism and whole-brain metabolic connectivity in 131 patients with pDLB. We also tested a comprehensive model focusing on the dopaminergic (DA), noradrenergic (NA), and cholinergic (Ch)-divisions systems to explore connectivity reconfiguration in major biochemical circuits for DLB. We evaluated connectivity changes in the resting-state networks (RSNs) that are linked to DLB core symptoms (Sala *et al.*, 2019). Clinical and demographic features of the pDLB group (males/females: 58/73) are reported in **Table 17**.

Table 17. Demographic and clinical features of Study 9 sample

	pDLB	**$pDLB_F$**	**$pDLB_M$**	**Sign.**
N	131	58	73	
Age (mean±sd)	72.34 ±7.8	72.43±8	72.27±7.7	0.91
Disease Duration (mean±sd)	2.26±1.8	2.47±2.13	2.12±1.5	0.332
MMSE (mean±sd)	18.9±5.2	18.6±5.2	19.05±5.3	0.714
Parkinsonism %	88%	89%	88%	0.884
Visual Hallucinations %	62%	52%	67%	0.183
Cognitive Fluctuations %	46%	41%	49%	0.490
RBD %	40.3%	31%	46%	0.216

Abbreviations: pDLB, probable dementia with Lewy bodies; RBD, rapid eye movement sleep behaviour disorder; SD, Standard Deviation.

Brain Metabolism

Brain hypometabolism pattern for both males and females corresponded to the prototypical DLB-like pattern, involving the bilateral medial and lateral occipital, temporoparietal, as well as dorsolateral prefrontal cortex (**Figure 27**). Direct statistical comparison between the two pDLB groups showed that $pDLB_M$ showed a more severe brain hypometabolism in the occipital, temporoparietal cortex, and cerebellum Crus I/II. Instead, $pDLB_F$ showed a more extended hypometabolism in the hippocampal structures, compared to $pDLB_M$ (**Figure 27**). In HC, we found statistically significant negative correlations between age and whole brain glucose metabolism in males and females.

Namely, an extended reduction of brain metabolism in the medial prefrontal cortex, anterior and middle cingulate gyrus in males, limited to the anterior cingulate cortex in females.

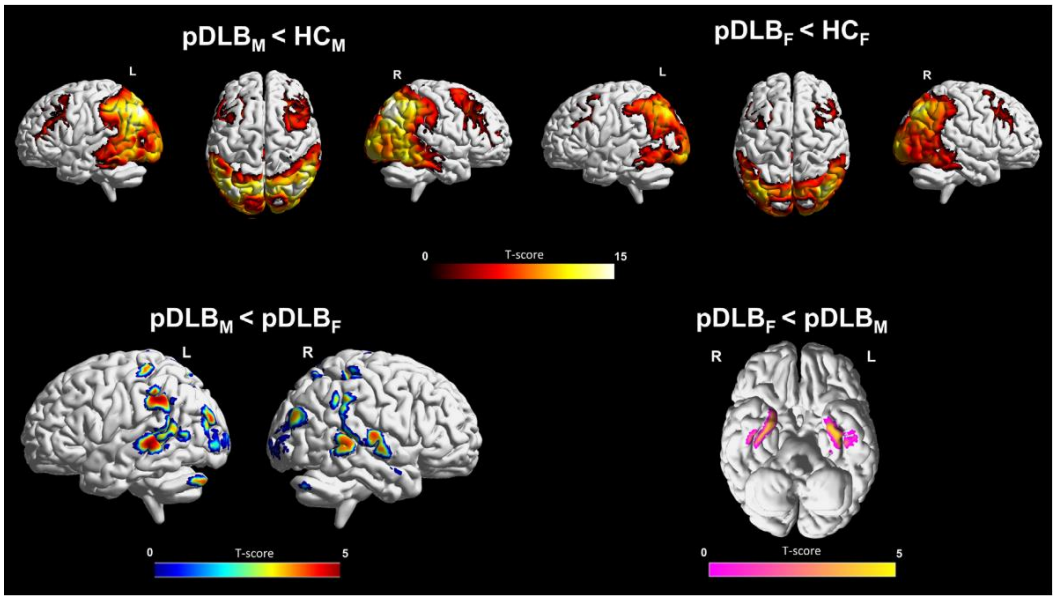

Figure 27. Topographical distribution of brain hypometabolism (Open access source). *Top: FDG-PET SPM group comparisons between pDLB and controls. Yellow/red scale represents hypometabolism severity in pDLB compared to HC (pFWE < 0.05, k = 100). Bottom: FDG-PET SPM group comparisons of $pDLB_M$ and $pDLB_F$. Blue/red scale represents hypometabolism in $pDLB_M$ versus $pDLB_F$ ($p < 0.001$, uncorrected, $k = 100$); Pink/yellow scale represents hypometabolism in $pDLB_F$ versus $pDLB_M$ ($p < 0.001$, uncorrected, $k = 100$). 3D renderings were obtained from BrainNet Viewer toolbox (Xia et al., 2013). Abbreviations: F, females; HC, healthy controls L, left; M, males; pDLB, probable dementia with Lewy bodies; R, right. The figure is from* (Caminiti, Boccalini, *et al.*, 2023) *in accordance to the fair use principle.*

Metabolic Connectivity

Whole-brain network – Overall, a pattern of significant whole-brain reconfigurations, mostly involving connectivity losses, was found in the two clinical groups as compared to HC (**Figure 28A**). The two groups shared 18% of altered connections according to the Jaccard (JSC) analysis. The $pDLB_M$ group showed a significantly higher proportion of altered connectivity (20%) than the $pDLB_F$ (9.7%) ($\chi^2 = 3.92$, $p < 0.05$). There were mostly connectivity losses in $pDLB_M$, involving temporal, insular, and cerebellar nodes, whereas female connectome featured patterns of increased connectivity; in particular, we found increased connectivity among the insula node and olfactory cortex, amygdala,

hippocampus, thalamus, putamen and pallidum, and the olfactory node with the insula, temporal pole, and occipital cortex (**Figure 28A**).

Hubs - In both groups, common pathological hubs were the bilateral angular gyrus and the Rolandic operculum, the left inferior parietal lobule, and the right insula (**Figure 28B**). All these hubs significantly lost reciprocal connections as well as with a series of widespread cortical nodes (**Figure 28A**). Then, we identified the nodes that resulted as pathological hubs only for males or females. The $pDLB_M$ showed selective pathological hubs in the inferior and right middle temporal gyrus, fusiform gyrus, left Rolandic operculum, left gyrus rectus, and right supramarginal gyrus. Instead, the $pDLB_F$ group showed selective pathological hubs in the superior and middle frontal cortex, left olfactory cortex, left insula, Heschl gyrus, right inferior parietal cortex, and precuneus (**Figure 28B**).

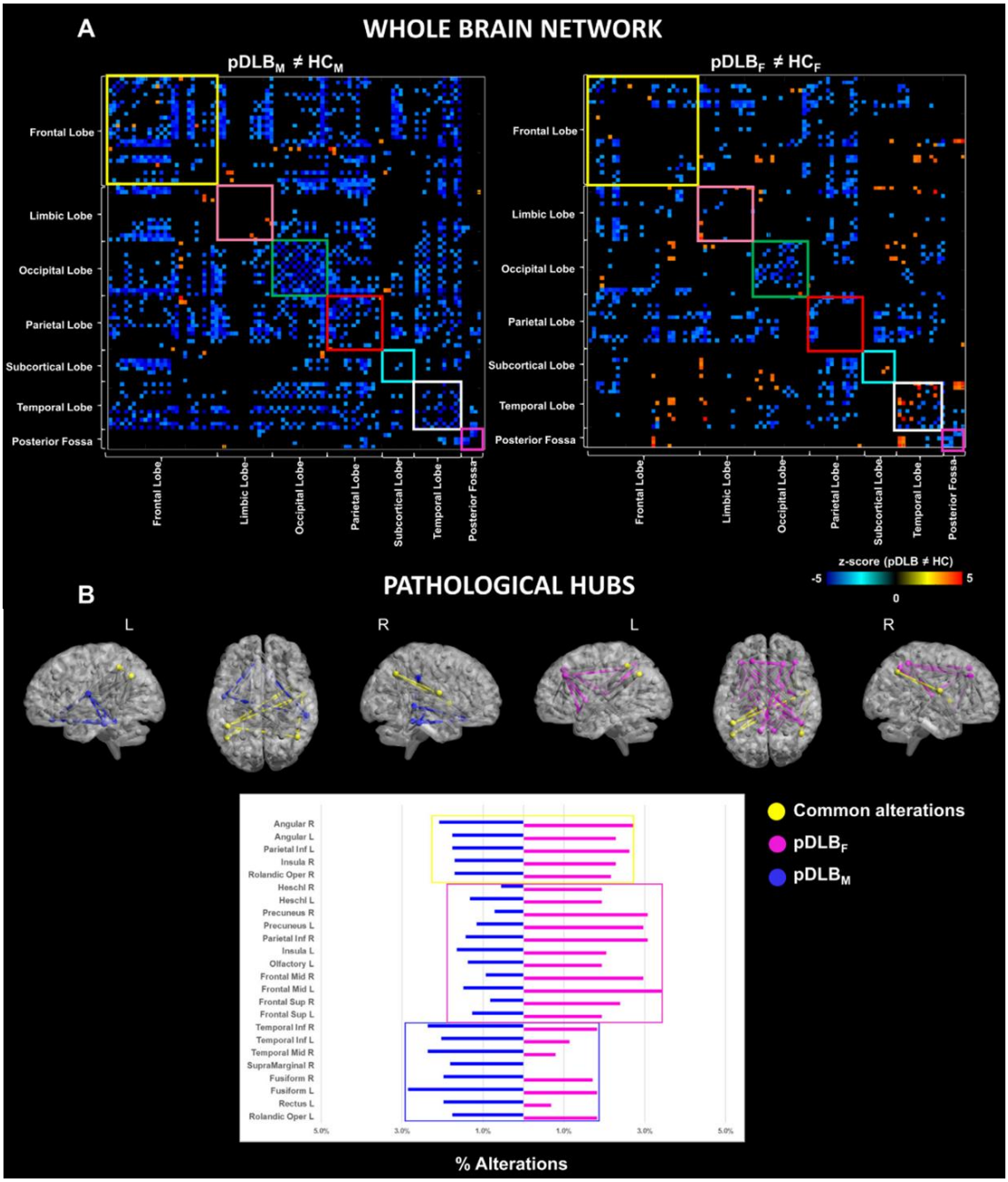

Figure 28. Whole-brain network analysis (Open access source). *(A) The matrices represent the significant differences obtained comparing adjacency matrices ($p < 0.05$, uncorrected for multiple comparisons) between $pDLB_M$ versus age-sex matched control group and $pDLB_F$ versus age-sex matched control group in the whole brain network. The connectivity loss is shown in cyan-blu, the gained connectivity in yellow-red, and the unchanged connectivity in black. (B) 3D brain showing pathological hubs shared by the two groups (yellow) or specifically affected only in $pDLB_M$ (blue) or $pDLB_F$ (pink) groups. The pyramid plot shows the distribution of altered connectivity of the pathological hubs normalized to the total number of connectivity alterations*

in pDLB versus HC comparisons. Automated Anatomical Labeling (AAL) (Tzourio-Mazoyer et al., 2002) atlas' labels were grouped into 7 macro-regions for visualization porpouse: Frontal Lobe (precentral gyrus, superior frontal gyrus, middle frontal gyrus, inferior frontal gyrus, Rolandic operculum, supplementary motor area, olfactory lobe, rectus gyrus), limbic lobe (insula, anterior cingulate cortex, middle cingulate cortex, posterior cingulate cortex, hippocampus, parahippocampal gyrus, amygdala), occipital lobe (calcarine cortex, cuneus, lingual gyrus, superior occipital gyrus, middle occipital gyrus, inferior occipital gyrus), parietal lobe (precentral gyrus, superior parietal lobule, inferior parietal lobule, supramarginal gyrus, angular gyrus, precuneus, paracentral lobule), subcortical lobe (caudate, putamen, thalamus, pallidum), temporal lobe (fusiform gyrus, Heschl gyrus, superior temporal gyrus, superior temporal pole, middle temporal gyrus, middle temporal pole, inferior temporal gyrus), and posterior fossa (cerebellum crus, lobules and vermis). Abbreviations: F, Females; HC, Healthy Controls; L, left; R, right; M, males; pDLB, probable dementia with Lewy bodies. The figure is from (Caminiti, Boccalini, *et al.*, 2023) *in accordance to the fair use principle.*

Dorsal DA network – The JSC analysis identified an overlap of 17% of connectivity alterations in the two DLB groups, with shared common striato-frontal connectivity alterations, specifically involving the dorsal putamen and the middle and superior frontal gyrus. There were also different connectivity patterns (**Figure 29**). For instance, the dorsal caudate connectivity was affected in males, but not in females who, instead, showed disconnections among cortical nodes.

Ventral DA network – We found a similar connectivity pattern of alterations in the two groups, supported by a JSC, equal to 22%. However, the $pDLB_M$ group showed connectivity alterations in 20% of nodes versus the 7% found in the $pDLB_F$ group ($\chi^2 = 7.24$, $p < 0.001$). In detail, both $pDLB_M$ and $pDLB_F$ showed a loss of connectivity between the right frontal cortex pars orbitalis and the left homologous region. We also found disconnections across the olfactory cortex, parahippocampal gyrus, and anterior cingulate cortex in the two pDLB groups (**Figure 29**). Of note, the ventral striatum was disconnected from the orbitofrontal cortex only in males. Moreover, the $pDLB_F$ group showed a prevalent connectivity loss on the right side of the network, which in the $pDLB_M$ extended to the contralateral side (**Figure 29**).

NA network – Overall, similar connectivity changes were found in the two groups, with a JSC equal to 25%, with a 16% and 12% connectivity alteration in $pDLB_M$ and $pDLB_F$,

respectively ($\chi^2 = 0.6645$, $p = 0.5$). We found common disconnections between the middle frontal cortex and the hypothalamus, amygdala, hippocampus, and precentral lobule. Furthermore, the precuneus was disconnected from the hypothalamus, amygdala, hippocampus, precentral, and postcentral lobule. Local disconnections between cerebellar nodes were also found in the two groups (**Figure 29**).

Ch3 network – This network showed no difference in the two clinical groups as compared to sex-matched HC.

Ch4-Perisylvian Network - We found no overlap in network alterations between the two groups. The Ch4-Perisylvian division showed 31.5% connectivity alterations in the $pDLB_M$, which was significantly different from a 7.6% alteration found in the $pDLB_F$ group ($\chi^2 = 18$, $p < 0.001$). The $pDLB_M$ was characterized by widespread loss of connectivity between the inferior frontal cortex nodes and the Rolandic operculum, Heshl gyrus, insula, and olfactory cortex. Instead, the $pDLB_F$ showed altered connectivity increases between the superior temporal pole and the Rolandic operculum, Heshl gyrus, insula, and olfactory cortex, without evidence of loss of connectivity.

Ch4-Median network – The two pDLB groups showed no overlap in the affected nodes (JSC = 0%). Specifically, the $pDLB_F$ group showed statistically significant altered connectivity only in 8% of nodes, with a loss of connections involving the superior frontal gyrus and anterior cingulate cortex, superior frontal gyrus pars orbitalis, and gyrus rectus. The $pDLB_M$ showed altered connectivity in 5% of nodes ($\chi^2 = 0.740$, $p = 0.39$), involving the middle, medial and superior frontal gyrus pars orbitalis, gyrus rectus, and anterior cingulate cortex (**Figure 29**). Male connectivity alterations involved both increases and decreases, whereas only decreases were present in females.

Ch5-6 network – Both groups showed increased connectivity as compared to HC, without evidence of reduced connectivity. According to the JSC analysis, we found no overlap in connectivity alterations between $pDLB_M$ and $pDLB_F$, with different nodes involved in males and females: the connectivity of dorsal putamen and pallidum were affected in $pDLB_F$, whereas in $pDLB_M$ the dorsal caudate and ventral striatum (**Figure 29**).

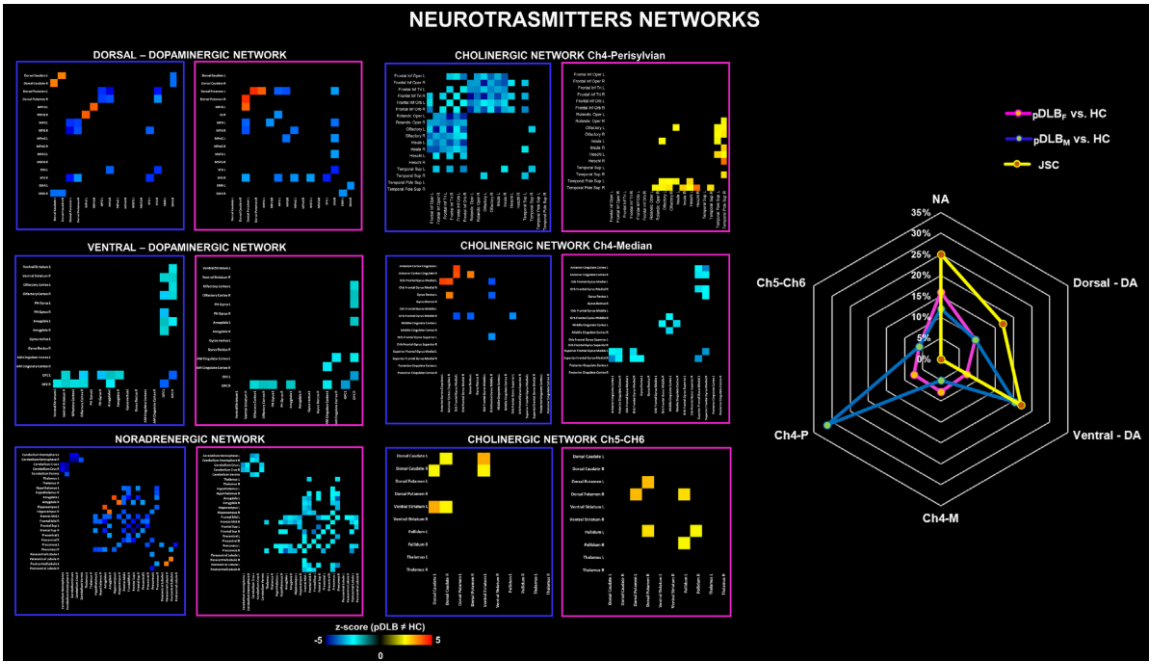

Figure 29. Neurotransmitter networks analysis (Open access source). *The matrices represent the significant differences obtained comparing adjacency matrices ($p < 0.05$, uncorrected for multiple comparisons) between $pDLB_M$ versus age-sex matched control group (square blue) and $pDLB_F$ versus age-sex matched control group (square pink) in the different neurotransmitter networks. The connectivity loss is shown in cyan, the gained connectivity in yellow, and the unchanged connectivity in black. Radar plot showing the percentage of altered connections in $pDLB_F$ (pink line), $pDLB_M$ (blue line), and the common alterations JSC (yellow line) in the two clinical groups. Abbreviations: Ch, Cholinergic; Ch-M, Cholinergic-Median; Ch-P, Cholinergic-Perisylvian; DA, dopaminergic; F, females; HC, healthy controls; JSC, Jaccard Similarity Coefficient; M, males; NA, noradrenergic; pDLB, probable dementia with Lewy bodies. The figure is from* (Caminiti, Boccalini, *et al.*, 2023) *in accordance to the fair use principle.*

RSNs – **Figure 30** illustrates the connectivity changes for each large-scale network in the two pDLB groups. There was a good overlap (JSC ≥ 40%) between $pDLB_F$ and $pDLB_M$ in most networks, except for the limbic and motor ones. The highest levels of overlap between the two clinical groups were found in the primary visual, posterior default mode, and attention networks. In these RSNs, both groups showed decreases in the overall connectivity strength as compared to HC (JSC ≤ 25%). Instead, connectivity alterations were prominent in the executive, limbic, and higher visual networks for $pDLB_M$ than $pDLB_F$ group as compared to HC. In particular, the high visual network was the most altered network for males (JSC = 20%), but not for females (JSC = 36%).

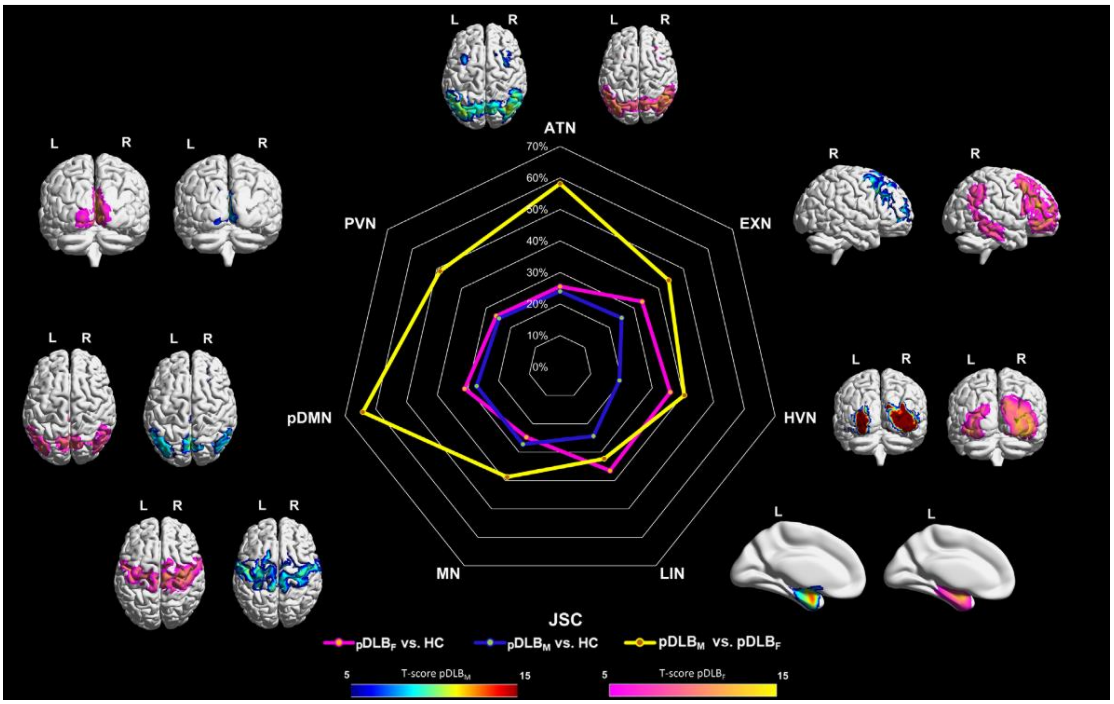

Figure 30. Resting state network analysis (Open access source). *Resting state network connectivity in pDLB males and females' groups. Blue/red scale represents correlation strength (T-score) between network's seed and the rest of the brain in pDLB$_M$ ($p < 0.05$, Family-wise Error corrected, $k = 100$); Pink/yellow scale represents correlation strength (T-score) between network's seed and the rest of the brain in pDLB$_F$ ($p < 0.05$, Family-wise Error corrected, $k = 100$). Radar plot showing JSC obtained comparing pDLB groups with HC and males and females DLB groups. The pink line indicates overlap, measured by JSC, between pDLB$_F$ and HC RSNs, the blue line indicates overlap between pDLB$_M$ and HC RSNs and the yellow line indicates the overlap between pDLB$_F$ and pDLB$_M$ in RSNs. 3D renderings were obtained from BrainNet Viewer toolbox (Xia et al., 2013). Abbreviations: ATN, attention network; EXN, executive network; F, females; HC, healthy controls; HVN, higher visual network; JSC, Jaccard Similarity Coefficient; LIN, limbic network; M, males; MN, motor network; pDLB probable dementia with Lewy Bodies; PVN, primary visual network; RSNs, resting state networks. The figure is from* (Caminiti, Boccalini, *et al.*, 2023) *in accordance to the fair use principle.*

4. Discussion

The studies included in this dissertation contributed to the evaluation of the role of molecular imaging biomarkers in LBDs, also exploring the promising potential of metabolic and molecular connectivity approaches. Moreover, the studies relied on advanced methods to disentangle the sources of clinical variability, focusing specifically on sex /gender differences in PD and DLB.

Most of following data are already published (Boccalini *et al.*, 2020, 2023; Carli *et al.*, 2021; Boccalini, Bortolin, *et al.*, 2022; Boccalini, Carli, Pilotto, *et al.*, 2022; Boccalini, Carli, Vanoli, *et al.*, 2022; Caminiti, Boccalini, *et al.*, 2023).

4.1 Imaging biomarkers for diagnosis and progression

4.1.1 Study 1: Distinctive clinical and imaging trajectories between SWEDD and Parkinson's disease patients (Boccalini, et al.) – submitted article

Study 1 demonstrated that [^{123}I]FP-CIT SPECT imaging can reliably reveal distinct dopaminergic alterations in early PD and SWEDD at baseline and their progression at a 2-year follow-up.

From a clinical standpoint, the two groups were comparable in terms of motor and cognitive symptoms at baseline (**Figure 6**). PD patients presented significantly more severe smell impairments than SWEDD, that instead showed more pronounced non-motor symptoms (even if mild), as measured by MDS-UPDRS part I (**Table 1**). Among non-motor symptoms, hyposmia has been widely recognized as an early discriminative sign of PD (Sprenger *et al.*, 2015; Taylor *et al.*, 2016). Our results further supported that hyposmia might be particularly useful to differentiate the two groups (**Table 1**). Previous literature reported discordant results regarding differences in non-motor symptoms, with a minor, comparable, or greater severity in SWEDD subjects (Balestrino *et al.*, 2021). The heterogenous clinical phenotypes encompassed by SWEDD subjects may at least partially explain the high degree of non-motor symptoms burden in SWEDD found here. Even if the motor, autonomic and cognitive symptoms similarly characterized both groups at baseline, worsening at 2-year follow-up occurred only in PD (**Table 2**). Specifically, PD patients worsened in all the MDS-UPDRS scales over time, while SWEDDs only showed a slight worsening in memory and visuospatial skills and MDS-

UPDRS total score, mostly driven by non-motor scores (**Table 2**). A lack of clinical progression in SWEDD strongly argues against a diagnosis of PD (and a neurodegenerative condition in general) (Marshall *et al.*, 2009; Nicastro, Burkhard and Garibotto, 2020; Balestrino *et al.*, 2021; Lee *et al.*, 2021). Notably, previous studies already demonstrated that in many SWEDD cases, the clinical diagnosis was revised in favour of dystonic tremor, or other alternative diagnoses included vascular parkinsonism, essential/atypical/monosymptomatic tremor, frontotemporal lobar degeneration with motor signs, functional (psychogenic) parkinsonism, drug-induced parkinsonism, and mild parkinsonian signs attributed to aging (see (Balestrino *et al.*, 2021) for a review).

From the imaging side, we applied two different approaches, namely a voxel-based approach and a subject-specific ROI approach based on the structure segmentation of MRI scans in each participant to increase the precision of [^{123}I]FP-CIT SBR extraction. PD subjects showed significantly lower binding in both striatal and extrastriatal regions compared with SWEDD and controls (**Table 3**, **Figures 7A** and **7B**). Importantly, given the limitations of the visual interpretation approach (Söderlund *et al.*, 2013; Batla *et al.*, 2014; Nicastro, Burkhard and Garibotto, 2018), SWEDDs were first semi-quantitatively evaluated by applying a voxel-wise comparison with a pool of HC. 26% (13/49) of scans initially reported as visually negative (SWEDD) were found abnormal after the voxel-wise semi-quantitative analysis and were excluded from the analyses. Of note, SPECT misinterpretation has emerged as an important contributor to the SWEDD population since a proportion of patients might have instead a degenerative condition (1.3%). When visual rating is combined with semi-quantification, a better diagnosis can be reached (Nicastro, Garibotto, Badoud, *et al.*, 2016; Nicastro, Burkhard and Garibotto, 2018).

To the best of our knowledge, only one previous study investigated extrastriatal [^{123}I]FP-CIT binding in SWEDD demonstrating preserved values comparably to HC in SWEDD whereas PD subjects showed reduced bindings in the insula and thalamus (Nicastro, Burkhard and Garibotto, 2020). Our results showed lower binding in the insula and thalamus but also in the hippocampus and parahippocampus for PD compared to SWEDDs (**Figure 7B** and **Table 3**). These extrastriatal regions harbor a variable proportion of SERT, beyond DAT, for which [^{123}I]FP-CIT has moderate affinity (Koch *et al.*, 2014), confirming a serotoninergic loss in PD. Serotonergic binding as assessed by DASB was diffusely reduced in the striatum, brainstem, and multiple cortical areas in PD

(Politis *et al.*, 2010). SWEDDs also had lower binding in the ACC, whose serotonergic dysfunction has a prominent role for apathy, depression and anxiety (Maillet *et al.*, 2021; Hsam and Kohl, 2023). Moreover, SWEDDs showed a higher hippocampal SBR compared to HC (Table S1) suggesting a possible altered serotoninergic transmission. The hypothesis of compensatory upregulation of serotonergic nerve terminals has been advanced to explain the relative preservation of 18F-dopa uptake in a genetic case of PD (Wile *et al.*, 2016). However, the possible contribution of serotoninergic system, as well as other neurotransmitter systems, to SWEDD symptomatology has never been directly explored. When we applied spatial association analysis with specific neurotransmitter maps (Dukart *et al.*, 2021), we found [^{123}I]FP-CIT binding alterations associated with SERT only in PD and only a trend for significance in SWEDD (**Figure 8**), likely because of the limited sample size.

Our longitudinal imaging results showed that striatal and extrastriatal deficit worsened at 2-year follow-up in PD but not in SWEDD patients (**Figure 7D** and **Table 3**), which is in line with previous DAT studies focusing on striatal binding (Marshall *et al.*, 2006; Batla *et al.*, 2014; Marek *et al.*, 2014; Lee *et al.*, 2021). The lack of dopaminergic depletion worsening in SWEDDs suggests that these subjects suffer from other conditions.

To assess the neural mechanisms underlying SWEDD, we also explored for the first time the molecular connectivity in the two main dopaminergic systems, finding out an extended cortical connectivity impairment characterizing the SWEDD group especially in the mesocorticolimbic system. Previous evidence in α-synucleinopathies showed a widespread impaired connectivity (see (Sala and Perani, 2019; Carli *et al.*, 2021) for reviews), revealing also molecular connectivity alterations within the nigrostriatal and mesocorticolimbic dopaminergic systems (Sala, S.P. Caminiti, *et al.*, 2017; Silvia Paola Caminiti *et al.*, 2017; Boccalini, Carli, Pilotto, *et al.*, 2022). Comparing the molecular connectivity profiles of both systems in SWEDD and PD groups, we found altered connectivity in both dopaminergic pathways, however involving distinct regions. Indeed, SWEDD group was characterized by more severe impaired connectivity in cortical areas. Regarding the nigrostriatal system, the PD profile was primarily characterized by a loss of interconnections within the basal ganglia, whereas SWEDD showed also cortical alterations. The group differences were more marked in the mesocorticolimbic system, with SWEDD showing greater connectivity alterations than

PD (**Figure 9**). These alterations involved the ventral striatum and many extrastriatal regions innervated also by other neurotransmission systems. Moreover, most of the alterations were represented by increases in connectivity in SWEDD rather than decreases, as occurring in PD. Molecular connectivity decreases might be indicative of selective denervation from the neurotransmitter nuclei projecting to the target regions, whereas interpreting the significance of connectivity increases (hyperconnectivity) is particularly complex. Increased connectivity might be indicative of a compensatory process, especially in the early disease stage, with the recruitment of brain regions that are still functional. But it can also represent a form of maladaptive functional reorganization where the proper connections usually characterizing healthy brains are replaced by a widespread dysfunctional connectivity pattern towards several regions (Hillary and Grafman, 2017). Moreover, the presence of cortical and extrastriatal connectivity alterations might suggest other possible neurotransmission abnormalities contributing to SWEDD symptomatology. Consensus about SWEDD is that it represents a variegated group of different conditions mimicking PD, including functional tremor, essential tremor or dystonia. Interestingly, altered connectivity in limbic areas has been observed in functional movement disorders (Morgante, Edwards and Espay, 2013), while we did not find such evidence for other conditions. Future molecular imaging studies using specific radiotracers are needed to understand the pathogenetic mechanisms and, thus, to address appropriate therapeutic options avoiding levodopa therapy, and prevent erroneous inclusion in clinical trials with consequent confounding outcomes and hazards for the patients.

Together with previous clinical and [^{123}I]FP-CIT PET results, the present findings highlight the distinct clinical and molecular trajectories of PD and SWEDD subjects. SWEDD subjects are characterised by prominent non-motor symptoms, absence of hyposmia, in addition to generally preserved dopaminergic binding but altered cortical connectivity. This scenario highlights the need for harmonizing methods for [^{123}I]FP-CIT-PET analyses and quantification to obtain univocal results. In this way, presynaptic dopaminergic SPECT images, investigated using semi-quantitative approaches, represent a reliable method in excluding or including the diagnosis of PD. Indeed, in the novel criteria for PD, a negative DaTSCAN represents an exclusion criterion for the diagnosis (Postuma *et al.*, 2018). One major question will remain to have a final diagnosis for

SWEDD, as they represent mostly a variegated group of non-degenerative conditions mimicking PD. Dopaminergic studies on each of these conditions (essential tremor, functional tremor, dystonia,..) would be useful to address this issue.

4.1.2 Study 2: Manual and semi-automated approaches to MIBG myocardial scintigraphy in patients with Parkinson's disease (Boccalini, Carli*, et al., 2022) – Published article*

[^{123}I]MIBG scintigraphy that assesses the denervation of the autonomic nervous system is another helpful tool included as supportive for PD diagnosis (Postuma *et al.*, 2018). *Study 2* (Boccalini, Carli, Vanoli, *et al.*, 2022) investigated the effects of different methods assessing [^{123}I]MIBG parameters on the clinical interpretation of [^{123}I]MIBG images. To do this, we evaluated the reproducibility of delayed and early H/M ratios using two types of approach: (i) manual-drawing method and (ii) fixed-size ROIs approach following literature guidelines proposed for heart failure (**Figure 10**) (Veltman *et al.*, 2012). Our results indicate that the use of fixed-size ROIs located following an "anatomical landmark square" (semiautomatic approach) improves the agreement among raters in classifying' H/M ratios as PD pathological or non-pathological. Of note, the semiautomatic procedure produced a perfect agreement between experienced and inexperienced observers (**Table 4**).

The use of a rectangular mediastinal ROI with unspecified size and manually drawn cardiac ROI is commonly used (van der Veen, Scholte and Stokkel, 2010). However, fixed-size ROIs are recommended in the proposal to standardise [^{123}I]MIBG parameters, but they were validated in patients with heart failure and without comparing the semiautomatic method with the standard visual one (Veltman *et al.*, 2012). Our results support and extend these findings in PD. The raters showed good inter and intra-rater agreements in early and late H/M ratios (continue values) applying manual-drawn and semiautomatic methods. This finding suggests that both methods for the calculation of the H/M ratios benefit from excellent reproducibility. However, the semiautomatic procedure showed a higher percentage of raters' consistency, assessing both early and late H/M ratios (**Table 4**).

The classification of the H/M ratios into pathological or not according to clinical cut-off (Nagamachi *et al.*, 2008) further highlighted the differences in the approaches. The agreement among raters in classifying patients into pathological or not, according to H/M ratios measures (categorical values) was higher in the semiautomatic procedure than in the manual one (**Table 4**). This variation might be explained by the fact that the expert and inexpert raters showed low agreement, especially in assessing early H/M ratio values using the manual method (Cohen Kappa 0.29). Instead, in the semiautomatic procedure, the consistency between the raters became perfect (Cohen Kappa 0.90). This improvement suggests that the semiautomatic procedure improves the interpretation of planar [^{123}I]MIBG images in clinical settings.

This study has some limitations, particularly the small sample size and the lack of a control group. The data used in the present study have been acquired in the context of a protocol aiming to profile the dementia risk in PD with imaging biomarkers, where the acquisition of healthy controls was not planned. Moreover, we are aware that the superimposition of noncardiac structures in the heart ROI might affect the [^{123}I]MIBG planar measures. This bias is intrinsic to the planar image technique because of the lack of three-dimensional information. A volumetric SPECT acquisition protocol would help to overcome this limitation, because of three-dimensional information. [^{123}I]MIBG-SPECT imaging can minimize the superimposition of the anatomic structures seen in 2-dimensional planar images (e.g., lungs overlapping the heart) (Oh *et al.*, 2015). We used the planar procedure in our study to obtain the [^{123}I]MIBG images because the quantification of global cardiac innervation using volumetric SPECT is less established than planar [^{123}I]MIBG imaging (van der Veen *et al.*, 2012). This bias would equally affect the H/M ratios obtained with manual and semi-automatic ROI placement, most likely not impacting our study's main result.

4.1.3 Study 3: Mapping brain metabolism, connectivity and neurotransmitters topography in early and late onset dementia with Lewy bodies – submitted article

Study 3 focused on a different molecular biomarker, namely [^{18}F]FDG-PET, in DLB. Brain hypometabolism as measured by [^{18}F]FDG-PET is an early biomarker of neurodegeneration, which has been associated with a variety of neuropathological events, including impaired neurotransmitter release (Kato *et al.*, 2016), consistently impacting on

large-scale brain networks (Seeley *et al.*, 2009). *Study 3* explored brain hypometabolism patterns in EO-DLB and LO-DLB and their association with the topography of specific brain neurotransmitter systems, and the metabolic connectivity in large-scale resting state networks. A recent clinico-pathological study showed that EO-DLB and LO-DLB are largely similar in core symptoms and with comparable distribution of limbic and neocortical Lewy pathology (Sim *et al.*, 2022). However, LO-DLB patients present more amnestic deficits that were accounted for by AD co-pathology, and EO-DLB can be predated by history of depression (Sim *et al.*, 2022). Our results of *Study 3* shows similarities between EO-DLB and LO-DLB in terms of clinical core symptom presentations and major brain hypometabolism hallmarks. However, we found that the LO-DLB individuals were characterized by a more severe hypometabolism in the dorsolateral frontal cortex, perisylvian/insular cortex and parahippocampal gyrus (**Figure 11**). The significant hypometabolism in parahippocampal gyri is in keeping with other structural grey-matter studies (Elder *et al.*, 2017). This is consistent also with amyloid and p-tau pathology reported in the medial temporal cortex of DLB cases, accounting for hypometabolism in the same region (Lee *et al.*, 2022). In a subgroup with available CSF data, we found also significantly higher p-tau pathology in the LO-DLB that may have a role on the parahippocampal hypometabolism found in this group. On the other hand, the EO-DLB showed more severe hypometabolism in the precuneus/PCC in the direct comparison with LO-DLB. Of note, subclinical depressive symptoms in ageing are linked with neurodegeneration biomarkers in the precuneus, PCC and fronto-temporal regions (Touron *et al.*, 2022). Previous studies reported the presence and intensity of depressive mood specifically characterized the clinico-pathological cohort of EO-DLB (Sim *et al.*, 2022). While we did not find differences between EO and LO-DLB in neuropsychiatric presentations, depression and apathy can be observed and linked to the above reported evidence when large cohort of subjects would be included. We must underline that our EO-DLB cases did not begin with a psychiatric- or delirium- onset, thus not representing this specific subtype (McKeith *et al.*, 2020).

Differences in EO-DLB and LO-DLB also emerged with the metabolic connectivity approaches (**Figures 12** and **13**). The whole-brain connectivity analysis revealed a severe disruption for both groups, however with some differences. The loss of connectivity arising from the occipital, inferior temporal and cerebellar nodes characterized both the

LO-DLB and EO-DLB. Noteworthy, increases and decreases in connectivity were present and differently expressed by EO-DLB and LO-DLB. Specifically, we observed in EO-DLB an higher amount of increased connectivity than LO-DLB, between frontal and posterior nodes. Increased connectivity among brain regions has been reported in prodromal DLB, Parkinson's disease, multiple sclerosis, traumatic brain injury, and stroke (Hillary and Grafman, 2017; Caminiti, Pilotto, *et al.*, 2023). While the mechanisms behind hyperconnectivity are still being studied, several valuable hypotheses have been proposed, such as adaptive or maladaptive mechanisms (Hillary and Grafman, 2017). Notably, this literature also reported a pattern of regionally increased functional connectivity during the early stages of neurodegenerative diseases, followed by a decline in connectivity. This might parallel our findings in EO vs. LO-DLB, the latter characterized by a more severe connectivity decrease. Concerning the RSNs analysis, the LO-DLB group showed loss of connectivity in the dorsolateral prefrontal part of the ATN. Attentional deficits are listed in the consensus clinical criteria for DLB diagnosis and are useful for differential diagnosis with dementia due to AD (Calderon *et al.*, 2001; McKeith *et al.*, 2017). Connectivity alterations in ATN were previously described in other studies conducted in DLB patients both in prodromal and dementia phases (Boccalini, Bortolin, *et al.*, 2022). Here it appears a functional marker of LO-DLB. EO-DLB instead, showed reduced connectivity in the frontal regions in EXN that are consistent with executive dysfunction and frontal connectivity alterations described in previous studies in DLB on both structural white-matter pathology (Lee *et al.*, 2010) and functional resting-state connectivity (Sourty *et al.*, 2016). In addition, the RSNs analysis supports the vulnerability of the DMN in EO-DLB - within both its anterior and posterior part. We found a loss of connectivity from the PCC node to the anterior part of the DMN and a loss of connectivity within the frontal aDMN. The PCC is a cortical region with high levels of metabolic demand and, together with the adjacent precuneus, represents the main hub of the pDMN (Leech, Braga and Sharp, 2012). Finally, EO-DLB group presented loss of connectivity within the LIN. Significant connectivity loss involved the limbic structures, from amygdala seed and thalamus. This finding indicates impaired limbic network connectivity and its possible relevance for the association with neuropsychiatric vulnerability previously reported in EO-DLB. Further studies are necessary for confirmation with large EO-DLB cohorts, here prevented by our limited sample size.

The spatial association analysis based on the metabolic differences in neurotransmission showed significant correlations with AChE, GABAa, SERT, DAT neurotransmitter maps and hypometabolism in both EO and LO DLB groups (**Figure 14**). Here, we found that the typical hypometabolism pattern was mostly driven by the AChT activity, as suggested by the highest correlation coefficient ($r=-0.368$, $p<0.001$). A widespread dysfunction of AChE activity was found in DLB (Lee *et al.*, 2010). Of note, the spatial coherence of AChE deficit and hypometabolism in DLB was reported in a multimodal neuroimaging study and was related to the degeneration of afferent cholinergic neocortical projections arising from the basal nucleus of Meynert (Klein *et al.*, 2010). The spatial association analysis based on metabolic differences in neurotransmission supports the hypothesis of a SERT system derangement as a major monoaminergic etiology differentiating EO-DLB from LO-DLB (Sim *et al.*, 2022). Indeed, we found a high correlation between hypometabolism and SERT map in EO-DLB, indicating a matched derangement in metabolism and 5-HTT SERT map. Loss of serotonergic neurons in the rostral raphe nuclei was reported in clinically diagnosed and neuropathologically confirmed DLB (Benarroch *et al.*, 2007). According to the Braak staging, the raphe nucleus is a subcortical region early affected by accumulations of Lewy bodies and neurites, even before the dopaminergic substantia nigra (Braak, Del, *et al.*, 2003).

In conclusion, this brain metabolic study using various analytic approaches revealed commonalities and differences between EO-DLB and LO-DLB. Specific neurotransmitter systems vulnerabilities and the presence of pure or mixed pathologies may have a role in the brain [^{18}F]FDG-PET results. These results add new biological evidence to the DLB syndromes.

We acknowledge some limitations of the study, mostly due to the retrospective observational design. First, a more comprehensive neuropsychological and neuropsychiatric assessment was not available to account for between-group differences that emerged in previous studies (e.g., (Sim *et al.*, 2022)). The role of serotonergic system dysfunction in EO-DLB should be confirmed by direct assessment with specific radiotracers for PET imaging.

4.2 Brain molecular imaging to achieve novel insights into the pathophysiology of neurodegenerative diseases

Brain connectivity approaches has allowed for remarkable advances in understanding neurodegenerative diseases' dysfunctional mechanisms, including LBDs ones (Carli *et al.*, 2021) – *Study 4*. Molecular approaches based on PET imaging provide evidence upon associations of brain metabolism and neurotransmitter systems and the combination of various imaging modalities represents an appealing approach to provide a comprehensive picture of neurodegenerative disease.

4.2.1 Study 5: Metabolic connectivity of resting-state networks in α synucleinopathies, from prodromal to dementia phase (Boccalini, et al., 2022) – Published article

Study 5 (Boccalini, Bortolin, *et al.*, 2022) assessed the large-scale brain network integrity in the spectrum of LB diseases, giving a comprehensive picture of connectivity reconfiguration from the prodromal to the overt clinical phases. We found altered connectivity patterns in the majority of the multiple large-scale brain networks, with interesting overlaps and differences within the disease spectrum. Distinct connectivity reconfigurations characterized the three clinical groups (iRBD, PD stable, and DLB). The SN and MN were the most severely affected networks in PD, and the LIN, ATTN, and PDMN in the DLB cohort. These specific patterns of connectivity reconfigurations might represent the dysfunctional substrates underlying the different clinical phenotypes. PD patients showed mainly motor symptoms (UPDRS III mean ± SD = 15.04 ± 7.02) and stable cognitive progression over time (no dementia evidence during 8 years of follow-up after the first clinical diagnosis). The SN and MN play a central role in preparing and executing the motor function (Tessitore, Cirillo and De Micco, 2019). Their connectivity in PD patients is frequently reported as disrupted (Caspers *et al.*, 2021; Chen *et al.*, 2021), and these functional changes are correlated with the motor symptoms' severity progression (Kojovic *et al.*, 2012). In DLB, metabolic connectivity alterations showed a severe involvement of PDMN, LN, and ATTN, consistently with the pathological and clinical heterogeneity of this condition (Iaccarino *et al.*, 2018; Sala *et al.*, 2019). In particular, PDMN and ATTN are associated with visual hallucination (Iaccarino *et al.*, 2018; Sala *et al.*, 2019), which were present as core symptoms in 73% (22 out of 30) of our DLB cohort. Notably, iRBD already showed severe alterations in PDMN and ATTN

networks compared to HC, sharing the same connectivity reconfiguration with DLB. On the contrary, iRBD and PD stable showed an overall low degree of similarity in metabolic connectivity reconfiguration in all the large-scale brain networks; in PDMN, the two groups showed the most prominent differences—likewise PD and DLB– (**Figure 16**). These results support that LB diseases are brain multisystem disorders, dynamically involving abnormal functioning of most large-scale networks, already in the prodromal phases. The high similarities between iRBD and DLB metabolic connectivity changes, together with the differences between PD and both iRBD and DLB, support the iRBD condition as a red flag for a progression to the severe phenotypes of α-synucleinopathies.

In the iRBD group, all networks showed a metabolic connectivity reconfiguration compared to HC, with the overlap ranging from poor to moderate (**Figure 17A**). MN, PDMN, and ATTN were the most altered networks. Connectivity alterations of the MN are in line with previous fMRI connectivity data (Ellmore *et al.*, 2013; Rolinski *et al.*, 2016; Yamada *et al.*, 2019; Wakasugi *et al.*, 2021). These fMRI studies report functional connectivity abnormalities in movement-related brain networks in iRBD patients, including sensory-motor networks. Rolinski et al. (2016) demonstrated that functional alteration of motor- related brain networks (basal ganglia network) is already present in iRBD and comparable to clinically manifested PD patients, despite the spared dopaminergic innervation. Thus, this study demonstrated that functional connectivity could be considered a sensitive measure to early brain changes, identifying brain alterations before a detectable neurotransmission impairment. A recent study further confirmed that motor-related networks (basal ganglia and sensory-motor networks) are dysfunctional in patients with iRBD without manifest motor deficits (Wakasugi *et al.*, 2021). In this study, we found a severe impairment of motor-related brain networks detected with metabolic connectivity measures for the first time (**Figure 16**). Thus, our findings, together with previous fMRI evidence, demonstrated the presence of early dysfunction in the motor large-scale brain networks in iRBD patients even before the onset of clinically relevant motor symptoms and dopaminergic impairments. Concerning the PDMN and ATTN, we found increased connectivity in iRBD patients compared to HC. Of note, iRBD showed a high overlap of metabolic connectivity reconfiguration in these networks with DLB patients, who showed increased anterior-posterior metabolic connections as well (**Figures 16**, **17B**, **18**). These functional connectivity alterations

related to posterior parietal regions agree with recent fMRI findings (Campabadal *et al.*, 2020). Campabadal et al. (2020) also found a correlation between functional connectivity in temporoparietal regions and cognitive performance in iRBD, suggesting a cognitive role of the derangement in posterior brain networks. In [^{18}F]FDG-PET studies—similar to fMRI data—connectivity changes are often explained in terms of function. Decreased connectivity indicates the functional separation between regions, whereas increased connectivity indicates increased functional pairing (Pievani *et al.*, 2014; Sala and Perani, 2019). Increased connectivity may indicate a "beneficial" compensatory process when increased connectivity affects metabolically spared brain regions. Thus, the recruitment of functionally spared brain regions might help cope with neurodegeneration. Most iRBD patients show hypometabolic patterns characterized by occipitoparietal hypometabolism with a sparing of frontal regions (Meles *et al.*, 2018; G. Carli, Caminiti, Galbiati, *et al.*, 2020), resembling those of DLB patients (Silvia Paola Caminiti *et al.*, 2019). In this context, the here reported increased functional connectivity between posterior regions and frontal brain area might represent compensation for the underlying neurodegeneration process in iRBD. Indeed, in DLB patients, we found the same compensatory metabolic connectivity signature, confirming previous results (S. Caminiti *et al.*, 2017; Sala *et al.*, 2019; G. Carli, Caminiti, Sala, *et al.*, 2020). Also, the visual networks, PVN and HVN, showed increased connectivity between the seed and occipital regions compared to HC (**Figures 16**, **17**). Conversely, DLB patients showed reduced metabolic connectivity within the same large-scale brain networks. Increased occipital connectivity in iRBD aligns with previous fMRI findings (Ellmore *et al.*, 2013; Byun *et al.*, 2020) and can support the recently proposed hypothesis about the cholinergic compensation to occipital damage in these patients (Bedard *et al.*, 2019; Byun *et al.*, 2020). Previous studies found that iRBD's cognitive performance positively correlates with functional measures of increased connectivity, indicating a possible ongoing compensation process linked to occipital regions (Byun *et al.*, 2020; Campabadal *et al.*, 2020). Moreover, recent molecular data (PET neuroimaging with the ^{18}F-fluoroethoxybenzovesamicol) demonstrated for the first time that the brain cholinergic alterations in patients with iRBD are characterized by increased cholinergic innervation in multiple brain areas (Bedard *et al.*, 2019), suggesting an ongoing compensatory cholinergic upregulation. The posterior occipital regions are crucial pathophysiological regions in cognitive decline in DLB and

PDD (A. Pilotto *et al.*, 2018; Silvia Paola Caminiti *et al.*, 2019). Indeed, in our study, DLB patients showed disrupted HVN and PVN metabolic connectivity connections. We hypothesize that increased occipital metabolic connectivity in iRBD patients may be a first protective compensatory response to early synucleinopathy-related changes in the occipital region, which is subsided by a connectivity decrease in DLB due to the advancement of the neurodegenerative processes and further accumulation of pathology.

In PD patients, we found a loss of connectivity mainly affecting the SN and MN networks showing a poor overlap with HC (**Figures 16**, **17**). These networks play a central role in motor function (Tessitore, Cirillo and De Micco, 2019) and are usually disrupted in PD patients (Caspers *et al.*, 2021; Chen *et al.*, 2021), leading to the motor symptoms' progression (Kojovic *et al.*, 2012). A recent multimodal imaging study demonstrated the close relationship between dopaminergic depletion, degeneration of nigrostriatal projection, and the destruction of sensory-motor networks in PD, mainly driven by the putamen's functional impairment (Ruppert *et al.*, 2020). In addition to SN and MN, we also found a decreased connectivity in ATTN, EXN, and PDMN, although less severe. These findings are consistent with previous metabolic connectivity data in PD (Sala, Silvia Paola Caminiti, *et al.*, 2017). PDMN showed a loss of connectivity between the seed and the anterior and posterior components. PDMN disruption was a direct consequence of PD pathology (Yao *et al.*, 2014) and is closely associated with PD dopaminergic depletion (Spetsieris *et al.*, 2015). Overall, the main connectivity alterations in PD are possibly led by the dopaminergic dysfunction characterizing this clinical entity. According to the dual syndrome hypothesis, the frontostriatal dysfunction is a characteristic of non-demented PD patients, as our cohort, and the posterior cortical dysfunction, found here in DLB and iRBD, is considered a signature of cognitive decline (Kehagia, Barker and Robbins, 2013). Consistently, we did not find a posterior connectivity alteration in PD, resembling a DLB pattern, as an early predictor of dementia. The frontal executive connectivity derangement seems to be disease-specific for stable PD, profoundly differing from connectivity alterations of iRBD and DLB.

In DLB patients, metabolic connectivity derangement involved PDMN, ATTN, and LIN, consistent with previous evidence (Sala *et al.*, 2019). DLB connectivity alterations in large-scale RSNs are also strongly related to clinical symptoms (Sala *et al.*, 2019). The alterations of PDMN, ATTN, and visual networks are associated with visual

hallucinations (Iaccarino *et al.*, 2018; Sala *et al.*, 2019). The biological explanation for these findings points to cholinergic damage, leading to the breakdown of the functional relationship among the calcarine cortex, lateral occipital cortex, and parietal cortex (Klein *et al.*, 2010). In our DLB group, both visual networks—PVN and HVN—showed decreased metabolic connectivity compared to HC (**Figures 16**, **17B**). On the other hand, PDMN and ATTN were characterized by abnormal connectivity increases involving the dorsolateral prefrontal cortex. As discussed above in iRBD, the increased poster-anterior connectivity can be interpreted as a compensative mechanism. In DLB patients, cognitive reserve proxies (i.e., education and specific occupational profiles) modulate both ATTN and PDMN throughout neural compensation mechanisms (Giulia Carli, Boccalini, *et al.*, 2020). Specifically, it has been demonstrated that highly educated DLB can engage the anterior brain regions to cope with posterior pathology. However, in overt DLB, the dorsolateral prefrontal cortex can be part of the hypometabolic pattern (Silvia Paola Caminiti *et al.*, 2019). When increased connectivity affects metabolically impaired brain regions, it may represent a form of maladaptive functional reorganization resulting from the brain's failure to cope with the damage. For instance, the proper one-to-one connection in healthy brains can be substituted by a widespread dysfunctional connectivity pattern toward several regions resulting in maladaptive connectivity increases. However, separating beneficial from maladaptive processes remains a challenge in need of longitudinal data and correlation with behavior (Schoonheim, 2017). Regarding LIN alterations in DLB, previous evidence showed that these are associated with the presence of clinical RBD (Sala *et al.*, 2019). Notably, the LIN seed is the amygdala which is considered an early site of LB accumulation (Braak, Del, *et al.*, 2003), and amygdala LB pathology has been associated with visual hallucinations (Harding and Halliday, 2001).

Overall, despite large-scale brain network alterations in all clinical groups, high topographical overlaps were found only in iRBD and DLB, and not in PD. Specifically, the involvement of the posterior and limbic networks appears as the DLB hallmark related to the clinical core symptoms, such as visual hallucinations (Sala *et al.*, 2019). These RSN alterations already in the iRBD phase may represent an early signature of future clinical progression. Similarly, the high spatial overlap in the ATTN between iRBD and DLB can be related to attentional and executive deficits in the two syndromes. Cognitive tests

assessing attention and executive functions strongly predict conversion to dementia in iRBD patients (Génier Marchand *et al.*, 2018). In conclusion, the findings of *Study 5* revealed that metabolic connectivity alterations in large-scale networks are already present in the iRBD phase. Strong connectivity similarities emerged between iRBD and DLB, showing comparable metabolic patterns in RSNs relevant for cognitive decline. Differently, PD's altered connectivity patterns support its more benign phenotype without dementia development. Thus, our findings showed the different RSNs derangement underlying the spectrum conditions. The disease-specific vulnerabilities shared by iRBD and DLB indicate that iRBD can be considered a risk factor for progression to a malignant α-synucleinopathy phenotype (Berg *et al.*, 2021).

4.3 Sex and gender as crucial sources of variability in LBD

Gender and sex are important sources of variance in LBDs clinical manifestation, characterized by marked heterogeneity and variable disease courses. Investigating in-depth the interaction between these factors and the underlying pathology is essential to implement tailored clinical work-up in terms of precision medicine.

4.3.1 Study 6: Gender-Related Vulnerability of Dopaminergic Neural Networks in Parkinson's Disease (Boccalini, et al., 2021) – Published article

Study 6 (Boccalini *et al.*, 2021) provides evidence of gender-specific effects on brain metabolic connectivity of dopaminergic networks in a cohort of PD patients. We considered the nigro-striato-cortical and the mesolimbic dopaminergic pathways linked to specific clinical PD features (Sulzer and Surmeier, 2013; Castrioto *et al.*, 2016). Our results show a widespread alteration of metabolic connectivity within the nigro-striato-cortical network in PD males (**Figures 19** and 2**1**). On the contrary, the connectivity of the mesolimbic dopaminergic system was remarkably reconfigured in women (**Figures 20** and **21**). On the methodological side, the present study is based on a metabolic connectivity approach that has demonstrated good reproducibility and applicability on PET-based assessments of brain connectivity (Veronese *et al.*, 2019), encouraging its use to investigate the neurotransmission network characteristics and the changes in neurological conditions. Subsequently, with the use of this approach, previously published studies revealed metabolic connectivity alterations within the nigrostriatal

dopaminergic and mesolimbic system, in PD and DLB (S. Caminiti *et al.*, 2017; Sala, Silvia Paola Caminiti, *et al.*, 2017). Sex hormones play a crucial role in gender differences in PD providing disease protection in women (Gillies and McArthur, 2010). The nigrostriatal dopaminergic system expresses high densities of estrogen and progesterone receptors in the human brain, determining its vulnerability to the modulation of sex hormones (Barth, Villringer and Sacher, 2015). Estrogens show neuroprotective effects on the nigrostriatal dopaminergic system. It has been proposed as a supportive effect of estradiol on DAT, leading to a greater amount of striatal dopamine availability in women (Gillies and McArthur, 2010). Following this evidence, we found a more preserved nigro-striato-cortical dopaminergic network in PD females compared with males, supporting a possible protective role of estrogens on the dopaminergic nigro-striato-cortical system. Thus, the development of symptomatic PD is delayed in women by higher physiological dopamine levels on the striatum due to the activity of estrogens. The estradiol-induced neuroprotection might be an adaptive response in the surviving neurons, restoring striatal dopaminergic functionality (Gillies and McArthur, 2010). In addition to sex hormones, a variety of broader social factors (e.g., role expectations and social attitudes) might modulate the course and outcome of neurodegenerative diseases. For example, gender differences can be noticed in the types of education and occupation due to gender roles, behaviors, and activities. A recent study highlighted gender differences in the effects of education and occupation on brain metabolism and cognitive reserve in AD (Malpetti *et al.*, 2017). In this context, the gender differences obtained in the metabolic connectivity may also be related to environmental factors, such as individual learning experiences, culture, or gender stereotypes. Indeed, gender roles, behaviors, and social activities due to historical and cultural aspects may influence the brain organization and the vulnerability and integrity of the brain itself. All the above suggest that different connectivity reconfigurations of dopaminergic networks that were revealed in women and men might be due to the interaction between sex-biological and social factors. α-synuclein plays a key role in dopaminergic neurotransmission pathways, regulating the filling and fusion of vesicles via vesicular monoamine transporter 2, the dopamine reuptake via DAT, and the postsynaptic dopamine activity (Calo *et al.*, 2016). Previous evidence acquired using the very same metabolic approach in a PD cohort showed a major vulnerability of the nigro-striato-cortical in comparison with the mesolimbic pathway (Sala, Silvia Paola

Caminiti, *et al.*, 2017). Considering PD males and females separately, specific metabolic connectivity alterations emerged in the present study, suggesting that gender may play a role in the variability of PD pathological substrate (**Figures 15** and **16**). Specifically, we found that the metabolic connectivity reconfiguration characterized by connectivity decreases and increases (**Figures 15** and **16**). Connectivity changes are usually interpreted in terms of function: connectivity decrements may indicate functional disconnection between regions, while connectivity increments indicate increased functional coupling between regions. However, increased connectivity that affects metabolically impaired brain regions might indicate a maladaptive mechanism, such as the disrupted excitatory–inhibitory balance of damaged networks due to underlying pathological processes (Pievani *et al.*, 2014; Sala and Perani, 2019). The present results concerning the nigro-striato-cortical pathway are in line with other data obtained in PD patients using single-photon emission computerized tomography imaging, where women show greater striatal DAT activity than men (Eusebio *et al.*, 2012; Koch *et al.*, 2014; Kaasinen *et al.*, 2015). The reduced vulnerability in the female nigro-striato- cortical dopaminergic system might be explained by the estradiol-induced neuroprotection on this system, as suggested (Haaxma *et al.*, 2007; Gillies and McArthur, 2010; Cerri, Mus and Blandini, 2019). It is well known that estradiol increases the synthesis, release, reuptake, and the turnover of dopamine (Cerri, Mus and Blandini, 2019). Studies mostly point toward a neuroprotective effect of estrogen on dopaminergic systems and toward a consequent reduction of risk for PD. These brain differences may account for the gender-related differences in motor symptoms that are primarily caused by the degeneration of the nigrostriatal dopamine neurons (McCann *et al.*, 2014). Coherently, greater motor impairment was found across a large PD cohort, mainly in men compared with women (Lubomski *et al.*, 2014). Specifically, men demonstrated higher UPDRS-III scores and required a significantly higher daily levodopa equivalent dose for therapy. Moreover, a recent study investigating the neurophysiological sex differences in early PD reported that female patients have a more favorable profile during transcranial magnetic stimulation, as suggested by the preserved physiological focal response to sensorimotor plasticity compared with men (Kolmancic *et al.*, 2019). However, the mechanisms through which estrogens act on the dopaminergic system protect against the a-synuclein-related neurodegeneration and the consequent motor clinical manifestations are not yet fully understood (Cerri, Mus and

Blandini, 2019). Moreover, there is also a lack of data regarding whether estrogen has a neuroprotective effect on the mesolimbic system, despite its involvement in PD clinical nonmotor symptoms. In this study, we also considered the mesolimbic system connectivity. Our results demonstrated a major vulnerability in PD females in this system, which is relatively spared in men (**Figures 20** and **21**). The mesolimbic system impairment in humans shows high intersubject variability, as demonstrated by postmortem studies (Surmeier and Sulzer, 2013) and *in vivo* molecular data (S. Caminiti *et al.*, 2017). Although the a-synuclein pathology is present in the ventral tegmental area (VTA), its neurons seem relatively spared to the overexpression of human A53T mutated a-synuclein compared with substantia nigra's neurons (Maingay *et al.*, 2006). The specific mechanisms defending VTA dopaminergic neurons from neurodegeneration are still unclear (Calo *et al.*, 2016). In this context, our findings suggest that gender may represent a crucial source of this variability in PD patients. This conclusion is consistent with previous studies that demonstrated that several psychiatric symptoms, such as apathy, depression, anxiety, and fatigue, are more common and severe in women (Martinez-Martin *et al.*, 2012). In PD, impairment in the mesolimbic dopaminergic system has been linked to nonmotor symptoms, in particular mood disorders, which may affect patients since or even before the initial clinical phase of PD (Gustafsson, Nordström and Nordström, 2015; Castrioto *et al.*, 2016). These findings would also fit with the higher rate of impulse compulsive disorder that resulted from the use of dopaminergic drugs observed in males (Premi *et al.*, 2016). Further studies will be critical for a better understanding of the neurobiological bases of the clinical different phenotypes in women and men. The gender-related vulnerabilities here reported might be explained also by sociodemographic factors, as briefly stated above. Educational, behavioral, and lifestyle choices might affect the organization of specific brain networks (Malpetti *et al.*, 2017). Limbic structures are sensitive to sex hormones, leading to high stress vulnerability of this system in females (McLaughlin, Baran and Conrad, 2009). Coherently, the mesolimbic dopamine system seems to be more sensitive to social defeat in females compared with males (Greenberg and Trainor, 2015). As supportive evidence, the cerebral metabolism and the metabolic connectivity in aging and AD dementia are affected by occupation and education with clear gender differences (Malpetti *et al.*, 2017). These gender brain discrepancies might be also explained by sociodemographic factors that can

consequently contribute to differences between females and males in brain functions and networks. The female widespread mesolimbic connectivity reconfiguration here reported could be explained as a function of gender-related interactions between biological and social elements.

Study 6 has some limitations, that we overcome with *Study 7* investigating gender differences in PD using [^{123}I]FP-CIT-SPECT. From the methodological standpoint, it must be acknowledged that despite the high accuracy and reproducibility of covariance [^{18}F]FDG-PET network analysis in the assessment of neurotransmitter system connectivity (Veronese *et al.*, 2019), some cortical regions receive overlapping projections from different neurotransmitter systems. Thus, results obtained with metabolic connectivity based on [^{18}F]FDG-PET data might lose a portion of their specificity. We also acknowledge that our data do not address the relationship between clinical characteristics and brain metabolic connectivity changes in the dopaminergic neural networks, due to data missing for the retrospective nature of the study.

4.3.2 Study 7: Gender differences in dopaminergic system dysfunction in de novo Parkinson's disease clinical subtypes (Boccalini, Carli*, et al., 2022) – Published article*

Study 7 (Boccalini, Carli, Pilotto, *et al.*, 2022) investigated gender differences in the large PPMI cohort of newly diagnosed and drug-naïve iPD patients, stratified according to clinical criteria in three groups: mild motor predominant, intermediate, and diffuse malignant (Fereshtehnejad *et al.*, 2017). The current study thus provides the first evidence of gender differences in clinical features, dopaminergic dysfunction, and molecular connectivity in well-defined iPD clinical subtypes. We found that in the mild motor and intermediate subtypes, male iPD patients had poorer cognitive abilities than females, who in contrast presented with more severe anxiety symptoms. Gender differences emerged also in the diffuse malignant subtype, with more severe motor impairment in males than females, the former with associated more severe SUVr in the putamen. The higher male vulnerability of the dopaminergic motor system also emerged in the mild motor and inter- mediate subtypes, with more severe and widespread connectivity alterations in the nigrostriatal dopaminergic pathway in males than females. As for the mesolimbic pathway, SUVr and molecular connectivity analyses demonstrated

lower [^{123}I]FP-CIT bindings in several limbic brain targets and a more massive reconfiguration of the mesolimbic system's connectivity in female than male patients. Of note, in females, high anxiety levels were associated with lower SUVr in the amygdala. Thus, the dysfunction of mesolimbic structures and their connectivity suggest a possible role of this endophenotypic pattern in the expression of psychiatric symptoms in females.

From a clinical standpoint, we found significant motor gender differences only in the diffuse malignant subtype, with males showing higher MDS-UPDRS III scores than females (**Table 12**). Since the diffuse malignant group expresses a more severe motor impairment, gender differences in the severity of motor symptoms could be more easily detectable in this subgroup than in the others (**Table 12**). This result agrees with previous reports of a more benign motor phenotype in iPD women than men (Haaxma *et al.*, 2007; Cerri, Mus and Blandini, 2019; Meoni, Macerollo and Moro, 2020). Consistent with the clinical difference, in the diffuse malignant subtype, we found a lower dopamine uptake in the putamen in males than females, and a significant correlation between reduced putaminal bindings and motor impairment as assessed by MDS- UPDRS III, only in males (**Table 14**) (as discussed below). Despite the limited sample size of this sub-group, these results surviving a conservative statistical threshold and based on a single subject-specific ROIs approach might support the hypothesis of a protective effect of female gender on motor impairment. A protective effect of estrogens on the nigrostriatal dopaminergic system has been proposed, with estradiol having suppressive effects on DAT, leading to a higher striatal dopamine availability in women (Gillies and McArthur, 2010). Following this hypothesis, the worsening of motor symptoms may be delayed in women by higher physiological dopamine levels in the striatum due to estrogens' protective activity and/or other female long-life reproductive factors (Haaxma *et al.*, 2007; Frentzel *et al.*, 2017). In the case of non-motor symptoms, gender differences were present in both mild-motor and intermediate subtypes. Males had lower performances than females in executive functions, memory, and processing speed (**Tables 11** and **12**). This cognitive picture is consistent with recent studies suggesting that male iPD patients are more prone to cognitive alterations (Reekes *et al.*, 2020). An exception was the visuospatial abilities in the intermediate subtype, which were lower in females than in males (**Table 12**). This is in keeping with previous studies in iPD (Locascio, Corkin and Growdon, 2003; Riedel *et al.*, 2008) and may be due to the higher performance of males in visuospatial tasks

reported in most general population studies (Weiss *et al.*, 2003; Curtis *et al.*, 2019). Moreover, males in the intermediate subtype had higher scores in the RBD questionnaire. The presence of RBD has prognostic relevance for progression to dementia in iPD (Postuma, Gagnon and Montplaisir, 2013; Anang *et al.*, 2014; Fereshtehnejad *et al.*, 2015). All in all, our results fit well with the evidence of an increased risk of PD-related cognitive impairment and dementia in males (Anang *et al.*, 2014; Pigott *et al.*, 2015). In the case of behavioral symptoms, female patients showed higher anxiety scores than males in the whole sample and especially in the intermediate subtype (**Tables 11** and **12**). Psychiatric symptoms, such as anxiety and depression, seem to be consistently associated with sex in iPD, with women presenting a higher burden than men (Scott *et al.*, 2000; Leentjens *et al.*, 2011; Martinez-Martin *et al.*, 2012; Liu *et al.*, 2015; Cerri, Mus and Blandini, 2019; Meoni, Macerollo and Moro, 2020). As for the [^{123}I]FP-CIT binding in the nigrostriatal dopaminergic system, gender differences emerged in all subtypes. Namely, i) the putamen binding was more preserved in females than males in the diffuse malignant subtype, supporting the more severe motor impairment observed in male patients; ii) female patients in the intermediate subtype presented a more significant DAT asymmetry in the putamen. Since the loss of side-to-side asymmetry is usually associated with disease worsening, this may indicate a less severe dopaminergic deficit (Nandhagopal *et al.*, 2009). These results, together with the mild alterations of molecular connectivity (see below) in females, are also in line with the hypothesis of estrogen-induced neuroprotection of the nigrostriatal system (Gillies and McArthur, 2010). The significant gender differences in striatal binding observed only in the diffuse malignant subtype may be due to the high disease burden than in the other subtypes, since PD motor symptoms do not manifest until a loss of 30–55% of putamen uptake (Lee *et al.*, 2000; Hilker *et al.*, 2005). Thus, gender differences in the intermediate subtype emerged as asymmetry in dopaminergic depletion. The protective effect of the female gender on motor system in severe PD phenotypes, however, needs to be replicated in larger age-matched samples. Major gender differences in [^{123}I]FP-CIT binding were present mainly in the extra-striatal regions belonging to the mesolimbic dopaminergic system, i.e. the hippocampus, amygdala, parahippocampus, insula, anterior, and middle cingulate cortex. This system was more affected in iPD females in the whole group and across all the subtypes (**Tables 13** and **14**). These mesolimbic regions receive dopamine projections

from the VTA, and ventral striatum neurons and their disruption is considered as the leading cause of neuropsychiatric symptoms in iPD (Castrioto *et al.*, 2016). In particular, the differences in [^{123}I]FP-CIT binding in the insula and amygdala, crucially affected by α- synuclein deposition in iPD, can be related to a wide range of non- motor symptoms, including socio-affective and behavioral changes (Criaud *et al.*, 2016), which were prominent in female patients. Of note, the lower female [^{123}I]FP-CIT binding in these extra-striatal regions is also due to loss of SERT (Koch *et al.*, 2014), suggesting an altered serotoninergic transmission. Thus, a more severe dopaminergic and serotoninergic dysfunction in iPD females may explain the higher incidence of severe psychopathological states (Gustafsson, Nordström and Nordström, 2015; Castrioto *et al.*, 2016), as observed in our female sample. In line with the clinical data, our correlation analysis revealed that the anxiety trait scores were associated with decreased [^{123}I]FP-CIT uptake in the amygdala, only in females. In addition, we found gender differences of [^{123}I]FP-CIT bindings in globus pallidus and thalamus, with female patients showing more significant binding reductions than men (**Tables 13** and **14**). The thalamus is an important hub for subcortical–cortical projections (Haber and Calzavara, 2009) and its molecular dysfunction might have long-distance effects on the limbic system (Pilotto, Schiano di Cola, *et al.*, 2019). On the other hand, the globus pallidus is the main target area for surgery and deep brain stimulation in PD (Vitek *et al.*, 2004). The neurotransmitter imbalance between GABAergic and dopaminergic activities in globus pallidus may contribute to resting tremor in iPD (Rajput *et al.*, 2008), a more common presenting motor symptom in women than in men (Cerri, Mus and Blandini, 2019; Meoni, Macerollo and Moro, 2020). We also report for the first time the presence of gender differences in the molecular connectivity of the dopaminergic circuitry in iPD and all subtypes. Following the metabolic connectivity evidence of *Study 5* (Boccalini *et al.*, 2021), we here confirm the gender differences in the vulnerability of the nigrostriatal and mesolimbic pathways in a large cohort of patients (**Figures 22** and **23**). Male patients showed extensive alterations in the molecular architecture of the nigrostriatal dopaminergic circuitry, with the primary loss of inter-connections at the level of basal ganglia, in all subtypes. Female patients showed alterations within the nigrostriatal system limited to the frontal cortical connections (opIFG and the precentral gyri). These regions also showed a higher dopaminergic depletion than in men, as revealed by SUVr

analysis, in mild motor and intermediate subtypes (**Table 14**). These gender-related connectivity reconfigurations might be again considered in the frame of hormone-induced neuroprotection on the nigrostriatal dopaminergic system. Of note, preclinical evidence has suggested a potential neuroprotective effect of estrogens through anti-inflammatory, anti-oxidative, and anti-apoptotic mechanisms, in addition to possible inhibitory effects on the formation and stabilization of α-synuclein fibrils (Jurado-Coronel *et al.*, 2018). The circulating estrogens determined by parity, duration of the fertile life span, age at menopause throughout a woman's life can lead to a later age at onset of PD (Haaxma *et al.*, 2007; Frentzel *et al.*, 2017). Thus, despite the advanced age of the women included in our sample, their advantage over men may be explained by hormonal and reproductive factors that have characterized their whole fertile life. Mesolimbic system impairment in iPD is characterized by high intersubject variability (Sulzer and Surmeier, 2013), and gender may represent a crucial source of this variability. Consistent with the low [^{123}I]FP-CIT bindings reported here in the limbic dopaminergic targets, we found a prominent connectivity alteration in the mesolimbic system in female patients, and for all groups (**Figures 22** and **23**). Male patients also showed some alterations in the mesolimbic system, but more limited. The topography changes were widespread in females, involving almost all the dopaminergic targets. The mesolimbic dopaminergic system is involved in non-motor symptoms, especially mood disorders. These symptoms are more common in iPD females and may affect patients since or even before the disease onset (Gustafsson, Nordström and Nordström, 2015; Castrioto *et al.*, 2016). Of note, the evidence of more extensive connectivity alterations of the mesolimbic pathway in females than males was significant in the intermediate subgroup, where gender differences in neuropsychiatric assessment emerged. Beyond sex-related factors, social factors might modulate the course and outcome of neurodegenerative diseases. An elderly cohort like ours could have been subject to gender disparities in education and occupation due to different social roles, behaviors, and activities. These flexible factors may influence the brain organization, vulnerability, and integrity of the brain itself. Limbic structures are highly interconnected and sensitive to stress and sex hormones, with high-stress vulnerability in females (McLaughlin, Baran and Conrad, 2009). Long-standing exposure to gender inequity is assumed to elicit sustained stress reactions, which is usually considered one of the main pathophysiological pathways linking social disadvantages to health (Hasselgren *et al.*,

2020). Thus, the life-long intricate networking of several factors, including genetics, environmental exposure, reproductive hormones, and neurotransmitters, might significantly impact the neurodegenerative processes and the clinical manifestations of diseases.

Concerning limitations of *Study 6*, we acknowledge that [^{123}I]FP-CIT binding in the extra-striatal regions is also due to SERT besides DAT density. However, our connectivity analysis addressed regions belonging to the nigrostriatal and mesolimbic dopamine structures and the target pathways rich in dopamine transporters. This finding was also considered additional evidence of serotoninergic gender differences in need of further research studies.

4.3.3 Study 8: Sex differences in dementia with Lewy bodies: an imaging study of neurotransmission pathways (Boccalini, et al., 2023) – Published article

Study 8 explores sex differences in pDLB by using [^{123}I]-FP- CIT-SPECT, also considering the affinity of the tracers for transporters involved in different neurotransmission systems (i.e., high-to-low affinity for DAT, SERT, and NET transporters, respectively). Thus, this study provided the first evaluation of the influence of sex on molecular endophenotypes in pDLB, considering neurotransmission impairments and molecular connectivity. We found comparable [^{123}I]FP-CIT binding decreases in dopaminergic systems in pDLB males and females in comparison to CTL. However, females showed more reduced extrastriatal binding than males (**Figure 24C**). As a trend toward similar sex differences was also found in the CTL group when comparing males and females, lower binding levels in these regions might represent a sex-related vulnerability to pathology. Connectivity of the nigrostriatal and mesolimbic systems was affected in both sex groups, but with different patterns. In line with the more extensive neurodegeneration hypothesis, beyond the striatal regions, pDLB females showed more long-distance connectivity alterations between subcortical and cortical regions belonging to the dopaminergic systems, in comparison to pDLB males. This study also revealed different molecular dysfunctions linked to monoaminergic transporters' availability. From a clinical standpoint, our data are in line with a male predominance in pDLB, as 62% of patients in our cohort were men. The male predominance is lower compared to previous works (Podcasy and Epperson, 2016; Van De Beek *et al.*, 2020);

however, it is consistent with the age of our cohort. Sex differences in prevalence are expected to be lower with increasing age (Mouton *et al.*, 2018; Van De Beek *et al.*, 2020), maybe in association with the drop in neuroprotective effects of estradiol (Mielke, Vemuri and Rocca, 2014). In addition, the more frequent concomitant AD pathology in females should be considered. AD co- pathology leads to more pronounced typical AD symptoms (Ferreira *et al.*, 2020), which can introduce a risk of underdiagnosing women with DLB in favor of AD (van de Beek *et al.*, 2020; Bayram *et al.*, 2021). Moreover, pDLB females in our cohort are older than males at the time of diagnosis (Bayram *et al.*, 2021) in line with the evidence that women meet clinical criteria for pDLB at an older age and after a longer latency from cognitive onset (Choudhury *et al.*, 2022). Despite women being less likely to meet clinical diagnostic criteria for pDLB, when symptoms are present, the clinical severity is not milder than in men (Bayram *et al.*, 2021). Accordingly, we did not find any significant differences in terms of clinical core features (frequency of parkinsonism, RBD, cognitive fluctuations, and visual hallucinations were similar in our cohorts) (**Table 15**). Here we show relevant data on the sex-specific alterations in [^{123}I]FP-CIT binding linked to other monoaminergic systems with sex differences to be considered for future studies assessing clinical phenotypes.

From the molecular perspective, both sex groups were characterized by loss of striatal DAT binding, a common hallmark of DLB (Wallert *et al.*, 2022), and also extrastriatal binding, in line with previous studies (Roselli *et al.*, 2010; Joling *et al.*, 2018). Moreover, we highlighted a tendency for sex-specific differences in [^{123}I]FP-CIT binding, also in CTL, that become significant in presence of pDLB diagnosis (**Figure 24A** and **B**). The comparison with CTL revealed a greater decrease in striatal bindings for pDLB males. Conversely, pDLB females showed lower [^{123}I]FP-CIT binding in cortical targets of the nigrostriatal dopaminergic system, i.e., middle frontal gyrus, precentral and postcentral gyri, but also in the extrastriatal regions belonging to the mesolimbic dopaminergic systems, i.e., amygdala, hippocampus, parahippocampus, insula, and cingulate gyrus compared to pDLB males (**Figure 24C**). Notably, the trend toward sex differences in the same extrastriatal regions in CTL suggests that sex vulnerabilities may not reflect a sole effect of DLB pathology, but a multifactorial mechanism which is present, albeit to a lesser extent, even in the absence of a neurodegenerative process. In pDLB, the females' lower binding in the cortical regions involved in the nigrostriatal

dopaminergic system is in line with the greater incidence of parkinsonism reported in our female sample as compared to males (**Table 16**). The great impairment of the nigrostriatal system was also supported by the sex difference in connectivity patterns involving connections between the frontoparietal cortical motor and striatal regions, which was only observed for females. Sex molecular differences emerged also in the mesolimbic structures' binding, with a sex-specific vulnerability disfavoring females. A lower [^{123}I]FP-CIT extrastriatal binding in females than males is found here also in CTL, without reaching the threshold for significant differences, as happened instead for pDLB. The limbic system is vulnerable to α- synuclein pathology and potentially explains autonomic and affective dysfunctions in DLB patients (Halliday *et al.*, 2011). Notably, a recent study found a similar limbic dopaminergic vulnerability in females with PD supporting the higher incidence of severe psychopathological states [25]. Taken together, these results suggest a common sex-dependent vulnerability of the mesolimbic system in α-synucleinopathies (Boccalini, Carli, Pilotto, *et al.*, 2022). In the absence of an interaction effect on the molecular binding in some regions applying the ROI-based approach, one can speculate that a sex-specific vulnerable ground could be present even in a healthy population (Malpetti *et al.*, 2017). Previous studies focused on sex differences in striatal DAT reporting healthy women to have higher striatal binding compared with healthy men that tend to disappear with aging (Shigemoto *et al.*, 2022). Albeit the sex-related differences are controversial (Nicastro, Garibotto, Poncet, *et al.*, 2016) and mostly based on conventional regions of interest-based analysis (Kaasinen *et al.*, 2015), our results extend the literature supporting that sex differences in [^{123}I]FP-CIT extrastriatal binding may exist in healthy populations and can influence the disease-related reduction in DAT. Limbic structures are highly interconnected and sensitive to stress and sex hormones, with high-stress vulnerability in females even in the healthy population (McLaughlin, Baran and Conrad, 2009). Then, the neurodegenerative processes might differently impact males and females depending also on several factors, including genetics, environmental exposure, and reproductive hormones. Noteworthy, α-synuclein pathology plays a key role in the neurotransmitter impairment affecting different clinically relevant systems, such as the dopaminergic, serotonergic, and noradrenergic ones (Uchihara and Giasson, 2016), for which [^{123}I]FP-CIT binding has high-to-low affinity, respectively (Scheffel *et al.*, 1997; Booij *et al.*, 2007; Booij and Kemp, 2008). To

explore the sex-specific alterations in [^{123}I]FP-CIT binding linked to other neurotransmitter systems beyond DAT, we applied spatial association analysis with specific neurotransmitter maps (Dukart *et al.*, 2021). We found [^{123}I]FP-CIT binding alterations associated also with SERT in both sex groups and NET only in females (**Figure 25**), which is consistent with the affinity of the tracer for transporters involved in these different neuro- transmission systems (Scheffel *et al.*, 1997; Booij *et al.*, 2007; Booij and Kemp, 2008) and supports their clinical relevance. Monoaminergic neurotransmitter alterations in DLB have been related to affective symptoms, such as depression and psychosis (Sharp *et al.*, 2008; Vermeiren *et al.*, 2015). Postmortem studies identified the decreased serotonergic neurotransmission as the main mono- aminergic etiology of depression in DLB, whereas impaired dopaminergic activity across the mesolimbic system might clinically account for psychosis (Vermeiren *et al.*, 2015). Noradrenergic deficiency is also of great magnitude, occurs early, and shows a strong correlation with disease severity in DLB, involving autonomic dysfunction, sleep disturbances, and cognitive decline (Vermeiren and De Deyn, 2017). Moreover, there is evidence that the presence of AD plaques and tangles in addition to Lewy body pathology further impairs noradrenergic neurotransmission in the locus coeruleus in DLB (Vermeiren *et al.*, 2015). Of relevance, we found that sex-related [^{123}I]FP-CIT binding alterations were associated with the NET system only in pDLB females, who usually present a great burden of AD pathology (Van De Beek *et al.*, 2020; Bayram, Coughlin and Litvan, 2022). A recent study explored the influence of concomitant AD pathology in DLB on both striatal and extrastriatal [^{123}I]FP-CIT binding, highlighting lower extrastriatal binding in the group with co-pathology (van der Zande *et al.*, 2020). The authors supported more extensive neurodegeneration, including the dopaminergic and serotonergic systems, in mixed pathology, possibly due to a synergistic effect of concomitant AD pathology. Further sex studies combining *in vivo* molecular imaging with amyloid and tau data are warranted to confirm our findings. Moreover, our results advocate future sex-related studies on the serotonergic and noradrenergic systems in DLB, using specific radiotracers, in large patient samples. Insights into the disease-specific sex effect on monoaminergic deficits might have implications for disease management in a precision medicine approach.

4.3.4 Study 9: Sex differences in brain metabolic connectivity architecture in probable dementia with Lewy bodies (Caminiti, Boccalini, et al., 2023) – Published article

Study 9 further deepened the knowledge of gender differences in pDLB by investigating how sex can modulate brain metabolism and metabolic connectivity (Caminiti, Boccalini, *et al.*, 2023). We applied metabolic connectivity approaches in a comprehensive whole brain and neural networks perspective to shed light on possible metabolic sex differences in pDLB. The results showed commonalities and differences in a large cohort of pDLB patients stratified by sex, and characterized by similar age, global cognitive functioning, and disease duration at the time of [^{18}F]FDG-PET exam. Both male and female pDLB groups showed the prototypical DLB-like hypometabolism, involving the occipital, temporoparietal cortex, and dorsolateral prefrontal cortex (**Figure 27**) (S.P. Caminiti *et al.*, 2019). However, the direct comparison revealed a more severe hypometabolism in temporoparietal and occipital DLB signature regions in male than female patients (**Figure 27**). Despite greater frontal and parietal volume loss in men than women have been reported in DLB contributing to cognitive dysfunction (Ballmaier *et al.*, 2004), this is the first time that sex differences in brain hypometabolism are investigated in pDLB. The more severe brain posterior hypometabolism in men compared to women may be due to the more diffuse neocortical LB pathology found in pDLB males (Nelson *et al.*, 2010), which is also considered the main determinant of occipital hypometabolism in DLB (Kasanuki *et al.*, 2012). The latter was associated with worse global cognitive dysfunction, visuo-spatial, and visuo-perceptive deficits, and with a higher likelihood of developing visual hallucinations in DLB (S.P. Caminiti *et al.*, 2019). Notably, male sex is considered the primary predictive factor in the transition from no cognitive impairment to mild cognitive impairment or dementia in patients with PD and men progress more rapidly than women (Cholerton *et al.*, 2018). Moreover, a recent longitudinal PET study reported an annually increased tau accumulation in the lateral occipital cortices, inferior parietal cortex, and fusiform gyrus in patients with DLB. The longitudinal increase in tau accumulation observed in both the fusiform gyrus and occipital cortex correlated also with global cognitive decline measures (Chen *et al.*, 2022). We also found more severe hypometabolism in the hippocampus in pDLB females than males (**Figure 27**). A recent postmortem study showed more severe hypometabolism in the hippocampus in patients with both concomitant LB and AD pathology than with

only LB (Lee *et al.*, 2022). Co-occurrent AD pathology is more often observed in DLB females than males (Coughlin, Hurtig and Irwin, 2020; Bayram *et al.*, 2021). Sex was found to significantly impact on AD copathology, with women showing a higher expression (Bayram, Coughlin and Litvan, 2022). In the present study we also evaluated the linear relationship between hypometabolism and age in the males and females HC. We found in both males and females a medial frontal cortex hypometabolism associated with aging, that was more extended in males than females. The present results confirm the previous evidence of a more extended frontal lobe vulnerability in males than females (Malpetti *et al.*, 2017). The frontal lobe vulnerability related to aging was consistently reported in the literature, and sex differences in age-related hypometabolism might reflect the faster age-related cognitive declines in males (Gur and Gur, 2022). In addition, in elderly males, declining levels of circulating testosterone are linked to changes in brain function and cognition (see (Giagulli *et al.*, 2016) for review).

Previously published studies revealed whole-brain metabolic connectivity alterations in synucleinopathies (S.P. Caminiti *et al.*, 2017; Sala, Silvia Paola Caminiti, *et al.*, 2017). A widespread impairment of brain metabolic connectivity architecture was also found here in the pDLB cohort, with a more pronounced connectivity loss in the pDLB males than females (**Figure 28B**). Considering pDLB males and females separately, shared or specific metabolic connectivity alterations emerged in the present study. The shared connectivity alterations involved insular and parietal nodes disconnecting with both cortical and subcortical nodes. The pathological hubs localized in temporoparietal regions were in line with the typical DLB hypometabolic pattern (S.P. Caminiti *et al.*, 2019). The insula emerged as an important pathological hub both in females and males showing disconnections from frontal and occipitoparietal regions. The insula is a complex structure multiconnected with several cortical regions. The insular lobe has the complex role of integrating information within and across cognitive, affective, visual, and sensorimotor tasks (Benarroch, 2019). Pathological studies found that this structure, in particular the anterior agranular insula, is an early site for pathological LB accumulations (Fathy *et al.*, 2019). Consistently, neuroimaging studies detected hypoperfusion (Nagahama *et al.*, 2010), dopamine deficit (Pilotto, Di Cola, *et al.*, 2019), decreased functional connectivity (Peraza *et al.*, 2014), and lower fractional anisotropy value (Lee *et al.*, 2010) in the insular cortex in DLB. Of note, together with

the olfactory cortex, the insula showed increased connectivity with basal ganglia and limbic regions in pDLB females. Increased connectivity is emerging as a fundamental response to the early phase of neurodegenerative processes (Hillary and Grafman, 2017). The insular hyperconnectivity found in females, is of particular interest, considering that the node emerged, instead, as a pathological hub for its prevalent losses in pDLB males. DLB females and males also showed specific sex-related pathological hubs: for females, hubs were localized in the precuneus, frontal and parietal regions, whereas for males, hubs were found in the inferior temporal and fusiform gyri. The different locations of pathological hubs according to sex, here might indicate specific regional vulnerability not only driven by the LB pathology. The brain multisystem connectivity impairment in DLB is paralleled by metabolic connectivity data targeting neurotransmission systems, such as the dopaminergic, noradrenergic, and cholinergic networks (S.P. Caminiti *et al.*, 2017; Giulia Carli, Caminiti, *et al.*, 2020). Here, the analysis of the neurotransmitters' networks showed that the two pDLB groups shared the most important connectivity alterations in the dorsal and ventral dopaminergic networks as well as in noradrenergic pathways (**Figure 29**). The dopaminergic network dysfunction was similar for the dorsal division in the groups but was slightly more affected in pDLB males for the ventral division. These results support the significant alteration of the dopaminergic networks in pDLB (Giulia Carli, Caminiti, *et al.*, 2020), independently of sex. Notably, we found more subcortical local alterations in men, involving the caudate and the ventral striatum compared to females whose alterations, instead, affected the subcortical-cortical connections. The noradrenergic network dysfunction is considered an early pathological event in the α-synuclein-spectrum and an extended reconfiguration of this network is already present in idiopathic RBD (Giulia Carli, Caminiti, *et al.*, 2020). Our data support that noradrenergic pathology deficiency is of great magnitude in synucleinopathies (Vermeiren and De Deyn, 2017) and can explain not only the autonomic and sleep disturbances but also cognitive performances (Gratwicke, Jahanshahi and Foltynie, 2015). In the current study, sex differences emerged in the connectivity of the cholinergic networks, with males showing more severe alterations with different connectivity patterns than females. The differences were strong in the Ch4-perisylvian division. Males showed the most important reduction in connectivity in this network affecting almost all nodes, females instead showed increased connectivity to the insula, frontal, temporal, and olfactory cortices. Comparable

sex differences emerged also in the Ch4-Median and Ch5-Ch6 divisions. According to the "compensatory hypothesis", increased cholinergic activity in cortical circuits may compensate for executive dysfunctions associated with striatal dopaminergic declines in the early stages of LB disorders (Bohnen *et al.*, 2018). In this perspective, the here reported increased cholinergic connectivity in pDLB females could represent an attempt to compensate for a system that is instead already disrupted in pDLB males. However, a form of maladaptive functional reorganization resulting from the brain's failure to cope with the damage cannot be excluded (Hillary and Grafman, 2017). For instance, the proper one-to-one connection in healthy brains can be replaced by a widespread dysfunctional connectivity pattern represented by increases between several regions. Moreover, it is worth noting that hyperconnectivity may also have a detrimental role in driving the spreading of neurodegeneration (Hillary and Grafman, 2017). However, separating beneficial from maladaptive processes remains challenging in need of correlations with clinical data (Schoonheim, 2017). The involvement of the Ch5-Ch6 pathway and the loss of Ch4 projections from the nucleus basalis of Meynert to cortical structures is in line with previous metabolic connectivity (S.P. Caminiti *et al.*, 2017) and tracer specific cholinergic neurotransmission studies (Kanel *et al.*, 2021). Cholinergic neurotransmission has a crucial role in cognitive function, supported also by the association between cholinergic depletion and cognitive decline in LB disorders (Bohnen *et al.*, 2018). However, no previous *in vivo* imaging studies focused on sex differences in the cholinergic system in DLB. Research in healthy animals revealed no marked difference in the general morphology of the brain cholinergic system, but subtle functional sex differences. In humans, sex differences in the nucleus basalis of Meynert exist (Giacobini and Pepeu, 2018). Many estradiol receptors are present in the basal forebrain cholinergic neurons and estradiol appears to modulate the cholinergic system through trophic effects (Newhouse and Dumas, 2015). Moreover, lifetime estrogen exposure might protect against the AD dementia risk that is associated with reduced estrogen levels (Zhu, Montagne and Zhao, 2021). Comparably, in PD, a possible neuroprotective effect of estradiol on this neurotransmission system is suggested, with the male sex as the main risk factor of progressing to dementia (Cholerton *et al.*, 2018). Further studies using specific radioligands for the vesicular acetylcholine transporter, such as [^{18}F]-fluoroethoxybenzovesamicol, might highlight the way DLB pathology

differently affects the cholinergic system and the related cognitive dysfunction in males and females.

Previous metabolic connectivity evidence showed a severe involvement of RSNs, such as the posterior cortical, the limbic, and the attention networks, whose disruption is strongly related to the DLB clinical symptoms (Sala *et al.*, 2019). Considering females and males separately, the RSNs showed similar reconfigurations in the two groups, with the confirmation of the main involvement of pDMN, attentive, and motor networks (**Figure 30**). A previous study investigating RSNs' integrity and their interactions with DLB core symptoms reported significant alterations of pDMN, as well as the limbic and attention networks in a DLB cohort (Sala *et al.*, 2019). Regarding sex-specific alterations, the limbic network was more dysfunctional in pDLB males than females. The amygdala is the seed driving the limbic network's construction. According to the recent "brain- first" hypothesis of α-synuclein spreading, the amygdala seems to be the most likely site of origin of LB pathology (Horsager *et al.*, 2020). The initial prevalent involvement of the amygdala was associated with an increased likelihood of PD evolving toward DLB (Blesa *et al.*, 2022). Recently, the amygdala volume has been reported to be associated with the trajectories of hallucinations, but not with other neuropsychiatric symptoms as happening in AD (Jaramillo-Jimenez *et al.*, 2021), and an increased burden of LB in the amygdala was present in DLB patients with visual hallucinations (O'brien *et al.*, 2020).

In conclusion, we identified a common metabolic connectivity substrate in men and women with a clinical diagnosis of pDLB. The shared connectivity alterations are also associated with the posterior cortical vulnerability which univocally characterizes the DLB condition, independently by sex effects. However, pDLB males showed more severe brain hypometabolism and long-distance connectivity alterations in the prototypical damaged DLB regions, which can explain a more clear-cut symptom-related diagnosis in males than females. Given the recent evidence of AD co-pathology as a possible driver of sex differences, further prospective studies combining brain metabolism and pathological measures, such as the CSF measures, are necessary. The lack of a comparable and full neuropsychological assessment in the present cohort represents a limitation preventing the evaluation of sex effects on the cognitive-neuroimaging correlations, a crucial point to be addressed by future studies.

4.4 Conclusion

This dissertation provides new evidence regarding the neurobiological mechanisms underlying different phenotypes and clinical trajectories in LBDs by using molecular neuroimaging. In these three years of PhD, I applied different methodological approaches and study designs to study molecular biomarkers with the goals of their better implementation in clinical practice and a deep understanding of the diseases. First, my studies focused on optimized univariate methods to analyze clinically useful biomarkers, such as [^{123}I]FP-CIT-SPECT, [^{18}F]FDG-PET and MIBG scintigraphy. Moreover, one of the main novelties is represented by the use of molecular connectivity on PET and SPECT data which represents an emerging approach for the study of neurodegenerative diseases. The exploration of molecular connectivity allows a detailed *in vivo* evaluation of the dynamic neurobiological changes underlying neurodegeneration. These both univariate and connectivity approaches have been then applied in my studies to reveal the endophenotypic variability in LBDs that could possibly explain the clinical heterogeneity linked also to different progression pathways. A deep focus has been then given to sex/gender contribution to α-synuclein-related neurodegeneration process and expression.

More in detail, the discussed studies support that a) semi-quantification of molecular biomarkers ([^{123}I]FP-CIT SPECT, [^{18}F]FDG-PET and MIBG) can improve the diagnosis and prognosis of LBDs identifying also different phenotypes (**Section 1**); b) molecular and metabolic connectivity can be valuable tools to comprehensively deepen neurodegenerative mechanisms (**Section 2**), in our case they were able to find alterations since the prodromal RBD stage resembling DLB ones; c) sex/gender differences exist in molecular endophenotypes assessed by different neuroimaging tools and are crucial to understand the variability of LBDs (**Section 3**).

Given my results of these three years, I can say that have explored and contributed to the study of LBDs variability based on multimodal imaging approaches. The multi-factorial protocol integrated epidemiological (e.g., gender) and clinical data, with neuroimaging measures to better understand the main sources of variability in LBDs. My results underline and confirm the complexity of these diseases and the existence of different

subtypes, difficult to ascribe to a single subtyping, but crucial to keep on studying to get ever closer to effective precision medicine.

As a general limitation, I acknowledge that a longitudinal design recruiting and following over time iRBD patients would have allowed strong prognostic consideration currently lacking in these studies. The identification of possible subtypes already in the prodromal stages of LBDs would be of crucial importance for early diagnosis and for recognizing different and specific progression trajectories.

5. Materials and Methods

The studies included in this dissertation relied on PET and SPECT data ([^{18}F]FDG-PET and [^{123}I]FP-CIT-SPECT) and the application of several imaging data approaches (univariate and advanced multivariate connectivity methods). Given that many procedures were shared among the studies, this section will first list the common analytical steps, with study-specific methodological details following, including the specific design and statistical analyses. Almost all the methods described below were published in peer-reviewed journals and are currently available online.

5.1 Clinical and cognitive assessment

For samples from the PPMI (*Studies 1* and *7*), clinical motor assessments included Movement Disorders Society-Unified Parkinson's Disease Rating Scale (MDS- UPDRS) and Hoehn and Yahr scales. SWEDD and PD subjects were subtyped into tremor dominant (TD), postural instability/gait difficulty (PIGD), and indeterminate (IT) subtypes, using the UPDRS items according to (Stebbins et al., 2013). Clinical non-motor assessments included Epworth Sleepiness Scale and a Rapid Eye Movement (REM) sleep behaviour disorder (RBD) questionnaire to assess sleep behaviour, Scales for Outcomes in PD-Autonomic (SCOPA-AUT) to assess autonomic function, and the 40- item University of Pennsylvania Smell Identification Test (UPSIT) to assess olfactory function. Global cognition was assessed with the Montreal Cognitive Assessment (MoCA). Cognitive testing included the Hopkins Verbal Learning Test-Revised (HLVT-R) to assess memory; Benton Judgment of Line Orientation (JOLO) 15-item version to assess visuospatial function; and Letter-Number Sequencing (LNS) and semantic fluency to assess executive abilities-working memory. Neurobehavioral testing included the Geriatric Depression Scale (GDS), State-Trait Anxiety Inventory (STAI), and Questionnaire for Impulsive-Compulsive Disorders (QUIP). All the assessments were also available and collected at follow-up for *Study 1*, except for the UPSIT.

5.2 [^{18}F]FDG-PET

5.2.1 Imaging acquisition

[^{18}F]FDG-PET images at Nuclear Medicine Unit, IRCCS San Raffaele Hospital, Milan, Italy, were acquired using a Discovery STE (GE Medical Systems, Milwaukee, WI) multi-ring PET tomography (PET-CT), and [^{18}F]FDG-PET images at Neurology Unit,

Department of Clinical and Experimental Sciences, University of Brescia, Brescia, Italy by a Discovery 690 (GE Healthcare) (*Studies 5* and *6*). [^{18}F]FDG-PET scans from Geneva University Hospitals were performed at the Nuclear Medicine and Molecular Imaging Division with Biograph128 mCT, Biograph128 Vision 600 Edge, Biograph40 mCT, or Biograph64 TruePoint PET scanners (Siemens Medical Solutions, USA) (*Studies 3* and *9*). [^{18}F]FDG-PET images belonging to ADNI subjects were obtained using ECAT HR + , General Electric Discovery LS, General Electric Discovery ST, General Electric Discovery STE, Siemens/ECAT HRRT, Siemens Biograph Hi-Rez, Philips Gemini TF, Siemens mCT and ECAT Biograph (*Study 3* and *9*). The acquisitions conformed to the European Association of Nuclear Medicine guidelines. Static emission images were acquired 30 to 45-minute after injecting 185–250 MBq of [^{18}F]FDG via an intravenous cannula. This postinjection time interval allows obtaining an equal distribution of the tracer across the entire brain, with negligible blood flow-dependent differences, thus achieving an optimal signal-to-noise ratio. The duration of scan acquisition was 15/20 minute. The 67 steady-state emission images obtained from the ADNI dataset were acquired 30 minute after injecting approximately 185MBq of [^{18}F]FDG, with a 30-minute scan acquisition duration. After realignment to correct for interframe motion, only the last three 5-minute frames were retrieved from the ADNI database and combined to obtain a single 15-minute static image, to increase uniformity across acquisition procedures. Uniform reconstruction protocols were applied, for example, the ordered subset expectation maximization algorithm and CT attenuation correction procedures.

5.2.2 Pre-processing and single-subject analyses

A rigorous quality control process was performed to check potential artifacts (e.g., acquisition issues, excessive patient motion) and issues related to technical characteristics, such as the use of compatible reconstruction algorithms. Then, [^{18}F]FDG-PET images of patients and controls were normalized to the optimized [^{18}F]FDG-PET template (Della Rosa *et al.*, 2014), using SPM12 (https://www.fil. ion.ucl.ac.uk/spm/). They were then scaled to the global mean of the activity within the brain and finally smoothed with an isotropic 3D Gaussian kernel (8 mm Full Width Half Maximum), accordingly to the validated pipeline proposed for our single-subject SPM- based analysis (Daniela Perani *et al.*, 2014). This method is based on a robust statistical comparison between a single patient and a large dataset of scans from normal controls including age

as a nuisance variable. This procedure allows identifying disease-specific brain hypometabolism patterns and has been demonstrated to provide reliable results regardless of the scanners used for image acquisition (Presotto *et al.*, 2017). This pipeline finally delivers patterns of brain hypometabolism at the voxel-level, or SPM-t thresholded maps, but also the so-called contrast images, which index relative hypometabolism, and intensity normalized images that can be used for 2nd level statistical analysis.

5.3 [^{123}I]FP-CIT-SPECT

5.3.1 Imaging acquisition

[^{123}I]FP-CIT SPECT for the DLB cohort (*Study 8*) was performed at Geneva University Hospitals (Switzerland). Patients received 185 MBq of [^{123}I]FP-CIT (ioflupane, DaTSCAN®, GE Healthcare, Glattbrugg, Switzerland) in slow IV injection and Lugol solution or sodium perchlorate to block thyroid uptake. SPECT/CT data acquisition started 4 h after ioflupane injection. The acquisition was performed on a triple-head gamma camera (GCA-9300A/ UI Toshiba Medical Systems AG, Oetwil am See, Switzerland) equipped with fan-beam low-energy high-resolution collimators.

For the PD cohort (*Studies 1* and 7), we downloaded reconstructed [^{123}I]FP-CIT SPECT (and MRI) imaging data from the PPMI website. Images were acquired on Siemens or General Electric SPECT tomographs, 3–4 h after [^{123}I]FP-CIT injection. The imaging protocol for the PPMI scans has been previously documented (Marek *et al.*, 2011, 2018).

5.3.2 Pre-processing and imaging analyses

Pre-processing of SPECT brain images was performed using Statistical Parametric Mapping (SPM12, Wellcome Trust Centre for Neuroimaging, London, UK, https://www.fil.ion.ucl.ac.uk/ spm/), running in MATLAB R2018b version 9.5.0 (MathWorks Inc., Sherborn, MA, USA).

SPECT images of DLB cohort were normalized based on an available [^{123}I]FP-CIT template (García-Gómez *et al.*, 2013), given the unavailability of MRI for all the subjects. Intensity-normalized parametric images were generated for each subject using the Image Calculator (ImCalc) function in SPM12. The cerebellar crus II uptake was used as the reference region to calculate the specific binding ratios (SBRs) as [(target region/reference region) − 1]. SBR images were saved for further voxel-wise analyses. Asymmetry index (AI) was calculated using [^{123}I]FP-CIT putaminal binding ratio (PBR)

and the following formula: $((PBR_{Higher\ side} - PBR_{Lower\ side})/ (PBR_{Higher\ side} + PBR_{Lower\ side})) \times 2 \times 100$, to have only positive values expressed in % (Nicastro, Burkhard and Garibotto, 2020). The use of the non-specific binding in the cerebellum crus as a reference was based on the observation that it is relatively free from both DAT and SERT (Kish *et al.*, 2005).

For PD cohort (PPMI) (*Studies 1* and *7*), SPECT images were co-registered to each patient's brain template in native space, obtained by integrating the grey and white tissue probability maps (obtained from T1 MRI) without non-brain tissue-specific for each patient. DAT SBR was calculated as [(target region/reference region)-1] for each subject-specific ROI. The lateral superior occipital cortex uptake was used as the reference region, given that the cerebellum is often not covered entirely in scans from PPMI, limiting its use.

We analysed striatal and extra-striatal subcortical structures variably innervated by the dopaminergic pathways, namely the caudate nucleus, putamen, globus pallidus, thalamus, amygdala, and hippocampus, bilaterally (**Figure 31**). We also considered cortical and deep brain ROIs with high dopaminergic innervations, belonging to the nigrostriatal and the mesolimbic dopaminergic pathways (**Figure 31C**). The mesolimbic targets consisted of the anterior and middle cingulate cortices, the olfactory cortex, the insula, the ventral and medial frontal areas, as well as the amygdala, hippocampus, and parahippocampal cortex. The nigrostriatal targets consisted of the frontal premotor, motor, dorsolateral frontal regions, and somatosensory cortex. Since the moderate affinity of [^{123}I]FP-CIT-SPECT for the serotonin transporter in extrastriatal regions, the signal extracted from basal ganglia was defined as "DAT binding"; instead, the signal extracted from extra-striatal regions was defined as "[^{123}I]FP-CIT-SPECT binding".

For the PPMI cohort, we obtained subject-specific ROIs through the automatic subcortical structure segmentation of each participant's MRI scans using the Volbrain platform (Manjón and Coupé, 2016). The whole putamen and caudate were subdivided into functional subregions (Tziortzi *et al.*, 2013), i.e., dorsal-motor and ventral divisions (**Figure 31**). For the DLB images (in MNI space) (*Study 8*), we used the same ROIs but derived from the Automated Anatomical Labelling atlas.For *Study 1*, we also generate the intensity-normalized parametric images in Montreal Neurologic Institute (MNI) for voxel-wise analyses: first the T1 MRI brain template of each subject was normalized to

the MNI space using tissue probability maps, then all SPECT images were aligned to the subject's respective brain template and normalized to the MNI space using the transformation matrix that was generated during the registration of the MRI images to the standard space. Intensity-normalized parametric images were generated using the lateral superior occipital regions as reference for each subject throughout the Image Calculator (ImCalc) function in SPM12. To confirm or not the SWEDD classification, images were semi quantitatively analyzed by a comparison with the pool of HC using Statistical Parametric Mapping (SPM 12; Wellcome Trust Centre for Neuroimaging), running in MATLAB R2018b, version 9.5 (MathWorks Inc.). Each SPECT image was tested for relative dopaminergic depletion by means of a 2-sample t-test in comparison with SPECT images of HC. The statistical threshold for the resulting SPM maps was set at a P value of 0.05, uncorrected for multiple comparisons, considering significant clusters containing more than 100 voxels.

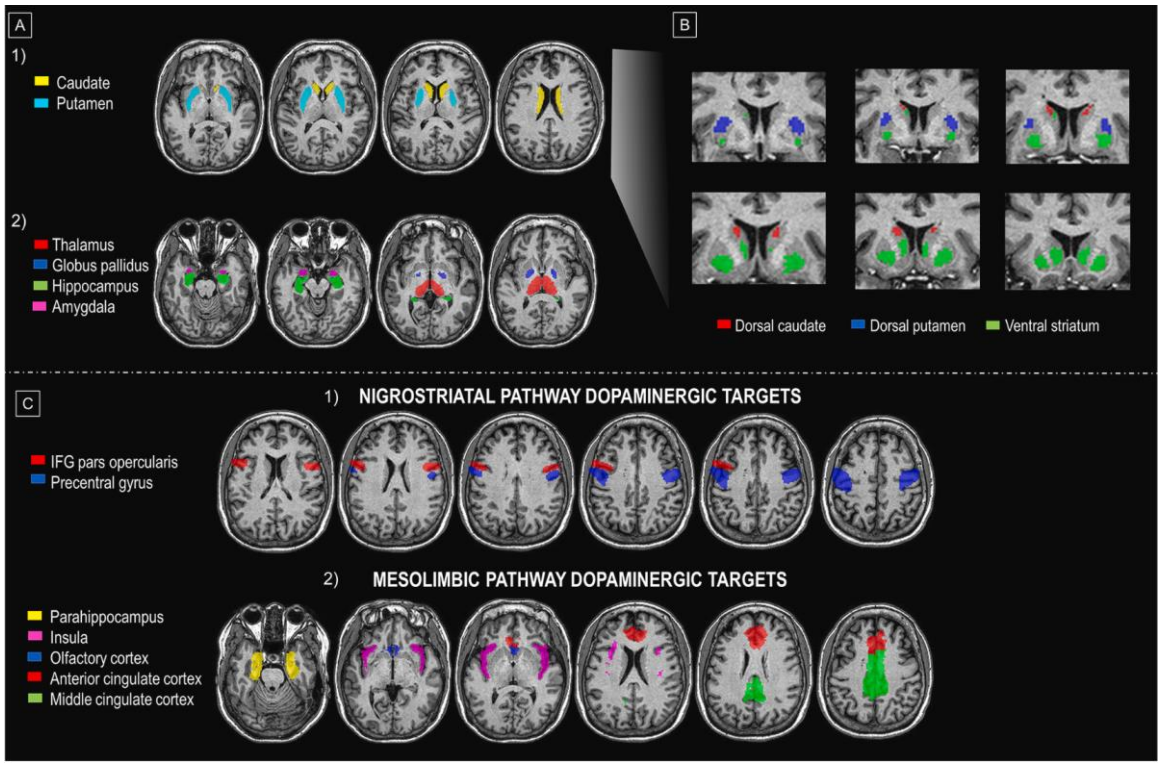

Figure 31. Subject-specific Regions of Interest (ROIs) (Open access source)*. Examples of anatomical subject-specific ROIs over-imposed on the relative MRI-T1 image in a patient's native space with idiopathic Parkinson's disease. The ROIs were obtained by the MRI scan's automatic anatomical subcortical structure segmentation, performed using Volbrain. The functional subdivision of the striatum was based on a multimodal imaging study (Tziortzi et al., 2013). The*

functional subdivision of the striatum includes dorsal and ventral divisions. A) The represented ROIs in axial view are: caudate nucleus and putamen (yellow and light blue) in panel A.1, globus pallidus (blue), thalamus (red), hippocampus (green), and amygdala (violet) in panel A.2. B) The functional subdivision of the striatum is displayed in coronal view showing ventral striatum (green), dorsal putamen (blue), dorsal caudate (red). C) The represented ROIs in axial view belong to the nigrostriatal (1) and mesolimbic pathways (2). The nigrostriatal cortical targets are the inferior frontal gyri pars opercularis (red) and the precentral gyri (blue); the mesolimbic targets are the parahippocampus (yellow), the insula (violet), the olfactory cortices (blue), the anterior cingulate (red), and the middle cingulate (green). The figure is from (Boccalini, Carli, Pilotto, *et al.*, 2022) *in accordance to the fair use principle.*

5.4 [^{123}I]MIBG myocardial scintigraphy

5.4.1 Imaging acquisition

[^{123}I]MIBG myocardial scintigraphy for PD sample (*Study 2*) was performed at the Nuclear Medicine Unit, San Raffaele Hospital, using (NM/CT 670, Milwaukee, WI, United States) manufactured by GE Healthcare medical systems, according to the standard procedure (Veltman *et al.*, 2012). All patients have suspended medication and stopped eating any food that could influence [^{123}I]MIBG myocardial uptake (Flotats *et al.*, 2010). A total of 111 MBq of [^{123}I]MIBG was injected intravenously. [^{123}I]MIBG planar images were obtained with a gamma camera in two temporal windows: 15 min after the injection (early-image) and 4 h after the injection (delayed- image). Static planar imaging was obtained with 256 × 256 matrix. Only planar images in thoracic anterior view were used for quantitative evaluation. All camera heads were equipped with low-energy high-resolution collimators and all images were acquired with a 15% energy window centred at the 159 keV photopeak of 123I. The image acquisition time was approximately 5 min. All planar images were analysed using Xeleris (Discovery NM/CT 670, GE Healthcare, Milwaukee, WI, United States) and PMOD software (PMOD Technologies Ltd.), for manual and semi-automatic methods respectively.

5.4.2 Pre-processing and imaging analyses

Early and late H/M ratios were calculated from [^{123}I]MIBG planar images using ROIs placed over the heart and the upper mediastinum. The ROIs were derived using two different approaches: manually drawn ROIs and semi-automatic fixed- size ROIs. In the first approach, a rectangular mediastinal ROI has been used with unspecified size. The

cardiac ROI was a polygonal manually drawn ROI including the myocardium and the left ventricular cavity (**Figure 10A**). The manual method was performed on a Xeleris workstation, following the recommendations described in the proposal for standardisation by Flotats et al. (Flotats *et al.*, 2010). For the semi-automatic method, we followed the guidelines of Veltman et al. (Veltman *et al.*, 2012) (**Figure 10B**). An "anatomical landmark square" was formed by the lung apexes (upper square border), the upper cardiac border (lower square border), and the medial contours of the lungs (medial square borders) to place fixed- size mediastinum and oval cardiac ROIs. Precisely, a fixed- size rectangular mediastinal ROI (13 × 20 pixel) and an oval cardiac ROI (60 × 70 pixel) were placed on [^{123}I]MIBG planar images. The mediastinal ROI was placed in the half of the "anatomical landmark square" formed by lungs apexes, the upper cardiac border, and the medial contours of the lung. The cardiac oval ROI was placed in the lower-right quadrant, over the myocardium, including the left ventricular cavity. The use of fixed-size ROI, which the operators only need to move according to the anatomical landmark square, gives partial automation to the method. This semiautomatic method was processed using the PMOD software. Three raters (expert, moderately-expert, and not expert) analysed the [^{123}I]MIBG images using both procedures. Of note, the inexpert rater followed a brief training (2 h) for the manual drawing analysis. The other raters were experienced in the analysis of [^{123}I]MIBG myocardial scintigraphy, with mean more than 5 and 10 years of experience, respectively. Anonymised data were analysed in a random order to avoid bias by order effects.

5.5 Metabolic and molecular connectivity analyses

5.5.1 Inter-regional correlation analysis (IRCA) for large-scale networks

In *Studies 5* and *9*, we performed IRCA using a voxel-wise SPM procedure (Lee *et al.*, 2008) to investigate the metabolic connectivity of the RSNs in different groups as compared to HC. The central assumption of this analysis dates to the work by Horwitz et al. (1984), demonstrating that brain regions whose glucose metabolism is correlated at rest are functionally associated (Horwitz, Duara and Rapoport, 1984). IRCA is a voxel-wise approach previously validated for [^{18}F]FDG-PET data that allows the derivation of RSNs from relevant seed regions selected based on previous literature (Horwitz, Duara and Rapoport, 1984; Lee *et al.*, 2008). It relies on selecting a ROI, or seed, from which the average tracer uptake value is extracted. The correlation between average uptake in

the seed and uptake in each voxel in the rest of the brain is then tested to estimate the connectivity profile, or connectivity map, of the seed of interest. Of note, brain networks estimated using [^{18}F]FDG-PET data benefit from disease specificity and robustness also in a small sample of patients (N ≥ 20)(Schindlbeck and Eidelberg, 2018; Ripp *et al.*, 2020). In this study, we applied IRCA analysis in three groups of patients and one HC cohort, ensuring a reliable number of subjects per group (N ≥ 25). In addition, to increase the reliability and reproducibility of RSNs, we considered the seeds of RSNs previously validated. Specifically, we considered the RSNs affected in PD and DLB, following the previous literature (S. Caminiti *et al.*, 2017; Sala, S.P. Caminiti, *et al.*, 2017; Iaccarino *et al.*, 2018; Sala *et al.*, 2019; Carli *et al.*, 2021), namely, the anterior and posterior default mode networks (ADMN and PDMN), the attentive network (ATTN), the frontal executive network (EXN), the limbic network (LIN), the motor network (MN), the somatosensory network (SN), the primary, and high visual networks (PVN and HVN; details on the selected ROIs are provided in **Table 7**). We used the REX toolbox to extract the mean metabolism values from the ROIs (seeds), entering as sources the scaled [^{18}F]FDG-PET images of patients and HC. Then, the average seed uptake was set as a variable of interest in a multiple regression model in SPM12, entering age and gender as nuisance covariates for each network.

5.5.2 Whole-brain and neurotransmitter networks analysis

Brain metabolic/molecular connectivity analyses were applied to investigate the molecular architecture of the whole-brain network (*Studies 3* and *9*) and neurotransmission circuits (*Studies 1*,*3*, *6*,*7*,*8*, and *9*), namely the nigro-striatal-cortical and mesolimbic dopaminergic, noradrenergic, and cholinergic pathways. These analyses are based on [^{18}F]FDG-PET data (*Studies 3,6,* and *9*) or [^{123}I]FP-CIT-SPECT data (*Studies 1*, *7*, and *8*) and rely on the combination of multivariate analysis methods and a priori selection of specific ROIs. Specifically, partial correlation analysis is a common ROI-based approach that allows for estimating the degree of linear association between each couple of selected ROIs, factoring the contribution of all remaining ROIs, providing reliable information on the molecular architecture of a given pathway in HC and neurodegenerative conditions. This brain connectivity approach assumes that regions with similar metabolic or molecular demands are functionally associated, and, thus, the

strength of the associations is proportional to the magnitude of the correlation coefficients.

The procedure consisted of the following steps:

i) selection of ROIs to reconstruct the network of interest. We considered the whole-brain network by applying the Automated anatomical labeling (AAL) (Tzourio-Mazoyer *et al.*, 2002) for cortical, subcortical, and cerebellar regions (95 × 95 ROIs). Neurotransmitter networks were assembled by considering the topographical organization of projections originating by specific brain nuclei based on biochemical, histochemical and anatomopathological findings (Sala and Perani, 2019; G. Carli, Caminiti, Sala, *et al.*, 2020) (see **Appendix** for the selected ROIs for each system).

ii) Average value of tracer uptake is then extracted from each ROI using scaled [^{18}F]FDG-PET or parametric [^{123}I]FP-CIT-SPECT images. The tracer uptake was extracted from each ROI composing different neurotransmitters networks using the REX toolbox for MATLAB (https://www.nitrc.org/projects/rex/).

iii) Application of partial correlation analyses computed using MATLAB's *parcorr* function on matrices composed by extracted data. Partial correlation is a statistical approach that allows assessing metabolic connectivity between two ROIs while controlling for the contributions of other regions (Huang *et al.*, 2010). In detail, to estimate the molecular architecture of each neurotransmission network, we created a subject-by-ROI matrix for each clinical group and HC. Each matrix's entries comprised the mean tracer uptake values derived for a specific ROI and subject. Based on these subject-by-ROI matrices, we computed partial correlation coefficients. The resulting partial correlation matrices were thresholded at $p < 0.01$, uncorrected for multiple comparisons, as a reasonable trade-off between statistical robustness and sensitivity. Age was included as a nuisance covariate in the analysis. To assess the connectivity alterations of the neurotransmission networks in each clinical group, we tested whether the strength of the partial correlation coefficients (indexing the strength of the metabolic connection) differed between the clinical and the HC groups. We thus first applied Fisher's transformation to

each coefficient resulting from partial correlation analysis. Then, a Z-test was used to test for significant changes in partial correlation coefficients.

5.6 Sample, methods and statistical analyses applied in different studies

5.6.1 Study 1: Distinctive clinical and imaging trajectories between SWEDD and Parkinson's disease patients (Boccalini, et al.) – submitted article

Sample

Data used in this study were obtained from the PPMI database (www. ppmi-info.org/data), an international, multiple-site, prospective, longitudinal cohort study (Marek et al., 2011, 2018).

We included 49 SWEDD patients from the PPMI who underwent baseline [^{123}I]FP-CIT SPECT imaging and T1-weighted MRI within one year. SWEDD subjects have no evidence of dopaminergic deficit in presynaptic dopaminergic scans and no expectation of PD medication within six months from baseline. The visual interpretation for normality was determined by the imaging core of PPMI and was informed to the referring physician. We randomly selected 49 de novo idiopathic PD and 49 healthy controls (HC) with baseline [^{123}I]FP-CIT SPECT imaging and T1-weighted MRI within one year, for comparison. PD patients were drug naïve and subjects with verified genetic mutations known to cause PD (GBA, LRRK2) have been excluded. 38 SWEDD and 40 PD patients underwent clinical assessment at 2 years follow-up and for 36 SWEDD and 39 PD of them [^{123}I]FP-CIT SPECT scans at 2 years follow-up were also available.

Statistical analyses and voxel-wise analyses

T-tests were used to compare demographics and clinical data between SWEDD and PD patients at baseline and follow-up. MANCOVA tests were applied to compare SBR imaging data using age, sex, and UPDRSIII as nuisance variables. Paired t-tests of difference images (baseline and follow-up) of clinical and SBR data within each group (SWEDD and PD) were also conducted. To investigate the differences between SWEDD and PD in cognitive changes over time we applied linear mixed-effects model for each clinical scale, that was used as a dependent variable. Then, applying the same longitudinal model, we examined differences in striatal SBR trajectories between SWEDD and PD. To further characterize the results of the ROI-based analysis, a complementary voxel-

based analysis was run. The [^{123}I]FP-CIT SBR parametric images were used in two-sample t-tests in SPM12, running in MATLAB, to compare SWEDD vs HC and PD vs HC at baseline and, directly SWEDD vs PD at baseline and follow-up. Age was included as a covariate of nuisance in the comparison with HC, and age, sex and UPDRSIII in the direct comparison between SWEDD and PD. Voxel-wise paired t-tests of difference images (baseline and follow-up) within each group (SWEDD and PD) were also run in SPM12. A threshold was set at $p = 0.005$, family-wise error (fwe)-corrected at the cluster level.

Connectivity analysis

Assessment of molecular connectivity between targets of each dopaminergic pathway (nigrostriatal and mesocorticolimbic) was performed via partial correlation analysis (see **Paragraph 5.5.2**). All the results were set at a statistical threshold of $p < 0.01$, uncorrected for multiple comparisons. In SWEDD and PD patients, we calculated the percentage of altered molecular connections in each network to quantify the severity of molecular connectivity alterations. Thus, we computed the number of altered connections divided by the total number of connections of each network to obtain the percentage of altered molecular connectivity. Then, we compared the number of altered molecular connections between patients for each network through the χ^2 test.

Spatial correlation analysis

We used the JuSpace toolbox (Dukart *et al.*, 2021) to our dataset to compute Spearman correlation (based on the Neuromorphometrics atlas; adjusted (adj) p values, N = 1000 permutations) between Z-scores (SWEDD vs HC and PD vs HC) and the DAT (Dukart *et al.*, 2018), serotonin transporter (SERT), and norepinephrine transporter (NET) (Hesse *et al.*, 2017) maps, derived from [^{123}I]FP-CIT, ^{11}C-3-amino-4-(2-dimethylaminomethyl-phenylsulfanyl)-benzonitrile (^{11}C-DASB), and (S,S)-^{11}C-Methylreboxetine ((S,S)-^{11}C-MRB) data, respectively. JuSpace is a comprehensive license-free toolbox running in MATLAB for the integration of positron emission tomography (PET)- and SPECT-derived maps with other brain imaging data (MRI, fMRI), allowing to examine specific neurotransmitter system changes as compared to HC. Briefly, the PET/SPECT maps were derived from average group maps of different healthy volunteers and consisted of maps of the binding signal intensity across the whole brain. Then, the data to generate a contrast between conditions (patients vs HC) were entered as input to be correlated with PET-

/SPECT-derived maps. The atlas is used to extract mean regional values from the input modalities to be correlated with respective mean values from maps, as a voxel-wise analysis would result in highly inflated degrees of freedom (Dukart *et al.*, 2021).

5.6.2 Study 2: Manual and semi-automated approaches to MIBG myocardial scintigraphy in patients with Parkinson's disease (Boccalini, Carli*, et al., 2022) – Published article*

The following data have been published (Boccalini, Carli, Vanoli, *et al.*, 2022).

Sample

The study included 35 patients fulfilling the PD clinical diagnostic criteria (Postuma *et al.*, 2018) who underwent [^{123}I]MIBG myocardial scintigraphy at San Raffaele Hospital, Milan, Italy.

The inter-rater agreements

The intraclass correlation coefficients (ICC) were used to assess agreement among independent raters, considering the H/M ratios as a continuous variable. ICC values < 0.5, between 0.5 and 0.75, between 0.75 and 0.9, and greater than 0.90 are indicative of poor, moderate, good, and excellent reliability, respectively. We applied previously published cut-off for pathological scans (<1.9 early ratios and <1.7 late ratios) to classify the H/M ratios into mutually exclusive categories (pathological and not). Following this categorisation, we calculated the Fleiss' kappa, κ to measure the inter-rater agreement between the raters. The following classification was suggested for assessing the strength of agreement: $\kappa < 0.20$ poor, 0.21–0.40 fair, 0.41–0.60 moderate, 0.61–0.80 good, and 0.81–1.00 very good. Last, Cohen's Kappa was also used to measure the agreement between two raters after classifying the H/M ratios as pathological or not. Cohen's Kappa values 0.01–0.20, 0.21– 0.40, 0.41–0.60, 0.61–0.80, and 0.81–1.00 were considered slight, fair, moderate, substantial, and perfect agreement, respectively. A Chi-square test was run to test differences in the proportion of patients classified as pathological or not by different raters.

The intra-rater agreements

The correlations between the H/M ratios obtained with the two methods by each rater were analysed by the Spearman correlation coefficients. The significance level was $p < 0.001$.

5.6.3 Study 3: Mapping brain metabolism, connectivity, and neurotransmitters topography in early and late onset dementia with Lewy bodies (Caminiti et al., 2023) – submitted article

Sample

We included N=62 patients with a clinical diagnosis of probable DLB (McKeith *et al.*, 2017) retrospectively evaluated from the clinical and imaging database of San Raffaele Hospital Milan, Italy, and Geneva University Hospitals, Switzerland. Participants were subsequently stratified into two clinical groups according to age at onset (EO-DLB ≤ 65 years, LO-DLB age at onset > 65 years). In addition, we collected prevalence of neuropsychiatric symptoms (i.e., depression, apathy, irritability, and anxiety) considering neuropsychiatric index (NPI) scores or medical records. Cerebrospinal Fluid (CSF) examination of β-amyloid (1-42), total-Tau and phospho-Tau, were available for 52%. Between-group differences in demographical and clinical measures were assessed by applying ANOVA and Chi-square test for continuous and discrete variables, respectively.

Brain hypometabolism maps

By considering SPM z-maps obtained from single-subject SPM preprocessing (D. Perani *et al.*, 2014), regional hypometabolism values (SPM z-scores) were extracted from a set of predefined (DLB typical hallmarks) and data driven (based on the results of univariate SPM group analysis) ROIs, namely Inferior, Middle and Superior Occipital Lobe, Calcarine Cortex, Lingual Gyrus, Fusiform Gyrus, Superior and Inferior Temporal Gyrus, inferior and superior parietal lobules, Middle Frontal Gyrus, posterior cingulate cortex, insula, supplementary motor area and parahippocampus. We also calculated the Cingulate Island Sign (CIS) ratio that was derived by dividing the [^{18}F]FDG uptake in the posterior cingulate cortex (PCC) with that in the precuneus and cuneus. The ROIs were derived from the Automated Anatomical Labelling (AAL) Atlas. Between-group differences in

brain hypometabolism within the DLB ROIs were assessed by means of a two-sample t-test on Statistical Package for Social Sciences (SPSS).

To describe group-level brain hypometabolism pattern characterizing the whole DLB cohort, patients' normalized images were compared to a set of 112 HC (age = 64.7 ± 9.3; Sex (male/female) = 53/59). Group comparison was performed by means of a two-sample t-test on SPM12 setting the statistical threshold at 0.05, family-wise error (FWE)-corrected for multiple comparisons. Only clusters containing more than 100 voxels were deemed to be significant. The same statistical design was applied to compare each DLB group with HC, as well as a head-to-head comparison of EO-DLB and LO-DLB. All SPM group analyses were performed considering age as nuisance variable.

Connectivity analysis

ROI-based metabolic connectivity analysis was applied to investigate the architecture of the whole-brain network (see **Paragraph 5.5.2**) and resting state networks (see **Paragraph 5.5.1**) for both DLB groups, and for the HC group for comparison. A group of 50 HC (for proper numerosity given the analysis) was randomly selected for comparison (mean age 65 yrs + 8).

Metabolic Spatial Distribution of Neurotransmitter Systems

We used JuSpace toolbox (Dukart *et al.*, 2021) for our dataset to test whether brain hypometabolism was spatially correlated with the distribution of specific neurotransmitter systems. We selected each subject's hypometabolism z-map (EO-DLB vs. HC; LO-DLB vs. HC) to compute Spearman correlations with provided PET and SPECT intensity maps of neurotransmitter systems. In details, PET/SPECT intensity maps covered the following receptor types: 5-HT1a (serotonin 5-hydroxytryptamine receptor subtype 1a), 5-HT1b (5-HT subtype 1b), 5-HT4 (5-HT subtype 4), dopamine transporter (DAT), GABAa (gamma-aminobutyric acid), NAT (noradrenaline transporter), SERT (serotonin transporter), and AChT (acetylcholine transporter). Specifically, the SERT map was obtained from HC images of 11C-DASB PET, a selective in vivo marker of 5-hydroxytryptamine transporter (5HTT) binding in humans. The neuromorphometric atlas from SPM12 was used to extract mean metabolic regional values from the input images to be correlated with the regional values of neurotransmitter maps. Then, we computed option 8 (extracts mean value per atlas region for each file

from list 1 and compares correlation coefficients for all images against null distribution) to compare the obtained Fisher's z-scores correlation coefficients against null distribution using a one-sample t-test. Exact permutation-based p-values (with N=10,000 permutations) were requested for this analysis.

The obtained Fisher's z-scores were then entered into a two-sample t-test on SPSS to directly compare the two DLB groups. Moreover, in a post-hoc analysis, the Fisher's z-scores of the neurotransmitter system which significantly differentiated the two groups were entered together with the individual SPM z-maps into a linear regression model to identify the brain hypometabolic regions driving the between-group neurotransmitter differences. We set statistical threshold at $p<0.05$, FWE-corrected for multiple comparisons, and we considered only clusters containing more than 100 voxels to be significant.

5.6.4 Study 5: Metabolic connectivity of resting-state networks in α-synucleinopathies, from prodromal to dementia phase (Boccalini, et al., 2022) – Published article

The following data have been published (Boccalini, Bortolin, *et al.*, 2022).

Sample

Thirty subjects with a polysomnography-confirmed diagnosis of iRBD (American Academy of Sleep Medicine, 2014) were retrospectively selected from the clinical database of the Sleep disorders Centre of Turro San Raffaele Hospital, Milan, Italy. Twenty-eight patients diagnosed with PD (Ronald B Postuma *et al.*, 2015) without cognitive impairment at baseline and follow-up (8 years) were retrospectively selected from the clinical and imaging database of the Neurology Unit, Department of Clinical and Experimental Sciences, at the University of Brescia, Brescia, Italy. Thirty patients with a diagnosis of probable DLB (McKeith *et al.*, 2017) were retrospectively selected from the clinical and imaging database of San Raffaele Hospital, Milan, Italy. Thirty HC were randomly selected for comparison from the internal database of the In Vivo Human Molecular and Structural Neuroimaging Unit, IRCCS San Raffaele Scientific Institute, Milan, Italy.

Metabolic connectivity comparison and metrics

We performed interregional correlation analysis (see **Paragraph 5.5.1**) to investigate RSNs in the three clinical groups (iRBD, PD, DLB) as compared to HC. The statistical threshold was set at $p = 0.001$, with Kep ≥ 100 voxels.

First, we aimed to evaluate the integrity of each RSN. To do that, we compared each clinical group with HC (iRBD vs. HC, PD vs. HC, and DLB vs. HC). We quantified the RSN extension and the overlap between each clinical group and HC. The difference in RSN extension between patients and HC may reflect two different and potentially malignant mechanisms: increased or decreased metabolic connectivity of the seed with a set of brain areas compared to healthy brain functioning. Then, the comparison of spatial topography aimed to evaluate if the set of areas metabolically connected to the seed is similar or different in patients and HC. We used well- established and validated connectivity metrics to quantify these differences. Differences in network extension and topography were measured according to the number of correlated voxels (Ballarini *et al.*, 2016; Galbiati *et al.*, 2021) and Dice (DC) similarity coefficient index (Savio *et al.*, 2017), respectively. When we found alterations compared to HC, we also evaluated the commonalities/differences of the pathological changes among the clinical spectrum (i.e., iRBD, PD, and DLB). To do that, we performed direct comparisons between clinical groups (i.e., iRBD vs. PD, iRBD vs. DLB, PD vs. DLB). Specifically, we evaluated the topographical differences, also considering the deviation from HC of each group, using a previously validated metabolic connectivity index: weighted DC coefficient (wDC) (G. Carli, Caminiti, Sala, *et al.*, 2020; Mencarelli *et al.*, 2020). Compared to the standard unweighted DC coefficient, the wDC provides a similarity index that considers not only spatial similarity between groups of patients but also the similarity of the connectivity changes that emerged in comparison with HC.

Network spatial extension (voxel count) - We extracted the number of seed-correlated voxels for each considered network in patients and control groups to quantify the degree and the direction of differences in the spatial extension of the metabolic connectivity. Specifically, computing the difference (Δ) between HC and clinical groups for each RSN for obtaining the degree (absolute value of Δ) and the direction of spatial differences (the sign of Δ, positive = increase and negative = decrease).

Network topography (Dice coefficient and weighted Dice coefficient) - Changes in RSNs connectivity between clinical groups and HC were assessed with the DC and computed using FSL software. DC measures similarity between large-scale networks by computing the normalized amount of their overlap (i.e., volume overlap between two binary masks divided by their mean volume). To evaluate the differences and similarities among clinical groups (i.e., iRBD vs. PD, iRBD vs. DLB, and PD vs. DLB), we computed the weighted wDC to account for their deviation from HC RSNs. Compared to the standard unweighted DC coefficient, the wDC provides a similarity index that advantageously considers not only spatial similarity but also the similarity of the connectivity signs [i.e., positive (higher connectivity than controls) and negative (lower connectivity than controls)]. To do so, we derived a ratio of the voxel count difference (SRΔ) between HC and clinical groups for each RSN:

$$SR\Delta = \frac{(Voxel\ count\ clinical\ group\ RSN) - (Voxel\ count\ RSN\ HC)}{(\ Voxel\ count\ RSN\ HC)}$$

Positive and negative ratios represented the increase and decrease of connectivity compared to HC in terms of spatial network extension. In other words, the SRΔ > 0 indicates that patients showed a higher extension of a specific RSN than HC, and SRΔ < 0 reflected a lower extension. In this way, the product sign reflects whether the groups had the same (both increase or decrease connectivity, positive sign) or different (one increase and the other decrease, or vice versa, negative sign) connectivity changes compared to HC. To obtain the wDC, we added the product of SRΔ of the two groups to the DC. For example, we did a linear computation to calculate the wDC for iRBD and PD groups; we first obtained the traditional DC, and then we added the product of SRΔs computed for iRBD and PD groups to DC. The wDC is a data-based similarity coefficient that measures similarity relative to the specific dataset investigated. Thus, this procedure quantifies the degree of similarity in connectivity alterations among the different clinical groups accounting for the connectivity networks' spatial changes compared to HC. Expressly, wDC values below or close to 0 indicated null or very low similarity between the two groups. The wDC is a relatively new index that can be applied in different ways and to different imaging modalities. Thus, we aimed to test whether the here computed index effectively measured the topographical differences between clinical groups, considering the deviation from HC in terms of RSNs extension. The wDC is supposed to

be higher when two groups of patients have a high percentage of topographical overlap (measured through the traditional DC), and/or both groups showed the same direction of changes compared to HC (increased or decreased network extension in comparison to HC). To verify that, we applied a ranking strategy. For each comparison (iRBD vs. PD, iRBD vs. DLB, and PD vs. DLB), we classified the nine RSN as concordant (both groups have increases/decreases) or discordant (one group has increases and the other decreases, or vice versa) in terms of extension compared to HC. For each comparison (iRBD vs. PD, iRBD vs. DLB, and PD vs. DLB), we also classified the RSNs with moderate-to-good overlap (DC > 0.40) or fair/poor overlap (DC < 0.40), according to the literature guidelines. Then, we defined a network similar when two groups showed either concordant direction of extension changes compared to HC or a moderate degree of overlap in DC. We defined a network not similar when it had discordant changes in extension compared to HC and fair/poor topographical overlap. Last, we tested whether the wDC was statistically different between similar and not similar RSNs for each comparison using ANOVA statistical models.

5.6.5 Study 6: Gender-Related Vulnerability of Dopaminergic Neural Networks in Parkinson's Disease (Boccalini, et al., 2021) – Published article

The following data have been published (Boccalini *et al.*, 2021).

Sample

Thirty-four PD patients (mean age in years – standard deviation [SD]: 62.97 – 10.48; gender [F/M]: 16/18) without cognitive impairment at baseline were retrospectively collected from the clinical and imaging data- base of the Neurology Unit, Department of Clinical and Experimental Sciences, at the University of Brescia, Brescia, Italy. All patients underwent MRI or CT to exclude cerebrovascular diseases or brain/iron accumulation. Patients with deep brain stimulation-verified genetic mutation known to cause PD, concomitant psychiatric or other neurological disorders, hallucination, psychosis or antipsychotic drug use, a background of drug or alcohol addiction, and mild cognitive impairment were excluded. Gender groups in the PD cohorts were compared through a one-way analysis of variance.

Metabolic connectivity measures and statistical analyses

Assessment of metabolic connectivity between targets of nigrostriatal and mesocorticolimbic dopaminergic pathways was performed via partial correlation analysis in each gender group (see **Paragraph 5.5.2**) in female and male groups as compared to gender-matched HC. All the results were set at a statistical threshold of $p < 0.01$, corrected for Bonferroni multiple comparisons.

We calculated the percentage of altered metabolic connections of each network (i.e., connections linking two nodes in the same matrix derived from the comparison between patients and HC) to quantify the severity of metabolic connectivity alterations in PD males and females. Specifically, we computed the total number of connections and the number of altered connections to calculate the percentage of altered metabolic connectivity of each network. Then, we compared the percentage of altered metabolic connections between males and females for each network through the chi-squared test. Thus, chi-square tests of independence examined the relationship between gender and the altered connectivity of dopaminergic networks.

5.6.6 Study 7: Gender differences in dopaminergic system dysfunction in de novo Parkinson's disease clinical subtypes (Boccalini, Carli*, et al., 2022) – Published article*

The following data have been published (Boccalini, Carli, Pilotto, *et al.*, 2022).

Sample

Data used in this study were obtained from the PPMI database (www. ppmi-info.org/data). We included 286 drug naïve iPD patients who underwent baseline [^{123}I]FP-CIT-SPECT imaging and T1-weighted MRI within one year. We excluded subjects with verified genetic mutations known to cause PD (GBA, LRRK2). For all iPD subjects, we collected clinical baseline data from the PPMI database. Following the practical clinical classification method provided by Fereshtehnejad et al. (2017), we assigned each patient to a specific subtype: the mild motor predominant (N = 155), the intermediate (N = 119), and the diffuse malignant (N = 12). The subtypes' definitions were based on the distribution of scores in motor and non-motor clusters. Both composite motor and non-motor summary scores are below the 75th percentile for the mild motor-predominant. For the diffuse malignant, either composite motor score should be greater than 75th

percentile, at least 1 out of 3 non-motor scores should be greater than 75th percentile, or all three non-motor scores greater than 75th percentile. The intermediate includes those patients not meeting criteria for other subtypes. Specifically, we utilized the 'Subtype Calculator' provided by Fereshtehnejad et colleagues, automatically calculating the appropriate category from clinical data.

We also included a pool of N = 73 HC subjects (mean age in years ± SD: 65.54 ± 9.67; gender [F/M]: 34/39) collected from the imaging database of the Neurology Unit, Department of Clinical and Experimental Sciences, at the University of Brescia, Brescia, Italy.

Statistical analyses

MANCOVA and ANOVA tests with Bonferroni correction were used to compare demographics, clinical, and SUVr imaging data between females and males. Age and education were entered as a covariate in the MANCOVA test for the comparison of clinical variables. Age, disease duration, UPDRS-III, and individual mean grey-matter volumes were used as nuisance variables in SUVr DAT imaging comparisons between sex. Notably, to limits the partial volume effects across subjects, we co-variated also ROIs structural volumes in the analysis of [^{123}I]FP-CIT binding data. Mann–Whitney U test was used to test gender differences in the degree of DAT and motor asymmetry, as measured by the side-to-side differences. We considered mean SUVr values for the left and right putamen to identify the DAT binding asymmetry in each patient. We also calculated the motor symptoms asymmetry (Kaasinen *et al.*, 2015). The 87% of patients showing DAT and motor asymmetry featured concordance in laterality (lower putamen uptake contralateral to the predominant symptoms). Thus, SUVr values for all selected ROIs were flipped ROI-by-ROI according to the DAT binding asymmetry index to set the symptomatic hemisphere on the left side and the predominant side of the DAT binding defect on the right side for all the patients. We employed ipsilateral (left) and contralateral (right) uptake values for statistical analyses.

Correlation analyses between DAT SUVr and clinical motor and behavioral scales showing significant gender differences were performed separately in females and males in the whole group, in the mild motor and intermediate subtypes. Age, disease duration, and ROIs' mean grey-matter volumes were used as covariates of no interest. We did not

perform correlation analyses in the diffuse malignant subtype because of the small sample size.

Connectivity analysis

Assessment of molecular connectivity between targets of each dopaminergic pathway (nigrostriatal and mesolimbic) was performed via partial correlation analysis (see **Paragraph 5.2.2**). Partial correlation analyses were performed in gender sub-groups of the whole iPD group and two subtypes (i.e., mild motor and intermediate). We did not perform connectivity analysis in diffuse malignant subtype because of the limited sample size. The samples sizes of the target population and the reference group of HC should be similar to ensure a robust statistical comparison of connectivity metrics. Thus, gender-matched iPD subgroups were randomly selected for comparison, with the same number of the same gender HC group (F/M = 34/39). In male and female patients, we calculated the percentage of altered molecular connections in each network (i.e., connections linking two nodes in the same matrix derived from comparing male/female clinical groups with relative male/female HC group) to quantify the severity of molecular connectivity alterations. Then, we compared the percentage of altered metabolic connections between male and female patients for each network through the chi-squared test.

5.6.7 Study 8: Sex differences in dementia with Lewy bodies: an imaging study of neurotransmission pathways (Boccalini, et al., 2023) – Published article

The following data have been published (Boccalini *et al.*, 2023).

Sample

We collected all [^{123}I]FP-CIT SPECT scans performed at Geneva University Hospitals (Switzerland) between 2013 and 2020 with the same acquisition protocol. Using the most recent clinical diagnostic criteria at the time of diagnosis (Mckeith *et al.*, 2005; McKeith *et al.*, 2017), we retrospectively included 123 subjects (male/female (M/F) = 77/46) with dementia fulfilling the diagnostic criteria of pDLB with available [^{123}I]FP-CIT SPECT images. Subjects have been evaluated in the Division of Neurology at Geneva University Hospitals by neurologists with expertise in movement disorders. For comparison, we included 78 control participants (CTL) (M/F = 34/44) with parkinsonism or tremor not associated with dopaminergic degeneration (e.g., functional tremor/parkinsonism, essential tremor, neuropathic tremor), and with a normal visual and semiquantitative

[^{123}I]FP-CIT SPECT assessment, already included in previous studies (Nicastro, Garibotto, Poncet, *et al.*, 2016; Nicastro, Burkhard and Garibotto, 2018; Nicastro *et al.*, 2020).

Statistical analyses

ANOVA tests were used to compare demographics and clinical data between females and males. $\chi 2$ test was performed for discrete variables, such as clinical symptoms' frequency. SBR imaging data were compared between females and males using MANCOVA test, including age as a covariate. A post hoc analysis was run, testing for sex × group (DLB vs CTL) interaction effect on regional SBR data.

[^{123}I]FP-CIT-SPECT voxel-wise analyses

To further characterize the results of the regional analysis, a complementary voxel-based analysis was run, assessing the voxel-wise distribution of [^{123}I]FP-CIT SBR sex differences. The [^{123}I]FP-CIT SBR parametric images were used in two-sample t-tests in SPM12, running in MATLAB, to compare pDLB females vs CTL females and pDLB males vs CTL males and, directly pDLB females vs pDLB males. Age was included as a covariate of nuisance. For all voxel-wise analyses, analyses, a threshold was set at $p = 0.005$, family-wise error (fwe)-corrected at the cluster level. We applied the JuSpace toolbox (Dukart *et al.*, 2021) to our dataset to compute Spearman correlation (based on the Neuromorphometrics atlas; adjusted (adj) p values, N = 10,000 permutations) between Z-scores (pDLB females vs CTL females and pDLB males vs CTL males) and the DAT (Dukart *et al.*, 2018), SERT, and NET (Hesse *et al.*, 2017) maps, derived from [^{123}I]FP-CIT, ^{11}C-DASB, and S,S-11C-MRB data, respectively. JuSpace is a comprehensive license-free toolbox running in MATLAB for the integration of positron emission tomography (PET)- and SPECT-derived maps with other brain imaging data (MRI, fMRI), allowing to examine specific neurotransmitter system changes as compared to CTL. Briefly, the PET/SPECT maps were derived from average group maps of different healthy volunteers and consisted of maps of the binding signal intensity across the whole brain. Then, the data to generate a contrast between conditions (patients vs CTL) were entered as input to be correlated with PET-/SPECT-derived maps. The atlas is used to extract mean regional values from the input modalities to be correlated with respective mean values from maps, as a voxel-wise analysis would result in highly inflated degrees of freedom.

Connectivity

Assessment of molecular connectivity between targets of each dopaminergic pathway (nigrostriatal and mesolimbic) was performed via partial correlation analyses in each gender group (see **Paragraph 5.5.2**). To ensure a robust statistical comparison of connectivity metrics, sex-matched DLB subgroups were randomly selected for comparison, with the same number of the same-sex CTL group (F/M = 44/34).

All the results were set at a statistical threshold of $p < 0.01$, uncorrected for multiple comparisons. In male and female patients, we calculated the percentage of altered molecular connections in each network to quantify the severity of molecular connectivity alterations. Thus, we computed the number of altered connections divided by the total number of connections of each network to obtain the percentage of altered molecular connectivity. Then, we compared the number of altered molecular connections between male and female patients for each network through the $\chi 2$ test.

5.6.8 Study 9: Sex differences in brain metabolic connectivity architecture in probable dementia with Lewy bodies (Caminiti, Boccalini, et al., 2023) – Published article

The following data have been published (Caminiti, Boccalini, *et al.*, 2023).

Sample

One hundred and thirty-one DLB patients (mean age in years ±standard deviation [SD]: 72 ±7.8; sex [F/M]: 58/73) fulfilling the latest consensus criteria for diagnosis of probable DLB (McKeith *et al.*, 2017)(pDLB) were retrospectively included from the clinical and imaging database of San Raffaele Hospital (Milan, Italy) and Geneva University Hospitals (Switzerland). The two gender groups (pDLB M and pDLB F) were compared through a one-way analysis of variance for continuous variables and Pearson's $\chi 2$ test for frequencies.

We selected [^{18}F]FDG-PET scans of 67 healthy controls (HC) from the control imaging database of the Nuclear Medicine Unit, San Raffaele Hospital, Milan. To obtain an equal sample size with the 2 pDLB groups and to avoid inter-scanner variability, we added 67 [^{18}F]FDG-PET images from the ADNI database (adni.loni.usc.edu). The final group of 134 HC comprised 75 males and 59 females with a similar age to DLB subjects (mean age F: 73 ± 4, t = -0.65 p = 0.52; M: 70 ± 6, t = 1.88 p = 0.07).

[^{18}F]FDG-PET voxel-wise analyses

A voxel-wise group analysis, employing a 2-sample t-test on SPM, was applied to compare the 2 pDLB groups with the sex- matched HC groups (pDLB M < HC M; pDLB F < HC F) thus obtaining the common hypometabolism patterns for pDLB M and pDLB F . The statistical threshold was set at p = 0.05, family-wise error (FWE)- corrected for multiple comparisons. Only clusters containing more than 100 voxels were deemed to be significant. Following the same approach, we directly compared the 2 pDLB groups (pDLB M < pDLB F; pDLB F < pDLB M). Due to the high level of brain metabolic similarity between the 2 clinical groups, the statistical threshold was set at p = 0.001, without applying a correction for multiple comparisons. All the SPM group comparisons were performed considering age as a variable of no interest. In addition, a linear regression analysis was applied in SPM12 to assess the voxel-level correlations between age and whole brain glucose metabolism, considering the smoothed and warped images of the HC males and females, separately.

Metabolic connectivity measures and statistical analyses

ROI-based connectivity approach (partial correlation analysis) was applied to investigate the molecular architecture of the whole-brain network and the major neurotransmission circuits (see **Paragraph 5.5.2**). Beyond the comparison of the percentage of altered metabolic connections between male and female patients for each network through the $\chi 2$ test, we also extracted the "pathological hub" defined as the ROIs with a percentage of altered connectivity one standard deviation above the total number of altered connections in the diagnostic group.

IRCA was applied to investigate RSNs, namely pDMN, PVN, HVN, ATN, LIN, MN, and EXN. Statistical significance was set at p < 0.05, FWE corrected for multiple comparisons, and at cluster extent > 100 voxels. The Jaccard Similarity Coefficient (JSC), a well-established and used metric for connectivity analysis was applied to assess the concordance of connectivity alterations found in pDLB groups in the whole-brain and neurotransmitters' networks. The JSC was computed by considering the commonly altered connections between the 2 groups normalized to the total number of connections in the same groups. JSC was also applied to measure the voxel-by-voxel spatial similarity of RSNs between pDLB and HC groups and between pDLB M and pDLB F. In this case,

the JSC was calculated considering the number of voxels in the intersection between the considered RSN binary masks, normalized to the number of voxels extracted from the sum of the RSN binary masks. JSC ranges from 0, indicating no overlap across the 2 groups, to 1, indicating complete overlap.

6. Bibliography

Adler, C.H. *et al.* (2019) 'Unified staging system for Lewy body disorders: Clinicopathologic correlations and comparison to Braak staging', *Journal of Neuropathology and Experimental Neurology*, 78(10), pp. 891–899. Available at: https://doi.org/10.1093/jnen/nlz080.

Albrecht, F. *et al.* (2019) 'FDG-PET hypometabolism is more sensitive than MRI atrophy in Parkinson's disease: A whole-brain multimodal imaging meta-analysis', *NeuroImage: Clinical*, 21(November 2018), p. 101594. Available at: https://doi.org/10.1016/j.nicl.2018.11.004.

Alcalay, R.N. *et al.* (2012) 'Cognitive performance of GBA mutation carriers with early-onset PD The CORE-PD study', *Neurology*, 78(18), pp. 1434–1440. Available at: https://doi.org/10.1212/WNL.0b013e318253d54b.

American Academy of Sleep Medicine (2014) *The international classification of sleep disorders (ICSD-3)*, *American Academy of Sleep Medicine*.

Anang, J.B.M. *et al.* (2014) 'Predictors of dementia in Parkinson disease: A prospective cohort study', *Neurology*, 83(14), pp. 1253–1260. Available at: https://doi.org/10.1212/WNL.0000000000000842.

Armstrong, M.J. and Okun, M.S. (2020) 'Diagnosis and Treatment of Parkinson Disease: A Review', *JAMA - Journal of the American Medical Association*, 323(6), pp. 548–560. Available at: https://doi.org/10.1001/jama.2019.22360.

Arnaldi, D. *et al.* (2021) 'Dopaminergic imaging and clinical predictors for phenoconversion of REM sleep behaviour disorder', *Brain*, 144(1), pp. 278–287. Available at: https://doi.org/10.1093/brain/awaa365.

Auning, E. *et al.* (2011) 'Early and presenting symptoms of dementia with Lewy bodies', *Dementia and Geriatric Cognitive Disorders*, 32(3), pp. 202–208. Available at: https://doi.org/10.1159/000333072.

Baba, T. *et al.* (2017) 'Longitudinal study of cognitive and cerebral metabolic changes in Parkinson's disease', *Journal of the Neurological Sciences*, 372, pp. 288–293. Available at: https://doi.org/10.1016/j.jns.2016.11.068.

Baldereschi, M. *et al.* (2000) 'Parkinson's disease and parkinsonism in a longitudinal

study: two-fold higher incidence in men', *Neurology*, 55(9), pp. 1358–1363.

Balestrino, R. *et al.* (2021) 'Unexpected (123I)FP-CIT SPECT findings: SWIDD, SWEDD and all DAT', *Journal of Neurology* [Preprint], (0123456789). Available at: https://doi.org/10.1007/s00415-021-10809-x.

Balestrino, R. and Schapira, A.H. V (2018) 'Glucocerebrosidase and Parkinson disease: molecular, clinical, and therapeutic implications', *The Neuroscientist*, 24(5), pp. 540–559.

Ballarini, T. *et al.* (2016) 'Neuropsychiatric subsyndromes and brain metabolic network dysfunctions in early onset Alzheimer's disease', *Human Brain Mapping*, 37(12), pp. 4234–4247. Available at: https://doi.org/10.1002/hbm.23305.

Ballmaier, M. *et al.* (2004) 'Comparing gray matter loss profiles between dementia with Lewy bodies and Alzheimer's disease using cortical pattern matching: Diagnosis and gender effects', *NeuroImage*, 23(1), pp. 325–335. Available at: https://doi.org/10.1016/j.neuroimage.2004.04.026.

Barth, C., Villringer, A. and Sacher, J. (2015) 'Sex hormones affect neurotransmitters and shape the adult female brain during hormonal transition periods', *Frontiers in Neuroscience*, 9(FEB), pp. 1–20. Available at: https://doi.org/10.3389/fnins.2015.00037.

Batla, A. *et al.* (2014) 'Patients with scans without evidence of dopaminergic deficit: A long-term follow-up study', *Movement Disorders*, 29(14), pp. 1820–1825. Available at: https://doi.org/10.1002/mds.26018.

Bauckneht, M. *et al.* (2018) 'Presynaptic dopaminergic neuroimaging in REM sleep behavior disorder: A systematic review and meta-analysis', *Sleep Medicine Reviews*, 41, pp. 266–274. Available at: https://doi.org/10.1016/j.smrv.2018.04.001.

Bayram, E. *et al.* (2021) 'Sex differences for phenotype in pathologically defined dementia with Lewy bodies', *Journal of Neurology, Neurosurgery and Psychiatry*, 92(7), pp. 745–750. Available at: https://doi.org/10.1136/jnnp-2020-325668.

Bayram, E., Coughlin, D.G. and Litvan, I. (2022) 'Sex Differences for Clinical Correlates of Alzheimer's Pathology in People with Lewy Body Pathology', *Movement Disorders*, pp. 1–11. Available at: https://doi.org/10.1002/mds.29044.

Beavan, M. *et al.* (2015) 'Evolution of prodromal clinical markers of parkinson disease

in a GBA mutation-positive cohort', *JAMA Neurology*, 72(2), pp. 201–208. Available at: https://doi.org/10.1001/jamaneurol.2014.2950.

Bedard, M.A. *et al.* (2019) 'Brain cholinergic alterations in idiopathic REM sleep behaviour disorder: a PET imaging study with 18 F-FEOBV', *Sleep Medicine*, 58, pp. 35–41. Available at: https://doi.org/10.1016/j.sleep.2018.12.020.

van de Beek, M. *et al.* (2020) 'Prodromal Dementia With Lewy Bodies: Clinical Characterization and Predictors of Progression', *Movement Disorders*, 35(5), pp. 859–867. Available at: https://doi.org/10.1002/mds.27997.

Van De Beek, M. *et al.* (2020) 'Sex-specific associations with cerebrospinal fluid biomarkers in dementia with Lewy bodies', *Alzheimer's Research and Therapy*, 12(1), pp. 1–8. Available at: https://doi.org/10.1186/s13195-020-00610-9.

Bega, D. *et al.* (2021) 'Clinical utility of DaTscan in patients with suspected Parkinsonian syndrome: a systematic review and meta-analysis', *npj Parkinson's Disease*, 7(1). Available at: https://doi.org/10.1038/s41531-021-00185-8.

Benarroch, E.E. *et al.* (2007) 'Rostral raphe involvement in Lewy body dementia and multiple system atrophy', *Acta Neuropathologica*, 114(3), pp. 213–220. Available at: https://doi.org/10.1007/s00401-007-0260-3.

Benarroch, E.E. (2019) 'Insular cortex: Functional complexity and clinical correlations', *Neurology*, 93(21), pp. 932–938.

Benedetti, M.D. *et al.* (2001) 'Hysterectomy, menopause, and estrogen use preceding Parkinson's disease: An exploratory case-control study', *Movement Disorders*, 16(5), pp. 830–837. Available at: https://doi.org/10.1002/mds.1170.

Berg, D. *et al.* (2021) 'Prodromal Parkinson disease subtypes — key to understanding heterogeneity', *Nature Reviews Neurology*, 0123456789. Available at: https://doi.org/10.1038/s41582-021-00486-9.

Bjornestad, A. *et al.* (2016) 'Risk and course of motor complications in a population-based incident Parkinson's disease cohort', *Parkinsonism & related disorders*, 22, pp. 48–53.

Blesa, J. *et al.* (2022) 'Motor and non-motor circuit disturbances in early Parkinson disease: which happens first?', *Nature Reviews Neuroscience*, 23(2), pp. 115–128.

Boccalini, C. *et al.* (2020) ‘Gender-Related Vulnerability of Dopaminergic Neural Networks in Parkinson’S Disease’, *Brain Connectivity*, pp. 1–28. Available at: https://doi.org/10.1089/brain.2020.0781.

Boccalini, C. *et al.* (2021) ‘Gender-Related Vulnerability of Dopaminergic Neural Networks in Parkinson’s Disease’, *Brain Connectivity*, 11(1), pp. 3–11.

Boccalini, C., Carli, G., Pilotto, A., *et al.* (2022) ‘Gender differences in dopaminergic system dysfunction in de novo Parkinson ’ s disease clinical subtypes’, *Neurobiology of Disease*, 167(October 2021), p. 105668. Available at: https://doi.org/10.1016/j.nbd.2022.105668.

Boccalini, C., Carli, G., Vanoli, E.G., *et al.* (2022) ‘Manual and semi-automated approaches to MIBG myocardial scintigraphy in patients with Parkinson ’ s disease’, (December), pp. 1–6. Available at: https://doi.org/10.3389/fmed.2022.1073720.

Boccalini, C., Bortolin, E., *et al.* (2022) ‘Metabolic connectivity of resting-state networks in alpha synucleinopathies , from prodromal to dementia phase’, (August), pp. 1–14. Available at: https://doi.org/10.3389/fnins.2022.930735.

Boccalini, C. *et al.* (2023) ‘Sex differences in dementia with Lewy bodies : an imaging study of neurotransmission pathways’, *European Journal of Nuclear Medicine and Molecular Imaging* [Preprint], (0123456789). Available at: https://doi.org/10.1007/s00259-023-06132-4.

Bodkin, C.L. (2019) ‘RBD: Gender Implications’, *Rapid-Eye-Movement Sleep Behavior Disorder*, pp. 215–222.

Boeve, B.F. (2010) ‘REM sleep behavior disorder: Updated review of the core features, the REM sleep behavior disorder-neurodegenerative disease association, evolving concepts, controversies, and future directions’, *Annals of the New York Academy of Sciences*, 1184, pp. 15–54. Available at: https://doi.org/10.1111/j.1749-6632.2009.05115.x.

Boeve, B.F. *et al.* (2013) ‘Clinicopathologic correlations in 172 cases of rapid eye movement sleep behavior disorder with or without a coexisting neurologic disorder’, *Sleep medicine*, 14(8), pp. 754–762.

Boeve, B.F. (2019) ‘REM Sleep Behavior Disorder Associated with Dementia with

Lewy Bodies BT - Rapid-Eye-Movement Sleep Behavior Disorder', in C.H. Schenck, B. Högl, and A. Videnovic (eds). Cham: Springer International Publishing, pp. 67–76. Available at: https://doi.org/10.1007/978-3-319-90152-7_6.

Bohnen, N. and Albin, R. (2011) 'The cholinergic system in Parkinson's disease', *Behav Brain Res.*, 221(2), pp. 564–573. Available at: https://doi.org/10.1016/j.bbr.2009.12.048.The.

Bohnen, N.I. *et al.* (2018) 'Recent Advances in Cholinergic Imaging and Cognitive Decline—Revisiting the Cholinergic Hypothesis of Dementia', *Current Geriatrics Reports*, 7(1), pp. 1–11. Available at: https://doi.org/10.1007/s13670-018-0234-4.

Booij, J. *et al.* (2007) 'Quantification of striatal dopamine transporters with123I-FP-CIT SPECT is influenced by the selective serotonin reuptake inhibitor paroxetine: A double-blind, placebo-controlled, crossover study in healthy control subjects', *Journal of Nuclear Medicine*, 48(3), pp. 359–366.

Booij, J. and Kemp, P. (2008) 'Dopamine transporter imaging with [123I]FP-CIT SPECT: Potential effects of drugs', *European Journal of Nuclear Medicine and Molecular Imaging*, 35(2), pp. 424–438. Available at: https://doi.org/10.1007/s00259-007-0621-0.

Borghammer, P. (2021) 'The α-Synuclein Origin and Connectome Model (SOC Model) of Parkinson's Disease: Explaining Motor Asymmetry, Non-Motor Phenotypes, and Cognitive Decline', *Journal of Parkinson's Disease*, 11(2), pp. 455–474. Available at: https://doi.org/10.3233/JPD-202481.

Borghammer, P. *et al.* (2022) 'A postmortem study suggests a revision of the dual-hit hypothesis of Parkinson's disease', *npj Parkinson's Disease*, 8(1), pp. 1–11. Available at: https://doi.org/10.1038/s41531-022-00436-2.

Borghammer, P. (2023) 'The brain-first vs. body-first model of Parkinson's disease with comparison to alternative models.', *Journal of neural transmission (Vienna, Austria : 1996)* [Preprint], (0123456789). Available at: https://doi.org/10.1007/s00702-023-02633-6.

Borghammer, P. and Van Den Berge, N. (2019) 'Brain-First versus Gut-First Parkinson's Disease: A Hypothesis', *Journal of Parkinson's Disease*, 9(s2), pp. S281–

S295. Available at: https://doi.org/10.3233/JPD-191721.

Braak, H., Del Tredici, K., *et al.* (2003) 'Staging of brain pathology related to sporadic Parkinson's disease', *Neurobiology of Aging*, 24(2), pp. 197–211. Available at: https://doi.org/10.1016/S0197-4580(02)00065-9.

Braak, H., Del, K., *et al.* (2003) 'Staging of brain pathology related to sporadic Parkinson ' s disease', *Neurobiology of aging*, 24, pp. 197–211.

Braak, H. *et al.* (2006) 'Pathology associated with sporadic Parkinson's disease - Where does it end?', *Journal of Neural Transmission, Supplement*, (70), pp. 89–97. Available at: https://doi.org/10.1007/978-3-211-45295-0_15.

Braak, H. *et al.* (2018) 'Staging of Brain Pathology Related to Sporadic Parkinson ' s Disease Staging of brain pathology related to sporadic Parkinson ' s disease', 24, pp. 197–211. Available at: https://doi.org/10.1016/S0197-4580(02)00065-9.

Brockmann, K. *et al.* (2011) 'GBA-associated PD presents with nonmotor characteristics', *Neurology*, 77(3), pp. 276–280. Available at: https://doi.org/10.1212/WNL.0b013e318225ab77.

Byun, J.-I. *et al.* (2020) 'Altered resting-state thalamo-occipital functional connectivity is associated with cognition in isolated rapid eye movement sleep behavior disorder', *Sleep Medicine*, 69, pp. 198–203.

Calderon, J. *et al.* (2001) 'Perception, attention, and working memory are disproportionately impaired in dementia with Lewy bodies compared with Alzheimer's disease', *Journal of Neurology Neurosurgery and Psychiatry*, 70(2), pp. 157–164. Available at: https://doi.org/10.1136/jnnp.70.2.157.

Calo, L. *et al.* (2016) 'Synaptic failure and α-synuclein', *Movement Disorders*, 31(2), pp. 169–177.

Caminiti, S. *et al.* (2017) 'Metabolic connectomics targeting brain pathology in dementia with Lewy bodies', *Journal of Cerebral Blood Flow and Metabolism*, 37(4), pp. 1311–1325. Available at: https://doi.org/10.1177/0271678X16654497.

Caminiti, Silvia Paola *et al.* (2017) 'Axonal damage and loss of connectivity in nigrostriatal and mesolimbic dopamine pathways in early Parkinson's disease', *NeuroImage: Clinical*, 14(October 2016), pp. 734–740. Available at:

https://doi.org/10.1016/j.nicl.2017.03.011.

Caminiti, S. P. *et al.* (2017) 'Evaluation of an optimized [18F]fluoro-deoxy-glucose positron emission tomography voxel-wise method to early support differential diagnosis in atypical Parkinsonian disorders', *European Journal of Neurology*, 24(5), pp. 1–8. Available at: https://doi.org/10.1111/ene.13269.

Caminiti, S.P. *et al.* (2017) 'Metabolic connectomics targeting brain pathology in dementia with Lewy bodies', *Journal of Cerebral Blood Flow and Metabolism*, 37(4). Available at: https://doi.org/10.1177/0271678X16654497.

Caminiti, Silvia Paola *et al.* (2019) 'Brain glucose metabolism in Lewy body dementia: implications for diagnostic criteria', *Alzheimer's Research & Therapy*, 11(1), p. 20.

Caminiti, S.P. *et al.* (2019) 'Brain glucose metabolism in Lewy body dementia: Implications for diagnostic criteria', *Alzheimer's Research and Therapy*, 11(1), p. 20. Available at: https://doi.org/http://dx.doi.org/10.1186/s13195-019-0473-4.

Caminiti, S.P., Pilotto, A., *et al.* (2023) 'Dopaminergic connectivity reconfiguration in the dementia with Lewy bodies continuum', *Parkinsonism & Related Disorders*, 108(January), p. 105288. Available at: https://doi.org/10.1016/j.parkreldis.2023.105288.

Caminiti, S.P., Boccalini, C., *et al.* (2023) 'Sex differences in brain metabolic connectivity architecture in probable dementia with Lewy bodies', 126, pp. 14–24. Available at: https://doi.org/10.1016/j.neurobiolaging.2023.02.004.

Campabadal, A. *et al.* (2020) 'Disruption of posterior brain functional connectivity and its relation to cognitive impairment in idiopathic REM sleep behavior disorder', *NeuroImage: Clinical*, 25, p. 102138.

Carli, Giulia, Caminiti, S.P., *et al.* (2020) 'Impaired metabolic brain networks associated with neurotransmission systems in the α-synuclein spectrum', *Parkinsonism and Related Disorders*, 81(July), pp. 113–122. Available at: https://doi.org/10.1016/j.parkreldis.2020.10.036.

Carli, G., Caminiti, S.P., Sala, A., *et al.* (2020) 'Impaired metabolic brain networks associated with neurotransmission systems in the α-synuclein spectrum', *Parkinsonism and Related Disorders*, 81. Available at: https://doi.org/10.1016/j.parkreldis.2020.10.036.

Carli, G., Caminiti, S.P., Galbiati, A., *et al.* (2020) 'In-vivo signatures of neurodegeneration in isolated rapid eye movement sleep behaviour disorder', *European Journal of Neurology*, 27(7), pp. 1285–1295. Available at: https://doi.org/10.1111/ene.14215.

Carli, Giulia, Boccalini, C., *et al.* (2020) 'Specific occupational profiles as proxies of cognitive reserve induce neuroprotection in dementia with Lewy bodies', *Brain Imaging and Behavior* [Preprint]. Available at: https://doi.org/10.1007/s11682-020-00342-2.

Carli, G. *et al.* (2021) 'Brain Molecular Connectivity in Neurodegenerative Conditions', 11. Available at: https://doi.org/https://doi.org/10.3390/ brainsci11040433.

Carrió, I. (2001) 'Cardiac neurotransmission imaging', *Journal of Nuclear Medicine*, 42(7), pp. 1062–1076.

Caspers, J. *et al.* (2021) 'Within-and across-network alterations of the sensorimotor network in Parkinson's disease', *Neuroradiology*, 63(12), pp. 2073–2085.

Castrioto, A. *et al.* (2016) 'Emotional manifestations of PD: Neurobiological basis', *Movement Disorders*, 31(8), pp. 1103–1113.

Catafau, A.M. *et al.* (2004) 'Impact of dopamine transporter SPECT using 123I-Ioflupane on diagnosis and management of patients with clinically uncertain parkinsonian syndromes', *Movement Disorders*, 19(10), pp. 1175–1182. Available at: https://doi.org/10.1002/mds.20112.

Cerami, C. *et al.* (2015) 'Brain metabolic maps in Mild Cognitive Impairment predict heterogeneity of progression to dementia', *NeuroImage: Clinical*, 7, pp. 187–194. Available at: https://doi.org/10.1016/j.nicl.2014.12.004.

Cereda, E. *et al.* (2013) 'Reproductive factors and clinical features of Parkinson's disease', *Parkinsonism and Related Disorders*, 19(12), pp. 1094–1099. Available at: https://doi.org/10.1016/j.parkreldis.2013.07.020.

Cerri, S., Mus, L. and Blandini, F. (2019) 'Parkinson's Disease in Women and Men: What's the Difference?', *Journal of Parkinson's Disease*, 9(3), pp. 501–515. Available at: https://doi.org/10.3233/JPD-191683.

Chen, L. *et al.* (2021) 'Dynamics of Top-Down Control and Motor Networks in Parkinson's Disease', *Movement Disorders*, 36(4), pp. 916–926.

Chen, Q. *et al.* (2022) ‘Longitudinal Tau Positron Emission Tomography in Dementia with Lewy Bodies’, *Movement Disorders* [Preprint].

Chiu, S.Y. *et al.* (2023) ‘Sex differences in dementia with Lewy bodies: Focused review of available evidence and future directions’, *Parkinsonism & Related Disorders*, 107(September 2022), p. 105285. Available at: https://doi.org/10.1016/j.parkreldis.2023.105285.

Cholerton, B. *et al.* (2018) ‘Sex differences in progression to mild cognitive impairment and dementia in Parkinson’s disease’, *Parkinsonism & related disorders*, 50, pp. 29–36.

Choudhury, P. *et al.* (2022) ‘The temporal onset of the core features in dementia with Lewy bodies’, *Alzheimer’s and Dementia*, 18(4), pp. 591–601. Available at: https://doi.org/10.1002/alz.12411.

Chung, E.J. and Kim, S.J. (2015) ‘123I-Metaiodobenzylguanidine Myocardial Scintigraphy in Lewy Body-Related Disorders: A Literature Review’, *Journal of Movement Disorders*, 8(2), pp. 55–66. Available at: https://doi.org/10.14802/jmd.15015.

Coughlin, D. *et al.* (2019) ‘Cognitive and Pathological Influences of Tau Pathology in Lewy Body Disorders’, *Annals of Neurology*, 85(2), pp. 259–271. Available at: https://doi.org/10.1002/ana.25392.

Coughlin, D.G. *et al.* (2020) ‘Multimodal in vivo and postmortem assessments of tau in Lewy body disorders’, *Neurobiology of Aging*, 96, pp. 137–147. Available at: https://doi.org/10.1016/j.neurobiolaging.2020.08.003.

Coughlin, D.G., Hurtig, H.I. and Irwin, D.J. (2020) ‘Pathological Influences on Clinical Heterogeneity in Lewy Body Diseases’, *Movement Disorders*, 35(1), pp. 5–19. Available at: https://doi.org/10.1002/mds.27867.

Criaud, M. *et al.* (2016) ‘Contribution of insula in Parkinson’s disease: A quantitative meta-analysis study’, *Human brain mapping*, 37(4), pp. 1375–1392.

Currie, L.J. *et al.* (2004) ‘Postmenopausal estrogen use affects risk for Parkinson disease’, *Archives of Neurology*, 61(6), pp. 886–888. Available at: https://doi.org/10.1001/archneur.61.6.886.

Curtis, A.F. *et al.* (2019) ‘Cognitive profile of non-demented Parkinson’s disease: Meta-analysis of domain and sex-specific deficits’, *Parkinsonism and Related Disorders*,

60(March 2018), pp. 32–42. Available at: https://doi.org/10.1016/j.parkreldis.2018.10.014.

Dauvilliers, Y. *et al.* (2018) 'REM sleep behaviour disorder', *Nature Reviews Disease Primers*, 4(1). Available at: https://doi.org/10.1038/s41572-018-0016-5.

Davidsson, A. *et al.* (2014) 'Comparison between visual assessment of dopaminergic degeneration pattern and semi-quantitative ratio calculations in patients with Parkinson's disease and Atypical Parkinsonian syndromes using DaTSCAN® SPECT', *Annals of Nuclear Medicine*, 28(9), pp. 851–859. Available at: https://doi.org/10.1007/s12149-014-0878-x.

Deramecourt, V. *et al.* (2006) 'Biochemical staging of synucleinopathy and amyloid deposition in dementia with Lewy bodies', *Journal of Neuropathology and Experimental Neurology*, 65(3), pp. 278–288. Available at: https://doi.org/10.1097/01.jnen.0000205145.54457.ea.

Di, X. and Biswal, A.B.B. (2012) 'Metabolic brain covariant networks as revealed by FDG-PET with reference to resting-state fMRI networks', *Brain connectivity*, 2(5), pp. 275–283.

Donadio, V. *et al.* (2017) 'A new potential biomarker for dementia with Lewy bodies', *Neurology*, 89(4), pp. 318–326. Available at: https://doi.org/10.1212/WNL.0000000000004146.

Drag, L.L. and Bieliauskas, L.A. (2010) 'Contemporary review 2009: Cognitive aging', *Journal of Geriatric Psychiatry and Neurology*, 23(2), pp. 75–93. Available at: https://doi.org/10.1177/0891988709358590.

Dukart, J. *et al.* (2018) 'Cerebral blood flow predicts differential neurotransmitter activity', *Scientific Reports*, 8(1), pp. 1–11. Available at: https://doi.org/10.1038/s41598-018-22444-0.

Dukart, J. *et al.* (2021) 'JuSpace: A tool for spatial correlation analyses of magnetic resonance imaging data with nuclear imaging derived neurotransmitter maps', *Human Brain Mapping*, 42(3), pp. 555–566. Available at: https://doi.org/10.1002/hbm.25244.

Van Den Eeden, S.K. *et al.* (2003) 'Incidence of Parkinson's disease: Variation by age, gender, and race/ethnicity', *American Journal of Epidemiology*, 157(11), pp. 1015–

1022. Available at: https://doi.org/10.1093/aje/kwg068.

Eidelberg, D. *et al.* (1994) 'The metabolic topography of Parkinsonism', *Journal of Cerebral Blood Flow and Metabolism*, 14(5), pp. 783–801. Available at: https://doi.org/10.1038/jcbfm.1994.99.

Eisinger, R.S. *et al.* (2017) 'Motor subtype changes in early Parkinson's disease', *Parkinsonism and Related Disorders*, 43, pp. 67–72. Available at: https://doi.org/10.1016/j.parkreldis.2017.07.018.

Elder, G.J. *et al.* (2017) 'The influence of hippocampal atrophy on the cognitive phenotype of dementia with Lewy bodies', *International Journal of Geriatric Psychiatry*, 32(11), pp. 1182–1189. Available at: https://doi.org/10.1002/gps.4719.

Ellmore, T.M. *et al.* (2013) 'Altered nigrostriatal and nigrocortical functional connectivity in rapid eye movement sleep behavior disorder', *Sleep*, 36(12), pp. 1885–1892.

Erro, R. *et al.* (2016) 'What do patients with scans without evidence of dopaminergic deficit (SWEDD) have? New evidence and continuing controversies', *Journal of Neurology, Neurosurgery and Psychiatry*, 87(3), pp. 319–323. Available at: https://doi.org/10.1136/jnnp-2014-310256.

Eusebio, A. *et al.* (2012) 'Voxel-based analysis of whole-brain effects of age and gender on dopamine transporter SPECT imaging in healthy subjects', *European journal of nuclear medicine and molecular imaging*, 39(11), pp. 1778–1783.

Fathy, Y.Y. *et al.* (2019) 'Differential insular cortex subregional vulnerability to α-synuclein pathology in Parkinson's disease and dementia with Lewy bodies', *Neuropathology and applied neurobiology*, 45(3), pp. 262–277.

Fedorova, T.D. *et al.* (2022) 'Imaging progressive peripheral and central dysfunction in isolated REM sleep behaviour disorder after 3 years of follow-up', *Parkinsonism and Related Disorders*, 101(May), pp. 99–104. Available at: https://doi.org/10.1016/j.parkreldis.2022.07.005.

Fereshtehnejad, S.M. *et al.* (2015) 'New clinical subtypes of Parkinson disease and their longitudinal progression a prospective cohort comparison with other phenotypes', *JAMA Neurology*, 72(8), pp. 863–873. Available at:

https://doi.org/10.1001/jamaneurol.2015.0703.

Fereshtehnejad, S.M. *et al.* (2017) 'Clinical criteria for subtyping Parkinson's disease: Biomarkers and longitudinal progression', *Brain*, 140(7), pp. 1959–1976. Available at: https://doi.org/10.1093/brain/awx118.

Ferini-Strambi, L. *et al.* (2019) 'Neuropsychological, electrophysiological, and neuroimaging biomarkers for REM behavior disorder', *Expert Review of Neurotherapeutics*, 19(11), pp. 1069–1087. Available at: https://doi.org/10.1080/14737175.2019.1640603.

Ferman, T.J. *et al.* (2011) 'Inclusion of RBD improves the diagnostic classification of dementia with Lewy bodies', *Neurology*, 77(9), pp. 875–882. Available at: https://doi.org/10.1212/WNL.0b013e31822c9148.

Ferman, T.J. *et al.* (2020) 'Subtypes of dementia with Lewy bodies are associated with α-synuclein and tau distribution', *Neurology*, 95(2), pp. E155–E165. Available at: https://doi.org/10.1212/WNL.0000000000009763.

Ferrando, R. and Damian, A. (2021) 'Brain SPECT as a Biomarker of Neurodegeneration in Dementia in the Era of Molecular Imaging: Still a Valid Option?', *Frontiers in Neurology*, 12(May), pp. 1–16. Available at: https://doi.org/10.3389/fneur.2021.629442.

Ferreira, D. *et al.* (2020) *β-Amyloid and tau biomarkers and clinical phenotype in dementia with Lewy bodies*, *Neurology*. Available at: https://doi.org/10.1212/WNL.0000000000010943.

Ferretti, M.T. *et al.* (2020) 'Sex and gender differences in Alzheimer's disease: current challenges and implications for clinical practice: Position paper of the Dementia and Cognitive Disorders Panel of the European Academy of Neurology', *European Journal of Neurology*, 27(6), pp. 928–943. Available at: https://doi.org/10.1111/ene.14174.

Flotats, A. *et al.* (2010) 'Proposal for standardization of 123 I-metaiodobenzylguanidine (MIBG) cardiac sympathetic imaging by the EANM Cardiovascular Committee and the European Council of Nuclear Cardiology', *European journal of nuclear medicine and molecular imaging*, 37(9), pp. 1802–1812.

Fornito, A., Zalesky, A. and Breakspear, M. (2015) 'The connectomics of brain

disorders', *Nature Reviews Neuroscience*, 16(3), pp. 159–172. Available at: https://doi.org/10.1038/nrn3901.

Frentzel, D. *et al.* (2017) 'Increase of reproductive life span Delays age of onset of parkinson's disease', *Frontiers in Neurology*, 8(AUG), pp. 2–8. Available at: https://doi.org/10.3389/fneur.2017.00397.

Gagnon, J.F. *et al.* (2009) 'Mild cognitive impairment in rapid eye movement sleep behavior disorder and Parkinson's disease', *Annals of Neurology*, 66(1), pp. 39–47. Available at: https://doi.org/10.1002/ana.21680.

Galbiati, A. *et al.* (2019) 'The risk of neurodegeneration in REM sleep behavior disorder: A systematic review and meta-analysis of longitudinal studies', *Sleep Medicine Reviews*, 43, pp. 37–46. Available at: https://doi.org/10.1016/j.smrv.2018.09.008.

Galbiati, A. *et al.* (2021) 'Exploring the functional role and neural correlates of K-complexes in isolated rapid eye movement sleep behavior disorder', *Cortex* [Preprint]. Available at: https://doi.org/https://doi.org/10.1016/j.cortex.2021.08.012.

Gan-Or, Z. *et al.* (2015) 'GBA mutations are associated with Rapid Eye Movement Sleep Behavior Disorder', *Annals of Clinical and Translational Neurology*, 2(9), pp. 941–945. Available at: https://doi.org/10.1002/acn3.228.

Garcia-Garcia, D. *et al.* (2012) 'Posterior parietooccipital hypometabolism may differentiate mild cognitive impairment from dementia in Parkinson's disease', *European Journal of Nuclear Medicine and Molecular Imaging*, 39(11), pp. 1767–1777. Available at: https://doi.org/10.1007/s00259-012-2198-5.

García-Gómez, F.J. *et al.* (2013) 'Elaboration of the SPM template for the standardization of SPECT images with 123I-Ioflupane', *Revista Española de Medicina Nuclear e Imagen Molecular (English Edition)*, 32(6), pp. 350–356. Available at: https://doi.org/10.1016/j.remnie.2013.09.003.

Gasca-Salas, C. *et al.* (2016) 'Significance of visual hallucinations and cerebral hypometabolism in the risk of dementia in Parkinson's disease patients with mild cognitive impairment', *Human Brain Mapping*, 37(3), pp. 968–977. Available at: https://doi.org/10.1002/hbm.23080.

Gatto, N.M. *et al.* (2014) 'Lifetime exposure to estrogens and Parkinson's disease in California teachers', *Parkinsonism and Related Disorders*, 20(11), pp. 1149–1156. Available at: https://doi.org/10.1016/j.parkreldis.2014.08.003.

Ge, J. *et al.* (2015) 'Assessing cerebral glucose metabolism in patients with idiopathic rapid eye movement sleep behavior disorder', *Journal of Cerebral Blood Flow & Metabolism*, 35(12), pp. 2062–2069.

Génier Marchand, D. *et al.* (2018) 'How does dementia with Lewy bodies start? prodromal cognitive changes in REM sleep behavior disorder', *Annals of Neurology*, 83(5), pp. 1016–1026. Available at: https://doi.org/10.1002/ana.25239.

Geser, F. *et al.* (2005) 'How to diagnose dementia with Lewy bodies: state of the art', *Movement disorders: official journal of the Movement Disorder Society*, 20(S12), pp. S11–S20.

Giacobini, E. and Pepeu, G. (2018) 'Sex and gender differences in the brain cholinergic system and in the response to therapy of Alzheimer disease with cholinesterase inhibitors', *Current Alzheimer Research*, 15(11), pp. 1077–1084.

Giagulli, V. *et al.* (2016) 'Serum testosterone and cognitive function in ageing male: updating the evidence', *Recent Patents on Endocrine, Metabolic & Immune Drug Discovery*, 10(1), pp. 22–30.

Giannoccaro, M.P. *et al.* (2020) 'Comparison of 123I-MIBG scintigraphy and phosphorylated α-synuclein skin deposits in synucleinopathies', *Parkinsonism and Related Disorders*, 81(June), pp. 48–53. Available at: https://doi.org/10.1016/j.parkreldis.2020.10.016.

Gillies, G.E. and McArthur, S. (2010) 'Estrogen actions in the brain and the basis for differential action in men and women: A case for sex-specific medicines', *Pharmacological Reviews*, 62(2), pp. 155–198. Available at: https://doi.org/10.1124/pr.109.002071.

Goedert, M., Clavaguera, F. and Tolnay, M. (2010) 'The propagation of prion-like protein inclusions in neurodegenerative diseases', *Trends in neurosciences*, 33(7), pp. 317–325.

Goedert, M., Jakes, R. and Spillantini, M.G. (2017) 'The Synucleinopathies: Twenty

Years on', *Journal of Parkinson's Disease*, 7(s1), pp. S53–S71. Available at: https://doi.org/10.3233/JPD-179005.

Gratwicke, J., Jahanshahi, M. and Foltynie, T. (2015) 'Parkinson's disease dementia: a neural networks perspective', *Brain*, 138(6), pp. 1454–1476.

Greenberg, G.D. and Trainor, B.C. (2015) *Sex Differences in the Social Behavior Network and Mesolimbic Dopamine System*, *Sex Differences in the Central Nervous System*. Elsevier Inc. Available at: https://doi.org/10.1016/B978-0-12-802114-9.00004-4.

Gur, R.E. and Gur, R.C. (2022) 'Gender differences in aging: cognition, emotions, and neuroimaging studies', *Dialogues in clinical neuroscience* [Preprint].

Gustafsson, H., Nordström, A. and Nordström, P. (2015) 'Depression and subsequent risk of Parkinson disease: a nationwide cohort study', *Neurology*, 84(24), pp. 2422–2429.

Haaxma, C.A. *et al.* (2007) 'Gender differences in Parkinson's disease', *Journal of Neurology, Neurosurgery and Psychiatry*, 78(8), pp. 819–824. Available at: https://doi.org/10.1136/jnnp.2006.103788.

Haba-Rubio, J. *et al.* (2018) 'Prevalence and determinants of rapid eye movement sleep behavior disorder in the general population', *Sleep*, 41(2), pp. 1–8. Available at: https://doi.org/10.1093/sleep/zsx197.

Haber, S.N. and Calzavara, R. (2009) 'The cortico-basal ganglia integrative network: the role of the thalamus', *Brain research bulletin*, 78(2–3), pp. 69–74.

Hall, C.B. *et al.* (2007) 'Education delays accelerated decline on a memory test in persons who develop dementia', *Neurology*, 69(17), pp. 1657–1664. Available at: https://doi.org/10.1212/01.wnl.0000278163.82636.30.

Halliday, G.M. *et al.* (2011) 'Neuropathology underlying clinical variability in patients with synucleinopathies', *Acta Neuropathologica*, 122(2), pp. 187–204. Available at: https://doi.org/10.1007/s00401-011-0852-9.

Harding, A.J. and Halliday, G.M. (2001) 'Cortical Lewy body pathology in the diagnosis of dementia', *Acta neuropathologica*, 102(4), pp. 355–363.

Hasselgren, C. *et al.* (2020) 'Sex differences in dementia: On the potentially mediating

effects of educational attainment and experiences of psychological distress', *BMC Psychiatry*, 20(1), pp. 1–13. Available at: https://doi.org/10.1186/s12888-020-02820-9.

Healy, D.G. *et al.* (2008) 'Phenotype, genotype, and worldwide genetic penetrance of LRRK2-associated Parkinson's disease: a case-control study', *The Lancet Neurology*, 7(7), pp. 583–590. Available at: https://doi.org/10.1016/S1474-4422(08)70117-0.

Heidebrink, J.L. (2002) 'Is dementia with Lewy bodies the second most common cause of dementia?', *Journal of Geriatric Psychiatry and Neurology*, 15(4), pp. 182–187. Available at: https://doi.org/10.1177/089198870201500402.

Hellwig, S. *et al.* (2012) '[18F] FDG-PET is superior to [123I] IBZM-SPECT for the differential diagnosis of parkinsonism', *Neurology*, 79(13), pp. 1314–1322.

Hely, M.A. *et al.* (2008) 'The Sydney multicenter study of Parkinson's disease: the inevitability of dementia at 20 years', *Movement disorders*, 23(6), pp. 837–844.

Henderson, M.X., Trojanowski, J.Q. and Lee, V.M.Y. (2019) 'α-Synuclein pathology in Parkinson's disease and related α-synucleinopathies', *Neuroscience Letters*, 709(June), p. 134316. Available at: https://doi.org/10.1016/j.neulet.2019.134316.

Hesse, S. *et al.* (2017) 'Central noradrenaline transporter availability in highly obese, non-depressed individuals', *European Journal of Nuclear Medicine and Molecular Imaging*, 44(6), pp. 1056–1064. Available at: https://doi.org/10.1007/s00259-016-3590-3.

Hilker, R. *et al.* (2005) 'Nonlinear progression of Parkinson disease as determined by serial positron emission tomographic imaging of striatal fluorodopa F 18 activity', *Archives of Neurology*, 62(3), pp. 378–382. Available at: https://doi.org/10.1001/archneur.62.3.378.

Hillary, F.G. and Grafman, J.H. (2017) 'Injured Brains and Adaptive Networks: The Benefits and Costs of Hyperconnectivity', *Trends in Cognitive Sciences*, 21(5), pp. 385–401. Available at: https://doi.org/10.1016/j.tics.2017.03.003.

Högl, B., Stefani, A. and Videnovic, A. (2018) 'Idiopathic REM sleep behaviour disorder and neurodegeneration—an update', *Nature Reviews Neurology*, 14(1), p. 40.

Höglinger, G.U. *et al.* (2015) 'A new dopaminergic nigro-olfactory projection', *Acta Neuropathologica*, 130(3), pp. 333–348. Available at: https://doi.org/10.1007/s00401-

015-1451-y.

Holtbernd, F. *et al.* (2015) ‘Dopaminergic correlates of metabolic network activity in Parkinson’s disease’, *Human brain mapping*, 36(9), pp. 3575–3585.

Horsager, J. *et al.* (2020) ‘Brain-first versus body-first Parkinson’s disease: a multimodal imaging case-control study’, *Brain*, pp. 1–12. Available at: https://doi.org/10.1093/brain/awaa238.

Horwitz, B., Duara, R. and Rapoport, S.I. (1984) ‘Intercorrelations of glucose metabolic rates between brain regions: application to healthy males in a state of reduced sensory input.’, *Journal of Cerebral Blood Flow and Metabolism*, 4(4), pp. 484–499. Available at: https://doi.org/10.1038/jcbfm.1984.73.

Hsam, O. and Kohl, Z. (2023) ‘Serotonin in synucleinopathies’, *Behavioural Brain Research*, 445(October 2022), p. 114367. Available at: https://doi.org/10.1016/j.bbr.2023.114367.

Huang, S. *et al.* (2010) ‘Learning brain connectivity of Alzheimer’s disease by sparse inverse covariance estimation’, *NeuroImage*, 50(3), pp. 935–949. Available at: https://doi.org/10.1016/j.neuroimage.2009.12.120.

Huber, M. *et al.* (2020) ‘Metabolic correlates of dopaminergic loss in dementia with lewy bodies’, *Movement disorders*, 35(4), pp. 595–605.

Iaccarino, L. *et al.* (2017) ‘The emerging role of PET imaging in dementia’, *F1000Research*, 6(0). Available at: https://doi.org/10.12688/f1000research.11603.1.

Iaccarino, L. *et al.* (2018) ‘The brain metabolic signature of visual hallucinations in dementia with Lewy bodies’, *Cortex*, 108, pp. 13–24.

Iranzo, A. *et al.* (2005) ‘Characteristics of idiopathic REM sleep behavior disorder and that associated with MSA and PD’, *Neurology*, 65(2), pp. 247–252. Available at: https://doi.org/10.1212/01.wnl.0000168864.97813.e0.

Iranzo, A. *et al.* (2013) ‘Neurodegenerative disease status and post-mortem pathology in idiopathic rapid-eye-movement sleep behaviour disorder: an observational cohort study’, *The Lancet Neurology*, 12(5), pp. 443–453.

Iranzo, A., Fernández-Arcos, A., *et al.* (2014) ‘Neurodegenerative disorder risk in idiopathic REM sleep behavior disorder: Study in 174 patients’, *PLoS ONE*, 9(2).

Available at: https://doi.org/10.1371/journal.pone.0089741.

Iranzo, A., Gelpi, E., *et al.* (2014) 'Neuropathology of prodromal Lewy body disease', *Movement Disorders*, 29(3), pp. 410–415.

Iranzo, A. *et al.* (2017) 'Dopamine transporter imaging deficit predicts early transition to synucleinopathy in idiopathic rapid eye movement sleep behavior disorder', *Annals of Neurology*, 82(3), pp. 419–428. Available at: https://doi.org/10.1002/ana.25026.

Irwin, D.J. and Hurtig, H.I. (2018) 'The contribution of tau, amyloid-beta and alpha-synuclein pathology to dementia in Lewy body disorders', *Journal of Alzheimer's disease & Parkinsonism*, 8(4).

Irwin, D.J., Lee, V.M.Y. and Trojanowski, J.Q. (2013) 'Parkinson's disease dementia: Convergence of α-synuclein, tau and amyloid-β pathologies', *Nature Reviews Neuroscience*, 14(9), pp. 626–636. Available at: https://doi.org/10.1038/nrn3549.

Ishii, K. *et al.* (2013) 'Comparative value of brain perfusion SPECT and I-123 MIBG myocardial scintigraphy for prediction of conversion to probable DLB in possible DLB subjects'. Soc Nuclear Med.

Jamadar, S.D. *et al.* (2021) 'Metabolic and Hemodynamic Resting-State Connectivity of the Human Brain: A High-Temporal Resolution Simultaneous BOLD-fMRI and FDG-fPET Multimodality Study', *Cerebral cortex (New York, N.Y. : 1991)*, 31(6), pp. 2855–2867. Available at: https://doi.org/10.1093/cercor/bhaa393.

Jaramillo-Jimenez, A. *et al.* (2021) 'Association Between Amygdala Volume and Trajectories of Neuropsychiatric Symptoms in Alzheimer's Disease and Dementia With Lewy Bodies', *Frontiers in Neurology*, 12(July), pp. 1–13. Available at: https://doi.org/10.3389/fneur.2021.679984.

Jellinger, K.A. (2012) 'Neuropathology of sporadic Parkinson's disease: evaluation and changes of concepts', *Movement disorders*, 27(1), pp. 8–30.

Jellinger, K.A. and Korczyn, A.D. (2018) 'Are dementia with Lewy bodies and Parkinson's disease dementia the same disease?', *BMC Medicine*, 16(1), pp. 1–16. Available at: https://doi.org/10.1186/s12916-018-1016-8.

Joling, M. *et al.* (2018) 'Lower 123I-FP-CIT binding to the striatal dopamine transporter, but not to the extrastriatal serotonin transporter, in Parkinson's disease

compared with dementia with Lewy bodies', *NeuroImage: Clinical*, 19(April), pp. 130–136. Available at: https://doi.org/10.1016/j.nicl.2018.04.009.

Joling, M. *et al.* (2019) 'Striatal DAT and extrastriatal SERT binding in early-stage Parkinson's disease and dementia with Lewy bodies, compared with healthy controls: An 123 I-FP-CIT SPECT study', *NeuroImage: Clinical*, 22(July 2018). Available at: https://doi.org/10.1016/j.nicl.2019.101755.

Jurado-Coronel, J.C. *et al.* (2018) 'Sex differences in Parkinson's disease: Features on clinical symptoms, treatment outcome, sexual hormones and genetics', *Frontiers in Neuroendocrinology*, 50(September), pp. 18–30. Available at: https://doi.org/10.1016/j.yfrne.2017.09.002.

Kaasinen, V. *et al.* (2015) 'Effects of aging and gender on striatal and extrastriatal [123I]FP-CIT binding in Parkinson's disease', *Neurobiology of Aging*, 36(4), pp. 1757–1763. Available at: https://doi.org/10.1016/j.neurobiolaging.2015.01.016.

Kanel, P. *et al.* (2021) 'Molecular Imaging of the Cholinergic System in Alzheimer and Lewy Body Dementias: Expanding Views', *Current Neurology and Neuroscience Reports*, 21(10), pp. 1–9. Available at: https://doi.org/10.1007/s11910-021-01140-z.

Kantarci, K. *et al.* (2012) 'Multimodality imaging characteristics of dementia with Lewy bodies', *Neurobiology of Aging*, 33(9), pp. 2091–2105. Available at: https://doi.org/10.1016/j.neurobiolaging.2011.09.024.

Kasanuki, K. *et al.* (2012) 'Neuropathological investigation of the hypometabolic regions on positron emission tomography with [18F] fluorodeoxyglucose in patients with dementia with Lewy bodies', *Journal of the Neurological Sciences*, 314(1–2), pp. 111–119. Available at: https://doi.org/10.1016/j.jns.2011.10.010.

Kato, T. *et al.* (2016) 'Brain fluorodeoxyglucose (FDG) PET in dementia', *Ageing Research Reviews*, 30, pp. 73–84. Available at: https://doi.org/10.1016/j.arr.2016.02.003.

Kehagia, A.A., Barker, R.A. and Robbins, T.W. (2013) 'Cognitive impairment in Parkinson's disease: the dual syndrome hypothesis', *Neurodegenerative diseases*, 11(2), pp. 79–92.

Kim, J.S. *et al.* (2009) 'Cardiac sympathetic denervation and its association with

cognitive deficits in Parkinson's disease', *Parkinsonism and Related Disorders*, 15(9), pp. 706–708. Available at: https://doi.org/10.1016/j.parkreldis.2009.01.008.

Kim, J.S. *et al.* (2015) '123I-MIBG myocardial scintigraphy and neurocirculatory abnormalities in patients with dementia with Lewy bodies and Alzheimer's disease', *Journal of the Neurological Sciences*, 357(1–2), pp. 173–177. Available at: https://doi.org/10.1016/j.jns.2015.07.025.

King, A.E., Mintz, J. and Royall, D.R. (2011) 'Meta-analysis of 123I-MIBG cardiac scintigraphy for the diagnosis of Lewy body–related disorders', *Movement Disorders*, 26(7), pp. 1218–1224.

Kish, S.J. *et al.* (2005) 'Regional distribution of serotonin transporter protein in postmortem human brain: Is the cerebellum a SERT-free brain region?', *Nuclear Medicine and Biology*, 32(2), pp. 123–128. Available at: https://doi.org/10.1016/j.nucmedbio.2004.10.001.

Klein, J. *et al.* (2010) 'Neurotransmitter changes in dementia with Lewy bodies and Parkinson disease dementia in vivo', *Neurology*, 74(11), pp. 885–892.

Knudsen, K. *et al.* (2018a) 'In-vivo staging of pathology in REM sleep behaviour disorder: a multimodality imaging case-control study', *The Lancet Neurology*, 17(7), pp. 618–628. Available at: https://doi.org/10.1016/S1474-4422(18)30162-5.

Knudsen, K. *et al.* (2018b) 'In-vivo staging of pathology in REM sleep behaviour disorder: a multimodality imaging case-control study', *The Lancet Neurology*, 17(7), pp. 618–628. Available at: https://doi.org/10.1016/S1474-4422(18)30162-5.

Knudsen, K. and Borghammer, P. (2018) 'Imaging the Autonomic Nervous System in Parkinson's Disease', *Current Neurology and Neuroscience Reports*, 18(11). Available at: https://doi.org/10.1007/s11910-018-0889-4.

Ko, J.H., Lee, C.S. and Eidelberg, D. (2017) 'Metabolic network expression in parkinsonism: Clinical and dopaminergic correlations', *Journal of Cerebral Blood Flow & Metabolism*, 37(2), pp. 683–693.

Koch, W. *et al.* (2014) 'Extrastriatal binding of [123 I] FP-CIT in the thalamus and pons: gender and age dependencies assessed in a European multicentre database of healthy controls', *European journal of nuclear medicine and molecular imaging*,

41(10), pp. 1938–1946.

Koedam, E.L.G.E. *et al.* (2008) 'Early-onset dementia is associated with higher mortality', *Dementia and Geriatric Cognitive Disorders*, 26(2), pp. 147–152. Available at: https://doi.org/10.1159/000149585.

Kojovic, M. *et al.* (2012) 'Functional reorganization of sensorimotor cortex in early Parkinson disease', *Neurology*, 78(18), pp. 1441–1448.

Kolmancic, K. *et al.* (2019) 'Sex differences in Parkinson's disease: A transcranial magnetic stimulation study', *Movement Disorders*, 34(12), pp. 1873–1881. Available at: https://doi.org/10.1002/mds.27870.

Komatsu, J. *et al.* (2018) '123I-MIBG myocardial scintigraphy for the diagnosis of DLB: a multicentre 3-year follow-up study', *Journal of Neurology, Neurosurgery and Psychiatry*, 89(11), pp. 1167–1173. Available at: https://doi.org/10.1136/jnnp-2017-317398.

Korat, Š. *et al.* (2021) 'Alpha-Synuclein PET tracer development-an overview about current efforts', *Pharmaceuticals*, 14(9). Available at: https://doi.org/10.3390/ph14090847.

Kosaka, K. (2014) 'Latest concept of Lewy body disease', *Psychiatry and Clinical Neurosciences*, 68(6), pp. 391–394. Available at: https://doi.org/10.1111/pcn.12179.

Krohn, L. *et al.* (2020) 'GBA variants in REM sleep behavior disorder: A multicenter study', *Neurology*, 95(8), pp. E1008–E1016. Available at: https://doi.org/10.1212/WNL.0000000000010042.

de Lau, L.M.L. *et al.* (2014) 'Relation of clinical subtypes in Parkinson's disease with survival', *Movement Disorders*, 29(1), pp. 150–151.

Lee, C.S. *et al.* (2000) 'In vivo positron emission tomographic evidence for compensatory changes in presynaptic dopaminergic nerve terminals in Parkinson's disease', *Annals of Neurology*, 47(4), pp. 493–503. Available at: https://doi.org/10.1002/1531-8249(200004)47:4<493::AID-ANA13>3.0.CO;2-4.

Lee, D.S. *et al.* (2008) 'Metabolic connectivity by interregional correlation analysis using statistical parametric mapping (SPM) and FDG brain PET; Methodological development and patterns of metabolic connectivity in adults', *European Journal of*

Nuclear Medicine and Molecular Imaging, 35(9), pp. 1681–1691. Available at: https://doi.org/10.1007/s00259-008-0808-z.

Lee, J.E. *et al.* (2010) 'A comparative analysis of cognitive profiles and white-matter alterations using voxel-based diffusion tensor imaging between patients with Parkinson's disease dementia and dementia with Lewy bodies', *Journal of Neurology, Neurosurgery & Psychiatry*, 81(3), pp. 320–326.

Lee, J.W. *et al.* (2021) 'Patients with scans without evidence of dopaminergic deficit (SWEDD) do not have early Parkinson's disease: Analysis of the PPMI data', *PLoS ONE*, 16(2 February), pp. 1–11. Available at: https://doi.org/10.1371/journal.pone.0246881.

Lee, P.C. *et al.* (2019) 'Examining the Reserve Hypothesis in Parkinson's Disease: A Longitudinal Study', *Movement Disorders*, 34(11), pp. 1663–1671. Available at: https://doi.org/10.1002/mds.27854.

Lee, Y. gun *et al.* (2022) 'Effects of Alzheimer and Lewy Body Disease Pathologies on Brain Metabolism', *Annals of Neurology*, 91(6), pp. 853–863. Available at: https://doi.org/10.1002/ana.26355.

Leech, R., Braga, R. and Sharp, D.J. (2012) 'Echoes of the brain within the posterior cingulate cortex', *Journal of Neuroscience*, 32(1), pp. 215–222. Available at: https://doi.org/10.1523/JNEUROSCI.3689-11.2012.

Leentjens, A.F.G. *et al.* (2011) 'Symptomatology and markers of anxiety disorders in Parkinson's disease: A cross-sectional study', *Movement Disorders*, 26(3), pp. 484–492. Available at: https://doi.org/10.1002/mds.23528.

Leitner, C. *et al.* (2023) 'Neuropsychological Changes in Isolated REM Sleep Behavior Disorder: A Systematic Review and Meta-analysis of Cross-sectional and Longitudinal Studies', *Neuropsychology Review* [Preprint]. Available at: https://doi.org/10.1007/s11065-022-09572-1.

Li, Y. *et al.* (2017) 'Predictive markers for early conversion of iRBD to neurodegenerative synucleinopathy diseases', *Neurology*, 88(16), pp. 1493–1500. Available at: https://doi.org/10.1212/WNL.0000000000003838.

Lin, Y.-Q. and Chen, S.-D. (2018) 'RBD: a red flag for cognitive impairment in

Parkinson's disease?', *Sleep medicine*, 44, pp. 38–44.

Liu, R. *et al.* (2015) 'Potential sex differences in nonmotor symptoms in early drug-naive Parkinson disease', *Neurology*, 84(21), pp. 2107–2115. Available at: https://doi.org/10.1212/WNL.0000000000001609.

Locascio, J.J., Corkin, S. and Growdon, J.H. (2003) 'Relation between clinical characteristics of Parkinson's disease and cognitive decline', *Journal of Clinical and Experimental Neuropsychology*, 25(1), pp. 94–109. Available at: https://doi.org/10.1076/jcen.25.1.94.13624.

Van Loenhoud, A.C. *et al.* (2019) 'Cognitive reserve and clinical progression in Alzheimer disease: A paradoxical relationship', *Neurology*, 93(4), pp. E334–E346. Available at: https://doi.org/10.1212/WNL.0000000000007821.

Lubomski, M. *et al.* (2014) 'Sex differences in Parkinson's disease', *Journal of Clinical Neuroscience*, 21(9), pp. 1503–1506. Available at: https://doi.org/10.1016/j.jocn.2013.12.016.

Lücking, C.B. *et al.* (2000) 'Association between early-onset Parkinson's disease and mutations in the parkin gene', *New England Journal of Medicine*, 342(21), pp. 1560–1567.

Maillet, A. *et al.* (2021) 'Serotonergic and Dopaminergic Lesions Underlying Parkinsonian Neuropsychiatric Signs', *Movement Disorders*, 36(12), pp. 2888–2900. Available at: https://doi.org/10.1002/mds.28722.

Maingay, M. *et al.* (2006) 'Ventral tegmental area dopamine neurons are resistant to human mutant alpha-synuclein overexpression', *Neurobiology of disease*, 23(3), pp. 522–532.

Malpetti, M. *et al.* (2017) 'Gender differences in healthy aging and Alzheimer's Dementia: A 18F-FDG-PET study of brain and cognitive reserve', *Human Brain Mapping*, 38(8), pp. 4212–4227. Available at: https://doi.org/10.1002/hbm.23659.

Mandelli, M.L. *et al.* (2016) 'Healthy brain connectivity predicts atrophy progression in non-fluent variant of primary progressive aphasia', *Brain*, 139(10), pp. 2778–2791. Available at: https://doi.org/10.1093/brain/aww195.

Manjón, J. V. and Coupé, P. (2016) 'Volbrain: An online MRI brain volumetry system',

Frontiers in Neuroinformatics, 10(JUL), pp. 1–14. Available at: https://doi.org/10.3389/fninf.2016.00030.

Marek, K. *et al.* (2011) 'The Parkinson Progression Marker Initiative (PPMI)', *Progress in Neurobiology*, 95(4), pp. 629–635. Available at: https://doi.org/10.1016/j.pneurobio.2011.09.005.

Marek, K. *et al.* (2014) 'Longitudinal follow-up of SWEDD subjects in the PRECEPT Study', *Neurology*, 82(20), pp. 1791–1797. Available at: https://doi.org/10.1212/WNL.0000000000000424.

Marek, K. *et al.* (2018) 'The Parkinson's progression markers initiative (PPMI) – establishing a PD biomarker cohort', *Annals of Clinical and Translational Neurology*, 5(12), pp. 1460–1477. Available at: https://doi.org/10.1002/acn3.644.

Marshall, V.L. *et al.* (2006) 'Two-year follow-up in 150 consecutive cases with normal dopamine transporter imaging', *Nuclear Medicine Communications*, 27(12), pp. 933–937. Available at: https://doi.org/10.1097/01.mnm.0000243374.11260.5b.

Marshall, V.L. *et al.* (2009) 'Parkinson's disease is overdiagnosed clinically at baseline in diagnostically uncertain cases: A 3-year European multicenter study with repeat [123I]FP-CIT SPECT', *Movement Disorders*, 24(4), pp. 500–508. Available at: https://doi.org/10.1002/mds.22108.

Martinez-Martin, P. *et al.* (2012) 'Gender-related differences in the burden of non-motor symptoms in Parkinson's disease', *Journal of Neurology*, 259(8), pp. 1639–1647. Available at: https://doi.org/10.1007/s00415-011-6392-3.

Marui, W. *et al.* (2002) 'Progression and staging of Lewy pathology in brains from patients with dementia with Lewy bodies', *Journal of the Neurological Sciences*, 195(2), pp. 153–159. Available at: https://doi.org/10.1016/S0022-510X(02)00006-0.

Massa, F. *et al.* (2019) 'Neuroimaging findings and clinical trajectories of Lewy body disease in patients with MCI', *Neurobiology of Aging*, 76, pp. 9–17. Available at: https://doi.org/10.1016/j.neurobiolaging.2018.12.001.

Massicotte-Marquez, J. *et al.* (2008) 'Executive dysfunction and memory impairment in idiopathic REM sleep behavior disorder', *Neurology*, 70(15), pp. 1250–1257. Available at: https://doi.org/10.1212/01.wnl.0000286943.79593.a6.

Mattioli, P. *et al.* (2023) ‘Derivation and Validation of a Phenoconversion-Related Pattern in Idiopathic Rapid Eye Movement Behavior Disorder’, *Movement Disorders*, 38(1), pp. 57–67. Available at: https://doi.org/10.1002/mds.29236.

Mazzulli, J.R. *et al.* (2011) ‘Gaucher disease glucocerebrosidase and α-synuclein form a bidirectional pathogenic loop in synucleinopathies’, *Cell*, 146(1), pp. 37–52.

McCann, H. *et al.* (2014) ‘α-Synucleinopathy phenotypes’, *Parkinsonism & related disorders*, 20, pp. S62–S67.

McKeith, I. (2007) ‘Dementia with Lewy bodies’, in *Handbook of clinical Neurology*. Elsevier, pp. 531–548.

Mckeith, I.G. *et al.* (2005) ‘Diagnosis and management of dementia with Lewy bodies third report of the DLB consortium’, *Neurology*, 65(12), pp. 1863–1872. Available at: https://doi.org/10.1212/01.wnl.0000187889.17253.b1.

McKeith, I.G. *et al.* (2017) ‘Diagnosis and management of dementia with Lewy bodies: Fourth consensus report of the DLB Consortium’, *Neurology*, 89(1), pp. 88–100.

McKeith, I.G. *et al.* (2020) ‘Research criteria for the diagnosis of prodromal dementia with Lewy bodies’, *Neurology*, 94(17), pp. 743–755. Available at: https://doi.org/10.1212/WNL.0000000000009323.

McLaughlin, K.J., Baran, S.E. and Conrad, C.D. (2009) ‘Chronic stress-and sex-specific neuromorphological and functional changes in limbic structures’, *Molecular neurobiology*, 40(2), pp. 166–182.

Meles, S.K. *et al.* (2018) ‘The Metabolic Pattern of Idiopathic REM Sleep Behavior Disorder Reflects Early-Stage Parkinson Disease’, *Journal of Nuclear Medicine*, 59(9), pp. 1437–1444.

Meles, S.K. *et al.* (2020) ‘Abnormal pattern of brain glucose metabolism in Parkinson’s disease: replication in three European cohorts’, *European Journal of Nuclear Medicine and Molecular Imaging*, 47(2), pp. 437–450. Available at: https://doi.org/10.1007/s00259-019-04570-7.

Mencarelli, L. *et al.* (2020) ‘Network Mapping of Connectivity Alterations in Disorder of Consciousness: Towards Targeted Neuromodulation’, *Journal of Clinical Medicine*, 9(3), p. 828.

Menšíková, K. *et al.* (2022) 'Lewy body disease or diseases with Lewy bodies?', *npj Parkinson's Disease*, 8(1). Available at: https://doi.org/10.1038/s41531-021-00273-9.

Meoni, S., Macerollo, A. and Moro, E. (2020) 'Sex differences in movement disorders', *Nature Reviews Neurology*, 16(2), pp. 84–96. Available at: https://doi.org/10.1038/s41582-019-0294-x.

Mielke, M.M., Vemuri, P. and Rocca, W.A. (2014) 'Clinical epidemiology of Alzheimer ' s disease : assessing sex and gender differences', *Clinical Epidemiology*, pp. 37–48.

Miglis, M.G. *et al.* (2021) 'Biomarkers of conversion to α-synucleinopathy in isolated rapid-eye-movement sleep behaviour disorder', *The Lancet Neurology*, 20(8), pp. 671–684. Available at: https://doi.org/10.1016/S1474-4422(21)00176-9.

Milber, J.M. *et al.* (2012) 'Lewy pathology is not the first sign of degeneration in vulnerable neurons in parkinson disease', *Neurology*, 79(24), pp. 2307–2314. Available at: https://doi.org/10.1212/WNL.0b013e318278fe32.

Minoshima, S. *et al.* (2001) 'Alzheimer's disease versus dementia with Lewy bodies: Cerebral metabolic distinction with autopsy confirmation', *Annals of Neurology*, 50(3), pp. 358–365. Available at: https://doi.org/10.1002/ana.1133.

Miyamoto, T. *et al.* (2008) '123I-MIBG cardiac scintigraphy provides clues to the underlying neurodegenerative disorder in idiopathic REM sleep behavior disorder', *Sleep*, 31(5), pp. 717–723. Available at: https://doi.org/10.1093/sleep/31.5.717.

Molano, J. *et al.* (2010) 'Mild cognitive impairment associated with limbic and neocortical lewy body disease: A clinicopathological study', *Brain*, 133(2), pp. 540–556. Available at: https://doi.org/10.1093/brain/awp280.

Morbelli, S. *et al.* (2019) 'Metabolic patterns across core features in dementia with lewy bodies', *Annals of Neurology*, 85(5), pp. 715–725. Available at: https://doi.org/10.1002/ana.25453.

Morgante, F., Edwards, M.J. and Espay, A.J. (2013) 'Psychogenic movement disorders', *Continuum: Lifelong Learning in Neurology*, 19(5 Movement Disorders), p. 1383.

Mouton, A. *et al.* (2018) 'Sex ratio in dementia with Lewy bodies balanced between Alzheimer's disease and Parkinson's disease dementia: A cross-sectional study', *Alzheimer's Research and Therapy*, 10(1), pp. 1–10. Available at:

https://doi.org/10.1186/s13195-018-0417-4.

Mueller, C. *et al.* (2017) 'The prognosis of dementia with Lewy bodies', *The Lancet Neurology*, 16(5), pp. 390–398.

Nagahama, Y. *et al.* (2010) 'Neural correlates of psychotic symptoms in dementia with Lewy bodies', *Brain*, 133(2), pp. 557–567.

Nagamachi, S. *et al.* (2008) 'Usefulness of rCBF analysis in diagnosing Parkinson's disease: supplemental role with MIBG myocardial scintigraphy', *Annals of nuclear medicine*, 22(7), pp. 557–564.

Nahimi, A. *et al.* (2018) 'Molecular Imaging of the Noradrenergic System in Idiopathic Parkinson's Disease', in *International review of neurobiology*. Elsevier, pp. 251–274.

Nalls, M.A. *et al.* (2013) 'A multicenter study of glucocerebrosidase mutations in dementia with Lewy bodies', *JAMA Neurology*, 70(6), pp. 727–735. Available at: https://doi.org/10.1001/jamaneurol.2013.1925.

Nandhagopal, R. *et al.* (2009) 'Longitudinal progression of sporadic Parkinson's disease: A multi-tracer positron emission tomography study', *Brain*, 132(11), pp. 2970–2979. Available at: https://doi.org/10.1093/brain/awp209.

Nelson, P.T. *et al.* (2010) 'Association between male gender and cortical Lewy body pathology in large autopsy series', *Journal of neurology*, 257(11), pp. 1875–1881.

Newhouse, P. and Dumas, J. (2015) 'Hormones and Behavior Estrogen – cholinergic interactions : Implications for cognitive aging ☆', *Hormones and Behavior*, 74, pp. 173–185. Available at: https://doi.org/10.1016/j.yhbeh.2015.06.022.

Nicastro, N., Garibotto, V., Poncet, A., *et al.* (2016) 'Establishing On-Site Reference Values for 123I-FP-CIT SPECT (DaTSCAN®) Using a Cohort of Individuals with Non-Degenerative Conditions', *Molecular Imaging and Biology*, 18(2), pp. 302–312. Available at: https://doi.org/10.1007/s11307-015-0889-6.

Nicastro, N., Garibotto, V., Badoud, S., *et al.* (2016) 'Scan without evidence of dopaminergic deficit: A 10-year retrospective study', *Parkinsonism and Related Disorders*, 31, pp. 53–58. Available at: https://doi.org/10.1016/j.parkreldis.2016.07.002.

Nicastro, N. *et al.* (2020) 'Extrastriatal 123I-FP-CIT SPECT impairment in degenerative

parkinsonisms', *Parkinsonism and Related Disorders*, 78(July), pp. 38–43. Available at: https://doi.org/10.1016/j.parkreldis.2020.07.008.

Nicastro, N., Burkhard, P.R. and Garibotto, V. (2018) 'Scan without evidence of dopaminergic deficit (SWEDD) in degenerative parkinsonism and dementia with Lewy bodies: A prospective study', *Journal of the Neurological Sciences*, 385(June 2017), pp. 17–21. Available at: https://doi.org/10.1016/j.jns.2017.11.039.

Nicastro, N., Burkhard, P.R. and Garibotto, V. (2020) 'Preserved Extrastriatal 123I-FP-CIT Binding in Scans Without Evidence of Dopaminergic Deficit (SWEDD)', *Molecular Imaging and Biology*, 22(6), pp. 1592–1599. Available at: https://doi.org/10.1007/s11307-020-01502-y.

Nicastro, N., Garibotto, V. and Burkhard, P.R. (2020) 'Extrastriatal 123I-FP-CIT SPECT impairment in Parkinson's disease-the PPMI cohort', *BMC Neurology*, 20(1), pp. 1–9. Available at: https://doi.org/10.1186/s12883-020-01777-2.

Niethammer, M. *et al.* (2013) 'Parkinson's disease cognitive network correlates with caudate dopamine', *Neuroimage*, 78, pp. 204–209.

Niethammer, M. and Eidelberg, D. (2012) 'Metabolic brain networks in translational neurology: Concepts and applications', *Annals of Neurology*, 72(5), pp. 635–647. Available at: https://doi.org/10.1002/ana.23631.

Nussbaum, R.L. (2018) 'Genetics of synucleinopathies', *Cold Spring Harbor Perspectives in Medicine*, 8(6). Available at: https://doi.org/10.1101/cshperspect.a024109.

Nutt, J.G. (2016) 'Motor subtype in Parkinson's disease: Different disorders or different stages of disease?', *Movement Disorders*, 31(7), pp. 957–961. Available at: https://doi.org/10.1002/mds.26657.

O'brien, J. *et al.* (2020) 'Visual hallucinations in neurological and ophthalmological disease: Pathophysiology and management', *Journal of Neurology, Neurosurgery and Psychiatry*, 91(5), pp. 512–519. Available at: https://doi.org/10.1136/jnnp-2019-322702.

Obeso, J.A. *et al.* (2017) 'Past, present, and future of Parkinson's disease: A special essay on the 200th Anniversary of the Shaking Palsy', *Movement Disorders*, 32(9), pp. 1264–1310.

Oh, J.-K. *et al.* (2015) 'Comparison of I-123 MIBG planar imaging and SPECT for the detection of decreased heart uptake in Parkinson disease', *Journal of Neural Transmission*, 122(10), pp. 1421–1427.

Oka, H. *et al.* (2007) 'Reduced cardiac 123I-MIBG uptake reflects cardiac sympathetic dysfunction in Lewy body disease', *Neurology*, 69(14), pp. 1460–1465.

Orimo, S. *et al.* (2012) '123I-MIBG myocardial scintigraphy for differentiating Parkinson's disease from other neurodegenerative parkinsonism: A systematic review and meta-analysis', *Parkinsonism and Related Disorders*, 18(5), pp. 494–500. Available at: https://doi.org/10.1016/j.parkreldis.2012.01.009.

Orimo, S. *et al.* (2016) '123I-meta-iodobenzylguanidine (MIBG) cardiac scintigraphy in α-synucleinopathies', *Ageing Research Reviews*, 30, pp. 122–133. Available at: https://doi.org/10.1016/j.arr.2016.01.001.

Outeiro, T.F. *et al.* (2019) 'Dementia with Lewy bodies: An update and outlook', *Molecular Neurodegeneration*, 14(1), pp. 1–18. Available at: https://doi.org/10.1186/s13024-019-0306-8.

De Pablo-Fernández, E. *et al.* (2019) 'Prognosis and Neuropathologic Correlation of Clinical Subtypes of Parkinson Disease', *JAMA Neurology*, 76(4), pp. 470–479. Available at: https://doi.org/10.1001/jamaneurol.2018.4377.

Pagonabarraga, J. and Kulisevsky, J. (2012) 'Cognitive impairment and dementia in Parkinson's disease', *Neurobiology of Disease*, 46(3), pp. 590–596. Available at: https://doi.org/10.1016/j.nbd.2012.03.029.

Palermo, G. *et al.* (2021) 'Dopamine transporter imaging, current status of a potential biomarker: A comprehensive review', *International Journal of Molecular Sciences*, 22(20). Available at: https://doi.org/10.3390/ijms222011234.

Palop, J.J., Chin, J. and Mucke, L. (2006) 'A network dysfunction perspective on neurodegenerative diseases', *Nature*, 443(7113), p. 768.

Papathanasiou, N.D. *et al.* (2012) 'Diagnostic accuracy of 123I-FP-CIT (DaTSCAN) in dementia with Lewy bodies: A meta-analysis of published studies', *Parkinsonism and Related Disorders*, 18(3), pp. 225–229. Available at: https://doi.org/10.1016/j.parkreldis.2011.09.015.

Pappatá, S. *et al.* (2011) 'Mild cognitive impairment in drug-naive patients with PD is associated with cerebral hypometabolism', *Neurology*, 77(14), pp. 1357–1362.

Parkkinen, L., Pirttilä, T. and Alafuzoff, I. (2008) 'Applicability of current staging/categorization of α-synuclein pathology and their clinical relevance', *Acta Neuropathologica*, 115(4), pp. 399–407. Available at: https://doi.org/10.1007/s00401-008-0346-6.

Paul, K.C. *et al.* (2018) 'Association of polygenic risk score with cognitive decline and motor progression in Parkinson disease', *JAMA Neurology*, 75(3), pp. 360–366. Available at: https://doi.org/10.1001/jamaneurol.2017.4206.

Peavy, G.M. *et al.* (2016) 'Phenotypic differences based on staging of Alzheimer's neuropathology in autopsy-confirmed dementia with Lewy bodies', *Parkinsonism & related disorders*, 31, pp. 72–78.

Perani, Daniela *et al.* (2014) 'Validation of an optimized SPM procedure for FDG-PET in dementia diagnosis in a clinical setting', *NeuroImage: Clinical*, 6, pp. 445–454. Available at: https://doi.org/10.1016/j.nicl.2014.10.009.

Perani, D. *et al.* (2014) 'Validation of an optimized SPM procedure for FDG-PET in dementia diagnosis in a clinical setting', *NeuroImage: Clinical*, 6, pp. 445–454. Available at: https://doi.org/10.1016/j.nicl.2014.10.009.

Perani, D. *et al.* (2020) 'PET Neuroimaging in Dementia Conditions', *PET and SPECT in Neurology*, pp. 211–282.

Peraza, L.R. *et al.* (2014) 'FMRI resting state networks and their association with cognitive fluctuations in dementia with Lewy bodies', *NeuroImage: Clinical*, 4, pp. 558–565. Available at: https://doi.org/10.1016/j.nicl.2014.03.013.

Periquet, M. *et al.* (2003) 'Parkin mutations are frequent in patients with isolated early-onset parkinsonism', *Brain*, 126(6), pp. 1271–1278.

Picillo, M. *et al.* (2017) 'Association between dopaminergic dysfunction and anxiety in de novo Parkinson's disease', *Parkinsonism and Related Disorders*, 37, pp. 106–110. Available at: https://doi.org/10.1016/j.parkreldis.2017.02.010.

Pievani, M. *et al.* (2014) 'Brain connectivity in neurodegenerative diseases-from phenotype to proteinopathy', *Nat Rev Neurol*, 10(11), pp. 620–633. Available at:

https://doi.org/10.1038/nrneurol.2014.178.

Pigott, K. *et al.* (2015) 'Longitudinal study of normal cognition in Parkinson disease', *Neurology*, 85(15), pp. 1276–1282. Available at: https://doi.org/10.1212/WNL.0000000000002001.

Pilotto, Andrea *et al.* (2018) 'Single-subject SPM FDG-PET patterns predict risk of dementia progression in Parkinson disease', *Neurology*, 90(12), pp. e1029–e1037. Available at: https://doi.org/10.1212/WNL.0000000000005161.

Pilotto, A. *et al.* (2018) 'Single-subject SPM FDG-PET patterns predict risk of dementia progression in Parkinson disease', *Neurology*, 90(12). Available at: https://doi.org/10.1212/WNL.0000000000005161.

Pilotto, A., Di Cola, F.S., *et al.* (2019) 'Extrastriatal dopaminergic and serotonergic pathways in Parkinson's disease and in dementia with Lewy bodies: a 123 I-FP-CIT SPECT study', *European journal of nuclear medicine and molecular imaging*, 46(8), pp. 1642–1651.

Pilotto, A., Schiano di Cola, F., *et al.* (2019) 'Extrastriatal dopaminergic and serotonergic pathways in Parkinson's disease and in dementia with Lewy bodies: a 123I-FP-CIT SPECT study', *European Journal of Nuclear Medicine and Molecular Imaging*, 46(8), pp. 1642–1651. Available at: https://doi.org/10.1007/s00259-019-04324-5.

Podcasy, J.L. and Epperson, C.N. (2016) 'Considering sex and gender in Alzheimer disease and other dementias', *Dialogues in Clinical Neuroscience*, 18(4), pp. 437–446.

Poewe, W. *et al.* (2017) 'Parkinson disease', *Nature Reviews Disease Primers*, 3, pp. 1–21. Available at: https://doi.org/10.1038/nrdp.2017.13.

Politis, M. *et al.* (2010) 'Staging of serotonergic dysfunction in Parkinson's Disease: An in vivo 11C-DASB PET study', *Neurobiology of Disease*, 40(1), pp. 216–221. Available at: https://doi.org/10.1016/j.nbd.2010.05.028.

Politis, M. (2014) 'Neuroimaging in Parkinson disease: from research setting to clinical practice', *Nature Reviews Neurology*, 10(12), p. 708.

Poston, K.L. and Eidelberg, D. (2010) 'FDG PET in the Evaluation of Parkinson's Disease.', *PET clinics*, 5(1), pp. 55–64. Available at:

https://doi.org/10.1016/j.cpet.2009.12.004.

Postuma, R.B., Gagnon, J.F., Vendette, M. and Montplaisir, J.Y. (2009) 'Markers of neurodegeneration in idiopathic rapid eye movement sleep behaviour disorder and Parkinson's disease', *Brain*, 132(12), pp. 3298–3307. Available at: https://doi.org/10.1093/brain/awp244.

Postuma, R.B., Gagnon, J.F., Vendette, M., Fantini, M.L., *et al.* (2009) 'Quantifying the risk of neurodegenerative disease in idiopathic REM sleep behavior disorder', *Neurology*, 72(15), pp. 1296–1300. Available at: https://doi.org/10.1212/01.wnl.0000340980.19702.6e.

Postuma, Ronald B *et al.* (2015) 'MDS clinical diagnostic criteria for Parkinson's disease', *Movement Disorders*, 30(12), pp. 1591–1601.

Postuma, Ronald B. *et al.* (2015) 'REM sleep behavior disorder and neuropathology in Parkinson's disease', *Movement Disorders*, 30(10), pp. 1413–1417. Available at: https://doi.org/10.1002/mds.26347.

Postuma, R.B. *et al.* (2018) 'Validation of the MDS clinical diagnostic criteria for Parkinson's disease', *Movement Disorders*, 33(10), pp. 1601–1608. Available at: https://doi.org/10.1002/mds.27362.

Postuma, R.B. *et al.* (2019) 'Risk and predictors of dementia and parkinsonism in idiopathic REM sleep behaviour disorder: A multicentre study', *Brain*, 142(3), pp. 744–759. Available at: https://doi.org/10.1093/brain/awz030.

Postuma, R.B., Gagnon, J.F. and Montplaisir, J. (2013) 'Rapid eye movement sleep behavior disorder as a biomarker for neurodegeneration: The past 10years', *Sleep Medicine*, 14(8), pp. 763–767. Available at: https://doi.org/10.1016/j.sleep.2012.09.001.

Poulin, J.F. *et al.* (2018) 'Mapping projections of molecularly defined dopamine neuron subtypes using intersectional genetic approaches', *Nature Neuroscience*, 21(9), pp. 1260–1271. Available at: https://doi.org/10.1038/s41593-018-0203-4.

Premi, E. *et al.* (2016) 'Impulse control disorder in PD: A lateralized monoaminergic frontostriatal disconnection syndrome?', *Parkinsonism and Related Disorders*, 30, pp. 62–66. Available at: https://doi.org/10.1016/j.parkreldis.2016.05.028.

Premi, E. *et al.* (2017) 'Source-Based Morphometry Multivariate Approach to Analyze

[123I]FP-CIT SPECT Imaging', *Molecular Imaging and Biology*, 19(5), pp. 772–778. Available at: https://doi.org/10.1007/s11307-017-1052-3.

Presotto, L. *et al.* (2017) 'Validation of 18F–FDG-PET Single-Subject Optimized SPM Procedure with Different PET Scanners', *Neuroinformatics*, 15(2), pp. 151–163. Available at: https://doi.org/10.1007/s12021-016-9322-9.

Rajput, A.H. *et al.* (2008) 'Globus pallidus dopamine and Parkinson motor subtypes: Clinical and brain biochemical correlation', *Neurology*, 70(16 PART 2), pp. 1403–1410. Available at: https://doi.org/10.1212/01.wnl.0000285082.18969.3a.

Rascol, O. and Schelosky, L. (2009) '123I-metaiodobenzylguanidine scintigraphy in Parkinson's disease and related disorders', *Movement Disorders*, 24(SUPPL. 2), pp. 732–741. Available at: https://doi.org/10.1002/mds.22499.

Raunio, A. *et al.* (2019) 'Lewy-related pathology exhibits two anatomically and genetically distinct progression patterns: a population-based study of Finns aged 85+', *Acta Neuropathologica*, 138(5), pp. 771–782. Available at: https://doi.org/10.1007/s00401-019-02071-3.

Reekes, T.H. *et al.* (2020) 'Sex specific cognitive differences in Parkinson disease', *npj Parkinson's Disease*, 6(1), pp. 1–6. Available at: https://doi.org/10.1038/s41531-020-0109-1.

Riedel, O. *et al.* (2008) 'Cognitive impairment in 873 patients with idiopathic Parkinson's disease: Results from the German Study on Epidemiology of Parkinson's Disease with Dementia (GEPAD)', *Journal of Neurology*, 255(2), pp. 255–264. Available at: https://doi.org/10.1007/s00415-008-0720-2.

Ripp, I. *et al.* (2020) 'Integrity of Neurocognitive Networks in Dementing Disorders as Measured with Simultaneous PET/Functional MRI', *Journal of nuclear medicine : official publication, Society of Nuclear Medicine*, 61(9), pp. 1341–1347. Available at: https://doi.org/10.2967/jnumed.119.234930.

Rolinski, M. *et al.* (2016) 'Basal ganglia dysfunction in idiopathic REM sleep behaviour disorder parallels that in early Parkinson's disease', *Brain*, 139(8), pp. 2224–2234.

Della Rosa, P.A. *et al.* (2014) 'A standardized [18 F]-FDG-PET template for spatial normalization in statistical parametric mapping of dementia', *Neuroinformatics*, 12(4),

pp. 575–593.

Roselli, F. *et al.* (2010) 'Midbrain SERT in degenerative parkinsonisms: A 123I-FP-CIT SPECT study', *Movement Disorders*, 25(12), pp. 1853–1859. Available at: https://doi.org/10.1002/mds.23179.

Rubinov, M. and Sporns, O. (2010) 'NeuroImage Complex network measures of brain connectivity : Uses and interpretations', *NeuroImage*, 52(3), pp. 1059–1069. Available at: https://doi.org/10.1016/j.neuroimage.2009.10.003.

Ruppert, M.C. *et al.* (2020) 'Network degeneration in Parkinson's disease: Multimodal imaging of nigro-striato-cortical dysfunction', *Brain*, 143(3), pp. 944–959. Available at: https://doi.org/10.1093/brain/awaa019.

Saeed, U. *et al.* (2017) 'Imaging biomarkers in Parkinson's disease and Parkinsonian syndromes: Current and emerging concepts', *Translational Neurodegeneration*, 6(1), pp. 1–25. Available at: https://doi.org/10.1186/s40035-017-0076-6.

Saito, Y. *et al.* (2003) 'Accumulation of Phosphorylated α-Synuclein in Aging Human Brain', *Journal of Neuropathology & Experimental Neurology*, 62(6), pp. 644–654. Available at: https://doi.org/10.1093/jnen/62.6.644.

Sala, A., Caminiti, S.P., *et al.* (2017) 'Altered brain metabolic connectivity at multiscale level in early Parkinson's disease', *Scientific Reports*, 7(1). Available at: https://doi.org/10.1038/s41598-017-04102-z.

Sala, A., Caminiti, Silvia Paola, *et al.* (2017) 'Altered brain metabolic connectivity at multiscale level in early Parkinson's disease', *Scientific Reports*, 7(1), pp. 1–12. Available at: https://doi.org/10.1038/s41598-017-04102-z.

Sala, A. *et al.* (2019) 'Vulnerability of multiple large-scale brain networks in dementia with Lewy bodies', *Human Brain Mapping*, 40(15), pp. 4537–4550. Available at: https://doi.org/10.1002/hbm.24719.

Sala, A. *et al.* (2022) 'Brain connectomics : time for a molecular imaging perspective ?', *Trends in Cognitive Sciences*, pp. 1–14. Available at: https://doi.org/10.1016/j.tics.2022.11.015.

Sala, A. and Perani, D. (2019) 'Brain Molecular Connectivity in Neurodegenerative Diseases: Recent Advances and New Perspectives Using Positron Emission

Tomography', *Frontiers in Neuroscience*, 13(June), pp. 1–15. Available at: https://doi.org/10.3389/fnins.2019.00617.

Sateia, M.J. (2014) 'International classification of sleep disorders', *Chest*, 146(5), pp. 1387–1394.

Savio, A. *et al.* (2017) 'Resting-state networks as simultaneously measured with functional MRI and PET', *Journal of Nuclear Medicine*, 58(8), pp. 1314–1317.

Scheffel, U. *et al.* (1997) 'N-substituted phenyltropanes as in vivo binding ligands for rapid imaging studies of the dopamine transporter', *Synapse*, 25(4), pp. 345–349. Available at: https://doi.org/10.1002/(SICI)1098-2396(199704)25:4<345::AID-SYN5>3.0.CO;2-A.

Schenck, C.H. (2019) 'Neuropathology of REM Sleep Behavior Disorder', in *Rapid-Eye-Movement Sleep Behavior Disorder*. Springer, pp. 579–587.

Schindlbeck, K.A. and Eidelberg, D. (2018) 'Network imaging biomarkers: insights and clinical applications in Parkinson's disease', *The Lancet Neurology*, 17(7), pp. 629–640.

Schneider, S.A. *et al.* (2007) 'Patients with adult-onset dystonic tremor resembling parkinsonian tremor have scans without evidence of dopaminergic deficit (SWEDDs)', *Movement disorders: official journal of the Movement Disorder Society*, 22(15), pp. 2210–2215.

Schoonheim, M.M. (2017) 'Functional reorganization is a maladaptive response to injury - Commentary', *Multiple Sclerosis*, 23(2), pp. 194–196. Available at: https://doi.org/10.1177/1352458516677593.

Schrag, A. *et al.* (2015) 'Prediagnostic presentations of Parkinson's disease in primary care: a case-control study', *The Lancet Neurology*, 14(1), pp. 57–64.

Schwartz, F. *et al.* (2019) 'Overlapping and distinct neural metabolic patterns related to impulsivity and hypomania in Parkinson's disease', *Brain Imaging and Behavior*, 13(1), pp. 241–254. Available at: https://doi.org/10.1007/s11682-017-9812-x.

Schwartz, J.R.L. and Roth, T. (2008) 'Neurophysiology of sleep and wakefulness: basic science and clinical implications', *Current neuropharmacology*, 6(4), pp. 367–378.

Scott, B. *et al.* (2000) 'Gender differences in Parkinson's disease symptom profile', *Acta Neurologica Scandinavica*, 102(1), pp. 37–43.

Seeley, W.W. *et al.* (2009) 'Neurodegenerative Diseases Target Large-Scale Human Brain Networks', *Neuron*, 62(1), pp. 42–52. Available at: https://doi.org/10.1016/j.neuron.2009.03.024.

Sharp, S.I. *et al.* (2008) 'Cortical serotonin 1A receptor levels are associated with depression in patients with dementia with lewy bodies and Parkinson's disease dementia', *Dementia and Geriatric Cognitive Disorders*, 26(4), pp. 330–338. Available at: https://doi.org/10.1159/000161058.

Shigemoto, Y. *et al.* (2022) 'Voxel-based analysis of age and gender effects on striatal [123I] FP-CIT binding in healthy Japanese adults', *Annals of Nuclear Medicine*, 36(5), pp. 460–467. Available at: https://doi.org/10.1007/s12149-022-01725-9.

Sidransky, E. *et al.* (2009) 'Multicenter analysis of glucocerebrosidase mutations in Parkinson's disease', *New England Journal of Medicine*, 361(17), pp. 1651–1661.

Sieber, B. *et al.* (2014) 'Prioritized research recommendations from the N ational I nstitute of N eurological D isorders and S troke P arkinson's D isease 2014 conference', *Annals of neurology*. Wiley Online Library, pp. 469–472.

Sim, J. *et al.* (2022) 'Clinical Manifestations of Early-Onset Dementia with Lewy Bodies Compared with Late-Onset Dementia with Lewy Bodies and Early-Onset Alzheimer Disease', *JAMA Neurology*, 79(7), pp. 702–709. Available at: https://doi.org/10.1001/jamaneurol.2022.1133.

Sisson, J.C. and Wieland, D.M. (1986) 'Radiolabeled meta-iodobenzylguanidine: pharmacology and clinical studies.', *American journal of physiologic imaging*, 1(2), pp. 96–103.

Sixel-Döring, F. *et al.* (2011) 'The role of 123 I-FP-CIT-SPECT in the differential diagnosis of Parkinson and tremor syndromes: a critical assessment of 125 cases', *Journal of neurology*, 258(12), pp. 2147–2154.

Smith, C. *et al.* (2019) 'Neuropathology of dementia in patients with Parkinson's disease: A systematic review of autopsy studies', *Journal of Neurology, Neurosurgery and Psychiatry*, 90(11), pp. 1234–1243. Available at: https://doi.org/10.1136/jnnp-2019-321111.

Söderlund, T.A. *et al.* (2013) 'Value of semiquantitative analysis for clinical reporting of

123I-2-β-carbomethoxy-3β-(4-iodophenyl)-N-(3-fluoropropyl) nortropane SPECT studies', *Journal of Nuclear Medicine*, 54(5), pp. 714–722. Available at: https://doi.org/10.2967/jnumed.112.110106.

Sourty, M. *et al.* (2016) 'Identifying Dynamic Functional Connectivity Changes in Dementia with Lewy Bodies Based on Product Hidden Markov Models', *Frontiers in Computational Neuroscience*, 10(June), pp. 1–11. Available at: https://doi.org/10.3389/fncom.2016.00060.

Spetsieris, P.G. *et al.* (2015) 'Metabolic resting-state brain networks in health and disease', *Proceedings of the National Academy of Sciences of the United States of America*, 112(8), pp. 2563–2568. Available at: https://doi.org/10.1073/pnas.1411011112.

Sprenger, F.S. *et al.* (2015) 'Nonmotor Symptoms in Subjects Without Evidence of Dopaminergic Deficits', *Movement Disorders*, 30(7), pp. 976–981. Available at: https://doi.org/10.1002/mds.26204.

Stebbins, G.T. *et al.* (2013) 'How to identify tremor dominant and postural instability/gait difficulty groups with the movement disorder society unified Parkinson's disease rating scale: Comparison with the unified Parkinson's disease rating scale', *Movement Disorders*, 28(5), pp. 668–670. Available at: https://doi.org/10.1002/mds.25383.

Stern, Y. (2013) 'Cognitive reserve in ageing', *Lancet Neurol.*, 11(11), pp. 1006–1012. Available at: https://doi.org/10.1016/S1474-4422(12)70191-6.Cognitive.

Stern, Y. *et al.* (2020) 'Whitepaper: Defining and investigating cognitive reserve, brain reserve, and brain maintenance', *Alzheimer's and Dementia*, 16(9), pp. 1305–1311. Available at: https://doi.org/10.1016/j.jalz.2018.07.219.

Stern, Y. and Barulli, D. (2019) 'Cognitive reserve', *Handbook of clinical neurology*, 167, pp. 181–190.

Stoessl, A.J. (2017) 'Glucose utilization: still in the synapse', *Nature neuroscience*, 20(3), pp. 382–384.

Stokholm, M.G. *et al.* (2016) 'Pathological α-synuclein in gastrointestinal tissues from prodromal Parkinson disease patients', *Annals of Neurology*, 79(6), pp. 940–949.

Available at: https://doi.org/10.1002/ana.24648.

Stubendorff, K. *et al.* (2012) 'The Impact of Autonomic Dysfunction on Survival in Patients with Dementia with Lewy Bodies and Parkinson's Disease with Dementia', *PLoS ONE*, 7(10), pp. 3–8. Available at: https://doi.org/10.1371/journal.pone.0045451.

Sulzer, D. and Surmeier, D.J. (2013) 'Neuronal vulnerability, pathogenesis, and Parkinson's disease', *Movement Disorders*, 28(6), pp. 715–724.

Surmeier, D.J., Obeso, J.A. and Halliday, G.M. (2017) 'Selective neuronal vulnerability in Parkinson disease', *Nature Reviews Neuroscience*, 18(2), pp. 101–113. Available at: https://doi.org/10.1038/nrn.2016.178.

Surmeier, D.J. and Sulzer, D. (2013) 'The pathology roadmap in Parkinson disease', *Prion*, 7(1), pp. 85–91.

Szwedo, A.A. *et al.* (2022) 'GBA and APOE Impact Cognitive Decline in Parkinson's Disease: A 10-Year Population-Based Study', *Movement Disorders*, 37(5), pp. 1016–1027. Available at: https://doi.org/10.1002/mds.28932.

Takeuchi, N., Sasai-Sakuma, T. and Inoue, Y. (2020) 'Gender differences in clinical findings and α-synucleiopathy-related markers in patients with idiopathic REM sleep behavior disorder', *Sleep Medicine*, 66, pp. 216–219. Available at: https://doi.org/10.1016/j.sleep.2019.11.1261.

Tang, C.C., Poston, K.L., Dhawan, V., *et al.* (2010) 'Abnormalities in metabolic network activity precede the onset of motor symptoms in Parkinson's disease', *Journal of Neuroscience*, 30(3), pp. 1049–1056.

Tang, C.C., Poston, K.L., Eckert, T., *et al.* (2010) 'Differential diagnosis of parkinsonism: a metabolic imaging study using pattern analysis', *The Lancet Neurology*, 9(2), pp. 149–158.

Taylor, S. *et al.* (2016) 'Progression of nonmotor symptoms in subgroups of patients with non-dopamine-deficient Parkinsonism', *Movement Disorders*, 31(3), pp. 344–351. Available at: https://doi.org/10.1002/mds.26456.

Terzaghi, M. *et al.* (2013) 'Cognitive performances and mild cognitive impairment in idiopathic rapid eye movement sleep behavior disorder: Results of a longitudinal follow-up study', *Sleep*, 36(10), pp. 1527–1532. Available at:

https://doi.org/10.5665/sleep.3050.

Tessitore, A., Cirillo, M. and De Micco, R. (2019) 'Functional Connectivity Signatures of Parkinson's Disease', *Journal of Parkinson's Disease*, 9(4), pp. 637–652. Available at: https://doi.org/10.3233/JPD-191592.

Teune, L.K. *et al.* (2010) 'Typical cerebral metabolic patterns in neurodegenerative brain diseases', *Movement Disorders*, 25(14), pp. 2395–2404. Available at: https://doi.org/10.1002/mds.23291.

Teune, L.K. *et al.* (2013) 'Validation of parkinsonian disease-related metabolic brain patterns', *Movement Disorders*, 28(4), pp. 547–551. Available at: https://doi.org/10.1002/mds.25361.

Thenganatt, M.A. and Jankovic, J. (2014) 'Parkinson disease subtypes', *JAMA Neurology*, 71(4), pp. 499–504. Available at: https://doi.org/10.1001/jamaneurol.2013.6233.

Tiraboschi, P. *et al.* (2006) 'What best differentiates Lewy body from Alzheimer's disease in early-stage dementia?', *Brain*, 129(3), pp. 729–735. Available at: https://doi.org/10.1093/brain/awh725.

Titova, N. *et al.* (2017) 'Parkinson's: a syndrome rather than a disease?', *Journal of Neural Transmission*, 124(8), pp. 907–914.

Toledo, J.B. *et al.* (2016) 'Pathological α-synuclein distribution in subjects with coincident Alzheimer's and Lewy body pathology', *Acta Neuropathologica*, 131(3), pp. 393–409. Available at: https://doi.org/10.1007/s00401-015-1526-9.

Tolosa, E. *et al.* (2021) 'Challenges in the diagnosis of Parkinson's disease', *The Lancet Neurology*, 20(5), pp. 385–397. Available at: https://doi.org/10.1016/S1474-4422(21)00030-2.

Tondo, G. *et al.* (2022) 'Brain Metabolism and Amyloid Load in Individuals With Subjective Cognitive Decline or Pre–Mild Cognitive Impairment', *Neurology* [Preprint].

Touron, E. *et al.* (2022) 'Depressive symptoms in cognitively unimpaired older adults are associated with lower structural and functional integrity in a frontolimbic network', *Molecular Psychiatry*, 27(12), pp. 5086–5095. Available at: https://doi.org/10.1038/s41380-022-01772-8.

Treglia, G., Cason, E. and Giordano, A. (2012) 'Diagnostic Performance of Myocardial Innervation Imaging Using MIBG Scintigraphy in Differential Diagnosis between Dementia with Lewy Bodies and Other Dementias: A Systematic Review and a Meta-Analysis', *Journal of Neuroimaging*, 22(2), pp. 111–117. Available at: https://doi.org/10.1111/j.1552-6569.2010.00532.x.

Tziortzi, A.C. *et al.* (2013) 'Connectivity-based functional analysis of dopamine release in the striatum using diffusion-weighted MRI and positron emission tomography', *Cerebral Cortex*, 24(5), pp. 1165–1177.

Tzourio-Mazoyer, N. *et al.* (2002) 'Automated anatomical labeling of activations in SPM using a macroscopic anatomical parcellation of the MNI MRI single-subject brain', *Neuroimage*, 15(1), pp. 273–289.

Uchihara, T. and Giasson, B.I. (2016) 'Propagation of alpha-synuclein pathology: hypotheses, discoveries, and yet unresolved questions from experimental and human brain studies', *Acta neuropathologica*, 131(1), pp. 49–73.

Ullah, M.F. *et al.* (2019) 'Impact of sex differences and gender specificity on behavioral characteristics and pathophysiology of neurodegenerative disorders', *Neuroscience and Biobehavioral Reviews*, 102(April), pp. 95–105. Available at: https://doi.org/10.1016/j.neubiorev.2019.04.003.

Utsumi, K. *et al.* (2020) 'Characteristics of initial symptoms and symptoms at diagnosis in probable dementia with Lewy body disease: incidence of symptoms and gender differences', *Psychogeriatrics*, 20(5), pp. 737–745. Available at: https://doi.org/10.1111/psyg.12586.

van der Veen, B.J. *et al.* (2012) 'Assessment of global cardiac I-123 MIBG uptake and washout using volumetric quantification of SPECT acquisitions', *Journal of Nuclear Cardiology*, 19(4), pp. 752–762.

van der Veen, L., Scholte, A. and Stokkel, M. (2010) 'Mathematical methods to determine quantitative parameters of myocardial 123I-MIBG studies: a review of the literature', *Nuclear medicine communications*, 31(7), pp. 617–628.

Veltman, C.E. *et al.* (2012) 'Reproducibility of planar 123I-meta-iodobenzylguanidine (MIBG) myocardial scintigraphy in patients with heart failure', *European Journal of*

Nuclear Medicine and Molecular Imaging, 39(10), pp. 1599–1608. Available at: https://doi.org/10.1007/s00259-012-2180-2.

Verger, A. *et al.* (2018) 'Brain PET substrate of impulse control disorders in Parkinson's disease: A metabolic connectivity study', *Human Brain Mapping*, 39(8), pp. 3178–3186. Available at: https://doi.org/10.1002/hbm.24068.

Vermeiren, Y. *et al.* (2015) 'The monoaminergic footprint of depression and psychosis in dementia with Lewy bodies compared to Alzheimer's disease', *Alzheimer's Research and Therapy*, 7(1), pp. 1–18. Available at: https://doi.org/10.1186/s13195-014-0090-1.

Vermeiren, Y. and De Deyn, P.P. (2017) 'Targeting the norepinephrinergic system in Parkinson's disease and related disorders: the locus coeruleus story', *Neurochemistry international*, 102, pp. 22–32.

Veronese, M. *et al.* (2019) 'Covariance statistics and network analysis of brain PET imaging studies', *Scientific Reports*, 9(1), pp. 1–15. Available at: https://doi.org/10.1038/s41598-019-39005-8.

Van Vickle, S.S. and Thompson, R.C. (2015) '123I-MIBG imaging: Patient preparation and technologist's role', *Journal of Nuclear Medicine Technology*, 43(2), pp. 82–86. Available at: https://doi.org/10.2967/jnmt.115.158394.

Vitek, J.L. *et al.* (2004) 'Acute stimulation in the external segment of the globus pallidus improves parkinsonian motor signs', *Movement disorders: official journal of the Movement Disorder Society*, 19(8), pp. 907–915.

Wakasugi, N. *et al.* (2021) 'Prefrontal network dysfunctions in rapid eye movement sleep behavior disorder', *Parkinsonism and Related Disorders*, 85(December 2020), pp. 72–77. Available at: https://doi.org/10.1016/j.parkreldis.2021.03.005.

Walker, Z. *et al.* (2004) 'Striatal dopamine transporter in dementia with Lewy bodies and Parkinson disease: A comparison', *Neurology*, 62(9), pp. 1568–1572. Available at: https://doi.org/10.1212/01.WNL.0000123248.39847.1D.

Wallert, E.D. *et al.* (2022) 'Imaging Dopaminergic Neurotransmission in Neurodegenerative Disorders', *Journal of Nuclear Medicine*, 63(Supplement 1), pp. 27S-32S. Available at: https://doi.org/10.2967/jnumed.121.263197.

Weintraub, D. *et al.* (2022) 'The neuropsychiatry of Parkinson's disease: advances and

challenges', *The Lancet Neurology*, 21(1), pp. 89–102. Available at: https://doi.org/10.1016/S1474-4422(21)00330-6.

Weiss, E. *et al.* (2003) 'Sex differences in brain activation pattern during a visuospatial cognitive task: a functional magnetic resonance imaging study in healthy volunteers', *Neuroscience letters*, 344(3), pp. 169–172.

Wile, D.J. *et al.* (2016) 'A scan without evidence is not evidence of absence: Scans without evidence of dopaminergic deficit in a symptomatic leucine-rich repeat kinase 2 mutation carrier', *Movement Disorders*, 31(3), pp. 405–409. Available at: https://doi.org/10.1002/mds.26450.

Wu, P. *et al.* (2014) 'Consistent abnormalities in metabolic network activity in idiopathic rapid eye movement sleep behaviour disorder', *Brain*, 137(12), pp. 3122–3128.

Yakushev, I., Drzezga, A. and Habeck, C. (2017) 'Metabolic connectivity: Methods and applications', *Current Opinion in Neurology*, 30(6), pp. 677–685. Available at: https://doi.org/10.1097/WCO.0000000000000494.

Yamada, G. *et al.* (2019) 'Nigrostriatal dopaminergic dysfunction and altered functional connectivity in REM sleep behavior disorder with mild motor impairment', *Frontiers in neurology*, p. 802.

Yao, N. *et al.* (2014) 'The default mode network is disrupted in Parkinson's disease with visual hallucinations', *Human brain mapping*, 35(11), pp. 5658–5666.

Yarnall, A.J. *et al.* (2014) 'Characterizing mild cognitive impairment in incident Parkinson disease : The ICICLE-PD Study', *Neurology*, 82(4), pp. 308–316. Available at: https://doi.org/10.1212/WNL.0000000000000066.

Yoon, E.J. *et al.* (2022) 'Brain Metabolism Related to Mild Cognitive Impairment and Phenoconversion in Patients With Isolated REM Sleep Behavior Disorder', *Neurology*, 98(24), pp. E2413–E2424. Available at: https://doi.org/10.1212/WNL.0000000000200326.

Zaccai, J., McCracken, C. and Brayne, C. (2005) 'A systematic review of prevalence and incidence studies of dementia with Lewy bodies', *Age and Ageing*, 34(6), pp. 561–566. Available at: https://doi.org/10.1093/ageing/afi190.

van der Zande, J.J. *et al.* (2020) 'Serotonergic deficits in dementia with Lewy bodies with concomitant Alzheimer's disease pathology: An 123I-FP-CIT SPECT study', *NeuroImage: Clinical*, 25(November 2019), p. 102062. Available at: https://doi.org/10.1016/j.nicl.2019.102062.

Zhao, P., Zhang, B. and Gao, S. (2012) '18[F]-FDG PET study on the idiopathic Parkinson's disease from several parkinsonian-plus syndromes', *Parkinsonism and Related Disorders*, 18(SUPPL. 1), pp. 60–62. Available at: https://doi.org/10.1016/s1353-8020(11)70513-2.

Zhou, J. *et al.* (2012) 'Predicting Regional Neurodegeneration from the Healthy Brain Functional Connectome', *Neuron*, 73(6), pp. 1216–1227. Available at: https://doi.org/10.1016/j.neuron.2012.03.004.

Zhou, J. *et al.* (2015) 'Gender differences in REM sleep behavior disorder: A clinical and polysomnographic study in China', *Sleep Medicine*, 16(3), pp. 414–418. Available at: https://doi.org/10.1016/j.sleep.2014.10.020.

Zhu, D., Montagne, A. and Zhao, Z. (2021) 'Alzheimer ' s pathogenic mechanisms and underlying sex difference', *Cellular and Molecular Life Sciences*, 78(11), pp. 4907–4920. Available at: https://doi.org/10.1007/s00018-021-03830-w.

Zis, P. *et al.* (2015) 'The range and nature of non-motor symptoms in drug-naive Parkinson's disease patients: a state-of-the-art systematic review', *npj Parkinson's Disease*, 1(1), pp. 1–8.

